

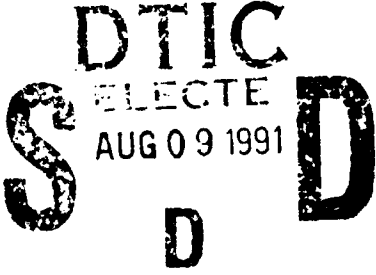
AD-A239 318



DOCUMENTATION PAGE

Form Approved
OMB No. 0704-0188

Information is estimated to average 1 hour per response, including the time for reviewing instructions, searching existing data sources, gathering and reviewing the material to be submitted, and completing and reviewing the collection of information. Send comments regarding this burden estimate or any aspect of this collection of information, including suggestions for reducing this burden, to Washington Headquarters Services, Directorate for Information Operations and Reports, 1215 Jefferson Davis Highway, Suite 1204, Arlington, VA 22202-4302, and to the Office of Management and Budget, Paperwork Reduction Project (0704-0188), Washington, DC 20503.

1. AGENCY USE ONLY (Leave blank)		2. REPORT DATE		3. REPORT TYPE AND DATES COVERED THESIS /DISSERTATION	
4. TITLE AND SUBTITLE Improved Finite Element Analysis of Thick Laminated Composite Plates by the Predictor Corrector Technique and Approximation of C ¹ Continuity with A New Least Squares Element				5. FUNDING NUMBERS	
6. AUTHOR(S) Jeffrey V. Kouri, Major				8. PERFORMING ORGANIZATION REPORT NUMBER AFIT/CI/CIA-91-003D	
7. PERFORMING ORGANIZATION NAME(S) AND ADDRESS(ES) AFIT Student Attending: Georgia Institute of Technology					
9. SPONSORING/MONITORING AGENCY NAME(S) AND ADDRESS(ES) AFIT/CI Wright-Patterson AFB OH 45433-6583				10. SPONSORING/MONITORING AGENCY REPORT NUMBER	
11. SUPPLEMENTARY NOTES					
12a. DISTRIBUTION/AVAILABILITY STATEMENT Approved for Public Release IAW 190-1 Distributed Unlimited ERNEST A. HAYGOOD, 1st Lt, USAF Executive Officer				12b. DISTRIBUTION CODE	
13. ABSTRACT (Maximum 200 words)					
					
<p>91-07321</p> 					
14. SUBJECT TERMS				15. NUMBER OF PAGES 214	
				16. PRICE CODE	
17. SECURITY CLASSIFICATION OF REPORT		18. SECURITY CLASSIFICATION OF THIS PAGE		19. SECURITY CLASSIFICATION OF ABSTRACT	
				20. LIMITATION OF ABSTRACT	

**IMPROVED FINITE ELEMENT ANALYSIS OF THICK LAMINATED
COMPOSITE PLATES BY THE PREDICTOR CORRECTOR
TECHNIQUE AND APPROXIMATION OF C^1 CONTINUITY WITH A
NEW LEAST SQUARES ELEMENT**

Jeffrey V. Kouri

214 pages

Directed by Dr. S. N. Atluri

The use of fiber reinforced composite laminates in engineering applications has been increasing rapidly. Along with this increase has come a rapid development in the analysis techniques to accurately model internal, as well as gross plate behaviors. Many improvements to laminated plate theory have been developed in the push for better analysis techniques. Improvements began with the application of Mindlin-Reissner shear deformation theory followed by higher order theories and discrete layer theories. With the drive for more accurate modeling, the cost has been increased complexity and computational time. Some of the higher order techniques lend themselves well to simplification, but in doing so they complicate the finite element analysis by creating a C^1 continuity requirement. The purpose of this work is to provide accurate, yet computationally efficient, improvements to the analysis of composite laminates.

One portion of this work shows that the higher order extensions to the first order shear deformation theory still do not correctly model the physics of the laminated plate problem. Results show that the first order theory can provide as good, if not better, results with the proper shear correction factor. This work uniquely implements a Predictor

Corrector technique into the finite element method to accurately calculate the shear correction factors. The technique provides excellent results with a simple Mindlin type plate element.

The second part of this research develops two new finite elements which approximate C^1 continuity through the use of a least squares technique. These Least Squares elements can be used to take advantage of the displacement field simplification techniques which, up until now, have seriously complicated the finite element application. The implementation of the elements are demonstrated using a piecewise, simplified third order displacement field. The Least Squares elements should prove to be useful tools in any finite element application where C^1 continuity is required.

The final portion of this work presents a study into the effects of stacking sequence, boundary conditions, pre-stress and plate aspect ratios on the fundamental frequency and buckling loads of laminated plates.

Approved For	
Date: 10/10/88	
By: [Signature]	
Availability Codes	
Dist	Availability of Special
A-1	

**IMPROVED FINITE ELEMENT ANALYSIS OF THICK
LAMINATED COMPOSITE PLATES BY THE
PREDICTOR CORRECTOR TECHNIQUE AND
APPROXIMATION OF C^1 CONTINUITY WITH A
NEW LEAST SQUARES ELEMENT**

A THESIS
Presented to
The Academic Faculty

by

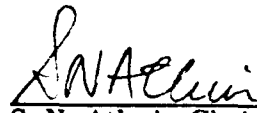
Jeffrey Victor Kouri
Major, USAF

In Partial Fulfillment
of the Requirements for the Degree
Doctor of Philosophy
in the School of Civil Engineering

Georgia Institute of Technology
March 6, 1991

IMPROVED FINITE ELEMENT ANALYSIS OF THICK
LAMINATED COMPOSITE PLATES BY THE
PREDICTOR CORRECTOR TECHNIQUE AND
APPROXIMATION OF C^1 CONTINUITY WITH A NEW
LEAST SQUARES ELEMENT

APPROVED:



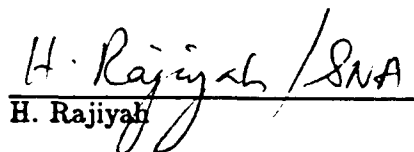
S. N. Atluri, Chairman



C. V. Smith



K. M. Will



H. Rajiyah



L. J. Jacobs

6 March 91

Date Approved by Chairman

*To my wonderful wife, Kris,
and my children, Jennifer and Brandon,
for their unending support and understanding.*

ACKNOWLEDGEMENTS

The author expresses his sincere gratitude to his academic advisor, Professor S. N. Atluri. He has provided guidance and suggestions which have been invaluable throughout the course of this research. The knowledge and experience gained through him far exceeds that which has actually been recorded on the pages of this thesis.

Thanks are also extended to the members of the thesis committee: Dr. H Rajiyah, Dr. C. V. Smith, Dr. K. M. Will, and especially Dr. L. J. Jacobs. Their questions and suggestions have been of great help throughout this work.

Most of all, the author wants to acknowledge the support and extreme patience of his wife, Kris, and children, Jennifer and Brandon. Without their encouragement and understanding this program could not have been completed.

Contents

I A REVIEW OF THE LITERATURE AND DEVELOPMENTS IN LAMINATED PLATE THEORIES	1
1.1 Introduction	1
1.2 A Brief Review of Basic Plate Theory	3
1.3 Further Developments in Shear Deformable Plate Theory	8
1.4 Laminated Fiber Reinforced Composite Plates	9
1.4.1 The Lamina	10
1.4.2 The Laminate	11
1.5 Evaluation of Current Analysis Methodologies	14
1.5.1 Higher order displacement fields	14
1.5.2 Discrete layer approach	16
1.5.3 Finite Element Analysis of Composite Materials	17
1.6 Analysis Approach	19
1.6.1 Improved First Order SDPT	19
1.6.2 Simplified Discrete Layer Approach with a Least Squares Element	19
1.6.3 Effect of Fiber Orientation and Stacking Sequence on Fundamental Frequency and Stability	20
II AN IMPROVED FIRST ORDER SHEAR DEFORMATION THEORY	

THROUGH THE USE OF THE PREDICTOR CORRECTOR TECH-	
NIQUE	21
2.1 Analysis Overview	21
2.2 Preliminary Development	22
2.2.1 Fundamental Equations	22
2.2.2 Internal Forces and Moments	25
2.3 Finite Element Formulation	27
2.3.1 Element Mathematical Considerations	27
2.3.2 Strain energy development	29
2.3.3 Kinetic energy development	33
2.3.4 Element stiffness and mass matrices	35
2.4 Analysis Method	37
2.4.1 Global matrix development	37
2.4.2 Solution to the eigenvalue problem	38
2.4.3 Updated natural frequency calculation	39
2.4.4 The equations of equilibrium	40
2.4.5 In-plane stress calculations	41
2.4.6 Derivatives of stresses	45
2.4.7 Shear correction coefficient calculations	48
III LEAST SQUARES ELEMENT DEVELOPMENT: C^1 CONTINUITY	
APPROXIMATION THROUGH A LEAST SQUARES METHOD	50
3.1 Background Information	50
3.2 Displacement Field Development	53
3.2.1 Displacement Field Basis	53
3.2.2 The Piecewise Continuous Displacement Field	55

3.3	Theory Development: Method I	57
3.3.1	The Domain Displacement Functions	57
3.3.2	Boundary Displacement Functions from Nodal Degrees of Freedom .	60
3.3.3	The Least Squares Implementation: Method I	64
3.4	Theory Development: Method II	68
3.4.1	The Domain Displacement Fields	68
3.4.2	The Element Boundary Displacements from Nodal Degrees of Freedom	68
3.4.3	The Least Squares Implementation: Method II	70
3.5	Preliminary Numerical Considerations: Method I -vs- Method II	73
3.6	Finite Element Formulation of the Least Squares Elements	76
3.6.1	Stiffness Matrix Development	76
3.6.2	Mass Matrix Development	82
3.6.3	Stress Stiffness Matrix Development	85
3.7	Finite Element Implementation of the Least Squares Elements	89
IV NUMERICAL RESULTS AND METHOD VALIDATIONS		91
4.1	Study Approach and Preliminary Information	91
4.2	Method Specific Behavior and Convergence	93
4.2.1	Predictor Corrector Technique	93
4.2.2	The Least Squares Method	96
4.3	Comparisons to Known Solutions	99
4.4	Stress Calculations	102
4.5	Conclusions From Method Evaluation	105
V NATURAL FREQUENCY AND STABILITY STUDIES FOR LAMI- NATED COMPOSITE PLATES		107

5.1 Study Approach	107
5.2 Initial Data Trends	110
5.3 Effects of Plate Aspect Ratio	111
5.4 Effects of Pre-Stress on Fundamental Frequency	111
5.5 Optimization of Fundamental Frequency and Buckling Loads	112
5.6 General Observations and Conclusions	114
VI CONCLUSIONS AND RECOMMENDATIONS	115
A Supplement to Equations	174
A.1 Supplement to equations Chapter III	174
B Calculation of Higher Order Derivatives	180
B.1 First Order Derivatives	180
B.2 Higher Order Derivatives	181
C BOUNDARY CONDITIONS	184
C.1 Boundary Conditions- Predictor Corrector Method	184
C.2 Boundary Conditions- Method I	184
C.3 Boundary Conditions- Method II	184

List of Tables

4.1	Material Properties.	92
5.1	Ply Angle Analysis Data/Figure* Correlation Grid.	109
5.2	Ply Angle Analysis Pre-stress Conditions.	110
C.1	Boundary Conditions: Predictor Corrector Method.	185
C.2	Boundary Conditions: Method I.	186
C.3	Boundary Conditions: Method II.	187

List of Figures

1.1	Deformation Geometry for CPT	4
1.2	Deformation Geometry for SDPT	5
1.3	Geometry of a Single Lamina	10
1.4	Laminate Deformation Geometry	11
2.1	Laminate Geometry	27
2.2	Eight Noded Isoparametric Element	28
2.3	Twelve Noded Isoparametric Element	43
3.1	Least Squares Element Domain	58
3.2	Least Squares Element with Nodes	61
3.3	Variation of Nodal variable q along element side.	62
3.4	Variation of Nodal variable w along element side.	63
4.1	Shear Correction Coefficient Variation Across Plate. Material I $a/b = 1$, 9 layer, [90/0/90/0/...], $h/b = 0.2$, BC-1, 5×5 quarter plate model.	117
4.2	Comparison of Transverse Shear Stress with Different Shear Correction Factors. Material I $a/b = 1$, 10 layer, [90/0/90/0/...], $h/b = 0.2$, BC-1, 3×3 quarter plate model.	118
4.3	Sensitivity of Natural Frequency to Shear Correction Coefficient. Cross ply laminate, Material II $a/b = 1$, $h/b = 0.2$, BC-1, 3×3 quarter plate model.	119
4.4	Variation of Shear Correction Coefficients with Number of Layers. Cross ply laminate, Material II $a/b = 1$, $h/b = 0.2$, BC-1, 4×4 quarter plate model.	120
4.5	Method I Interelement Compatibility. [0/90/0] simply supported $a/b = 1$, Material III, $b/h=4$, Location: $x = 0.16667$, $y = 0.133333$, 3×3 quarter plate model.	121

4.6	Method II Interelement Compatibility. [0/90/0] simply supported $a/b = 1$, Material III, $b/h=4$, Location: $x = 0.16667$, $y = 0.133333$, 3×3 quarter plate model.	122
4.7	Method I Convergence. [0/90/90/0] simply supported (BC-1), $a/b = 1$, Material VII, $b/h=5$, quarter plate model.	123
4.8	Method II Convergence. [0/90/90/0] simply supported (BC-1), $a/b = 1$, Material VII, $b/h=5$, quarter plate model.	124
4.9	Method I Convergence. Ten layer [-45/ + 45/ - 45/ . . .] simply supported (BC-1), $a/b = 1$, Material I, quarter plate model.	125
4.10	Method II Convergence. Ten layer [-45/ + 45/ - 45/ . . .] simply supported (BC-1), $a/b = 1$, Material I, quarter plate model.	126
4.11	Method I Convergence. 16 Layer Hybrid- Materials IV & V, simply supported (BC-1), $a/b = 1$, quarter plate model.	127
4.12	Method II Convergence. 16 Layer Hybrid- Materials IV & V, simply supported (BC-1), $a/b = 1$, quarter plate model.	128
4.13	Method Comparison of Non-dimensional Natural Frequency -vs- Anisotropy Ratio. [0/90/90/0], Material VII, $b/h = 5$, $\omega_n = (\omega b^2/h) (\rho/E_2)^{1/2}$, $a/b = 1$, Simply supported (BC-1)	129
4.14	Method Comparison of Non-dimensional Buckling Coefficient -vs- Anisotropy Ratio. [0/90/90/0], Material VII, $b/h = 5$, $\lambda_b = n_1 b^2/h^3 E_2$, $a/b = 1$, Simply supported (BC-1)	130
4.15	Method Comparison of Percent Error in Natural Frequency -vs- Anisotropy Ratio. [0/90/90/0], Material VII, $b/h = 5$, $a/b = 1$, Simply supported (BC-1)	131
4.16	Method Comparison of Percent Error in Buckling Coefficient -vs- Anisotropy Ratio. [0/90/90/0], Material VII, $b/h = 5$, $a/b = 1$, Simply supported (BC-1)	132
4.17	Method Comparison of Percent Error in Natural Frequency -vs- Thickness Ratio. 10 layer, [-45/+45/-45/ . . .], Material I, $a/b = 1$, Simply supported (BC-1)	133
4.18	Method Comparison of Percent Error in Natural Frequency -vs- Thickness Ratio. 16 layer Hybrid- Materials IV & V, $a/b = 1$, Simply supported (BC-1)	134
4.19	In-plane Displacements -vs- z Location. 10 layer, Material I, [90/0/90/ . . .], $a/b = 1$, $h/b = 0.2$, Simply supported (BC-1), 3×3 quarter plate model, $x = 0.29167$, $y = 0.29167$	135

4.20 In-plane Stresses -vs- z Location. 10 layer, Material I, [90/0/90/...], $a/b = 1$, $h/b = 0.2$, Simply supported (BC-1), 3×3 quarter plate model, $x = 0.29167$, $y = 0.29167$	136
4.21 In-plane Shear stress -vs- z Location. 10 layer, Material I, [90/0/90/...], $a/b = 1$, $h/b = 0.2$, Simply supported (BC-1), 3×3 quarter plate model, $x = 0.29167$, $y = 0.29167$	137
4.22 Transverse Shear Stresses -vs- z Location. 10 layer, Material I, [90/0/90/...], $a/b = 1$, $h/b = 0.2$, Simply supported (BC-1), 3×3 quarter plate model, $x = 0.29167$, $y = 0.29167$	138
4.23 Method Comparison of Transverse Shear Stresses. 10 layer, Material I, [90/0/90/...], $a/b = 1$, $h/b = 0.2$, Simply supported (BC-1), 3×3 quarter plate model, $x = 0.29167$, $y = 0.29167$	139
4.24 In-plane Stress Comparison: Method I -vs- Elasticity. 10 layer, Material VI, [90/0/90/...], $a/b = 1$, $h/b = 0.2$, Simply supported (BC-1), 4×4 quarter plate model, $x = 0.29167$, $y = 0.29167$	140
4.25 Transverse Shear Stress Comparison: Method I -vs- Elasticity. 10 layer, Material VI, [90/0/90/...], $a/b = 1$, $h/b = 0.2$, Simply supported (BC-1), 4×4 quarter plate model, $x = 0.29167$, $y = 0.29167$	141
4.26 In-plane Displacements -vs- z Location. 9 layer, Material I, [90/0/90/...], $a/b = 1$, $h/b = 0.2$, Simply supported (BC-1), 3×3 quarter plate model, $x = 0.29167$, $y = 0.29167$	142
4.27 In-plane Stresses -vs- z Location. 9 layer, Material I, [90/0/90/...], $a/b = 1$, $h/b = 0.2$, Simply supported (BC-1), 3×3 quarter plate model, $x = 0.29167$, $y = 0.29167$	143
4.28 In-plane Shear stress -vs- z Location. 9 layer, Material I, [90/0/90/...], $a/b = 1$, $h/b = 0.2$, Simply supported (BC-1), 3×3 quarter plate model, $x = 0.29167$, $y = 0.29167$	144
4.29 Transverse Shear Stresses -vs- z Location. 9 layer, Material I, [90/0/90/...], $a/b = 1$, $h/b = 0.2$, Simply supported (BC-1), 3×3 quarter plate model, $x = 0.29167$, $y = 0.29167$	145
4.30 Method Comparison of Transverse Shear Stresses. 9 layer, Material I, [90/0/90/...], $a/b = 1$, $h/b = 0.2$, Simply supported (BC-1), 3×3 quarter plate model, $x = 0.29167$, $y = 0.29167$	146

4.31	In-plane Displacements -vs- z Location. 16 Layer Hybrid, Materials IV & V, $a/b = 1$, $h/b = 0.3$, Simply supported (BC-1), 3×3 quarter plate model, $x = 0.29167$, $y = 0.29167$	147
4.32	In-plane Stresses -vs- z Location. 16 Layer Hybrid, Materials IV & V, $a/b = 1$, $h/b = 0.3$, Simply supported (BC-1), 3×3 quarter plate model, $x = 0.29167$, $y = 0.29167$	148
4.33	In-plane Shear stress -vs- z Location. 16 Layer Hybrid, Materials IV & V, $a/b = 1$, $h/b = 0.3$, Simply supported (BC-1), 3×3 quarter plate model, $x = 0.29167$, $y = 0.29167$	149
4.34	Transverse Shear Stresses -vs- z Location. 16 Layer Hybrid, Materials IV & V, $a/b = 1$, $h/b = 0.3$, Simply supported (BC-1), 3×3 quarter plate model, $x = 0.29167$, $y = 0.29167$	150
4.35	Method Comparison of Transverse Shear Stresses. 16 Layer Hybrid, Materials IV & V, $a/b = 1$, $h/b = 0.3$, Simply supported (BC-1), 3×3 quarter plate model, $x = 0.29167$, $y = 0.29167$	151
5.1	Eigenvalue Coefficients -vs- Ply Angle. Case A, 6 Layer $[+\theta/ - \theta/\dots]$, Material II, $a/b = 0.7$, $h/b = 0.1$, Simply supported (BC-6), 3×4 full plate model.	152
5.2	Pre-Stressed Natural Frequency -vs- Ply Angle. Case A, 6 Layer $[+\theta/ - \theta/\dots]$, Material II, $a/b = 0.7$, $h/b = 0.1$, Simply supported (BC-6), 3×4 full plate model.	153
5.3	Eigenvalue Coefficients -vs- Ply Angle. Case A, 6 Layer $[+\theta/ - \theta/\dots]$, Material II, $a/b = 0.7$, $h/b = 0.1$, Clamped, (BC-13), 3×4 full plate model.	154
5.4	Pre-Stressed Natural Frequency -vs- Ply Angle. Case A, 6 Layer $[+\theta/ - \theta/\dots]$, Material II, $a/b = 0.7$, $h/b = 0.1$, Clamped (BC-13), 3×4 full plate model.	155
5.5	Eigenvalue Coefficients -vs- Ply Angle. Case B, 6 Layer $[+\theta/ - \theta/\dots]$, Material II, $a/b = 1.0$, $h/b = 0.1$, Simply supported (BC-6), 4×4 full plate model.	156
5.6	Pre-Stressed Natural Frequency -vs- Ply Angle. Case B, 6 Layer $[+\theta/ - \theta/\dots]$, Material II, $a/b = 1.0$, $h/b = 0.1$, Simply supported (BC-6), 4×4 full plate model.	157
5.7	Eigenvalue Coefficients -vs- Ply Angle. Case B, 6 Layer $[+\theta/ - \theta/\dots]$, Material II, $a/b = 1.0$, $h/b = 0.1$, Clamped, (BC-13), 4×4 full plate model.	158

5.8	Pre-Stressed Natural Frequency -vs- Ply Angle. Case B, 6 Layer [+ θ / - θ /...], Material II, $a/b = 1.0$, $h/b = 0.1$, Clamped (BC-13), 4×4 full plate model	159
5.9	Eigenvalue Coefficients -vs- Ply Angle. Case C, 6 Layer [+ θ / - θ /...], Material II, $a/b = 1.4286$, $h/b = 0.1$, Simply supported (BC-6), 4×3 full plate model.	160
5.10	Pre-Stressed Natural Frequency -vs- Ply Angle. Case C, 6 Layer [+ θ / - θ /...], Material II, $a/b = 1.4286$, $h/b = 0.1$, Simply supported (BC-6), 4×3 full plate model.	161
5.11	Eigenvalue Coefficients -vs- Ply Angle. Case C, 6 Layer [+ θ / - θ /...], Material II, $a/b = 1.4286$, $h/b = 0.1$, Clamped, (BC-13), 4×3 full plate model.	162
5.12	Pre-Stressed Natural Frequency -vs- Ply Angle. Case C, 6 Layer [+ θ / - θ /...], Material II, $a/b = 1.4286$, $h/b = 0.1$, Clamped (BC-13), 4×3 full plate model	163
5.13	Eigenvalue Coefficients -vs- Ply Angle. Case D, 6 Layer [+ θ / - θ /...], Material II, $a/b = 1.7$, $h/b = 0.1$, Simply supported (BC-6), 5×3 full plate model.	164
5.14	Pre-Stressed Natural Frequency -vs- Ply Angle. Case D, 6 Layer [+ θ / - θ /...], Material II, $a/b = 1.7$, $h/b = 0.1$, Simply supported (BC-6), 5×3 full plate model.	165
5.15	Eigenvalue Coefficients -vs- Ply Angle. Case D, 6 Layer [+ θ / - θ /...], Material II, $a/b = 1.7$, $h/b = 0.1$, Clamped, (BC-13), 5×3 full plate model.	166
5.16	Pre-Stressed Natural Frequency -vs- Ply Angle. Case D, 6 Layer [+ θ / - θ /...], Material II, $a/b = 1.7$, $h/b = 0.1$, Clamped (BC-13), 5×3 full plate model.	167
5.17	Natural Frequency -vs- Ply Angle for All Aspect Ratios. 6 Layer [+ θ / - θ /...], Material II, $h/b = 0.1$, Simply Supported (BC-6), Various mesh full plate models.	168
5.18	Natural Frequency -vs- Ply Angle for All Aspect Ratios. 6 Layer [+ θ / - θ /...], Material II, $h/b = 0.1$, Clamped (BC-13), Various mesh full plate models.	169

5.19 Uniaxial Buckling Coefficient -vs- Ply Angle for All Aspect Ratios. 6 Layer [+ θ / - θ /...], Material II, $h/b = 0.1$, Simply Supported (BC-6), Various mesh full plate models.	170
5.20 Uniaxial Buckling Coefficient -vs- Ply Angle for All Aspect Ratios. 6 Layer [+ θ / - θ /...], Material II, $h/b = 0.1$, Clamped (BC-13), Various mesh full plate models.	171
5.21 Biaxial Buckling Coefficient -vs- Ply Angle for All Aspect Ratios. 6 Layer [+ θ / - θ /...], Material II, $h/b = 0.1$, Simply Supported (BC-6), Various mesh full plate models.	172
5.22 Biaxial Buckling Coefficient -vs- Ply Angle for All Aspect Ratios. 6 Layer [+ θ / - θ /...], Material II, $h/b = 0.1$, Clamped (BC-13), Various mesh full plate models.	173

SUMMARY

The use of fiber reinforced composite laminates in engineering applications has been increasing rapidly. Along with this increase has come a rapid development in the analysis techniques to accurately model internal, as well as gross plate behaviors. Many improvements to laminated plate theory have been developed in the push for better analysis techniques. Improvements began with the application of Mindlin-Reissner shear deformation theory followed by higher order theories and discrete layer theories. With the drive for more accurate modeling, the cost has been increased complexity and computational time. Some of the higher order techniques lend themselves well to simplification, but in doing so they complicate the finite element analysis by creating a C^1 continuity requirement. The purpose of this work is to provide accurate, yet computationally efficient, improvements to the analysis of composite laminates.

One portion of this work shows that the higher order extensions to the first order shear deformation theory still do not correctly model the physics of the laminated plate problem. Results show that the first order theory can provide as good, if not better, results with the proper shear correction factor. This work uniquely implements a Predictor Corrector technique into the finite element method to accurately calculate the shear correction factors. The technique provides excellent results with a simple Mindlin type plate element.

The second part of this research develops two new finite elements which approximate C^1 continuity through the use of a least squares technique. These Least Squares elements can be used to take advantage of the displacement field simplification techniques which, up until now, have seriously complicated the finite element application. The implementation of the elements are demonstrated using a piecewise, simplified third order displacement field. The Least Squares elements should prove to be useful tools in any finite element

application where C^1 continuity is required.

The final portion of this work presents a study into the effects of stacking sequence, boundary conditions, pre-stress and plate aspect ratios on the fundamental frequency and buckling loads of laminated plates.

CHAPTER I

A REVIEW OF THE LITERATURE AND DEVELOPMENTS IN LAMINATED PLATE THEORIES

1.1 Introduction

Laminated fiber reinforced composite materials have provided engineers with the ability to design and build structures as never before. The use of composites has been growing rapidly over the past twenty years and is continuing to do so at an increased rate. Early in their existence, their use was primarily associated with spacecraft and aircraft because of their high strength to weight ratios, in spite of their high cost. Recently however, reduced manufacturing costs are making composites attractive to many other industries. Composites are now being used for automobiles, sporting goods, pressure vessels and a multitude of other applications. Composite materials will eventually be able to benefit virtually any engineering application because of their design advantages. Today's technology has only begun to realize the resource that is becoming available in the composite material world. The engineer has the ability to not only design directional strength, but also thermal and electrical conductivity, radar absorption, thermal expansion, fracture characteristics and stiffness, to only mention a few parameters. As research into composite materials continues, more and more of these design parameters will be developed, and more and more applications will arise. In reality, the composite material science is probably in its very infancy, and as it continues to grow, so must the ability to perform accurate engineering

analyses.

The engineering analysis of composite materials is in itself a relatively new field and has just begun to grow. The mathematical modeling of the mechanics of composite materials dates back only thirty years ago when classical laminated plate theory, as we know it today, was developed by Reissner and Stavsky (1961) [121]. It remains today as the main tool available to the practicing engineer. However, as the field grows so will its complexity, and classical laminated plate theory (CLPT) will not be a sufficient analysis tool. As the field grows, more accurate and efficient modeling techniques must be developed. The inherent complex nature of composite laminates often necessitates complex mathematical models. Unfortunately, complex models are difficult to implement in practical engineering analysis, so the need for accurate, yet efficient, methods will remain high. No matter how accurate or simple a mathematical model is, it has very limited engineering applicability if it cannot be applied to general shapes and boundary conditions. The finite element method is the tool which is generally used to achieve this capability. However, the finite element implementation of new mathematical formulations can be difficult and the end product is not always useful. Accuracy in the finite element method many times corresponds to increased computational costs. For example, a recent article by Jing and Liao (1989) [39] proposes a new element which gives excellent results for laminated composites. The element is employed in *each* layer of the laminate. Thus, each layer is modeled by a twenty-node mixed field hexahedron with three degrees of freedom at each node and fourteen stress parameters. One can see that for a laminate with a moderate number of layers the analysis can quickly become numerically intractable.

Based upon the above discussion, we see that the future calls for not only increased understanding and more complex mathematical modeling of composite materials, but also for fresh ideas and approaches on how to effectively and economically model laminate

behavior. It is hoped that this work will present some novel approaches in the analysis methods of composite materials which will provide simple, yet powerful, tools to be used in engineering design analysis. In addition, it may possibly initiate a new methodology for future work in laminated composite plates and shells.

1.2 A Brief Review of Basic Plate Theory

The mathematical analysis of plates has been a much studied area in the engineering world for many years. The use of plates as major structural components has driven researchers to find a way to accurately predict their behavior from a static, dynamic and stability point of view. The first major achievements in modern engineering plate analysis, as stated by McFarland et al (1972) [74], were begun in the early 1800's and are accredited to Cauchy, Poisson, Navier, Lagrange and Kirchhoff. However, the development of what we know today as classical plate theory (CPT) is generally attributed to Kirchhoff [55] for his work in 1850.

In CPT certain assumptions are made simplifying the problem to one that is more easily solved. The Kirchhoff assumptions, as they are sometimes called, parallel the ideas behind simple beam theory. We first assume that a normal to the midplane of the plate before deformation remains normal and inextensionable after deformation. Also, we assume that normal stresses in the transverse direction to the plate are small compared with the other stresses and can be neglected. The geometry of the deformation is shown in Figure 1.1. One can see that the in-plane displacements are composed of a translation and a rotation. They can be written as:

$$\begin{aligned} u &= u_o - z \frac{\partial w_o}{\partial x} \\ v &= v_o - z \frac{\partial w_o}{\partial y} \end{aligned} \quad (1.1)$$

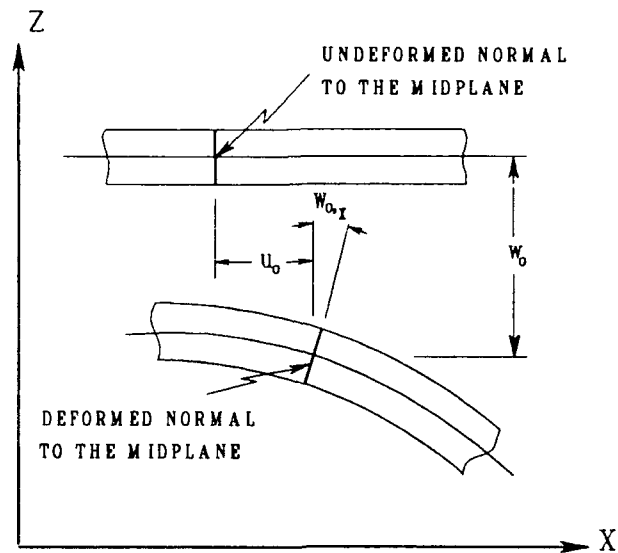


Figure 1.1: Deformation Geometry for CPT

$$w = w_0$$

The Kirchhoff assumptions are valid for many cases, and accurate results can be achieved with them for engineering problems. Problems are restricted to thin plates free from any large transverse loads. However, there is an important concept to remember when working with the Kirchhoff assumptions. One must remember that in assuming that the normals to the midplane remain normal after deformation, one does *not* preclude transverse stresses¹. Just as in beam theory, it means that the additional deformation caused by these stresses is negligible. This is a valid assumption as long as the shear rigidity for the transverse strain is on the same order of magnitude as the elastic modulus, which is the case for most isotropic engineering materials.

The next major advancement in plate theory was the logical step to include the effects of transverse shear deformation into the governing equations. Including transverse shear allows the normals to the midplane to deform. The work in this area closely parallels

¹Throughout this work, 'transverse stresses' and 'transverse strains' will imply the shear components only, and not the normal components (unless otherwise specified).

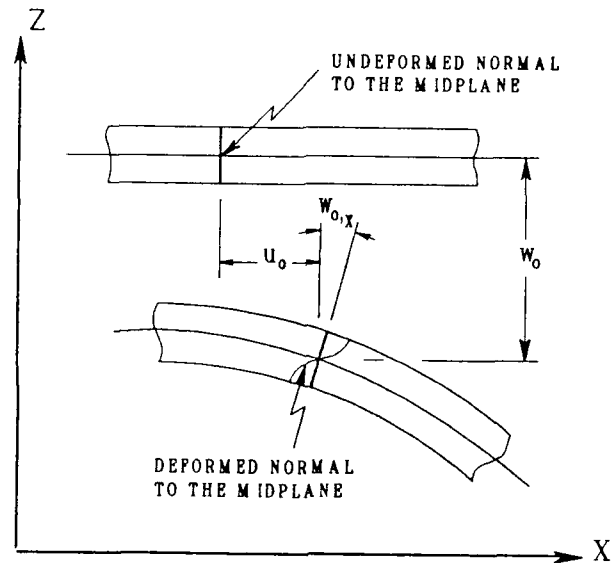


Figure 1.2: Deformation Geometry for SDPT

that done in beam theory. Transverse shear deformation effects are included in going from Bernoulli-Euler beam theory to Timoshenko beam theory. The inclusion of transverse shear into plate theory has taken many forms and was proposed in many different ways by several investigators. In a survey article Reddy (1985) [114] presented a brief account of the development in this area. It appears that work to include transverse shear effects into plate theory was first published by Basset [8] in 1890, followed by Reissner (1945) [118], Hencky (1947) [30], Hildebrand (1949) [32], Reissner (1947) [119] and Mindlin (1951) [76]. Today the development of shear deformable plate theory (SDPT) is sometimes categorized as a Reissner-Mindlin plate theory. The difference being that Reissner used a stress based approach and Mindlin used a displacement based approach, as did Basset, Hildebrand and Hencky.

In SDPT the Kirchhoff assumption that the normals to the midplane remain normal after deformation is removed. The result is that the displacements in the u and v directions are no longer constrained to be equal to the rotation of a midplane normal. Such a deformation is depicted in Figure 1.2. In its general form, this deformation can be

represented as a power series expansion in z , with the number of terms carried in the expansion being determined by the order of the theory desired. In the initial work with Reissner-Mindlin SDPT, the displacements are assumed to be of the form

$$u = u_o + z\phi_x \quad (1.2)$$

$$v = v_o + z\phi_y \quad (1.3)$$

$$w = w_o \quad (1.4)$$

where u_o , v_o , w_o , ϕ_x and ϕ_y are all functions of x and y . Here, the u and v displacements are linear in z , while w is constant with respect to z . Thus, the deformed normal would maintain a straight line appearance but be inclined to the midplane. For obvious reasons, the SDPT with this form of displacements will be referred to as the first order theory. Just as a point of comparison, if the Kirchhoff assumption is invoked on these displacements we have

$$\phi_x = -\frac{\partial w}{\partial x} \quad (1.5)$$

$$\phi_y = -\frac{\partial w}{\partial y} \quad (1.6)$$

which reduces the deformation back to a translation and the same rotation as in eqns (1.1). This, in effect, couples ϕ_x and ϕ_y to w . In SDPT w_o is uncoupled from ϕ_x and ϕ_y creating the required deformation through the thickness. Substitution of eqns (1.2)-(1.4) into the linear strain displacement equations gives, for the six strains:

$$\epsilon_x = \frac{\partial u}{\partial x} = u_{o,x} + z\phi_{x,x} = \epsilon_x^o + z\kappa_x \quad (1.7)$$

$$\epsilon_y = \frac{\partial v}{\partial y} = v_{o,y} + z\phi_{y,y} = \epsilon_y^o + z\kappa_y \quad (1.8)$$

$$\epsilon_z = \frac{\partial w}{\partial z} = 0 \quad (1.9)$$

$$\gamma_{xz} = \frac{\partial u}{\partial z} + \frac{\partial w}{\partial x} = \phi_x + w_{,x} \quad (1.10)$$

$$\gamma_{yz} = \frac{\partial v}{\partial z} + \frac{\partial w}{\partial y} = \phi_y + w_{,y} \quad (1.11)$$

$$\gamma_{xy} = \frac{\partial u}{\partial y} + \frac{\partial v}{\partial x} = u_{o,y} + v_{o,x} + z(\phi_{x,y} + \phi_{y,x}) = \gamma_o + z\kappa_{xy} \quad (1.12)$$

(Note the use of commas denoting partial differentiation.)

The results in eqns (1.7)-(1.12) show an important aspect of the first order theory. This is the fact that the assumed displacement fields for u and v presuppose constant values of transverse shear strains in the thickness direction. Hence, for a homogeneous plate the shear stress is also constant through the thickness. Again parallel to beam theory, this obviously cannot be the case, as the top and bottom surfaces should be free of any surface tractions (for the free vibration case). The result of this violation is that the amount of transverse strain energy is overestimated, and the plate model is actually more stiff than it should be. To remedy this, a shear correction factor is normally introduced. The correction factor multiplies the transverse shear stiffness coefficients, thus reducing the stiffness in these directions. For an isotropic material the coefficients could be introduced as

$$\sigma_{xz} = k \cdot G\gamma_{xz} \quad (1.13)$$

$$\sigma_{yz} = k \cdot G\gamma_{yz} \quad (1.14)$$

The value for k can be shown to be dependent upon the cross section of the beam or plate. For an isotropic material with a rectangular cross section the value becomes 5/6. This factor is due to the fact that the exact solution is parabolic. This shortcoming of the first order theory has not proven to be of any detriment to the results obtainable using it. With the correct shear correction factor, the theory provides very accurate results

for the gross plate behavior. It is understandable that the integral average of transverse stresses can be predicted accurately, but their distribution through the thickness cannot. Also, the assumed displacements result in in-plane stresses which are antisymmetric about the midplane of the plate. Thus, inaccurate results may be achieved for cases where the loading conditions may preclude such a solution.

1.3 Further Developments in Shear Deformable Plate Theory

Since the development of SDPT many researchers have published works on variations of the Reissner-Mindlin approach. Since 1957 many higher order displacement fields have been used in an attempt to achieve more accurate results and to eliminate the shortcomings of the first order theory. The desire has mainly been to eliminate the need for a shear correction factor. The landmark article into improving first order SDPT was published by Lo, Christensen and Wu (1977) [67]. In their article the authors review some of the different higher order displacement fields which have been used over the years. Most significant, however, is that they themselves present a higher order theory using displacements of the form:

$$\begin{aligned}
 u &= u_o + z\phi_x + z^2\psi_x + z^3\zeta_x \\
 v &= v_o + z\phi_y + z^2\psi_y + z^3\zeta_y \\
 w &= w_o + z\phi_z + z^2\psi_z
 \end{aligned}
 \tag{1.15}$$

In their work Lo et al show that this form of a displacement field alleviates the necessity for a shear correction factor for homogeneous plates, and that one can get better results for cases with certain loading conditions which result in non-antisymmetric in-plane stresses. They also briefly discuss some of the other forms of higher order displacement fields which

have been studied. The end result appears to be that the required form of the displacement field is closely tied to several items. The choice of the displacement field depends on the type of problem being solved, which variables are needed as a result of the analysis and the required level of accuracy for those variables.

For gross plate behavior, and accurate in-plane stresses, the first order theory has provided very satisfactory results over the past forty five years. At the cost of increased complexity, the higher order approaches have not been applied in any extent to isotropic plate theory. In fact, it was not until the advent of laminated composite plates that higher order approaches were considered to any extent at all. In the above mentioned work by Lo et al, their third order SDPT was developed and demonstrated for isotropic plates, but it was immediately applied to laminated plates [68], the real motivation for their work. It is the fact that first order SDPT has many disadvantages when it comes to laminated composite plates that has prompted the search for an improvement in the analysis of such structures. This search has lead to the multitude of higher order applications of SDPT that can be found in the literature over the past twenty years. However, before we can accurately and efficiently apply the theories available to us, we must first study the fundamentals of the problem.

1.4 Laminated Fiber Reinforced Composite Plates

Research into the analysis of laminated plates began in the late 1950's by Stavsky (1959) [133] and Lekhnitsky (1968) [62] (originally published in Russian in 1957), but classical laminated plate theory (CLPT) as we know it today is credited to Reissner and Stavsky [121] for their work in 1961. The development of the CLPT equations will be developed later in Section 2.2.1, so for now we will concentrate on understanding the physics of the deformation of laminated fiber reinforced composite plates.

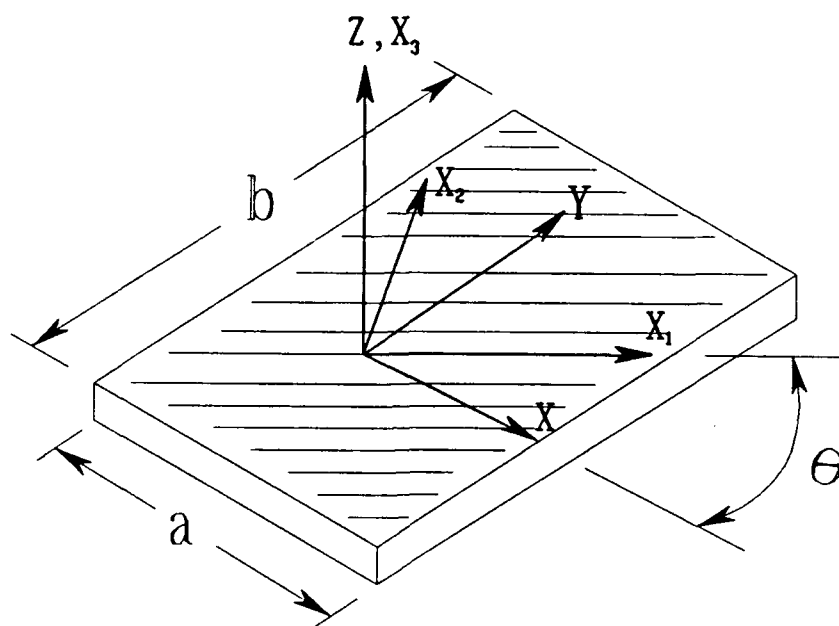


Figure 1.3: Geometry of a Single Lamina

1.4.1 The Lamina

The geometry of a lamina is shown in Figure 1.3. The material properties and constitutive equations of the lamina are described originally with respect to the material coordinates, the x_1 , x_2 and x_3 axis, and then transformed into the global coordinates through a simple transformation. The details of this will be presented in Section 2.2.1. At this point it is important to understand the material properties of the lamina in Figure 1.3. The elastic modulus is generally much higher in the x_1 direction than in the x_2 direction. Typical values for E_1/E_2 can be on the order of 40. In addition, and perhaps more importantly, the values for shear rigidity are small compared to the elastic modulus. A typical value for G_{23}/E_2 is 0.35, while G_{13}/E_1 can be less than 0.01. These big discrepancies in rigidities make shear deformation considerations very important in the analysis of composite materials. Early investigators found that they could no longer neglect the contribution of transverse shear deformation to the overall deformation, even in relatively thin laminates.

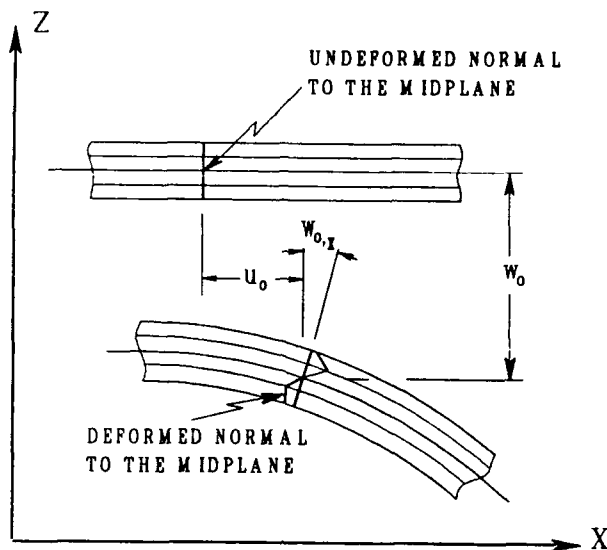


Figure 1.4: Laminate Deformation Geometry

(See Reissner (1945) [118], Mindlin (1951) [76], Whitney (1969) [141] and Whitney and Pagano (1970) [144].) These properties of a lamina are compounded when multiple lamina are stacked to form a laminate.

1.4.2 The Laminate

The real advantage of using composite materials in the design of structures is realized when multiple layers are stacked with varying ply angles. This allows the engineer to tailor the material properties to fit a specific purpose. This process, while providing great design capabilities, creates great difficulty in accurate analysis of the plate parameters. A laminated plate may appear to behave externally like an isotropic plate, but internally it is totally different. Figure 1.4 depicts the cross section of a laminated plate.

As discussed above in Section 1.4.1, transverse shear effects are extremely important in the analysis of composite materials. The inclusion of transverse shear effects in the study of composite plates was first done by Yang, Norris and Stavsky (1966) [145] in their

work on elastic wave propagation in heterogeneous plates. This first work was nothing more than the application of a Mindlin displacement form, as in eqns (1.2)-(1.4), to the classical laminated plate theory equations. This approach, despite its simplicity, has been the mainframe for the analysis of transverse shear effects in fiber reinforced composite laminated plates. In fact, commercial analysis codes used in industry rely upon this first order SDPT. This theory has been used in one form or another extensively over the past twenty eight years. Most of the advances and improvements in the analysis methods since 1968 have been extensions in one form or another of this work. To understand how to improve upon this theory, we must look at the physics of the problem.

We begin by taking a close look at the deformation field of composite plates. It is assumed that the layers of the laminate are perfectly bonded together so that no slip can occur between them. The deformation of a normal to the midplane of the laminate is no longer a smooth continuous function as it was for an isotropic plate as depicted in Figure 1.2, but instead is piecewise continuous (not piecewise linear, however). This can easily be understood by considering that the material properties can change drastically at the layer interfaces. One can gain better understanding into the physics of the problem by studying it in such manner. Next, we let u_i be the three displacements at any point, each being a general function of x_j . (Here $i, j = 1, 2, 3$ and x_j represents the three coordinate directions.) The deformation field depicted in Figure 1.4 can be deduced by the following items:

1. The functions $u_i(x_j)$ must be continuous in x_j to satisfy compatibility.
2. In the 1-2 plane, since there is no slip or gaps between layers, the material on each side of the interface must have the same displacement, and hence, displacement gradient. In other words, $u_{i,\alpha}$ (here $\alpha = 1, 2$) must be continuous across the layer interface. Let us write this as $u_{i,\alpha}^+ = u_{i,\alpha}^-$.

3. Since $\epsilon_{\alpha\beta} = \frac{1}{2}(u_{\alpha,\beta} + u_{\beta,\alpha})$, then 2 above implies $\epsilon_{\alpha\beta}$ must be continuous across the interface, ie. $\epsilon_{\alpha\beta}^+ = \epsilon_{\alpha\beta}^-$.
4. Since $\epsilon_{\alpha\beta}^+ = \epsilon_{\alpha\beta}^-$, then $\sigma_{\alpha\beta}^+ \neq \sigma_{\alpha\beta}^-$ in general. This is due to the possibility of the material constants changing across the layer interface.
5. Based simply on Newton's Third Law, σ_{3j} must be continuous across the layer interface, ie. $\sigma_{3j}^+ = \sigma_{3j}^-$.
6. From item 5 we find $\epsilon_{3j}^+ \neq \epsilon_{3j}^-$. This again is due to the changing of material properties from layer to layer.
7. Since $\epsilon_{3j}^+ \neq \epsilon_{3j}^-$, and $\epsilon_{3j} = \frac{1}{2}(u_{3,j} + u_{j,3})$, then $u_{j,3}^+ \neq u_{j,3}^-$. (See also item 2 above.)

These seven ideas are very important when studying composite laminates. If one uses a displacement based approach in analyzing laminated plates these ideas should be kept in mind as the model is developed. In doing so, the limitations and strengths of any specific theory can be realized. We can summarize the above items into one general observation worthy of special note. This is as follows:

Observation 1 *The displacement field, $u_i(x_j)$, for a laminated composite plate must be continuous for all x_j , but it need not have a unique $u_{i,3}$ across the interfaces of the lamina.*

This observation tells us in no uncertain terms what form our displacement field takes. An exact solution to the laminated composite plate cannot be achieved if this observation is violated. This observation is supported by exact, three-dimensional analysis of composite laminates published by Pagano (1969) [96] and (1970) [97].

1.5 Evaluation of Current Analysis Methodologies

1.5.1 Higher order displacement fields

As discussed in Section 1.3 there have been many attempts at improving the analysis of laminated composite plates. A large number of these concentrated upon trying to gain more accuracy by carrying more terms in the series expansion of the displacements. In other words, higher order SDPT's are used as in eqns (1.15). One of the disadvantages of the higher order approach is that the number of unknowns in the problem quickly becomes large. In addition, it becomes difficult to physically understand and to prescribe boundary conditions for these additional terms. The order of the expansion by no means needs to be limited to three as is shown in eqns (1.15). A few of the works in this area have been published by Nelson and Lorch (1974) [84], Kant et al (1988) [46], Murty and Vellaichamy (1987) [83], Pandya and Kant (1988) [104], Lo et al (1977) [67, 68], Mallikarjuna and Kant (1989) [71, 45], Mottram (1989) [78] and Murty (1977) [80].

Modifications of the higher order approach are also quite common in current research. They are referred to as the simplified higher order methods. Through setting the transverse stresses on the top and bottom surfaces of the plate equal to zero, the number of unknowns in the displacement field can be reduced by four terms. For example, the most common simplified higher order method found in the literature begins with cubic forms for u and v and a constant w (with respect to z). This nine parameter displacement field can then be reduced to one of only five parameters, the same number as found in the first order theory. This specific example will be discussed in more detail in Section 3.1. Some examples of simplified higher order approaches can be found in references published by Reddy (1984) [113, 112], Kant and Pandya (1988) [44], Senthilnathan et al (1988) [124, 65], Reddy and Phan (1985) [117], Murty (1987) [81] and Khdeir (1989) [53].

These higher order approaches theoretically make sense, but outside of the realm of

homogeneous materials, carrying a finite number of higher order terms does not coincide with the physics of the problem. A higher order SDPT has unique values of $u_{i,3}$ across the lamina interfaces. Thus, a higher order SDPT does not have the freedom to fully comply with Observation 1. The advantage to a higher order theory is that a traction free condition on the top and bottom surfaces can be satisfied, and the need for a shear correction coefficient is *reduced*. However, accurate prediction of the transverse stresses cannot be done directly. We use the word *directly* here because the transverse stresses can be found by integrating the equations of equilibrium through the thickness of the plate. This is done utilizing the calculated in-plane stresses which are generally accurate. This technique is used quite often when transverse stresses are desired. Some examples of this are included in the works by Nishioka and Atluri (1979) [85], Murty (1987) [82], Kant and Pandya (1988) [44], Noor and Burton (1989) [88] and Reddy et al (1989) [116]. Also, note the above emphasis on the word *reduced* with regards to the shear correction coefficient. Since the assumed deformation field is not exact, then the calculated transverse strain energy is going to deviate from the true energy, and a shear correction coefficient would be beneficial to adjust this difference. If the assumed deformation closely approximates the true one, then the shear correction coefficient would be insignificant. In other words, in studying an isotropic plate one would expect a third order theory to give excellent results without a shear correction factor, as such a field follows an elasticity solution. However, depending upon the makeup of a composite laminate, a third order theory cannot accurately describe a piecewise continuous displacement field. Based upon this discussion, it is reasonable to assume that the first order SDPT with the *correct* shear correction coefficients can give better results for certain cases than a higher order theory without any correction. This time, notice that the emphasis is placed upon the word *correct* with regard to the shear correction coefficients. One of the purposes of this work is to

demonstrate that the shear correction coefficients can be calculated accurately, allowing the first order SDPT to provide as good, if not better, results than the higher order approaches with their added complexities.

1.5.2 Discrete layer approach

Up to this point we have not considered the obvious methodology for the laminated composite plate problem. This, of course, is to assume a piecewise continuous displacement field through the thickness of the laminate as depicted in Figure 1.4. Within each layer the displacements can be chosen to be linear or of a higher order form. This form of displacement field should provide us with more accurate results than a finite term higher order approach and is often referred to as a discrete layer approach. The discrete layer approach is nothing more than modeling each individual layer of the laminate as a separate plate. The obvious drawback to such an approach is that the number of unknowns in the problem becomes tied to the number of layers in the laminate. A problem can quickly become intractable for thick plates with a large number of layers. A few of the works published in this area include those by Srinivas (1973) [130], Reddy et al (1989) [116], Barbero and Reddy (1990) [6] and Alam and Asnani (1984) [2, 3].

Just as there was a simplified version of the higher order approach, there is also a simplified discrete layer approach. In assuming a piecewise continuous displacement field, the number of unknowns can be reduced by enforcing displacement continuity, as well as transverse shear traction continuity, at the layer interfaces. In this manner the number of unknowns can be made to be independent of the number of layers. (This will be developed in more detail in Section 3.2.2.) The simplified discrete layer approach has been demonstrated to provide accurate results for thick composite laminates and has the potential to become an efficient and powerful tool in the analysis of laminated composite plates. A few examples of the simplified discrete layer approach include Sciuva (1987)

[123], Mawenya and Davies (1974) [73] and Lee et al (1990) [59].

It is interesting to note that a piecewise continuous displacement field results in a smooth transverse stress field rather than a piecewise continuous one through the thickness. This is because when the interlaminar transverse stress continuity is enforced across a lamina interface, either in the discrete layer or simplified discrete layer theory, the derivatives (slopes) with respect to z of these functions are also the same. Thus, a smooth function through the thickness results. The end result is that in order to calculate the transverse stresses, one must rely upon integrating the equations of equilibrium as discussed in Section 1.5.1.

1.5.3 Finite Element Analysis of Composite Materials

Finite element analysis of laminated plates began with the work of Pryor and Barker (1971) [42]. In their work they developed an element based upon the deformation field given in eqns (1.2)-(1.4), and established seven degrees of freedom at each node ($u_o, v_o, w_o, \phi_x, \phi_y, \gamma_{xz}$ and γ_{yz}). This basic development has been the fundamental basis for much of the finite element work done with composite materials to date, with the only difference being that five degrees of freedom per node are generally used (u_o, v_o, w_o, ϕ_x and ϕ_y). This basic approach is the back-bone of composite analyses, and most commercial finite element codes are based upon this theory. Many different elements and implementations have been devised, but generally the first order shear deformation theory is the basis behind them. Some of the works published in the past several years using a first order shear deformation approach include: Moser and Schmid (1989) [77], Craig and Dawe (1987) [24], Kumar and Rao (1988) [57], Fuehne and Engblom (1989) [26], Lardeur and Batoz (1989) [58], Zienkiewicz and Lefebvre (1988) [147], Oñate and Suarez (1983) [95], Reddy (1980) [110], Suresh et al (1979) [103] and Irons and Zienkiewicz (1970) [38]. As one might expect, the first order theory is burdened with the shear correction coefficient

problem as discussed in Section 1.3. This problem is even more difficult with laminates than with homogeneous plates, because the coefficients not only depend upon geometry, but also on ply orientation and material properties. In addition, because of this, different coefficients are also needed for different directions in the plate. However, despite this drawback, the first order approach has remained popular because of its low computational cost. Implementation of higher order approaches has also been well documented in the published work. These include works by Kant et al (1988) [46, 44, 104], Mallikarjuna and Kant (1989) [71] and Reddy (1989) [115]. The advantage of these, as discussed previously, is the reduced need for shear correction coefficients, while the disadvantage is the increased complexity. The simplified higher order approaches, even with lower numbers of degrees of freedom, have increased complexity in that they have increased continuity requirements. This will be discussed in more detail in Section 3.2.

The discrete layer and simplified discrete layer approaches have also been employed in finite element analyses. The full discrete layer approaches are computationally more intense than other methods and are not widely found in the literature. Examples include those by Reddy et al (1989) [116] and Barbero and Reddy (1990) [6]. Examples of the simplified discrete layer approaches are computationally efficient and include: Lee et al (1990) [59].

All of the above mentioned finite element analyses are displacement based approaches. Along with these come the lack of direct transverse stress calculations and increased continuity requirements for the finite element model. These inherent problems have led to much research in the areas of mixed and hybrid methods which eliminate these problems. These methods have demonstrated excellent results, but again at the cost of excessive computations. Research in these areas include: Putchu and Reddy (1986) [106], Jing and Liao (1989) [39], Spilker (1982) [128], Spilker et al (1977) [129], Mau, Tong and Pian

(1972) [72] and Liou and Sun (1987) [66].

As a final note, there have been a few survey and overview articles by Reddy (1985) [114], (1981) [111], (1989) [115], which have appeared in the past several years. The interested reader may find them beneficial if more information is desired.

1.6 Analysis Approach

1.6.1 Improved First Order SDPT

As discussed above in Section 1.5.1 the first order SDPT has the potential to provide accurate results as long as the correct shear correction coefficients can be calculated. In Chapter II we will develop a finite element method based upon first order SDPT which can accurately calculate the vibration characteristics of thick laminated composite plates. The method will include the calculation of accurate shear correction coefficients by comparing the first order transverse strain energy to a more accurate strain energy. This more accurate strain energy will be calculated based upon the transverse stresses found from integrating the equations of equilibrium through the thickness of the plate.

1.6.2 Simplified Discrete Layer Approach with a Least Squares Element

Chapter III of this work will develop two new Least Squares finite elements. The elements will utilize a unique Least Squares method to allow an element's displacement functions to approximate C^1 continuous functions on the boundaries of the element. This technique will allow the element to behave as one with C^1 continuity. Thus, it will enable the use of displacement functions which normally would require C^1 continuous interpolation functions. The Least Squares element would be applicable to either a simplified higher order approach or a simplified discrete layer approach with a simplified higher order piecewise continuous function as the basis for the displacement field. These forms of displacement functions will be shown to contain differentials of the out-of-plane displacement, which up

until now could not easily be analyzed without the use of C^1 continuous elements. The simplified discrete layer field, based upon the simplified higher order approach, will be used to demonstrate the technique.

1.6.3 Effect of Fiber Orientation and Stacking Sequence on Fundamental Frequency and Stability

The Least Squares finite element technique will be used to perform a study of the effects of fiber orientation angle, stacking sequence, boundary conditions, aspect ratios and pre-stressing on the fundamental frequencies and buckling loads of composite laminates. The study will concentrate upon optimizing frequency and buckling load while varying the other parameters. The purpose of the study is to provide new information for the design engineer to aid in the designing of composite laminated materials.

CHAPTER II

AN IMPROVED FIRST ORDER SHEAR DEFORMATION THEORY THROUGH THE USE OF THE PREDICTOR CORRECTOR TECHNIQUE

2.1 Analysis Overview

In this part of the work we will investigate the feasibility of developing a finite element model which is based upon a first order SDPT. The method stands out from any other finite element models of this type because it will include the ability to calculate accurate shear correction coefficients for any particular laminate being considered. With accurate shear correction coefficients, the first order SDPT will give very good results. This technique has been successfully applied analytically by Noor and Peters (1989) [91] and Noor and Burton (1989) [88], (1990) [89], but implementation of the technique into a finite element analysis has not been published.

In the following sections we will first develop a first order plate bending model for a general composite laminate. This development will be the basis for the development of the finite element model to be used for a vibration analysis. The finite element model will be developed to include the integration of the equilibrium equations through the thickness of the plate to obtain the transverse stresses. These stresses will then be used to calculate the transverse strain energy which will be compared to those obtained using the first order theory. This comparison will yield the above mentioned shear correction coefficient which

then will be used to calculate an updated natural frequency and mode shape.

2.2 Preliminary Development

2.2.1 Fundamental Equations

As presented and discussed above in Section 1.2, the assumed displacements for a first order SDPT are represented by eqns (1.2)-(1.4). These equations will form the basis for our analysis. In terms of these variables, eqns (1.7)-(1.12) represent the strains.

Next, we can begin to introduce some of the standard equations used when working with fiber reinforced composite materials (see texts by Jones [41] and Christensen [22].

First we define:

$$\{\sigma\} = \begin{Bmatrix} \sigma_{11} \\ \sigma_{22} \\ \sigma_{33} \\ \sigma_{12} \\ \sigma_{13} \\ \sigma_{23} \end{Bmatrix}, \text{ and } \{\epsilon\} = \begin{Bmatrix} \epsilon_{11} \\ \epsilon_{22} \\ \epsilon_{33} \\ \gamma_{12} \\ \gamma_{13} \\ \gamma_{23} \end{Bmatrix}$$

for a single layer of a composite material related through the constitutive equation

$$\{\sigma\} = [C] \{\epsilon\} \quad (2.1)$$

where $[C]$ are the stiffnesses in the 1-2-3 coordinate system as depicted in Figure 1.3. If we assume two orthogonal planes of material property symmetry for the material under consideration, then $[C]$ takes the standard form:

$$[C] = \begin{bmatrix} C_{11} & C_{12} & C_{13} & 0 & 0 & 0 \\ C_{12} & C_{22} & C_{23} & 0 & 0 & 0 \\ C_{13} & C_{23} & C_{33} & 0 & 0 & 0 \\ 0 & 0 & 0 & C_{66} & 0 & 0 \\ 0 & 0 & 0 & 0 & C_{44} & 0 \\ 0 & 0 & 0 & 0 & 0 & C_{55} \end{bmatrix} \quad (2.2)$$

The values for the C_{ij} are:

$$\begin{aligned}
C_{11} &= E_1 (1 - \nu_{32}\nu_{23}) / A, & C_{12} &= E_2 (\nu_{12} + \nu_{13}\nu_{32}) / A, & C_{44} &= G_{13} \\
C_{13} &= E_3 (\nu_{13} + \nu_{12}\nu_{23}) / A, & C_{22} &= E_2 (1 - \nu_{31}\nu_{13}) / A, & C_{55} &= G_{23} \\
C_{23} &= E_3 (\nu_{23} + \nu_{13}\nu_{21}) / A, & C_{33} &= E_3 (1 - \nu_{12}\nu_{21}) / A, & C_{66} &= G_{12}
\end{aligned} \tag{2.3}$$

where

$$A = (1 - \nu_{23}\nu_{32} - \nu_{12}\nu_{21} - \nu_{13}\nu_{31} - \nu_{12}\nu_{23}\nu_{31} - \nu_{13}\nu_{32}\nu_{21})$$

We also define the Poisson's ratio, ν_{ij} , to be the ratio of the deformation in the j direction to that in the i direction when pulled in the i direction.

The next step is to then transform $[C]$ into the x, y, z coordinate system to get the form:

$$\begin{Bmatrix} \sigma_{xx} \\ \sigma_{yy} \\ \sigma_{zz} \\ \sigma_{xy} \\ \sigma_{xz} \\ \sigma_{yz} \end{Bmatrix} = \begin{bmatrix} \bar{C}_{11} & \bar{C}_{12} & \bar{C}_{13} & \bar{C}_{16} & 0 & 0 \\ \bar{C}_{12} & \bar{C}_{22} & \bar{C}_{23} & \bar{C}_{26} & 0 & 0 \\ \bar{C}_{13} & \bar{C}_{23} & \bar{C}_{33} & \bar{C}_{36} & 0 & 0 \\ \bar{C}_{16} & \bar{C}_{26} & \bar{C}_{36} & \bar{C}_{66} & 0 & 0 \\ 0 & 0 & 0 & 0 & \bar{C}_{44} & \bar{C}_{45} \\ 0 & 0 & 0 & 0 & \bar{C}_{45} & \bar{C}_{55} \end{bmatrix} \begin{Bmatrix} \epsilon_{xx} \\ \epsilon_{yy} \\ \epsilon_{zz} \\ \gamma_{xy} \\ \gamma_{xz} \\ \gamma_{yz} \end{Bmatrix} \tag{2.4}$$

where ($n = \sin \theta$, $m = \cos \theta$):

$$\begin{aligned}
\bar{C}_{11} &= m^4 C_{11} + 2m^2 n^2 (C_{12} + 2C_{66}) + n^4 C_{22} \\
\bar{C}_{12} &= m^2 n^2 (C_{11} + C_{22} - 4C_{66}) + (m^4 + n^4) C_{12} \\
\bar{C}_{22} &= n^4 C_{11} + 2m^2 n^2 (C_{12} + 2C_{66}) + m^4 C_{22} \\
\bar{C}_{16} &= -mn [n^2 C_{11} - m^2 C_{22} - (m^2 - n^2) (C_{12} + 2C_{66})] \\
\bar{C}_{26} &= -mn [m^2 C_{11} - n^2 C_{22} + (m^2 - n^2) (C_{12} + 2C_{66})] \\
\bar{C}_{66} &= m^2 n^2 (C_{11} + C_{22} - 2C_{12}) + (m^4 - n^4) C_{66}
\end{aligned} \tag{2.5}$$

$$\begin{aligned}
\bar{C}_{13} &= m^2 C_{13} + n^2 C_{23} & \bar{C}_{44} &= m^2 C_{44} + n^2 C_{55} \\
\bar{C}_{23} &= n^2 C_{13} + m^2 C_{23} & \bar{C}_{36} &= (C_{32} - C_{31}) nm \\
\bar{C}_{45} &= (C_{44} - C_{55}) nm & \bar{C}_{55} &= m^2 C_{55} + n^2 C_{44} \\
\bar{C}_{33} &= C_{33}
\end{aligned}$$

We can next eliminate the σ_{zz} equation from eqn (2.4). One can solve for ϵ_{zz} from eqn (2.4) to get

$$\epsilon_{zz} = \frac{1}{\bar{C}_{33}} (\sigma_{zz} - \bar{C}_{13}\epsilon_{xx} - \bar{C}_{32}\epsilon_{yy} - \bar{C}_{36}\gamma_{xy}) \quad (2.6)$$

which can then be substituted back into eqn (2.4) to yield:

$$\begin{Bmatrix} \sigma_{xx} \\ \sigma_{yy} \\ \sigma_{xy} \\ \sigma_{xz} \\ \sigma_{yz} \end{Bmatrix} = \begin{bmatrix} \bar{Q}_{11} & \bar{Q}_{12} & \bar{Q}_{16} & 0 & 0 \\ \bar{Q}_{12} & \bar{Q}_{22} & \bar{Q}_{26} & 0 & 0 \\ \bar{Q}_{16} & \bar{Q}_{26} & \bar{Q}_{66} & 0 & 0 \\ 0 & 0 & 0 & \bar{Q}_{44} & \bar{Q}_{45} \\ 0 & 0 & 0 & \bar{Q}_{45} & \bar{Q}_{55} \end{bmatrix} \begin{Bmatrix} \epsilon_{xx} \\ \epsilon_{yy} \\ \gamma_{xy} \\ \gamma_{xz} \\ \gamma_{yz} \end{Bmatrix} - \frac{\sigma_{zz}}{\bar{C}_{33}} \begin{Bmatrix} \bar{C}_{13} \\ \bar{C}_{23} \\ \bar{C}_{36} \\ 0 \\ 0 \end{Bmatrix} \quad (2.7)$$

The values, \bar{Q}_{ij} , are the reduced stiffness coefficients developed by Whitney (1969) [141], and are defined in terms of the \bar{C}_{ij} as:

$$\begin{aligned}
\bar{Q}_{ij} &= \bar{C}_{ij} - (\bar{C}_{i3} \cdot \bar{C}_{j3}) / \bar{C}_{33} & i, j &= 1, 2, 6 \\
\bar{Q}_{ij} &= \bar{C}_{ij} & i, j &= 4, 5
\end{aligned} \quad (2.8)$$

Next, before moving on, it will be convenient to have $[\bar{Q}]$ partitioned into two matrices, $[Q]$ and $[\bar{Q}]$, defined as

$$[\bar{Q}] = \begin{bmatrix} [Q] & 0 \\ 0 & [\bar{Q}] \end{bmatrix} \quad (2.9)$$

The reason for breaking $[\bar{Q}]$ up like this will be apparent in the next section. Lastly, from this point on, we will drop the term containing σ_{zz} in eqn (2.7). In other words we assume that the transverse normal stress has little effect on our solution.

2.2.2 Internal Forces and Moments

At this point it is convenient to define the internal force and moment relations for a composite laminate. The forces per unit width of the plate are found by integrating the stresses through the thickness to get

$$\begin{Bmatrix} N_x \\ N_y \\ N_{xy} \end{Bmatrix} = \{\mathbf{N}\} = \int_{-h/2}^{h/2} \begin{Bmatrix} \sigma_{xx} \\ \sigma_{yy} \\ \sigma_{xy} \end{Bmatrix} dz = \int_{-h/2}^{h/2} [Q] \begin{Bmatrix} \epsilon_{xx} \\ \epsilon_{yy} \\ \gamma_{xy} \end{Bmatrix} dz \quad (2.10)$$

$$\begin{Bmatrix} Q_x \\ Q_y \end{Bmatrix} = \{\mathbf{Q}\} = \int_{-h/2}^{h/2} \begin{Bmatrix} \sigma_{xz} \\ \sigma_{yz} \end{Bmatrix} dz = (k_i k_j)^{\frac{1}{2}} \int_{-h/2}^{h/2} [\bar{Q}] \begin{Bmatrix} \gamma_{xz} \\ \gamma_{yz} \end{Bmatrix} dz \quad (2.11)$$

where we have introduced k_i and k_j , the shear correction coefficients, which will be discussed in more detail later. Similarly, the moments per unit width are

$$\begin{Bmatrix} M_x \\ M_y \\ M_{xy} \end{Bmatrix} = \{\mathbf{M}\} = \int_{-h/2}^{h/2} \begin{Bmatrix} \sigma_{xx} \\ \sigma_{yy} \\ \sigma_{xy} \end{Bmatrix} \cdot z \cdot dz = \int_{-h/2}^{h/2} [Q] \begin{Bmatrix} \epsilon_{xx} \\ \epsilon_{yy} \\ \gamma_{xy} \end{Bmatrix} \cdot z \cdot dz \quad (2.12)$$

Next, we use eqns (1.7)-(1.12) to express the strains in terms of midplane strains and curvatures. The result is

$$\{\mathbf{N}\} = \int_{-h/2}^{h/2} [Q] \begin{Bmatrix} \epsilon_x^o + z\kappa_x \\ \epsilon_y^o + z\kappa_y \\ \gamma_o + z\kappa_{xy} \end{Bmatrix} dz = \int_{-h/2}^{h/2} ([Q] \{\epsilon_o\} + [Q]z \{\kappa\}) dz \quad (2.13)$$

$$\{Q\} = (k_i k_j)^{\frac{1}{2}} \int_{-h/2}^{h/2} [\bar{Q}] \begin{Bmatrix} w_{,x} + \phi_x \\ w_{,y} + \phi_y \end{Bmatrix} dz = (k_i k_j)^{\frac{1}{2}} \int_{-h/2}^{h/2} [\bar{Q}] \{\vartheta\} dz \quad (2.14)$$

$$\{M\} = \int_{-h/2}^{h/2} [Q] \begin{Bmatrix} \epsilon_x^o + z\kappa_x \\ \epsilon_y^o + z\kappa_y \\ \gamma_o + z\kappa_{xy} \end{Bmatrix} \cdot z \cdot dz = \int_{-h/2}^{h/2} ([Q]z \{\epsilon_o\} + [Q]z^2 \{\kappa\}) dz \quad (2.15)$$

In the above three equations, the $[Q]$ and $[\bar{Q}]$ are piecewise constant with respect to the integration through the thickness of the laminate. Thus, as is commonly done, we establish matrices $[A]$, $[\bar{A}]$, $[B]$ and $[D]$ whose elements are defined by:

$$A_{ij} = \int_{-h/2}^{h/2} Q_{ij} dz = \sum_{k=1}^n (Q_{ij})_k \cdot t_k \quad (2.16)$$

$$\bar{A}_{ij} = (k_i k_j)^{\frac{1}{2}} \int_{-h/2}^{h/2} \bar{Q}_{ij} dz = (k_i k_j)^{\frac{1}{2}} \sum_{k=1}^n (\bar{Q}_{ij})_k \cdot t_k \quad (2.17)$$

$$B_{ij} = \int_{-h/2}^{h/2} Q_{ij} z \cdot dz = \sum_{k=1}^n (Q_{ij})_k \cdot t_k \cdot \bar{z}_k \quad (2.18)$$

$$D_{ij} = \int_{-h/2}^{h/2} Q_{ij} z^2 \cdot dz = \sum_{k=1}^n (Q_{ij})_k \left(t_k \cdot \bar{z}_k^2 + \frac{t_k^3}{12} \right) \quad (2.19)$$

where $\bar{z}_k = z_k - z_{k-1}$, and t_k and z_k are defined as in Figure 2.1. Finally, since $\{\epsilon_o\}$, $\{\kappa\}$ and $\{\vartheta\}$ are independent of z , they can be pulled outside of the integral. The end result is a convenient representation of the internal forces and moments in the laminate:

$$\begin{Bmatrix} N \\ M \\ Q \end{Bmatrix} = \begin{bmatrix} A & B & 0 \\ B & D & 0 \\ 0 & 0 & \bar{A} \end{bmatrix} \begin{Bmatrix} \epsilon_o \\ \kappa \\ \vartheta \end{Bmatrix} \quad (2.20)$$

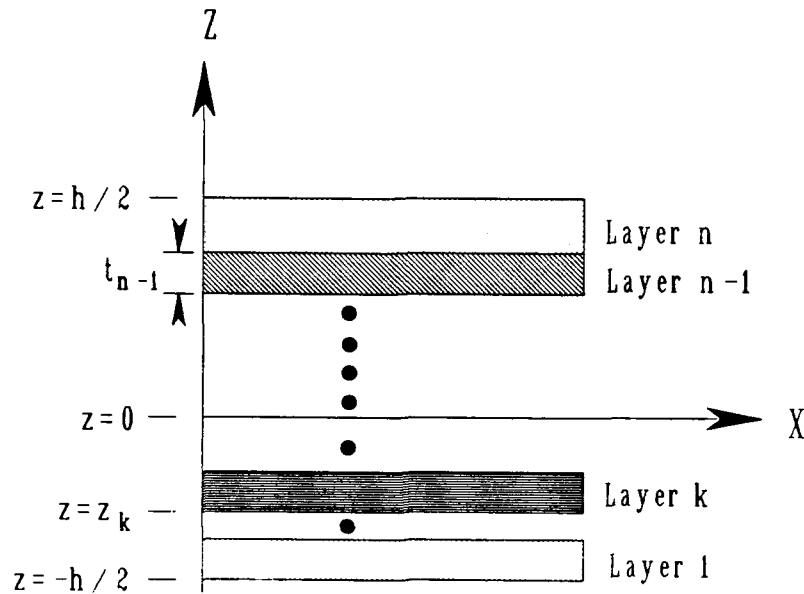


Figure 2.1: Laminate Geometry

These equations will now be used in the finite element formulation.

2.3 Finite Element Formulation

2.3.1 Element Mathematical Considerations

As discussed in the previous section, the basis for this analysis is a first order shear deformation theory. The displacements through the thickness of the plate will be described with three displacements and two rotations. As a result, a two dimensional element is all that is required rather than a three dimensional solid one. The quadratic, eight noded, isoparametric element is often used in modeling plates with accurate results. For this reason it will be used for this analysis. The eight noded element will have the three displacements and two rotations at each node for a total of 40 degrees of freedom. The element is shown in Figure 2.2.

The element parameters will be described through standard shape functions derived

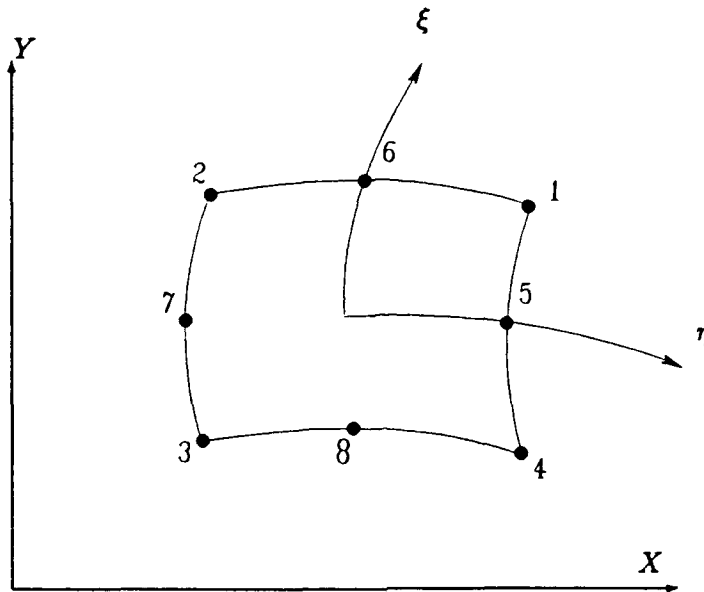


Figure 2.2: Eight Noded Isoparametric Element

for the serendipity family of elements as given in any standard finite element text. (See Zienkiewicz [146], Cook [23], Tong and Rossettos [136] or Bathe [9].) The eight shape functions are

$$\begin{aligned}
 N_i &= \frac{1}{4} (1 + \eta\eta_i) (1 + \xi\xi_i) (\xi\xi_i + \eta\eta_i - 1) & i = 1, 2, 3, 4 \\
 N_i &= \frac{1}{2} (1 + \eta\eta_i) (1 - \xi^2) & i = 5, 7 \\
 N_i &= \frac{1}{2} (1 - \eta^2) (1 + \xi\xi_i) & i = 6, 8
 \end{aligned} \tag{2.21}$$

where here η_i and ξ_i are the coordinates of the i th node, and η and ξ are the coordinates of any desired point in the element. The disadvantage of this element, which will be discussed in detail later, is that it is only capable of having a quadratic variation of the primary variables throughout it. Thus, the stresses will be linear and derivatives of stresses constant. This restriction can be overcome, but as mentioned above, will be discussed later.

The finite element model used in this analysis is based upon finding a stationary value of the element's total energy. For our problem, the energy is composed of both internal strain energy, U_{se} , and kinetic energy, U_{ke} . The internal strain energy is defined as

$$U_{se} = \int_V U_o dV = \frac{1}{2} \int_V \sigma_{ij} \epsilon_{ij} dV \quad (2.22)$$

and the kinetic energy becomes

$$U_{ke} = \frac{1}{2} \int_V \rho |\bar{V}|^2 dV = \frac{1}{2} \int_V \rho (\sqrt{\dot{u}^2 + \dot{v}^2 + \dot{w}^2})^2 dV \quad (2.23)$$

The total energy, Π , is then

$$\Pi = U_{se} + U_{ke} \quad (2.24)$$

Finding an extremum of this functional leads to the stiffness and mass matrices.

2.3.2 Strain energy development

In the above discussion, eqn (2.22) can readily be adapted for the case of the composite laminate. If we perform an integration through the thickness of the laminate, just as performed in the development of eqn (2.20), it can be shown that the expression for the strain energy of the system becomes

$$U_{se} = \frac{1}{2} \int_A \left(\left\{ \begin{matrix} \mathbf{N} \\ \mathbf{M} \end{matrix} \right\}^T \left\{ \begin{matrix} \epsilon^o \\ \kappa \end{matrix} \right\} + \{\mathbf{Q}\}^T \{\vartheta\} \right) dA \quad (2.25)$$

where it is now written in terms of the internal forces and moments and is an area integral

rather than a volume integral. The goal is to write this expression ultimately in terms of the nodal degrees of freedom of the element. From eqn (2.20) $\{N\}$, $\{M\}$, and $\{Q\}$ can be written as

$$\begin{Bmatrix} N \\ M \end{Bmatrix} = \begin{bmatrix} A & B \\ B & D \end{bmatrix} \begin{Bmatrix} \epsilon^o \\ \kappa \end{Bmatrix} \quad (2.26)$$

$$(2.27)$$

$$\{Q\} = [\bar{A}] \{\vartheta\}$$

Next, recalling the definitions of $\{\epsilon^o\}$, $\{\kappa\}$, and $\{\vartheta\}$, (see eqns (1.7)-(1.12)), we can express them as

$$\begin{aligned} \begin{Bmatrix} \epsilon^o \\ \kappa \end{Bmatrix} &= \begin{Bmatrix} u_{o,x} \\ v_{o,y} \\ v_{o,x} + u_{o,y} \\ \phi_{x,x} \\ \phi_{y,y} \\ \phi_{x,y} + \phi_{y,x} \end{Bmatrix} = \begin{bmatrix} 1 & 0 & 0 & 0 & 0 & 0 & 0 & 0 \\ 0 & 0 & 0 & 1 & 0 & 0 & 0 & 0 \\ 0 & 1 & 1 & 0 & 0 & 0 & 0 & 0 \\ 0 & 0 & 0 & 0 & 1 & 0 & 0 & 0 \\ 0 & 0 & 0 & 0 & 0 & 0 & 0 & 1 \\ 0 & 0 & 0 & 0 & 0 & 1 & 1 & 0 \end{bmatrix} \begin{Bmatrix} u_{o,x} \\ u_{o,y} \\ v_{o,x} \\ v_{o,y} \\ \phi_{x,x} \\ \phi_{x,y} \\ \phi_{y,x} \\ \phi_{y,y} \end{Bmatrix} \\ &= [I] \{\delta'_{xy}\} \end{aligned} \quad (2.28)$$

$$\begin{aligned} \{\vartheta\} &= \begin{Bmatrix} w_{,x} + \phi_x \\ w_{,y} + \phi_y \end{Bmatrix} = \begin{bmatrix} 1 & 0 & 1 & 0 \\ 0 & 1 & 0 & 1 \end{bmatrix} \begin{Bmatrix} \phi_x \\ \phi_y \\ w_{o,x} \\ w_{o,y} \end{Bmatrix} \\ &= [\bar{I}] \{\bar{\delta}'_{xy}\} \end{aligned} \quad (2.29)$$

Next, $\{\delta'_{xy}\}$ and $\{\bar{\delta}'_{xy}\}$, which are expressed in terms of the derivatives with respect to x and y , need to be written in terms of the derivatives with respect to η and ξ . This can easily be done through the standard use of the Jacobian matrix, $[J]$, which relates the

derivatives of the two coordinate systems. If we define

$$[\Gamma] = [J]^{-1}$$

then we can write:

$$\{\delta'_{xy}\} = \begin{bmatrix} \Gamma & 0 & 0 & 0 \\ 0 & \Gamma & 0 & 0 \\ 0 & 0 & \Gamma & 0 \\ 0 & 0 & 0 & \Gamma \end{bmatrix} \begin{Bmatrix} u_{,\eta} \\ u_{,\xi} \\ v_{,\eta} \\ \vdots \\ \phi_{y,\xi} \end{Bmatrix} = [II] \{\delta'_{\eta\xi}\} \quad (2.30)$$

$$\{\tilde{\delta}'_{xy}\} = \begin{bmatrix} I & 0 \\ 0 & \Gamma \end{bmatrix} \begin{Bmatrix} \phi_x \\ \phi_y \\ w_{,\eta} \\ w_{,\xi} \end{Bmatrix} = [\tilde{II}] \{\tilde{\delta}'_{\eta\xi}\} \quad (2.31)$$

where I used in $[\tilde{II}]$ is the identity matrix. The final step is to now represent $\{\delta'_{\eta\xi}\}$ and $\{\tilde{\delta}'_{\eta\xi}\}$ in terms of the forty nodal degrees of freedom. First, we establish the order of the nodal degrees of freedom (eight sets of the five displacements) to be

$$\{\Delta\} = \begin{Bmatrix} (u_o)_1 \\ (v_o)_1 \\ (w_o)_1 \\ (\phi_x)_1 \\ (\phi_y)_1 \\ \vdots \\ (\phi_y)_8 \end{Bmatrix} \quad (2.32)$$

so that through the use of the shape functions we can represent

$$\{\delta'_{\eta\xi}\} = \begin{bmatrix} N_{1,\eta} & 0 & 0 & 0 & 0 & N_{2,\eta} & 0 & \dots & 0 \\ N_{1,\xi} & 0 & 0 & 0 & 0 & N_{2,\xi} & 0 & \dots & 0 \\ 0 & N_{1,\eta} & 0 & 0 & 0 & 0 & N_{2,\eta} & \dots & 0 \\ 0 & N_{1,\xi} & 0 & 0 & 0 & 0 & N_{2,\xi} & \dots & 0 \\ \vdots & & & & \ddots & & & & \vdots \\ \vdots & & & & & & & \ddots & \vdots \\ 0 & 0 & 0 & 0 & N_{1,\xi} & \dots & \dots & \dots & N_{8,\xi} \end{bmatrix} \begin{Bmatrix} \Delta \end{Bmatrix}$$

$$= [III] \{\Delta\} \quad (2.33)$$

$$\begin{aligned} \left\{ \tilde{\delta}'_{\eta\xi} \right\} &= \begin{bmatrix} 0 & 0 & 0 & N_1 & 0 & 0 & 0 & 0 & N_2 & \cdots & 0 \\ 0 & 0 & 0 & 0 & N_1 & 0 & 0 & 0 & 0 & \cdots & 0 \\ 0 & 0 & N_{1,\eta} & 0 & 0 & 0 & 0 & N_{2,\eta} & 0 & \cdots & 0 \\ 0 & 0 & N_{1,\xi} & 0 & 0 & 0 & 0 & N_{2,\xi} & 0 & \cdots & 0 \end{bmatrix} \left\{ \Delta \right\} \\ &= [I\bar{I}I] \{\Delta\} \end{aligned} \quad (2.34)$$

So now we have in total

$$\begin{Bmatrix} \epsilon_o \\ \kappa \end{Bmatrix} = [I][II][III] \{\Delta\} = [\beta] \{\Delta\} \quad (2.35)$$

$$\{\vartheta\} = [\bar{I}][\bar{I}I][I\bar{I}I] \{\Delta\} = [\bar{\beta}] \{\Delta\} \quad (2.36)$$

Substituting these into eqns (2.26)-(2.28), the equations for the internal forces and moments we get:

$$\begin{Bmatrix} N \\ M \end{Bmatrix} = \begin{bmatrix} A & B \\ B & D \end{bmatrix} [\beta] \{\Delta\} \quad (2.37)$$

$$\{Q\} = [\bar{A}] [\bar{\beta}] \{\Delta\} \quad (2.38)$$

With these representations, the expression for total strain energy can now be expressed as

$$U_{se} = \frac{1}{2} \int_A \left(\{\Delta\}^T [\beta]^T \begin{bmatrix} A & B \\ B & D \end{bmatrix}^T [\beta] \{\Delta\} + \{\Delta\}^T [\bar{\beta}]^T [\bar{A}]^T [\bar{\beta}] \{\Delta\} \right) dA \quad (2.39)$$

2.3.3 Kinetic energy development

The mass matrix for the dynamic analysis of the composite plate comes from the expression for the kinetic energy of the plate given in eqn (2.23) . The time derivatives of the displacements in eqns (1.2)-(1.4) become

$$\begin{aligned}\dot{u} &= \dot{u}_o + z\dot{\phi}_x \\ \dot{v} &= \dot{v}_o + z\dot{\phi}_y \\ \dot{w} &= \dot{w}_o\end{aligned}\quad (2.40)$$

Substituting these expressions into eqn (2.23) gives

$$U_{ke} = \frac{1}{2} \int_V \rho \left[\dot{u}_o^2 + \dot{v}_o^2 + 2z (\dot{u}_o \dot{\phi}_x + \dot{v}_o \dot{\phi}_y) + \dot{w}_o^2 + z^2 (\dot{\phi}_x^2 + \dot{\phi}_y^2) \right] dV \quad (2.41)$$

If the displacement functions are assumed to be harmonic functions of time, each one can be assumed to be premultiplied by $e^{i\omega t}$. With this, the time derivatives can be written as the displacements themselves multiplied by $i\omega$. To aid in the development of the mass matrix we define the following expressions:

$$\begin{Bmatrix} \dot{u}_o \\ \dot{v}_o \\ \dot{w}_o \\ 0 \\ 0 \end{Bmatrix} = i\omega \begin{bmatrix} 1 & 0 & 0 & 0 & 0 \\ 0 & 1 & 0 & 0 & 0 \\ 0 & 0 & 1 & 0 & 0 \\ 0 & 0 & 0 & 0 & 0 \\ 0 & 0 & 0 & 0 & 0 \end{bmatrix} \{\delta\} = i\omega [I_1] \{\delta\} \quad (2.42)$$

$$\begin{Bmatrix} 0 \\ 0 \\ 0 \\ \dot{\phi}_x \\ \dot{\phi}_y \end{Bmatrix} = i\omega \begin{bmatrix} 0 & 0 & 0 & 0 & 0 \\ 0 & 0 & 0 & 0 & 0 \\ 0 & 0 & 0 & 0 & 0 \\ 0 & 0 & 0 & 1 & 0 \\ 0 & 0 & 0 & 0 & 1 \end{bmatrix} \{\delta\} = i\omega [I_2] \{\delta\} \quad (2.43)$$

$$\begin{pmatrix} \dot{\phi}_x \\ \dot{\phi}_y \\ 0 \\ \dot{u}_o \\ \dot{v}_o \end{pmatrix} = i\omega \begin{bmatrix} 0 & 0 & 0 & 1 & 0 \\ 0 & 0 & 0 & 0 & 1 \\ 0 & 0 & 0 & 0 & 0 \\ 1 & 0 & 0 & 0 & 0 \\ 0 & 1 & 0 & 0 & 0 \end{bmatrix} \{\delta\} = i\omega [I_3] \{\delta\} \quad (2.44)$$

$$\begin{pmatrix} \dot{u}_o \\ \dot{v}_o \\ 0 \\ \dot{\phi}_x \\ \dot{\phi}_y \end{pmatrix} = i\omega \begin{bmatrix} 1 & 0 & 0 & 0 & 0 \\ 0 & 1 & 0 & 0 & 0 \\ 0 & 0 & 0 & 0 & 0 \\ 0 & 0 & 0 & 1 & 0 \\ 0 & 0 & 0 & 0 & 1 \end{bmatrix} \{\delta\} = i\omega [I_4] \{\delta\} \quad (2.45)$$

Now, with these equations defined, we can write eqn (2.41) as

$$U_{ke} = -\frac{1}{2}\omega^2 \int_V \rho \left(\{\delta\}^T [I_1]^T [I_1] \{\delta\} + z^2 \{\delta\}^T [I_2]^T [I_2] \{\delta\} + z \{\delta\}^T [I_3]^T [I_4] \{\delta\} \right) dV \quad (2.46)$$

which simplifies to, (due to the nature of the matrices),

$$U_{ke} = -\frac{1}{2}\omega^2 \int_V \rho \left(\{\delta\}^T [I_1] \{\delta\} + z^2 \{\delta\}^T [I_2] \{\delta\} + z \{\delta\}^T [I_3] \{\delta\} \right) dV \quad (2.47)$$

In this equation, only ρ and z vary through the thickness, so as before, we can easily perform the integration in the z direction, and reduce it down to an area integral. The result is

$$U_{ke} = -\frac{1}{2}\omega^2 \int_A \left(P \{\delta\}^T [I_1] \{\delta\} + I \{\delta\}^T [I_2] \{\delta\} + R \{\delta\}^T [I_3] \{\delta\} \right) dV \quad (2.48)$$

where

$$P = \int_{-h/2}^{h/2} \rho dz = \sum_{k=1}^n \rho_k \cdot t_k \quad (2.49)$$

$$R = \int_{-h/2}^{h/2} \rho_k z \cdot dz = \sum_{k=1}^n \rho_k \cdot t_k \cdot z_k \quad (2.50)$$

$$I = \int_{-h/2}^{h/2} \rho_k z^2 \cdot dz = \sum_{k=1}^n \rho_k \left(t_k \cdot z_k^2 + \frac{t_k^3}{12} \right) \quad (2.51)$$

The final form for U_{ke} follows after writing $\{\delta\}$ in terms of $\{\Delta\}$ and the shape functions.

We have

$$\begin{aligned} \{\delta\} &= \begin{bmatrix} N_1 & 0 & 0 & 0 & 0 & N_2 & 0 & 0 & \cdots & 0 \\ 0 & N_1 & 0 & 0 & 0 & 0 & N_2 & 0 & \cdots & 0 \\ 0 & 0 & N_1 & 0 & 0 & 0 & 0 & N_2 & \cdots & 0 \\ 0 & 0 & 0 & N_1 & 0 & 0 & 0 & 0 & \cdots & 0 \\ 0 & 0 & 0 & 0 & N_1 & 0 & 0 & 0 & \cdots & N_8 \end{bmatrix} \{\Delta\} \\ &= [N] \{\Delta\} \end{aligned} \quad (2.52)$$

Now we can write our final form of U_{ke} as

$$\begin{aligned} U_{ke} &= -\frac{1}{2} \omega^2 \int_A \left(\{\Delta\}^T [N]^T \begin{bmatrix} P & 0 \\ 0 & I \end{bmatrix} [N] \{\Delta\} \right. \\ &\quad \left. + \{\Delta\}^T [N]^T \begin{bmatrix} 0 & R \\ R & 0 \end{bmatrix} [N] \{\Delta\} \right) dA \end{aligned} \quad (2.53)$$

where $P[I_1]$ and $I[I_2]$ have been combined into one matrix. With this equation, along with eqn (2.39), we have what is needed to minimize the energy functional and get an expression for the stiffness and mass matrices.

2.3.4 Element stiffness and mass matrices

In the last two sections we developed expressions for both the strain energy, eqn (2.39) , and kinetic energy, eqn (2.53) , for a general composite laminate. Substituting these two

equations into eqn (2.24) , the expression for total energy, results in

$$\begin{aligned} \Pi = & \frac{1}{2} \int_A \left(\{\Delta\}^T [\beta]^T \begin{bmatrix} A & B \\ B & D \end{bmatrix}^T [\beta] \{\Delta\} + \{\Delta\}^T [\tilde{\beta}]^T [\tilde{A}]^T [\tilde{\beta}] \{\Delta\} \right) dA \\ & - \frac{1}{2} \omega^2 \int_A \left(\{\Delta\}^T [N]^T \begin{bmatrix} P & 0 \\ 0 & I \end{bmatrix} [N] \{\Delta\} \right. \\ & \left. + \{\Delta\}^T [N]^T \begin{bmatrix} 0 & R \\ R & 0 \end{bmatrix} [N] \{\Delta\} \right) dA \end{aligned} \quad (2.54)$$

If we extremize this equation with respect to the nodal degrees of freedom, the result is

$$\begin{aligned} & \int_A \left([\beta]^T \begin{bmatrix} A & B \\ B & D \end{bmatrix}^T [\beta] + [\tilde{\beta}]^T [\tilde{A}]^T [\tilde{\beta}] \right) \{\Delta\} dA \\ & - \omega^2 \int_A \left([N]^T \begin{bmatrix} P & 0 \\ 0 & I \end{bmatrix} [N] \right. \\ & \left. + [N]^T \begin{bmatrix} 0 & R \\ R & 0 \end{bmatrix} [N] \right) \{\Delta\} dA = 0 \end{aligned} \quad (2.55)$$

This equation is of the form

$$([k] - \omega^2 [m]) \{\Delta\} = 0 \quad (2.56)$$

giving us our eigenvalue problem to solve for the natural frequencies and mode shapes of our problem. From eqn (2.55) the elemental stiffness matrix is

$$[k] = \int_A \left([\beta]^T \begin{bmatrix} A & B \\ B & D \end{bmatrix}^T [\beta] + [\tilde{\beta}]^T [\tilde{A}]^T [\tilde{\beta}] \right) dA \quad (2.57)$$

and the elemental mass matrix is

$$[m] = \int_A \left([N]^T \begin{bmatrix} P & 0 \\ 0 & I \end{bmatrix} [N] + [N]^T \begin{bmatrix} 0 & R \\ R & 0 \end{bmatrix} [N] \right) dA \quad (2.58)$$

At this point it is important to remember that the integration must be done in the η - ξ coordinate system since the displacements have been represented in terms of the shape functions. Thus, the differential area element becomes:

$$dA = \|J\| d\eta d\xi$$

2.4 Analysis Method

2.4.1 Global matrix development

In Section 2.3.4 we developed expressions for the elemental stiffness and mass matrices for a laminated composite plate which was based upon an eight noded isoparametric element. The expressions, given by eqn (2.57) and eqn (2.58), are the basis for developing the global system of equations in the finite element problem.

The process of building global stiffness and mass matrices follows the standard procedure of discretizing the domain in question to establish an elemental mesh. The elements and nodes are numbered, and the integration of eqn (2.57) and eqn (2.58) is performed over each element. Thus, we build the element's stiffness and mass matrices. The results for each element are then assembled into a global mass and stiffness matrix resulting in a matrix equation of the form:

$$\left([K] - \omega^2 [M] \right) \{ \Delta \} = 0. \quad (2.59)$$

In carrying out the integration of eqn (2.57) and eqn (2.58) one can easily employ the Gauss quadrature technique. Unfortunately, the number of integration points used for the

different terms in the equations varies. For example, in eqn (2.58) the integrand contains the squares of the shape functions given in eqn (2.21). The result is an expression with terms on the order of η^4 and ξ^4 . Thus, to get an accurate integration of the mass and inertia terms, a three by three point Gaussian integration must be performed. Unfortunately, eqn (2.57) presents another case. The first terms, which represent the bending stiffnesses, are on the order of η^2 and ξ^2 , so can be integrated with a two by two scheme. The next expression contains the shear stiffness terms which are on the order of η^4 and ξ^4 , as well as η^2 and ξ^2 . The fourth order terms result from the fact that the transverse shear contains ϕ_x and ϕ_y and not their derivatives. However, despite the higher order of the shear stiffness terms, it is often recommended that a one point integration scheme be used to give the best results when solving eqn (2.59) for the natural frequencies. This need for under integration follows from the presence of the shear locking phenomenon as described in the text by Hughes [36]. When the shear terms are integrated with a lower order than the bending terms, it is referred to as *reduced selective integration*. In the present analysis of thick plates it was found that there was no need to selectively integrate the shear terms over the bending terms. The final analysis discussed in the results section was done with a two point integration on the bending terms and a three point integration on both the mass and shear stiffness terms.

The last step in developing the final form of the global stiffness and mass matrices is the elimination of the fixed degrees of freedom to implement the boundary conditions. For each fixed degree of freedom, the corresponding row and column are eliminated from $[K]$ and $[M]$. With this performed, eqn (2.59) is ready to be solved.

2.4.2 Solution to the eigenvalue problem

In the last section we discussed the integration of eqn (2.57) and eqn (2.58) to establish the global matrix equation, (eqn (2.59)). The eigenvalues and eigenvectors of this equation

provide the natural frequencies and mode shapes of the modeled plate. They are found computationally using an appropriate linear algebra technique. For this task, the present investigation utilized the IMSL-10 scientific package which is readily available on the CYBER 990 computer. The IMSL-10 package has a routine which solves the general eigenvalue problem for the case when $[M]$ is positive definite, as we have for this problem. The routine is efficient and returns all of the desired eigenvalues and their corresponding eigenvectors. The eigenvalues are ordered from lowest to highest, but, if under integration is being used for the transverse shear terms, care must be taken in choosing the first fundamental frequency. In investigating the effects of under integrating these terms, one finds that it causes both kinematic and zero energy deformation modes to be present in the solution. Thus, all zero (or near zero) frequencies need to be overlooked, as well as any whose deformation carries a zero energy deformation mode in any of its elements. The zero energy deformation modes can easily be spotted by looking at the mode shapes for the frequency in question.

2.4.3 Updated natural frequency calculation

As stated in Section 1.6, the purpose of this study is to develop a technique to accurately calculate the shear correction coefficients so that we can perform an accurate vibration analysis of a composite structure. Having accurate values of the shear correction coefficients allows us to account for the appropriate transverse shear contribution in our strain energy expressions, and thus we can receive accurate results. The first order shear deformation theory establishes a constant value of transverse shear strain through the thickness of the plate. In reality, it is well known that this is not the case. In an isotropic, rectangular cross-section beam or plate, the exact elasticity solution establishes a parabolic distribution. These two strain distributions result in different transverse strain energy density distributions, which can then be used to calculate the shear correction factors.

This is exactly the technique which will be used in this analysis, not through an exact method, but by an approximate numerical method. We will calculate the strain energy per unit area of the plate based on the first order theory and compare it to the strain energy calculated using another more accurate technique. Both methods will use the preliminary mode shape and natural frequency obtained using the finite element analysis. The values received for the shear correction coefficients should primarily be functions only of the plate geometry and lay-up. It should not be a function of the deformation or location in the plate. The coefficients should be a constant for a given plate, but k_x can be different from k_y due to inherent differences in the material properties for the two directions.

The transverse strain energy per unit area can be accurately calculated if one knows the transverse stress distributions through the thickness of the plate, along with the plate's constitutive properties. In this analysis the transverse stress distribution through the thickness of the plate will be calculated by integrating the equations of equilibrium with respect to the out-of-plane direction. Since the in-plane stresses are accurately calculated using the first order analysis, we can expect to get reasonable results for the transverse stresses. Thus, with this approach we can find accurate values for the shear correction coefficients and ultimately the natural frequencies and mode shapes.

2.4.4 The equations of equilibrium

The equations of equilibrium for three dimensional elasticity are given by:

$$\begin{aligned}\sigma_{xx,x} + \sigma_{xy,y} + \sigma_{xz,z} + f_x &= \rho\ddot{u} \\ \sigma_{xy,x} + \sigma_{yy,y} + \sigma_{yz,z} + f_y &= \rho\ddot{v} \\ \sigma_{zx,x} + \sigma_{zy,y} + \sigma_{zz,z} + f_z &= \rho\ddot{w}\end{aligned}\tag{2.60}$$

where f_i are any body forces present. The first two terms, along with the fourth term on the left hand sides can be brought over to the right and these forms then integrated with

respect to z . The results are:

$$\begin{aligned}\sigma_{xz}(z) &= \int_{-h/2}^z (\rho\ddot{u} - \sigma_{xx,x} - \sigma_{xy,y} - f_x) dz \\ \sigma_{yz}(z) &= \int_{-h/2}^z (\rho\ddot{v} - \sigma_{xy,x} - \sigma_{yy,y} - f_y) dz \\ \sigma_{zz}(z) &= \int_{-h/2}^z (\rho\ddot{w} - \sigma_{zx,x} - \sigma_{zy,y} - f_z) dz\end{aligned}\tag{2.61}$$

The first two of these equations provide us with a method to calculate the transverse stresses σ_{xz} and σ_{yz} . Once this is done, the third provides us with an expression for σ_{zz} , if so desired. Obviously to perform the integration through the thickness of the plate we must first find the in-plane stresses and then their derivatives.

2.4.5 In-plane stress calculations

Once we have found the first eigenvalue and eigenvector of eqn (2.59), we know all of the nodal displacements of the plate model within a constant. This constant will prove to be inconsequential later, as we will be interested only in ratios of the strain energy densities. The stresses within the plate can be found from the displacements through eqns (1.7)-(1.12) and eqn (2.4). Once these are known at various locations, the derivatives follow.

From a computational point of view, the stresses can be calculated at a point within an element based upon the element's nodal displacements. The usual procedure is to perform the differentiation of the displacements by differentiating the shape function representation of the displacements and scaling them to the global coordinates through the Jacobian. The location of the most accurate stress calculations can be shown to be at the Gauss integration points. Once the stresses are known at the Gauss points, their derivatives can be found in a similar manner. In Section 2.3.1 we briefly discussed a drawback to

the quadratic element chosen for this analysis, and it is now clear that the problem will be in calculating accurate derivatives of the stress within an element. The displacements within an element will, at best, be quadratic and after differentiation will provide us with linear stresses (in certain directions). The required additional differentiation leaves us with constant stress derivatives, and hence, constant strain energy per unit area throughout the element (again in certain directions). As a result, we will have a mismatch when we compare this strain energy to the strain energy calculated using the first order theory, which results in a higher order function. To alleviate this problem, a technique has been developed to globally smooth the nodal displacements to a higher order polynomial. When the new displacements are used in conjunction with higher order shape functions, the end result is a higher order variation of transverse strain energy within the element. We will find that this linear variation will be sufficient in calculating the new shear correction coefficients.

The method is begun by considering each element individually. Using a cubic least squares curve fit routine, we calculate the four polynomial coefficients for w , ϕ_x and ϕ_y on each side of the element. In other words, we end up with the coefficient data for twelve curves for each element. The curve fitting is done utilizing five points per side. We use the original three data points plus two additional ones. If the element is an interior element, a data point from either side is taken. If it is a boundary element, two points from the adjacent interior element are used. After this is completed, the next step is to temporarily *transform* our eight noded element into a twelve noded one, as depicted in Figure 2.3. The shape functions associated with this element are established as:

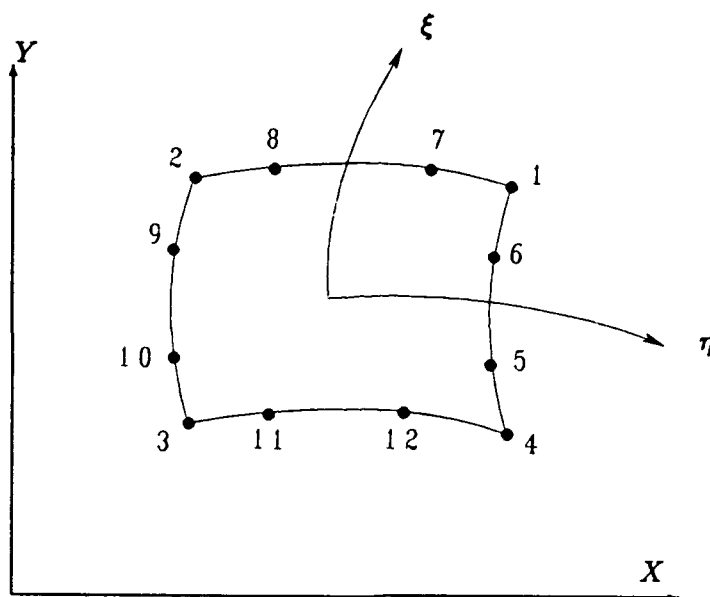


Figure 2.3: Twelve Noded Isoparametric Element

$$\begin{aligned}
 N_i &= \frac{1}{32} (1 + \xi\xi_i) (1 + \eta\eta_i) (9\xi^2 + 9\eta^2 - 10) & i = 1, 2, 3, 4 \\
 N_i &= \frac{9}{32} (1 + \xi\xi_i) (1 + 9\eta\eta_i) (1 - \eta^2) & i = 7, 8, 11, 12 \\
 N_i &= \frac{9}{32} (1 + 9\xi\xi_i) (1 + \eta\eta_i) (1 - \xi^2) & i = 5, 6, 9, 10
 \end{aligned} \tag{2.62}$$

Next, we proceed to build an element displacement vector, $\{\Delta\}_c$, consisting of sixty terms and defined as

$$\{\Delta\}_c = \left\{ \begin{array}{l} (u_o)_1 \\ (v_o)_1 \\ (w_o)_1 \\ (\phi_x)_1 \\ (\phi_y)_1 \\ \vdots \\ (\phi_y)_{12} \end{array} \right\}_c \tag{2.63}$$

Note that the c subscript distinguishes this displacement vector from the original one defined in eqn (2.32). In building $\{\Delta\}_c$, the original displacements are retained for the

corner nodes, and the values for the side nodes are calculated using the polynomial curve fits. In this manner, the displacements which originally varied quadratically, now vary cubically.

Next, the stresses are calculated at the twelve nodes. We start by finding the strains from the derivatives of displacements at each node by establishing

$$\begin{Bmatrix} \epsilon_o \\ \kappa \end{Bmatrix} = [\beta^*] \{\Delta\}_c \quad (2.64)$$

where $[\beta^*]$ is defined exactly as $[\beta]$ was defined in eqns (2.28)-(2.35) with the exception that $[III]$ is expanded out to include the extra four shape functions. It is important to remember that eqn (2.64) provides the midplane strains and curvatures at a specific point in the element. The three in-plane strains at this point can be represented as a function of z by

$$\begin{Bmatrix} \epsilon_x \\ \epsilon_y \\ \gamma_{xy} \end{Bmatrix} = \begin{bmatrix} 1 & 0 & 0 & z & 0 & 0 \\ 0 & 1 & 0 & 0 & z & 0 \\ 0 & 0 & 1 & 0 & 0 & z \end{bmatrix} [\beta^*] \{\Delta\}_c$$

$$= [Z] [\beta^*] \{\Delta\}_c \quad (2.65)$$

The stresses at this specific point in the plate's thickness become

$$\begin{Bmatrix} \sigma_{xx} \\ \sigma_{yy} \\ \sigma_{xy} \end{Bmatrix} = [Q]_k [Z] [\beta^*] \{\Delta\}_c \quad (2.66)$$

where $[Q]_k$ represents the $[Q]$, as defined in eqn (2.9), for the k th layer of the laminate, and z falls in this layer. Thus, eqn (2.66) allows us to calculate the stress at a specific

η, ξ, z location in the element. This is the first necessary step in calculating the derivatives of the stresses in the element.

2.4.6 Derivatives of stresses

In Section 2.4.4 we established that in order to calculate the transverse stresses, and ultimately the transverse strain energy in the laminated plate, we needed to calculate the derivatives of the in-plane stresses with respect to the in-plane directions. Above, in Section 2.4.5, we established a method to calculate the in-plane stresses at any location within the element using eqn (2.66). This equation will become the basis for the next calculations.

We start by choosing a convenient set of points at which to determine our desired parameters. Through experimentation and ease of computational implementation, it was found best to use eight interior points coinciding to the Gauss integration points for a three by three integration, (the center point is discarded). The stresses, as given by eqn (2.66), are calculated as a function of z at each of these eight interior points. The result is established in matrix notation as:

$$\left\{ \begin{array}{c} (\sigma)_1 \\ (\sigma)_2 \\ \vdots \\ (\sigma)_8 \end{array} \right\} = \left\{ \begin{array}{c} \left\{ \begin{array}{c} \sigma_{xx} \\ \sigma_{yy} \\ \sigma_{xy} \end{array} \right\}_1 \\ \vdots \\ \left\{ \begin{array}{c} \sigma_{xx} \\ \sigma_{yy} \\ \sigma_{xy} \end{array} \right\}_8 \end{array} \right\} \quad (2.67)$$

Turning our attention now to the derivatives of the stresses, we establish only the terms needed and write them as

$$\begin{Bmatrix} \sigma_{xx,x} \\ \sigma_{yy,y} \\ \sigma_{xy,x} \\ \sigma_{xy,y} \end{Bmatrix} = \begin{bmatrix} \Gamma_{11} & \Gamma_{12} & 0 & 0 & 0 & 0 \\ 0 & 0 & \Gamma_{21} & \Gamma_{22} & 0 & 0 \\ 0 & 0 & 0 & 0 & \Gamma_{11} & \Gamma_{12} \\ 0 & 0 & 0 & 0 & \Gamma_{21} & \Gamma_{22} \end{bmatrix} \begin{Bmatrix} \sigma_{xx,\eta} \\ \sigma_{xx,\xi} \\ \sigma_{yy,\eta} \\ \sigma_{yy,\xi} \\ \sigma_{xy,\eta} \\ \sigma_{xy,\xi} \end{Bmatrix} \quad (2.68)$$

where

$$\begin{bmatrix} \Gamma_{11} & \Gamma_{12} \\ \Gamma_{21} & \Gamma_{22} \end{bmatrix} = [J]^{-1} \quad (2.69)$$

The column matrix on the right hand side of eqn (2.68) can now be established through eqn (2.67) and the derivatives of eqn (2.62). The result is

$$\begin{Bmatrix} \sigma_{xx,\eta} \\ \sigma_{xx,\xi} \\ \sigma_{yy,\eta} \\ \sigma_{yy,\xi} \\ \sigma_{xy,\eta} \\ \sigma_{xy,\xi} \end{Bmatrix} = \begin{bmatrix} N_{1,\eta} & 0 & 0 & N_{2,\eta} & 0 & 0 & \cdots & 0 \\ N_{1,\xi} & 0 & 0 & N_{2,\xi} & 0 & 0 & \cdots & 0 \\ 0 & N_{1,\eta} & 0 & 0 & N_{2,\eta} & 0 & \cdots & 0 \\ 0 & N_{1,\xi} & 0 & 0 & N_{2,\xi} & 0 & \cdots & 0 \\ 0 & 0 & N_{1,\eta} & 0 & 0 & N_{2,\eta} & \cdots & N_{8,\eta} \\ 0 & 0 & N_{1,\xi} & 0 & 0 & N_{2,\xi} & \cdots & N_{8,\xi} \end{bmatrix} \begin{Bmatrix} (\sigma)_1 \\ (\sigma)_2 \\ \vdots \\ (\sigma)_8 \end{Bmatrix} \quad (2.70)$$

We can combine eqn (2.68) and eqn (2.70) to get an expression for the derivatives of stresses at any η, ξ as a function of z . The result is:

$$\begin{Bmatrix} \sigma_{xx,x} \\ \sigma_{yy,y} \\ \sigma_{xy,x} \\ \sigma_{xy,y} \end{Bmatrix} = [G][N] \begin{Bmatrix} (\sigma)_1 \\ (\sigma)_2 \\ \vdots \\ (\sigma)_8 \end{Bmatrix} \quad (2.71)$$

where the rectangular matrices in eqn (2.68) and eqn (2.70) have been represented by $[G]$ and $[N]$ respectively.

Body force or dynamic terms

The representation of the body forces, or the dynamic terms, is the final item required before the integration of eqn (2.61) can be performed. For the case of free vibration, the inertia terms of the plate can be treated either way with no difference, as the sign difference drops out. Recalling the discussion in Section 2.3.3 we can express the required acceleration terms as:

$$\begin{aligned}\ddot{u} &= -\omega^2 (u_o + z\phi_x) \\ \ddot{v} &= -\omega^2 (v_o + z\phi_y) \\ \ddot{w} &= -\omega^2 w_o\end{aligned}\tag{2.72}$$

These equations are the final expressions we need to calculate the transverse stress distributions.

Putting it all together

Equation 2.71 and eqn (2.72) provide the appropriate expressions to place into eqn (2.61) so that the integration can be accomplished. The integration can be performed numerically using a trapezoidal rule, or other simple integration method, starting at $z = -h/2$ with σ_{xz} and σ_{yz} equal to zero, or to whatever surface tractions exist. The final values of σ_{xz} and σ_{yz} at $z = h/2$ should correspond to the tractions on the top surface of the plate, which are zero for the free vibration case. The end results of the calculations are the determinations of the transverse shear distributions through the thickness of the plate at some specific η, ξ location.

2.4.7 Shear correction coefficient calculations

First order strain energy calculations

The transverse strain energy densities calculated using the first order theory are U_{xz} and U_{yz} . They are defined by

$$U_{xz} = \frac{1}{2} C_{xz} \gamma_{xz}^2 \quad (2.73)$$

$$U_{yz} = \frac{1}{2} C_{yz} \gamma_{yz}^2 \quad (2.74)$$

where

$$C_{xz} = \int_{-h/2}^{h/2} \bar{C}_{44} dz$$

$$C_{yz} = \int_{-h/2}^{h/2} \bar{C}_{55} dz$$

and γ_{xz} and γ_{yz} are given in eqns (1.10)-(1.11).

Improved strain energy calculations

As discussed earlier, through the use of the accurate in-plane stresses and the equilibrium equations, we can calculate a more accurate representation of the transverse strain energies. The transverse stress distributions, as functions of z , are found by substituting eqn (2.71) and eqn (2.72) into eqn (2.61). The result of this provides us with through-the-thickness distributions of both σ_{xz} and σ_{yz} . The transverse strain energies due to these stresses are defined as:

$$\bar{U}_{xz} = \frac{1}{2} \int_{-h/2}^{h/2} \bar{C}_{44} (\bar{\gamma}_{xz}^2) dz \quad (2.75)$$

$$\bar{U}_{yz} = \frac{1}{2} \int_{-h/2}^{h/2} \bar{C}_{55} (\bar{\gamma}_{yz}^2) dz \quad (2.76)$$

where

$$\bar{\gamma}_{xz} = S_{44}\sigma_{xz} + S_{45}\sigma_{yz}$$

$$\bar{\gamma}_{yz} = S_{54}\sigma_{xz} + S_{55}\sigma_{yz}$$

Here

$$\begin{bmatrix} S_{44} & S_{45} \\ S_{54} & S_{55} \end{bmatrix} = \begin{bmatrix} \bar{Q}_{44} & \bar{Q}_{45} \\ \bar{Q}_{54} & \bar{Q}_{55} \end{bmatrix}^{-1} \quad (2.77)$$

Transverse strain energy comparisons

In the previous two sections we have developed expressions for the transverse strain energy using the results from a first order theory (eqns (2.73)-(2.74)) and by integrating the equations of equilibrium through the thickness of the plate (eqns (2.75)-(2.76)). By comparing the results of the two different methods we can obtain a new shear correction factor with which an updated natural frequency can be calculated. If we let k_x^o and k_y^o be the original shear correction coefficients, then

$$(k_i)^2 \bar{U}_{iz} = (k_i^o)^2 U_{iz} \quad (2.78)$$

should hold true, and hence new shear correction coefficients can be found.

CHAPTER III

LEAST SQUARES ELEMENT DEVELOPMENT: C^1 CONTINUITY APPROXIMATION THROUGH A LEAST SQUARES METHOD

3.1 Background Information

As discussed in Section 1.3, one approach to improving laminated plate theory is to assume a displacement field with higher order terms in the z coordinate. For example, a typical form often seen (see eqns (1.15)) assumes u and v cubic in z and w quadratic. Rewriting the displacement field here for convenience, we have:

$$\begin{aligned}u &= u_o + z\phi_x + z^2\psi_x + z^3\zeta_x \\v &= v_o + z\phi_y + z^2\psi_y + z^3\zeta_y \\w &= w_o + z\phi_z + z^2\psi_z\end{aligned}\tag{3.1}$$

The motivation behind cubic functions for u and v stems from the fact that transverse shear should at least be quadratic in z . This allows the top and bottom surfaces to be free from tractions, if conditions warrant this. The expression for w is generally simplified by dropping the terms involving z , thus making w a constant. This displacement field has been shown to be an improvement over the first order theory, mainly for the reason of producing acceptable results without the use of shear correction factors. The disadvantage is that the displacement field is now an eleven parameter field as shown above, or assuming

w as a constant, a nine parameter field. When compared to the five parameter first order theory, this difference represents a significant increase in the number of unknown functions in the problem. The nine parameter field can easily be simplified, as has been done beginning in 1984 by Reddy [113], by setting the transverse stress to zero on the top and bottom surfaces of the plate. These four conditions are used to eliminate the variables ψ_x, ψ_y, ζ_x and ζ_y from the u and v displacements. The end result is:

$$\begin{aligned} u &= u_o + z \left[\phi_x - \frac{4z^2}{3h^2} (\phi_x + w_{o,x}) \right] \\ v &= v_o + z \left[\phi_y - \frac{4z^2}{3h^2} (\phi_y + w_{o,y}) \right] \end{aligned} \quad (3.2)$$

$$w = w_o$$

This field is readily seen to now have five unknowns, which is the same number as the first order theory. This displacement field provides very good results when applied to laminated plates and is considered an improvement over the first order theory. It performs well without shear correction coefficients and provides improved in-plane responses, and hence, can be used to provide better out-of-plane results following the method outlined in Section 2.4.7. This improvement does not come without cost, however. Even though the number of unknown functions is the same as in the first order theory, the finite element formulation of this field is hampered by the form of eqns (3.2), which include derivatives of w in the u and v displacements. In other words, the terms $w_{,x}$ and $w_{,y}$, found in the expressions for u and v , make the problem not one of C^0 continuity, as it was for the first order and higher order theories, but make it now one requiring C^1 continuity for w . This requirement is the reason that the displacement field in eqns (3.2) is not

widely used. The C^1 continuity problem has long plagued finite element developers and is usually avoided if at all possible. In fact, one of the biggest advantages of the five parameter Mindlin style displacement field was that it changed the plate bending problem from one of C^1 continuity found in the Kirchhoff theory, to one of C^0 continuity. The standard isoparametric shape functions, given in eqn (2.21), insure that the degrees of freedom are continuous from element to element but do nothing to maintain continuity in the derivatives of the functions. In most analysis this fact only becomes significant when differentials of the degrees of freedom are used, for instance, as required in stress calculations. The stresses are discontinuous between elements because of the discontinuity in the shape function differentials from element to element. In the case of eqns (3.8), the discontinuity of $w_{,x}$ and $w_{,y}$ immediately cause discontinuities in u and v . Thus, the global displacement field contains gaps, violating one of the requirements for convergence¹. The result is a formulation which is generally too soft and has poor convergence qualities. In fact, a displacement field of the form given in eqn (3.2) was implemented into a C^0 element formulation during this course of study with very poor results.

Successful use of eqns (3.2) in a finite element formulation has been demonstrated by Reddy and Phan (1985) [105], but formulations of this type are by no means common. The problem was solved by utilizing Hermite polynomials for the element shape functions which satisfy the C^1 continuity requirement. However, the practicability of Hermitian polynomials is questionable based upon the lack of published work utilizing them. In fact, most finite element text books have little or no reference to them. See Zienkiewicz [146], Bathe [9] and Cook [23]. In the book by Zienkiewicz, he states that elements using Hermitian interpolation functions have little engineering applicability.

In the past, researchers have proposed several other methods to solve the C^1 continuity

¹It can be shown that convergence can still be achieved if gaps go to zero in the limit

problem. One common method discussed by Zienkiewicz has been the use of non-conformal elements, which allow gaps, but satisfy convergence. This method has been used with some success in other problems, but it immediately restricts the elements to being straight sided rectangles. Another possible solution includes the use of conforming triangular elements as developed by Anderheggen (1970) [4] and Irons (1969) [37]. These have been demonstrated for thin plates.

All of the above mentioned techniques to solve the C^1 continuity problem generally are not without their drawbacks. It is the intent of this research to present a simple, unique and computationally effective method to approximate a C^1 continuous element which produces accurate results for laminated composite plates. In the next several sections, the new Least Squares element will be developed in detail and will approximate C^1 continuity with very little increase in complexity over traditional finite element techniques. We will show that fields of the form of eqns (3.2) can be used easily with very good results.

3.2 Displacement Field Development

3.2.1 Displacement Field Basis

For this work we will develop a displacement field similar to that given in eqns (3.2), but which will be better suited for our needs later in developing a piecewise continuous displacement field. We begin by assuming a symmetric, parabolic, transverse strain field of the form:

$$\gamma_{\alpha z} = \varphi_{\alpha}(a_0 + a_1 z^2), \quad (3.3)$$

where φ_{α} is a transverse shear strain, $\alpha = x, y$ and a_0 and a_1 are constants. If we force the transverse stress (strain) to go to zero at $z = \pm \frac{h}{2}$, we can eliminate the two constants.

The result can be written as:

$$\gamma_{\alpha z} = \varphi_{\alpha} \left(1 - \frac{4z^2}{h^2} \right) \quad (3.4)$$

Next, substituting eqn (3.4) into the strain displacement relations for transverse strain, (see eqns (1.10)-(1.11)), and solving for $u_{\alpha,z}$, we can write:

$$u_{\alpha,z} = \varphi_{\alpha} \left(1 - \frac{4z^2}{h^2} \right) - w_{,\alpha} . \quad (3.5)$$

Integrating this with respect to z yields

$$u_{\alpha} = u_{\alpha o} + \varphi_{\alpha} \left(z - \frac{4z^3}{3h^2} \right) - zw_{,\alpha} . \quad (3.6)$$

The end result is a displacement field of the form:

$$\begin{aligned} u &= u_o + \varphi_x \left(z - \frac{4z^3}{3h^2} \right) - zw_{,x} \\ v &= v_o + \varphi_y \left(z - \frac{4z^3}{3h^2} \right) - zw_{,y} \\ w &= w(x, y) \end{aligned} \quad (3.7)$$

A displacement field of this form was published by Bhimaraddi and Stevens [16] in 1984, but it was presented with no justification or explanation of how or why it was chosen. The displacement field is somewhat similar to that given in eqns (3.2), but instead of a rotation angle, ϕ_{α} , we have a measure of transverse shear strain, φ_{α} .

The field in eqns (3.7) has no immediate advantage over eqns (3.2), as they both require C^1 continuity. In fact, eqns (3.7) are at somewhat of a disadvantage over eqns (3.2) if one intends to compare any results to those of a first order shear deformation analysis because of the differences between ϕ_α and φ_α . The advantage to eqns (3.7) comes into play when it is used as a basis for a simplified piecewise continuous displacement model. The algebra involved in satisfying continuity becomes much simpler. Therefore, throughout this section, eqns (3.7) will be utilized as the displacement field of choice.

3.2.2 The Piecewise Continuous Displacement Field

As discussed earlier in Section 1.4.2, a continuous, smooth function cannot accurately represent the displacements through the thickness of a laminated composite plate. To improve the accuracy of the analysis, we must turn to a piecewise continuous function through the thickness where each layer is modeled with its own smooth function. This allows for slope discontinuities at the layer interfaces. Towards this end, we assume a function of the form given in eqns (3.7), but to begin with, we allow each layer to have its own values for u_o, v_o, φ_x and φ_y . This can be written as:

$$\begin{aligned} u^n &= u_o^n + \varphi_x^n \left(z - \frac{4z^3}{3h^2} \right) - zw_{,x} \\ v^n &= v_o^n + \varphi_y^n \left(z - \frac{4z^3}{3h^2} \right) - zw_{,y} \end{aligned} \quad (3.8)$$

$$w^n = w(x, y)$$

where the superscript n refers to the n th layer of the laminate, and z is a global coordinate running from $-\frac{h}{2}$ to $+\frac{h}{2}$.

The piecewise displacement field presented in eqns (3.8) must be modified to meet

some of the requirements listed in Section 1.4.2, namely transverse traction continuity and displacement continuity at the layer interfaces. Using eqns (3.8), we can calculate the transverse stresses on either side of the layer interfaces and set them equal to one another. In doing so we find out that the values for φ_α^n can all be related to the φ_α of one reference layer. If we choose the bottom layer as the reference layer, we can write:

$$\varphi_x^n = \left(\frac{\bar{C}_{44}^1}{\bar{C}_{44}^n} \right) \varphi_x^1 = \alpha_n \varphi_x^1 \quad (3.9)$$

$$\varphi_y^n = \left(\frac{\bar{C}_{55}^1}{\bar{C}_{55}^n} \right) \varphi_y^1 = \beta_n \varphi_y^1 \quad (3.10)$$

where \bar{C}_{44}^n and \bar{C}_{55}^n are from eqn (2.5) for the n th layer. Similarly, enforcing u and v to be continuous functions across the layer interfaces results in the expressions

$$u_o^n = u_o^1 + \sum_{k=1}^n \left(z_k - \frac{4z_k^3}{3h^2} \right) (\alpha_{k-1} - \alpha_k) \varphi_x^1 \quad (3.11)$$

$$v_o^n = v_o^1 + \sum_{k=1}^n \left(z_k - \frac{4z_k^3}{3h^2} \right) (\beta_{k-1} - \beta_k) \varphi_y^1 \quad (3.12)$$

where the bottom layer is once again the reference layer. With these expressions, eqns (3.8) can be written as:

$$\begin{aligned} u^n &= u_o^1 + \left(\sum_{j=1}^n P_j \right) \varphi_x^1 + \alpha_n \varphi_x^1 \left(z - \frac{4z^3}{3h^2} \right) - zw_{,x} \\ v^n &= v_o^1 + \left(\sum_{j=1}^n \bar{P}_j \right) \varphi_y^1 + \alpha_n \varphi_y^1 \left(z - \frac{4z^3}{3h^2} \right) - zw_{,y} \end{aligned} \quad (3.13)$$

$$w^n = w(x, y)$$

where

$$P_j = \left(z_j - 4z_j^3/3h^2 \right) (\alpha_{j-1} - \alpha_j)$$

$$\bar{P}_j = \left(z_j - 4z_j^3/3h^2 \right) (\beta_{j-1} - \beta_j)$$

and here z_j is the distance to the bottom of j th layer. This piecewise continuous, simplified higher order displacement field will be the one used to demonstrate the effectiveness of the Least Squares element in the sections to follow. A field of this form was used by Lee et al (1990) [59].

At this time an important distinction is made in terminology. The three equations above will be referred to as the *displacement fields*, while the five terms on the right hand side, u_o , v_o , φ_x , φ_y and w , will be termed the *displacement functions*. This terminology will help make the following sections less confusing. Note also that the superscript 1 has been dropped. It will be implied from this point on.

3.3 Theory Development: Method I

3.3.1 The Domain Displacement Functions

We begin by assuming the element domain shown in Figure 3.1 with a local η - ξ coordinate system as shown. Within this domain we have displacements represented by eqns (3.13) in terms of five domain *displacement functions* u_o , v_o , w , φ_x and φ_y . Each of these functions is represented by an n term polynomial expansions in η and ξ with n unknown constants α_i . The expressions can be written as:

$$u_o = \alpha_1 + \alpha_2\eta + \alpha_3\xi + \alpha_4\eta^2 + \alpha_5\xi^2 + \alpha_6\eta\xi + \dots$$

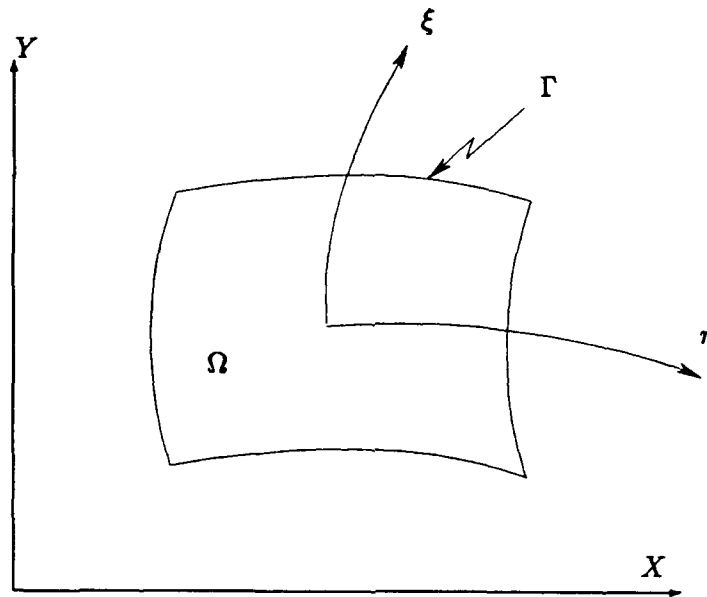


Figure 3.1: Least Squares Element Domain

$$\begin{aligned}
 v_o &= \alpha_{n+1} + \alpha_{n+2}\eta + \alpha_{n+3}\xi + \alpha_{n+4}\eta^2 + \alpha_{n+5}\xi^2 + \alpha_{n+6}\eta\xi + \dots \\
 \varphi_x &= \alpha_{2n+1} + \alpha_{2n+2}\eta + \alpha_{2n+3}\xi + \alpha_{2n+4}\eta^2 + \alpha_{2n+5}\xi^2 + \alpha_{2n+6}\eta\xi + \dots \quad (3.14) \\
 \varphi_y &= \alpha_{3n+1} + \alpha_{3n+2}\eta + \alpha_{3n+3}\xi + \alpha_{3n+4}\eta^2 + \alpha_{3n+5}\xi^2 + \alpha_{3n+6}\eta\xi + \dots \\
 w &= \alpha_{4n+1} + \alpha_{4n+2}\eta + \alpha_{4n+3}\xi + \alpha_{4n+4}\eta^2 + \alpha_{4n+5}\xi^2 + \alpha_{4n+6}\eta\xi + \dots
 \end{aligned}$$

We can write these expressions in matrix notation, (using $n = 10$ for example), as:

$$\begin{Bmatrix} u_o \\ v_o \\ \varphi_x \\ \varphi_y \\ w \end{Bmatrix} = \begin{bmatrix} \alpha_1 & \dots & \dots & \alpha_{10} \\ \vdots & \ddots & & \vdots \\ \vdots & & \ddots & \vdots \\ \alpha_{41} & \dots & \dots & \alpha_{50} \end{bmatrix} \{\mathbf{A}\} \quad (3.15)$$

where

$$\{\mathbf{A}\}^T = [\mathbf{A}] = [1 \ \eta \ \xi \ \eta\xi \ \eta^2 \ \xi^2 \ \eta^2\xi \ \eta\xi^2 \ \eta^3 \ \xi^3] \quad (3.16)$$

Or we can write the functions in terms of α 's as:

$$\begin{Bmatrix} u_o \\ v_o \\ \varphi_x \\ \varphi_y \\ w \end{Bmatrix} = [\mathcal{A}'] \{\alpha\} \quad (3.17)$$

where

$$[\mathcal{A}'] = \begin{bmatrix} \mathbf{A} & 0 & 0 & 0 & 0 \\ 0 & \mathbf{A} & 0 & 0 & 0 \\ 0 & 0 & \mathbf{A} & 0 & 0 \\ 0 & 0 & 0 & \mathbf{A} & 0 \\ 0 & 0 & 0 & 0 & \mathbf{A} \end{bmatrix} \quad (3.18)$$

and $\{\alpha\}$ is a column vector of all the α 's (50 for this case). Next, we add the local derivatives of w to these expressions to get:

$$\begin{Bmatrix} u_o \\ v_o \\ \varphi_x \\ \varphi_y \\ w \\ w_{,\eta} \\ w_{,\xi} \end{Bmatrix} = [\mathcal{A}] \{\alpha\} \quad (3.19)$$

where

$$[\mathcal{A}] = \begin{bmatrix} \mathbf{A} & 0 & 0 & 0 & 0 \\ 0 & \mathbf{A} & 0 & 0 & 0 \\ 0 & 0 & \mathbf{A} & 0 & 0 \\ 0 & 0 & 0 & \mathbf{A} & 0 \\ 0 & 0 & 0 & 0 & \mathbf{A} \\ 0 & 0 & 0 & 0 & \mathbf{A}_{,\eta} \\ 0 & 0 & 0 & 0 & \mathbf{A}_{,\xi} \end{bmatrix} \quad (3.20)$$

We now have everything we need to write the domain *displacement field* given in eqns (3.13) in terms of the domain functions given in eqns (3.14). The result is

$$\begin{Bmatrix} u \\ v \\ w \end{Bmatrix} = [T][A] \{\alpha\} \quad (3.21)$$

Here

$$[T] = \begin{bmatrix} 1 & 0 & c_1 & 0 & 0 & c_2\Gamma_{11} & c_2\Gamma_{12} \\ 0 & 1 & 0 & \bar{c}_1 & 0 & c_2\Gamma_{21} & c_2\Gamma_{22} \\ 0 & 0 & 0 & 0 & 1 & 0 & 0 \end{bmatrix} \quad (3.22)$$

where

$$c_1 = \sum_{j=1}^n P_j + z\alpha_k - \frac{4z^3}{3h^2}\alpha_k \quad (3.23)$$

$$\bar{c}_1 = \sum_{j=1}^n \bar{P}_j + z\beta_k - \frac{4z^3}{3h^2}\beta_k \quad (3.24)$$

$$c_2 = -\frac{4z^3}{3h^2} \quad (3.25)$$

This now gives an expression for the domain *displacement field* in terms of the α 's . The next step is to develop a boundary *displacement field* written in terms of nodal degrees of freedom.

3.3.2 Boundary Displacement Functions from Nodal Degrees of Freedom

The element domain shown in Figure 3.1 is now modified to include eight boundary nodes. The element is shown in Figure 3.2 and now resembles a standard quadratic isoparametric element. However, we define the nodal degrees of freedom as

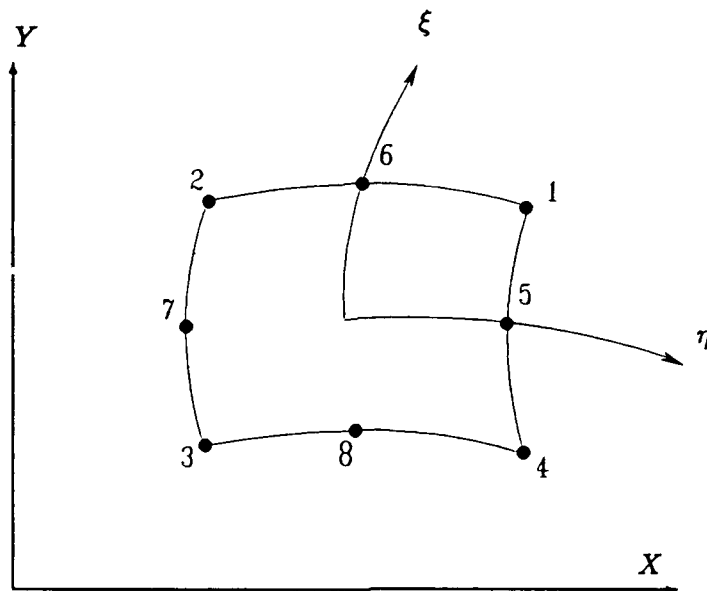


Figure 3.2: Least Squares Element with Nodes

$$\{\delta_i\}^T = [u_o \ v_o \ \varphi_x \ \varphi_y \ w \ w_{,x} \ w_{,y}] \quad i = 1, 2, 3, 4 \quad (3.26)$$

$$\{\delta_i\}^T = [u_o \ v_o \ \varphi_x \ \varphi_y] \quad i = 5, 6, 7, 8 \quad (3.27)$$

giving the side nodes and the corner nodes different numbers of degrees of freedom for a total of 44 degrees of freedom per element. For future use, we define a vector containing all 44 degrees of freedom as:

$$\{\Delta\} = \begin{Bmatrix} \delta_1 \\ \delta_2 \\ \vdots \\ \delta_8 \end{Bmatrix} \quad (3.28)$$

Along each edge of the element we have two corner nodes with 7 degrees of freedom

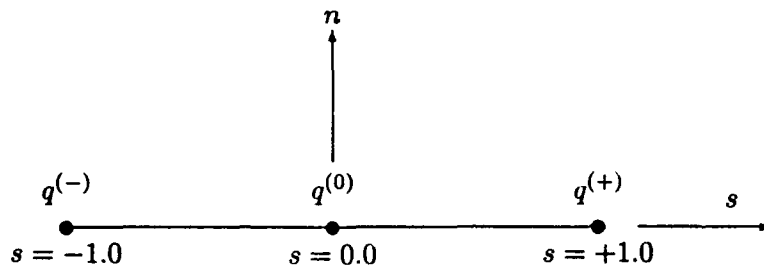


Figure 3.3: Variation of Nodal variable q along element side.

and one side node with only four degrees of freedom, as described above. With this, u_o , v_o , φ_x and φ_y are defined by three quantities along the edge, one at each node. Any one of these four quantities, call it q , defines a quadratic curve in the boundary variable s , which varies from -1.0 to $+1.0$ along each of the four sides. See Figure 3.3. We can easily establish the second order equation for any of the four degrees of freedom from the following equation:

$$q(s) = \frac{1}{2} (-s + s^2) q_{(-)} + (1 - s^2) q_{(0)} + \frac{1}{2} (s + s^2) q_{(+)} \quad (3.29)$$

The function w , on the other hand, is defined by six nodal variables. We define first $w_{,s}$ as the derivative of w tangent to the side in the direction of s , and $w_{,n}$ as the derivative of w normal to the direction of s . See Figure 3.4. For a rectangular element aligned with the global x - y coordinate system these two derivatives correspond identically to either $w_{,x}$ or $w_{,y}$ depending upon which side one looks at. If the element is not straight sided or not aligned with the global coordinate system, the two derivatives will each be a linear combination of both $w_{,x}$ and $w_{,y}$ related through the standard Jacobian matrix. With this in mind, we see that w is defined by four variables, the two values of w and the two

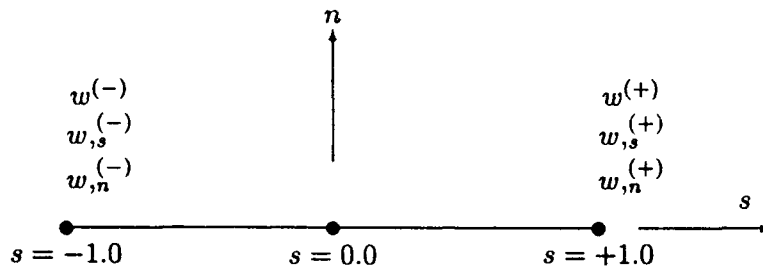


Figure 3.4: Variation of Nodal variable w along element side.

values $w_{,s}$. Thus, w can be fit by a cubic equation, making $w_{,s}$ quadratic. In addition, $w_{,n}$ is defined only by two points, one $w_{,n}$ at each end, thus making it vary only linearly. The required equations for w and its derivatives become:

$$w(s) = \left(\frac{1}{2} - \frac{3}{4}s + \frac{1}{4}s^3\right) w^{(-)} + \frac{1}{4} (1 - s - s^2 + s^3) w_{,s}^{(-)} + \left(\frac{1}{2} + \frac{3}{4}s - \frac{1}{4}s^3\right) w^{(+)} + \frac{1}{4} (-1 - s + s^2 + s^3) w_{,s}^{(+)} \quad (3.30)$$

$$w_{,s}(s) = \frac{3}{4} (-1 + s^2) w^{(-)} + \frac{1}{4} (-1 - 2s + 3s^2) w_{,s}^{(-)} + \frac{3}{4} (1 - s^2) w^{(+)} + \frac{1}{4} (-1 + 2s + 3s^2) w_{,s}^{(+)} \quad (3.31)$$

$$w_{,n}(s) = \left(\frac{1}{2} - \frac{s}{2}\right) w_{,n}^{(-)} + \left(\frac{1}{2} + \frac{s}{2}\right) w_{,n}^{(+)} \quad (3.32)$$

The significant point here is that all functions, including $w_{,s}$ and $w_{,n}$, can be expressed along an edge of an element in terms of *only* the nodal values along that particular edge. This will become an important fact to help insure compatibility from element to element.

The final step is to compile eqns (3.29)-(3.32) into a matrix format. It is convenient

to write:

$$\left\{ \begin{array}{c} u_o \\ v_o \\ \varphi_x \\ \varphi_y \\ w \\ w_{,x} \\ w_{,y} \end{array} \right\}_i = [\mathcal{F}]_i \{\Delta\} \quad (3.33)$$

where the subscript i refers to the i th side of the element, and the matrix $[\mathcal{F}]$ contains the necessary terms from eqns (3.29)-(3.32) as well as Jacobian terms relating the local differentials to the global ones.

3.3.3 The Least Squares Implementation: Method I

In the past two sections we have developed two different methods for finding expressions for the five *displacement functions*, u_o , v_o , φ_x , φ_y and w , as well as for the differentials of w . In Section 3.3.1, eqn (3.19) defined the functions anywhere in the element's domain in terms of unknown α 's. In Section 3.3.2, eqn (3.33) defined the seven functions only on the element's boundary and in terms of the nodal degrees of freedom. Let us refer to column vectors of these seven functions from each of these two equations as $\{\delta_\Omega\}$ and $\{\delta_\Gamma\}$ respectively. Here the symbols Ω and Γ correspond, of course, to domain and boundary. The vector $\{\delta_\Omega\}$ gives the seven functions in terms of the local coordinates, η and ξ , while $\{\delta_\Gamma\}$ gives them as functions of a boundary variable, s .

The basis for the formulation of the Least Squares element begins with these two vectors. The vector $\{\delta_\Omega\}$ is evaluated on the boundary by setting the appropriate variable, either η or ξ , to ± 1.0 while the other varies as s . This new vector will be referred to as $\{\delta_\Omega\}_\Gamma$, in other words, the domain displacement functions evaluated on the boundary. Next, we define a functional, I , as the integral of the square of the difference between the

domain *displacement functions* evaluated on the boundary and the boundary *displacement functions* established from the nodal degrees of freedom. This is written as:

$$I = \int_{\Gamma} (\{\delta_{\Omega}\}_{\Gamma} - \{\delta_{\Gamma}\})^2 d\Gamma \quad (3.34)$$

Substituting in the expressions from eqn (3.19) and eqn (3.33) the above equation becomes:

$$I = \int_{\Gamma} ([\mathcal{A}] \{\alpha\} - [\mathcal{F}]_i \{\Delta\})^2 d\Gamma \quad (3.35)$$

The functional I can now be minimized with respect to the α 's to obtain the expression

$$\frac{\partial I}{\partial \alpha} = \int_{\Gamma} ([\mathcal{A}]^T [\mathcal{A}] \{\alpha\} - [\mathcal{A}]^T [\mathcal{F}]_i \{\Delta\}) d\Gamma = 0 \quad (3.36)$$

(The constant 2 has been divided out.) The next step is to perform the integration and solve for the α 's in terms of the nodal degrees of freedom. As indicated in eqn (3.36), the integration is performed over the element's boundary. The integrand is defined as a function of the boundary variable s , but care must be taken in how the integration is performed to insure the correct sign on the integral for each side. Upon performing the integration, the expression can be solved for the α 's². The result is

$$\{\alpha\} = ([\mathcal{A}]^T [\mathcal{A}])^{-1} [\mathcal{A}]^T [\mathcal{F}] \{\Delta\} \quad (3.37)$$

or

²Note: To keep the number of symbols used to a minimum, the same symbols are used after the integration to represent the variables. The difference is understood.

$$\{\alpha\} = [H_I] \{\Delta\} \quad (3.38)$$

where

$$[H_I] = \left([A]^T [A] \right)^{-1} [A]^T [F] \quad (3.39)$$

This result is the basis for the Least Squares Element. The unknowns, (the α 's), of the domain displacement functions which make up the displacement fields, are chosen in such a manner as to *force* these functions to match those on the boundary which are determined from the nodal degrees of freedom. Since the functions on each side of the element are determined only from the nodal degrees of freedom on that side, interelement compatibility is *met*. Note, in the last two sentences the words 'force' and 'met' were emphasized. This is because the desired action is only accomplished in an approximate manner. The values of the functions may not match exactly, but their differences are minimized. Thus, compatibility is not met unconditionally, but it is met in a least squared sense.

With eqn (3.38) we now have the ability to update eqn (3.19). Substituting in the expression for $\{\alpha\}$, the domain *displacement functions* become:

$$\left\{ \begin{array}{c} u_o \\ v_o \\ \varphi_x \\ \varphi_y \\ w \\ w_{,\eta} \\ w_{,\xi} \end{array} \right\} = [A] [H_I] \{\Delta\} \quad (3.40)$$

Remembering that these domain *displacement functions* form the basis for the element *displacement field* throughout the domain, we can also update eqn (3.21) to now be:

$$\begin{Bmatrix} u \\ v \\ w \end{Bmatrix} = [T][A][H_I]\{\Delta\} \quad (3.41)$$

With eqn (3.41) we now have an expression for the element *displacement field*. This *displacement field* formulation is quite different from that of a standard isoparametric formulation and has some points worthy of discussion. First of all, the matrix $[A]$ is a function of the elements local coordinate system variables η and ξ . The order of the terms is dependant upon the value of n chosen in eqns (3.14). Thus, eqn (3.41) represents the *displacement field* already in terms of the element local coordinate system. The role usually performed by shape functions has already been filled directly for the Least Squares element. First, the strain field, or any desired differential field for that matter, is found by directly differentiating $[A]$ in eqn (3.41). Next, the development of $[H_I]$ in eqns (3.35)-(3.38) has insured that the domain *displacement field* has been determined such that it matches a specific function determined from nodal degrees of freedom on each specific edge of the element. This specific function is quadratic for u_o , v_o , φ_x and φ_y . This is essentially the same as what is provided by the shape functions in eqn (2.21). In fact, if n in eqn (3.14) is chosen to provide a biquadratic function (with the $\eta^2\xi^2$ term removed) the formulation for these four domain functions should be identical with that found using the standard shape function interpolations. However, unlike eqn (2.21) , the formulation in eqn (3.41) allows for a cubic variation of w along its edges, and hence a quadratic tangential derivative, while establishing a linear normal derivative of w along each edge. This is where the power of the Least Squares element comes into play. All three variables, w , $w_{,x}$ and $w_{,y}$, will remain compatible along common element boundaries. As a result, so will u and v .

3.4 Theory Development: Method II

3.4.1 The Domain Displacement Fields

In Section 3.3.1 we defined the domain *displacement functions* for the element domain. The unknowns in these expressions were then chosen to minimize the difference between them and the boundary *displacement functions* in terms of the nodal degrees of freedom. Method II will utilize the *displacement fields* themselves in the Least Squares method rather than the *displacement functions*. The minimization process will minimize the gaps between elements directly rather than through the functions making them up.

The domain *displacement field* is given by eqn (3.21). We use this form exactly as developed before and write it as:

$$\left\{ \begin{array}{c} u \\ v \\ w \end{array} \right\}_{\Omega} = [I] [A] \{\alpha\} \quad (3.42)$$

where the subscript Ω was added to denote that this is the *displacement field* defined at any point in the domain.

3.4.2 The Element Boundary Displacements from Nodal Degrees of Freedom

We now establish an element pictured exactly as in Figure 3.2. This time however, instead of nodal degrees of freedom as defined in eqns (3.26)-(3.27) we define them as

$$\{\delta_i\}^T = [u_o \quad v_o \quad \varphi_x \quad \varphi_y \quad w] \quad i = 1, 2, 3, 4, 5, 6, 7, 8 \quad (3.43)$$

and $\{\Delta\}$ is defined exactly as in eqn (3.28), with the exception that now $\{\Delta\}$ is a 40 term vector rather than one with 44 terms. This form for the elemental degrees of freedom is

identical to the standard, eight noded isoparametric element used in Section 2.3.1. The only difference is that the use of shape functions has not been established. Instead, we follow the method of Section 3.3.2 to define the actual displacements on the boundary in terms of the forty nodal degrees of freedom. We assume a quadratic variation on the boundary of the element for each of the five degrees of freedom. Now eqn (3.29) and Figure 3.3 can be used to write

$$\begin{Bmatrix} u_o \\ v_o \\ \varphi_x \\ \varphi_y \\ w \end{Bmatrix}_i = [G]_i \{ \Delta \} \quad (3.44)$$

where again the subscript i denotes the i th side, and the matrix $[G]$ contains the necessary terms from eqn (3.29).

We cannot use eqns (3.13) to establish the displacements on the boundary. This is because the boundary *displacement functions* in terms of the nodal degrees of freedom, given in eqn (3.44), do not include the $w_{,x}$ and $w_{,y}$ terms. If we were to restrict the analysis to rectangular elements aligned with the global axis system, we would have either $w_{,x}$ or $w_{,y}$ on any one side. This would enable the displacements parallel to each side to be calculated. A more desirable option would be to define new functions for u , v and w . Proceeding in this direction, we define

$$\begin{aligned} u_b^n &= u_o^1 + \sum_{j=1}^n P_j \varphi_x^1 + \alpha_n \varphi_x^1 \left(z - \frac{4z^3}{3h^2} \right) \\ v_b^n &= v_o^1 + \sum_{j=1}^n \tilde{P}_j \varphi_y^1 + \alpha_n \varphi_y^1 \left(z - \frac{4z^3}{3h^2} \right) \end{aligned} \quad (3.45)$$

$$w_b^n = w_o$$

where the subscript b denotes a boundary displacement. These expressions for the *displacement fields* are the same as those in eqns (3.13) with the w_x and w_y terms removed, making it a C^o continuous field. The displacements along the i th side can now be written as:

$$\{\mathbf{u}\}_{\Gamma_i} = \left\{ \begin{array}{c} u \\ v \\ w \end{array} \right\}_{\Gamma_i} = \begin{bmatrix} 1 & 0 & c_1 & 0 & 0 \\ 0 & 1 & 0 & \bar{c}_1 & 0 \\ 0 & 0 & 0 & 0 & 1 \end{bmatrix} \left\{ \begin{array}{c} u_o \\ v_o \\ \varphi_x \\ \varphi_y \\ w \end{array} \right\}_i \quad (3.46)$$

where the subscript b has given way to a subscript Γ , and c_1 and \bar{c}_1 are the same as defined eqns (3.23)-(3.24). Upon substituting in eqn (3.44), the above becomes:

$$\{\mathbf{u}\}_{\Gamma_i} = \begin{bmatrix} 1 & 0 & c_1 & 0 & 0 \\ 0 & 1 & 0 & \bar{c}_1 & 0 \\ 0 & 0 & 0 & 0 & 1 \end{bmatrix} [\mathcal{G}]_i \{\Delta\} \quad (3.47)$$

For convenience, we let

$$[\mathcal{J}] = \begin{bmatrix} 1 & 0 & c_1 & 0 & 0 \\ 0 & 1 & 0 & \bar{c}_1 & 0 \\ 0 & 0 & 0 & 0 & 1 \end{bmatrix} \quad (3.48)$$

so eqn (3.47) can be written as:

$$\{\mathbf{u}\}_{\Gamma_i} = [\mathcal{J}][\mathcal{G}]_i \{\Delta\} \quad (3.49)$$

3.4.3 The Least Squares Implementation: Method II

In the last two sections we established expressions for the displacements: first, within the domain *displacement field*, (Section 3.4.1), and then for the *displacement field* on the

boundary, (Section 3.4.2). We now proceed in the same manner as in Section 3.3.3 and develop an element domain *displacement field* in terms of the nodal degrees of freedom. This time however, the Least Squares method will be used to minimize the difference between the actual *displacement fields* on the boundary and not the *displacement functions*, which are their components.

We establish a functional, I , as being the integral of the squares of the difference between the domain *displacement field* evaluated on the element boundary and the boundary *displacement field* in terms of the nodal degrees of freedom. This can be written as:

$$I = \int_{\Gamma} \int_{-h/2}^{h/2} (\{\mathbf{u}_{\Omega}\}_{\Gamma} - \{\mathbf{u}_{\Gamma}\})^2 dz \cdot d\Gamma \quad (3.50)$$

Again, the symbol Γ refers to boundary so the first term in the integrand is interpreted as the domain *displacement field* evaluated on the boundary. This equation is very similar to eqn (3.34) with two notable exceptions. The first, as already mentioned, is the obvious difference of the type of variables in the integrand, actual displacements rather than *displacement functions*. The second difference, which is a result of the first, is that the integral now has another dimension added to it. This is because the terms under the integral, the *displacement fields*, are functions of z as well as x and y . Hence, in minimizing the difference between the displacements on the boundary, the thickness of the element must also be considered. Upon substituting in eqn (3.42) and eqn (3.49), we can write the above functional as:

$$I = \int_{\Gamma} \int_{-h/2}^{h/2} ([\mathcal{I}] [\mathcal{A}] \{\alpha\} - [\mathcal{J}] [\mathcal{G}] \{\Delta\})^2 dz \cdot d\Gamma \quad (3.51)$$

Minimizing this with respect to the α 's, we get:

$$\frac{\partial I}{\partial \alpha} = \int_{\Gamma} \int_{-h/2}^{h/2} ([\mathcal{A}]^T [\mathcal{I}]^T [\mathcal{I}] [\mathcal{A}] - [\mathcal{A}]^T [\mathcal{I}]^T [\mathcal{J}] [\mathcal{G}]) dz \cdot d\Gamma = 0 \quad (3.52)$$

Again, the factor 2 has been divided out. Also note that the differential area has been split up into a differential length and thickness because it will be convenient to perform the thickness integration first to simplify the expression. Noting that the only z dependency is in $[\mathcal{I}]$ and $[\mathcal{J}]$, we can write:

$$\int_{\Gamma} ([\mathcal{A}]^T [\mathcal{M}] [\mathcal{A}] - [\mathcal{A}]^T [\mathcal{N}] [\mathcal{G}]) d\Gamma = 0 \quad (3.53)$$

where

$$[\mathcal{M}] = \int_{-h/2}^{h/2} [\mathcal{I}]^T [\mathcal{I}] dz \quad (3.54)$$

$$[\mathcal{N}] = \int_{-h/2}^{h/2} [\mathcal{I}]^T [\mathcal{J}] dz \quad (3.55)$$

Now, eqn (3.53) can be evaluated in the same manner as eqn (3.36) and the end result solved for the α 's in terms of the nodal degrees of freedom. The result is :

$$\{\alpha\} = ([\mathcal{A}]^T [\mathcal{M}] [\mathcal{A}])^{-1} [\mathcal{A}]^T [\mathcal{N}] [\mathcal{G}] \{\Delta\} \quad (3.56)$$

or

$$\{\alpha\} = [H_{II}] \{\Delta\} \quad (3.57)$$

where

$$[H_{II}] = ([\mathcal{A}]^T [\mathcal{M}] [\mathcal{A}])^{-1} [\mathcal{A}]^T [\mathcal{N}] [\mathcal{G}] \quad (3.58)$$

This result is now the basis for the second version of the Least Square element. Just as

with Method I, we now have the ability to write the element *displacement field* anywhere in the domain in terms the local coordinates and the nodal degrees of freedom. The result is

$$\begin{Bmatrix} u \\ v \\ w \end{Bmatrix} = [Z][A][H_{II}]\{\Delta\} \quad (3.59)$$

Except for the differences between $[H_I]$ and $[H_{II}]$ there is no difference between eqn (3.41) and eqn (3.59). All of the discussion at the end of Section 3.3.3 concerning the implementation of the expressions for the displacements, is applicable to both Method I and II.

3.5 Preliminary Numerical Considerations: Method I -vs- Method II

The idea of approximating a C^1 continuous element through the Least Squares method is the same in both Method I in Section 3.3 and Method II in Section 3.4. However, the details of the developments are quite different, and as would be expected, the two methods will result in two different elements. It is beneficial to discuss some of the differences at this time.

First, and probably most obvious, the element from Method I requires 44 degrees of freedom, while the one from Method II has only 40. Having fewer degrees of freedom may make Method II computationally more efficient. In addition, the w displacement in Method I is defined by twelve degrees of freedom, requiring at least twelve α 's in the initial function for w . Method II requires no more than eight α 's to describe each unknown, as each displacement variable is defined by eight degrees of freedom. Requiring fewer unknowns in the initial representation of the displacement field (fewer α 's) is important,

for it makes the matrix inversion required to find $[H_{II}]$ easier than for that required to find $[H_I]$. (See eqn (3.37) and eqn (3.56).) In fact, the inversion of these matrices becomes a limiting factor into future research into developing more Least Squares elements. In eqn (3.14) the number of terms carried in the expressions quickly reaches a maximum. Since the integrations of eqn (3.36) and eqn (3.53) are carried out in the local coordinate system, one variable varies from -1 to +1, while the other is equal to ± 1 . Upon integration, the evaluation of odd terms go to zero, and the even terms remain. Consider the matrix $[O]$, where

$$[O] = [A]^T [A] \quad (3.60)$$

and $[A]$ is defined by eqn (3.20). Upon integrating $[O]$ over the boundary of the element, as in eqn (3.36), it can be shown that the diagonal is positive definite, because the terms come from the squares of the individual terms. However, the off-diagonal terms come from the even terms in the original polynomial expression. If n in eqn (3.14) is chosen so that the expressions are complete biquadratic³, then $[O]$ is ill-conditioned, and not invertible. The term $\eta^2\xi^2$ is the one which causes this problem. So, in order to get twelve unknown α 's in each displacement function of eqn (3.14), this biquadratic term, $\eta^2\xi^2$, must be dropped. The expression for $[A]$, as shown in eqn (3.16), must be modified to be

$$\{A\}^T = [A] = [1 \quad \eta \quad \xi \quad \eta\xi \quad \eta^2 \quad \xi^2 \quad \eta^2\xi \quad \eta\xi^2 \quad \eta^3 \quad \xi^3 \quad \eta^3\xi \quad \eta\xi^3] \quad (3.61)$$

With this form, $[O]$ is well conditioned can be inverted easily. This inversion problem is by no means new and has previously been encountered. In an article addressing the use of

³By biquadratic we mean the product of complete quadratic polynomials in each variable.

the Least Squares method to smooth discontinuous stresses, Hinton and Campbell (1974) [33] state that the tendency towards ill-conditioning “may be overcome to some extent” by using orthogonal polynomials such as Legendre polynomials. If formulations requiring a higher number of alphas are required, a few more higher order odd terms may be added before $[O]$ becomes ill-conditioned. In addition, it may be possible to experiment with trigonometric functions in order to add more unknowns, if necessary, while still maintaining the ability to invert the matrix. If judiciously chosen, the trigonometric functions could be under integrated after the inversion process to approximate the original polynomial terms.

Lastly, but probably more importantly, we need to consider the more conceptual difference between the two new Least Squares methods. In Method I, the Least Squares technique enforced the constituent functions, the *displacement functions* of the *displacement fields*, to be compatible across element boundaries. This indirectly enforces compatibility along element boundaries in the displacements. In contrast, Method II enforces compatibility directly to the actual *displacement fields* by forcing them through the Least Squares technique to fit a known compatible *displacement field*. Looking at the mechanism of the methods more closely, we see that Method I forces the normal derivative of w along each side of the element to be linear. In other words, at the element boundary the slope of the plate will become a linear function normal to the edge, but it will be quadratic parallel to it. Method II, on the other hand, forces the displacements to be like those with $w_{,x}$ and $w_{,y} = 0$ on the boundary. In effect, Method II will force the w displacement to be a constant along the boundaries of the elements, if allowed to do so. This sounds like an unacceptable approximation. However, if we choose w to be an eight term quadratic, then w cannot be constant on the boundaries except for the trivial solution of $w = 0$ everywhere. Thus, through the Least Squares method, the *displacement fields* represent

those which minimize the gaps between the elements.

In light of the above discussion, Method II is presented along with Method I, not for its direct engineering applicability, but as a demonstration of the power of the Least Squares method. Method II will be shown to provide some encouraging results despite the unacceptable approximation discussed above. The intent is to demonstrate a second method which may be applied more effectively for other problems. It could be greatly improved if a better choice of displacement functions, based upon the nodal degrees of freedom, can be found.

3.6 Finite Element Formulation of the Least Squares Elements

The development of the stiffness and mass matrices for the Least Squares elements follow the basic procedure used in Section 2.3. However, due to the increase in complexity in the displacement field, the equations and matrix algebra become much more complicated. As a result, the following derivation presents some of the intermediate matrices by symbol only, and the interested reader is referred to Appendix A for the details.

3.6.1 Stiffness Matrix Development

The expressions for in-plane strains within any layer of an element can be found by substituting eqns (3.13) into the appropriate strain displacement relations resulting in

$$\begin{aligned}\epsilon_x^k &= u_{o,x}^1 + \sum_{j=2}^k P_j \varphi_{x,x}^1 - zw_{,xx} + \alpha_k \varphi_{x,x}^1 \left(z - \frac{4z^3}{3h^2} \right) \\ \epsilon_y^k &= v_{o,y}^1 + \sum_{j=2}^k \bar{P}_j \varphi_{y,y}^1 - zw_{,yy} + \beta_k \varphi_{y,y}^1 \left(z - \frac{4z^3}{3h^2} \right)\end{aligned}\quad (3.62)$$

$$\begin{aligned} \gamma_{xy}^k = & u_{o,y}^1 + v_{o,x}^1 + \sum_{j=2}^k (P_j \varphi_{x,y}^1 + \bar{P}_j \varphi_{y,x}^1) \\ & - 2zw_{,xy} + (\alpha_k \varphi_{x,y} + \beta_k \varphi_{y,x}) \left(z - \frac{4z^3}{3h^2} \right) \end{aligned}$$

The transverse strains simply become

$$\begin{aligned} \gamma_{xz}^k &= \alpha_k \varphi_x^1 \left(1 - \frac{4z^2}{h^2} \right) \\ \gamma_{yz}^k &= \beta_k \varphi_y^1 \left(1 - \frac{4z^2}{h^2} \right) \end{aligned} \tag{3.63}$$

In order to keep future equations less cumbersome, as well as for convenience, the superscript 1, which implies the value of the parameter for the reference (first) layer, will be dropped. In other words, the variables u_o , v_o , φ_x and φ_y will be understood to refer to the values for the first layer of the laminate. We can express eqn (3.62) in matrix notation as

$$\begin{Bmatrix} \epsilon_x \\ \epsilon_y \\ \gamma_{xy} \end{Bmatrix}^k = \{\epsilon\}^k = [S] \{\delta\} \tag{3.64}$$

where the forms of $[S]$ and $\{\delta\}$ (see Appendix A) were purposefully chosen to aid the computations to follow. Similarly, eqn (3.63) is written as

$$\begin{Bmatrix} \gamma_{xz} \\ \gamma_{yz} \end{Bmatrix}^k = \{\gamma\}^k = [S_i] \{\delta^t\} \tag{3.65}$$

Referring to Appendix A, we see that $[S]$ is a 3 by 18 element matrix, while $[S_i]$ is a 2 by 4 matrix.

With the above equations, the expression for in-plane strain energy, U , can be written as:

$$\begin{aligned}
 U &= \frac{1}{2} \int_V \{\sigma\}^T \{\epsilon\} dV \\
 &= \frac{1}{2} \int_V \{\epsilon\}^T [Q] \{\epsilon\} dV \\
 &= \frac{1}{2} \int_V \{\delta\}^T [S]^T [Q] [S] \{\delta\} dV \tag{3.66}
 \end{aligned}$$

where $[Q]$ was defined in Section 2.2.1. Similarly the transverse strain energy, U_t , becomes:

$$\begin{aligned}
 U_t &= \frac{1}{2} \int_V \{\gamma\}^T [\bar{Q}] \{\gamma\} dV \\
 &= \frac{1}{2} \int_V \{\delta^t\}^T [S_t]^T [\bar{Q}] [S_t] \{\delta^t\} dV \tag{3.67}
 \end{aligned}$$

Next, we perform the integration through the thickness of the element. In doing so, the results can be written as:

$$U = \frac{1}{2} \int_A \{\delta\}^T [\Omega] \{\delta\} dA \tag{3.68}$$

$$U_t = \frac{1}{2} \int_A \{\delta^t\}^T [\Omega^t] \{\delta^t\} dA \tag{3.69}$$

where

$$[\Omega] = \int_{-h/2}^{h/2} [S]^T [Q] [S] dz \quad (3.70)$$

$$[\Omega^t] = \int_{-h/2}^{h/2} [S_t]^T [\bar{Q}] [S_t] dz \quad (3.71)$$

The matrices defined in eqn (3.70) and eqn (3.71) are counterparts to the extensional, bending and coupling stiffness matrices defined in eqns (2.16)-(2.19) in Section 2.2.1. These $[A]$, $[B]$ and $[D]$ matrices have specific physical interpretations to them and are discussed in any fundamental composites textbook (see Jones [41], Tsai and Hahn [137] or Christensen [22]). Unfortunately, the components of $[\Omega]$ and $[\Omega_t]$ do not lend themselves to as nice a physical description. The two matrices can be broken down into extensional, bending, coupling and so-forth submatrices, but there is nothing to be gained at this point from doing so. If computational efficiency for specific laminates were desired, then knowing which submatrices go to zero for these cases would be beneficial. The form of $[S]$ and $[S_t]$ were chosen to make the integrations in eqn (3.70) and eqn (3.71) as easy as possible.

The next step in the finite element formulation is to write $\{\delta\}$ and $\{\delta_t\}$ in terms of the nodal degrees of freedom. We first establish a simplified version of $\{\delta\}$ and $\{\delta_t\}$. We define $[L_1]$ and $[L_1^t]$ (see Appendix A) such that

$$\{\delta\} = [L_1] \{\delta_{xy}\} \quad (3.72)$$

$$\{\delta^t\} = [L_1^t] \{\delta_{xy}^t\} \quad (3.73)$$

where

$$\{\delta_{xy}\}^T =$$

$$[u_{o,x} \ u_{o,y} \ v_{o,x} \ v_{o,y} \ \varphi_{x,x} \ \varphi_{x,y} \ \varphi_{y,x} \ \varphi_{y,y} \ w_{o,xx} \ w_{o,xy} \ w_{o,yy}] \quad (3.74)$$

and

$$\{ \delta_{xy}^t \}^T = [\varphi_x \ \varphi_y \ w_{o,x} \ w_{o,y}] \quad (3.75)$$

Next, in preparation for integration in the local coordinate system, the conversions of the global derivatives to the local coordinate system are established. We establish $[L_2]$ and $[L_2^t]$ (see Appendix A) such that

$$\{ \delta_{xy} \} = [L_2] \{ \delta_{\eta\xi} \} \quad (3.76)$$

$$\{ \delta_{xy}^t \} = [L_2^t] \{ \delta_{\eta\xi}^t \} \quad (3.77)$$

where

$$\{ \delta_{\eta\xi} \}^T = [u_{o,\eta} \ u_{o,\xi} \ v_{o,\eta} \ v_{o,\xi} \ \varphi_{x,\eta} \ \varphi_{x,\xi} \ \varphi_{y,\eta} \ \varphi_{y,\xi} \ F_1(w) \ F_2(w) \ F_3(w)] \quad (3.78)$$

and

$$\{ \delta_{\eta\xi}^t \}^T = [\varphi_x \ \varphi_y \ w_{o,\eta} \ w_{o,\xi}] \quad (3.79)$$

In eqn (3.78) the terms $F_1(w)$, $F_2(w)$ and $F_3(w)$ arise from the required higher derivatives of w . They are defined by:

$$\begin{aligned} F_1(w) &= w_{,\eta\eta} - c_3 x_{,\eta\eta} - c_4 y_{,\eta\eta} \\ F_2(w) &= w_{,\eta\xi} - c_3 x_{,\eta\xi} - c_4 y_{,\eta\xi} \\ F_3(w) &= w_{,\xi\xi} - c_3 x_{,\xi\xi} - c_4 y_{,\xi\xi} \end{aligned} \quad (3.80)$$

where

$$\begin{aligned} c_3 &= \Gamma_{11}w_{,\eta} + \Gamma_{12}w_{,\xi} \\ c_4 &= \Gamma_{21}w_{,\eta} + \Gamma_{22}w_{,\xi} \\ \Gamma_{ij} &= \text{Componentsof } [J]^{-1} \end{aligned}$$

These equations have become complicated because of the second derivatives of w in eqn (3.74). These require new transformations relating the higher order derivatives in the global to the local coordinate systems. These transformations show up in both eqns (3.80) and in $[L_2]$. The complete details of these transformations, which are not normally seen in the literature ⁴, can be found in Appendix B. In a final sequence into developing the element stiffness matrix, we establish a new column matrix containing all of the required local derivatives of the displacement functions

$$\begin{aligned} \{\delta_{\eta\xi}\}^T &= [u_{o,\eta} \quad u_{o,\xi} \quad v_{o,\eta} \quad v_{o,\xi} \quad \varphi_{x,\eta} \\ &\quad \varphi_{x,\xi} \quad \varphi_{y,\eta} \quad \varphi_{y,\xi} \quad w_{,\eta} \quad w_{,\xi} \quad w_{,\eta\eta} \quad w_{,\eta\xi} \quad w_{,\xi\xi}] \end{aligned} \quad (3.81)$$

This matrix is found through differentiation of eqn (3.40) with either $[H_I]$ or $[H_{II}]$ depending upon whether Method I or Method II is being used. The terminology $[H]$ will hereafter imply either Method I or Method II. We can write

$$\{\delta_{\eta\xi}\} = [\mathcal{A}_{\eta\xi}][H]\{\Delta\} \quad (3.82)$$

$$\{\delta'_{i,\xi}\} = [\mathcal{A}'_{\eta\xi}][H]\{\Delta\} \quad (3.83)$$

⁴In the literature search for this work, only one article with similar derivations was found. See Reddy (1989) [116].

where $[\mathcal{A}_{\eta\xi}]$ and $[\mathcal{A}_{\eta\xi}^t]$ are differentiated versions of $[\mathcal{A}]$, and are defined in Appendix A.

The matrix $\{\delta_{\eta\xi}\}$ is related to $\{\delta_{\eta\xi}\}$ through the relation

$$\{\delta_{\eta\xi}\} = [L_3] \{\delta_{\eta\xi}\} \quad (3.84)$$

where $[L_3]$ is given in Appendix A. Substituting eqns (3.72)-(3.83) into eqn (3.68) and eqn (3.69), the expression for the elements total strain energy, $U_{se} = U + U_t$, becomes

$$U_{se} = \frac{1}{2} \int_a \left(\{\Delta\}^T [\beta]^T [[\Omega] \beta] \{\Delta\} + \{\Delta\}^T [\beta^t]^T [\Omega^t] [\beta^t] \{\Delta\} \right) dA \quad (3.85)$$

where

$$\begin{aligned} [\beta] &= [L_1][L_2][L_3][\mathcal{A}_{\eta\xi}][H] \\ [\beta^t] &= [L_1^t][L_2^t][\mathcal{A}_{\eta\xi}^t][H] \end{aligned}$$

Minimizing eqn (3.85) with respect to $\{\Delta\}$ gives the stiffness matrix. The result is:

$$[k] = \int_a \left([\beta]^T [[\Omega] \beta] + [\beta^t]^T [\Omega^t] [\beta^t] \right) dA \quad (3.86)$$

3.6.2 Mass Matrix Development

The mass matrix development follows much the same procedure as in Section 2.3.3. The expression for kinetic energy, U_{ke} , can be written as

$$U_{ke} = -\frac{1}{2}\omega^2 \int_V \rho (u^2 + v^2 + w^2) dV \quad (3.87)$$

or

$$U_{ke} = -\frac{1}{2}\omega^2 \int_V \rho \{u\}^T \{u\} dV \quad (3.88)$$

where

$$\{u\} = [u \quad v \quad w] \quad (3.89)$$

Following the same general procedure as in Section 3.6.1, we establish a matrix, $[S_m]$, so that we can write:

$$\{u\} = [S_m] \{\delta^m\} \quad (3.90)$$

where

$$\{\delta^m\}^T = [u_o \quad v_o \quad w_o \quad \vartheta_x \quad \vartheta_y \quad \vartheta_x \quad \vartheta_y \quad \vartheta_x \quad \vartheta_y \quad w_{,x} \quad w_{,y}] \quad (3.91)$$

and $[S_m]$ is defined in Appendix A by eqn (A.18). With these equations, eqn (3.88) becomes:

$$U_{ke} = -\frac{1}{2}\omega^2 \int_V \rho \{\delta^m\}^T [S_m]^T [S_m] \{\delta^m\} dV \quad (3.92)$$

This expression can be integrated through the thickness resulting in

$$U_{ke} = -\frac{1}{2}\omega^2 \int_A \{\delta^m\}^T [\Omega_m] \{\delta^m\} dA \quad (3.93)$$

where

$$[\Omega_m] = \int_{-h/2}^{h/2} \rho [S_m]^T [S_m] dz \quad (3.94)$$

The next task is to represent $\{\delta^m\}$ in terms $\{\Delta\}$. Towards this end, we establish a new column matrix

$$\{\delta_{\eta\xi}^m\}^T = [u_o \quad v_o \quad \vartheta_x \quad \vartheta_y \quad w \quad w_{,\eta} \quad w_{,\xi}] \quad (3.95)$$

where

$$\{\delta_{\eta\xi}^m\} = [A][H]\{\Delta\} \quad (3.96)$$

In this equation, the matrix $[A]$ is exactly as defined in eqn (3.20). Finally, $\{\delta^m\}$ is related to $\{\delta_{\eta\xi}^m\}$ through

$$\{\delta^m\} = [L_m]\{\delta_{\eta\xi}^m\} \quad (3.97)$$

where $[L_m]$ is defined in Appendix A. Putting all of the above equations together allows U_{ke} to be expressed in terms of $\{\Delta\}$. The result is

$$U_{ke} = -\frac{1}{2}\omega^2 \int_A \{\Delta\}^T [\beta_m]^T [\Omega_m] [\beta_m] \{\Delta\} dA \quad (3.98)$$

where

$$[\beta_m] = [L_m][A][H] \quad (3.99)$$

To find the expression for the mass matrix, we minimize eqn (3.98) with respect to $\{\Delta\}$.

The result is

$$[m] = \int_A [\beta_m]^T [\Omega_m] [\beta_m] dA \quad (3.100)$$

This is the final expression for the element mass matrix.

3.6.3 Stress Stiffness Matrix Development

The finite element coding for Method I and Method II will be extended to include both the buckling problem and the pre-stressed vibration problem. To accomplish this, we develop the initial stress stiffness matrix, $[k_\sigma]$, following the procedure outline in Cook [23]. We assume that the strains are composed of both linear and nonlinear portions. The are written as:

$$\{\epsilon\} = \{\epsilon_L\} + \{\epsilon_{NL}\} \quad (3.101)$$

The nonlinear portion of the strains $\{\epsilon_{NL}\}$ includes the higher order terms as in the Lagrangian strain definitions. The buckling and pre-stressed vibration analysis will be limited to include only the in-plane normal stresses in the following development, but they could easily be modified to include in-plane shear and transverse stresses quite easily.

The strain energy due to the nonlinear portion of eqn (3.101) can be expressed in terms of the nonlinear portion and the pre-stress present in the element. Thus

$$U_{NL} = \frac{1}{2} \int_V \left\{ \begin{matrix} \epsilon_x \\ \epsilon_y \end{matrix} \right\}_{NL}^T \left\{ \begin{matrix} \sigma_{xo} \\ \sigma_{yo} \end{matrix} \right\} dV \quad (3.102)$$

The nonlinear portions of the strains are written as

$$\left\{ \begin{matrix} \epsilon_x \\ \epsilon_y \end{matrix} \right\}_{NL} = \frac{1}{2} \begin{bmatrix} u_{,x} & v_{,x} & w_{,x} & 0 & 0 & 0 \\ 0 & 0 & 0 & u_{,y} & v_{,y} & w_{,y} \end{bmatrix} \left\{ \begin{matrix} u_{,x} \\ v_{,x} \\ w_{,x} \\ u_{,y} \\ v_{,y} \\ w_{,y} \end{matrix} \right\}$$

$$= \frac{1}{2} [Q] \{u_{xy}\} \quad (3.103)$$

From eqn (3.90) we can write:

$$\begin{Bmatrix} u_{,x} \\ v_{,x} \\ w_{,x} \end{Bmatrix} = [S_m] \{\delta_{,x}^m\} \quad (3.104)$$

where $\{\delta_{,x}^m\}$ is the derivative of eqn (3.91) with respect to x . Similarly we can write:

$$\begin{Bmatrix} u_{,y} \\ v_{,y} \\ w_{,y} \end{Bmatrix} = [S_m] \{\delta_{,y}^m\} \quad (3.105)$$

which now allows us write:

$$\begin{Bmatrix} u_{,x} \\ v_{,x} \\ w_{,x} \\ u_{,y} \\ v_{,y} \\ w_{,y} \end{Bmatrix} = \begin{bmatrix} S_m & 0 \\ 0 & S_m \end{bmatrix} \begin{Bmatrix} \delta_{,x}^m \\ \delta_{,y}^m \end{Bmatrix} \quad (3.106)$$

Next we establish

$$\begin{Bmatrix} \delta_{,x}^m \\ \delta_{,y}^m \end{Bmatrix} = [I_B] \{\delta_{xy}^m\} \quad (3.107)$$

where $[I_B]$ and $\{\delta_{xy}^m\}$ are defined in Appendix A. We can now write:

$$\begin{Bmatrix} \epsilon_x \\ \epsilon_y \end{Bmatrix}_{NL} = \frac{1}{2} \begin{bmatrix} S_m & 0 \\ 0 & S_m \end{bmatrix} [I_B] \{\delta_{xy}^m\} \quad (3.108)$$

Next, in a sequence very similar to that in eqns (3.73)-(3.84), we establish the following

relation to relate $\{\delta_{xy}^m\}$ to the nodal degrees of freedom. (Note: The details of the following terms are omitted, but the matrices are very similar to those in eqns (3.73)-(3.84) and are distinguished through the use of the ' symbol.)

$$\{\delta_{xy}^m\} = [L'_2] [L'_3] [A'_{\eta\xi}] [H] \{\Delta\} \quad (3.109)$$

At this point it is convenient to define:

$$[\beta'] = [I_B] [L'_2] [L'_3] [A'_{\eta\xi}] [H] \quad (3.110)$$

so that we can simply write

$$\begin{Bmatrix} \epsilon_x \\ \epsilon_y \end{Bmatrix}_{NL} = \frac{1}{2} \begin{bmatrix} S_m & 0 \\ 0 & S_m \end{bmatrix} [\beta'] \{\Delta\} \quad (3.111)$$

This equation can be substituted into eqn (3.102) to give:

$$U_{NL} = \frac{1}{4} \int_V \{\Delta\}^T [\beta']^T \begin{bmatrix} S_m & 0 \\ 0 & S_m \end{bmatrix}^T [Q]^T \begin{Bmatrix} \sigma_{xo} \\ \sigma_{yo} \end{Bmatrix} dV \quad (3.112)$$

We manipulate the last two terms in the integrand to give:

$$\begin{aligned} [Q]^T \begin{Bmatrix} \sigma_{xo} \\ \sigma_{yo} \end{Bmatrix} &= \begin{bmatrix} \sigma_{xo} & 0 & 0 & 0 & 0 & 0 \\ 0 & \sigma_{yo} & 0 & 0 & 0 & 0 \\ 0 & 0 & \sigma_{xo} & 0 & 0 & 0 \\ 0 & 0 & 0 & \sigma_{yo} & 0 & 0 \\ 0 & 0 & 0 & 0 & \sigma_{xo} & 0 \\ 0 & 0 & 0 & 0 & 0 & \sigma_{xo} \end{bmatrix} \{u_{xy}\} \\ &= [\sigma_o] \{u_{xy}\} \end{aligned} \quad (3.113)$$

Substitution of the expressions for $\{u_{xy}\}$ into eqn (3.113) and the result into eqn (3.112), gives the required form to provide a symmetric matrix. The result is:

$$U_{NL} = \frac{1}{4} \{\Delta\}^T \int_V [\beta']^T \begin{bmatrix} S_m & 0 \\ 0 & S_m \end{bmatrix}^T [\sigma_o] \begin{bmatrix} S_m & 0 \\ 0 & S_m \end{bmatrix} [\beta'] \{\Delta\} dV \quad (3.114)$$

The element stress stiffness matrix is now established through minimization of eqn (3.114) after integration through the thickness. The end result is

$$[k_\sigma] = \int_A [\beta']^T [O_B] [\beta'] dA \quad (3.115)$$

where the integration through the thickness produced the matrix $[O_B]$ and is defined as

$$[O_B] = \int_{-h/2}^{h/2} \begin{bmatrix} S_m & 0 \\ 0 & S_m \end{bmatrix}^T [\sigma_o] \begin{bmatrix} S_m & 0 \\ 0 & S_m \end{bmatrix} dz \quad (3.116)$$

It turns out that $[O_B]$ can be written in terms of the matrix $[\Omega_m]$ defined in eqn (3.94).

The relationship is:

$$[O_B] = \begin{bmatrix} p_{xo} [\Omega_m] & 0 \\ 0 & p_{yo} [\Omega_m] \end{bmatrix} \quad (3.117)$$

Here, the terms p_{xo} and p_{yo} are pre-stress forces per unit width stemming from the integration of the pre-stresses through the thickness. The inclusion of material properties in the displacement field has added a complexity to the calculations involved in calculating the stress stiffness matrix. In most mechanics problems this matrix is found through much simpler means.

3.7 Finite Element Implementation of the Least Squares Elements

In the past three sections we have developed equations for the element stiffness (eqn (3.86)), mass (eqn (3.100)) and stress stiffness (eqn (3.115)) matrices. These three element matrices can be assembled into the global matrices following standard finite element techniques. The resulting equation to be solved becomes

$$\left([K] - \omega^2 [M] - p_o [K_\sigma] \right) \{ \Delta \} = 0 \quad (3.118)$$

where here we have assumed $p_{x_o} = p_{y_o} = p_o$. If the value of p_o is zero, then eqn (3.118) reduces down to the vibration eigenvalue problem of eqn (2.59) in Section 2.4.1. To solve the buckling problem, we set the second term equal to zero and solve the eigenvalue problem for p_o . For the pre-stress problem, we set p_o equal to some value less than the critical buckling load and solve the resulting eigenvalue problem for ω .

Stress calculations for the Least Squares method are done in a manner similar to that already discussed for the Predictor Corrector method. Stresses are calculated at the three by three Gauss points, which are then treated as the nodes for a *reduced* eight noded element. The stress data from these eight *nodes* are then used to find the derivatives of the stress. The derivatives of the stresses are needed to put into the equations of equilibrium, which are integrated to give the transverse stresses.

The formulation of the Least Squares element presented here is unique. There exists no formulations like it in the literature. In fact, the only previous works which were found, used the least squares process as a tool to smooth finite element results, in particular stresses. A few papers appeared over a short period of time, but none of these implemented a least squares approach to smoothing functions to approximate a C^1 continuous element.

Published works using the least squares method for smoothing functions include Hinton and Campbell (1974) [33], Lynn and Arya (1973) [70] and (1974) [69], Hinton, Scott and Ricketts (1975) [34] and Razzaque (1973) [109].

CHAPTER IV

NUMERICAL RESULTS AND METHOD VALIDATIONS

4.1 Study Approach and Preliminary Information

The implementation of the Predictor Corrector and the two Least Squares techniques into the finite element method was presented in great detail in Chapters II and III. This Chapter will present the basic numerical findings of these methods. The approach will be to compare numerical results obtained with all three of these methods to existing data found in the current literature. The intent is to provide an understanding into the capabilities and limitations of the techniques. The primary study will concentrate on the solutions of the eigenvalue problems encountered when finding the natural frequency and the critical buckling load. The vibration problem will be analyzed with all three techniques. However, the stability problem was only implemented into the two Least Squares methods, so will not be addressed by the Predictor Corrector technique. In addition, there will not be a rigorous mathematical convergence study but only a demonstration and discussion of the convergence characteristics.

In comparing the methods to existing data found in the literature, an attempt has been made to provide results for a wide range of possible laminates. While the emphasis is placed on thick laminates, the number of layers does not necessarily have to be large. The laminates studied range from as little as three layers to as many as sixteen. The ply angles were not limited to the standard 0, 90 and ± 45 degrees, and both symmetric

Table 4.1: Material Properties.

MATERIAL	E_L/E_T	G_{LT}/E_T	G_{TT}/E_T	ν_{LT}	ν_{TT}
I	15	0.5	.35	.3	.49
II	40	0.6	.5	.25	.25
III	25	0.5	.2	.25	.25
IV	4.46	.566	.395	.415	.49
V*	11.49	.566	.28	.38	.49
VI	30	.6	.5	.25	.25
VII	?†	.6	.5	.25	.25

*For this material: $E_T = 1.14E_{T(IV)}$ and $\rho = 0.846\rho_{(IV)}$

† Indicates variable ratio.

and anti-symmetric laminates are considered. In addition, to a wide range of material properties, a laminate made up of two separate materials (hybrid) was also considered. In choosing such a wide range of variables for the different laminates, an appreciation for the capability and limitations can be realized. The material properties which are used are listed in Table 4.1. The ply layup of the hybrid laminate considered in this analysis is $[45/-45/0/90/45/-45/0/90]_{AS}$. The middle eight layers are Material IV, and the top four and bottom four layers are Material V. This laminate was chosen to match that analyzed by Noor (1990) [89].

Throughout this research many different boundary conditions were considered and investigated. It is worth mentioning at this point, with more to follow later, that the boundary conditions are believed to be a source of variance for the Least Squares methods when comparing them to 3-D elasticity solutions. The boundary conditions used in the remainder of this work are given in Appendix C.

4.2 Method Specific Behavior and Convergence

4.2.1 Predictor Corrector Technique

The finite element program for the Predictor Corrector technique, as described in Chapter II, was implemented in FORTRAN on the CYBER 990 computer. Since the main part of the program is based upon a standard quadratic isoparametric Mindlin plate element, there is no need to spend much effort on evaluating its performance. This type of element is well understood and is one of the most widely used elements in plate analysis. Thus, we will concentrate on the performance of the Predictor Corrector method to calculate accurate shear correction coefficients and the resulting improvement in the eigenvalues.

As discussed previously in Section 2.4.3, the shear correction coefficients should primarily be functions of the plate's material properties and cross sectional shape, and hence, they should be relatively constant throughout the plate. Figure 4.1 provides some typical examples of the shear correction factors calculated at different locations in a quarter plate model. The data points represent a different x or y location in the plate. Data near locations where the shear stresses are zero are disregarded, as these are not accurate. One can see that the lines are relatively constant, and an average value of the shear correction factors can easily be calculated. It was found that it becomes difficult to calculate the shear correction coefficients anywhere where the transverse shear stresses are small. This is understandable from a numerical viewpoint when one considers the method involved in calculating these numbers. The integration through the thickness of the plate relies upon the addition of many numbers, which results in inaccuracies if the numbers are small. The coefficients themselves are then found by dividing a small number by another. The result is likely to be inaccurate. The important point is that the shear correction coefficients should be calculated from the data found surrounding an area in the plate where the stresses are relatively high.

No attempt was made to automate the calculation of the shear correction coefficients into successive runs of the finite element program. In determining the natural frequency of a particular laminate, the program was first run with both shear correction coefficients equal to one and the resulting average shear correction coefficients determined. The program was then run a second time with the new coefficients and the updated natural frequency determined. The calculations involved in calculating the shear correction coefficients were avoided in this second run. It is interesting to note that there is no need to iterate a solution to find the most accurate shear correction factors. Noor (1989) [88] also found this to be the case. Figure 4.2 presents the calculated transverse stress for a laminate calculated with shear correction coefficients equal to 1.0 and then with the coefficients equal to 0.79. Note that there is no change in the shape of the curves. The lines fall exactly on top of one another.

To validate the program's ability to calculate the shear correction factors in the present analysis, the results are compared to those obtained by Noor [88]. For example, the values published by Noor for a 9 layer crossply laminate are $k_x = 0.838$ and $k_y = 0.730$. The data from this analysis is presented in Figure 4.1. The current analysis provides averages of $k_x = 0.841$ and $k_y = 0.732$. As a further check, the shear correction factors were calculated for a homogeneous aluminum plate. These values came out to be very close to 5/6.

The sensitivity of the natural frequency to the shear correction factor is shown in Figure 4.3. The figure shows that ω_n is almost linear with respect to the shear correction factor. This is independent of the number of layers. Based upon this data, one could update ω_n with relative confidence knowing the relationship $\partial\omega_n/\partial k_\alpha$. The relationship of the actual shear correction coefficients with the number of layers is quite different, however. Referring to Figure 4.4, one can see that the shear correction factors do not follow any particular relationship.

It was no surprise that the finite element program converges rapidly to the first fundamental frequency. It was found that 9, 16 and 25 element, quarter plate meshes yielded essentially the same answer. In fact, both a nine element full plate and quarter plate model give the same natural frequency. The shear correction factors, however, do not converge as fast, as can be expected. Because of the need for accurate data fitting in calculating the coefficients, at least a 16 element quarter plate model is needed. A finer mesh is probably desirable. A 25 element mesh was used for Figure 4.1. This fact presents a problem for cases where the ply layups preclude quarter plate symmetry, requiring then full plate modeling. In order to get accurate shear correction coefficients at least 64 or 100 elements are required. This was found to be a serious drawback to the Predictor Corrector method. The computational time and storage required to solve a problem quickly became large.

If this program is to be implemented in an analysis, new methods of curve fitting the nodal displacements should be studied to provide more accuracy and flexibility. The present analysis was restricted to rectangular elements because of the methods used in curve fitting the data. There is a lot of room for improvement in calculating the shear correction coefficients and there is no reason that the method cannot be improved upon significantly. If accurate single element shear correction coefficient calculations can be made, the computational time can be greatly reduced. The need for fine meshes can be avoided. For maximum efficiency, multiple mesh runs may be required. A finer mesh may be needed in calculating the shear correction coefficients and then a coarse mesh used to calculate the updated natural frequency. Also, this technique could easily be extended to solve the general shell problem.

4.2.2 The Least Squares Method

The behaviors of the two Least Squares elements developed in Chapter III require more investigation than the standard isoparametric Mindlin element used in the Predictor Corrector program. The elements are non-conforming in the sense that they are not free from gaps¹ between elements, but they do differ in that the gaps are minimized in a least squares sense. In the finite element method incompatibilities between elements normally result in a reduction in stiffness, but in Methods I and II the minimization of the incompatibilities through the Least Squares method should also minimize this expected effect. However, this least squares minimization of the gaps between the elements can be expected to change the convergence properties of the elements. Recalling the difference between Methods I and II, we can also expect that the two methods themselves may have different convergence properties. In Method I, the normal derivative of the out-of-plane displacement along an edge of an element was forced to be linear, while the tangential derivative was quadratic. With a displacement field of sufficient order, these requirements can be enforced. Thus, the gaps, which are minimized by enforcing these requirements, should tend to zero. This should be true especially as the number of elements increases. However, one must also consider the vehicle used in minimizing the gaps. In minimizing the gaps, the element is *warped* into a shape not commensurate with the true solution. Thus, the element may start out soft due to the presence of gaps, but becomes more stiff as the number of elements increases. It may also converge to a slightly stiffer solution.

Method II, on the other hand, minimizes the gaps by forcing the out-of-plane displacement to be equal to one where the slopes of this displacement are zero. If the displacement field is of sufficient order to allow this, the slope of the plate would tend to zero at the element boundaries causing a large increase in stiffness. This is indeed what happens and

¹The word *gap* is used loosely to refer to both gaps and overlaps.

is stated without proof. It suffices to say that when a high order displacement field is used, the element becomes unreasonably stiff and gives very poor results. As was discussed in Section 3.5, if the field for w is restricted to being quadratic, it cannot meet the zero slope case at all edges of the element, and hence, through the Least Squares technique should not be too stiff. Thus, Method II is expected to have gaps, but the effect of them should be minimized through the Least Squares method.

The results received from Methods I and II follow the discussion in the last two paragraphs. The gaps between elements are most easily observed when considering thick laminates made up of just a few layers. Typical examples of the incompatibilities for Methods I and II are given in Figure 4.5 and Figure 4.6. These figures, for a three layer cross-ply, show that Method I essentially has interelement compatibility, while Method II has definite gaps between the elements. One can visually see, however, that the gaps are indeed zero in a least squares sense. Figure 4.7 and Figure 4.12 show the convergence of Methods I and II respectively for a four layer cross ply laminate. The plots both show the ratio of $\omega^2/\omega_{Exact}^2$ as a function of E_1/E_2 . Note that Method I produces a stiffer solution as the mesh is refined, while Method II gets less stiff as the number of elements increases. In addition, note that Method I is converging as the mesh is refined, while Method II is neither converging nor diverging to a solution and is moving away from the exact solution. A different convergence study is presented in Figure 4.9 and Figure 4.10, this time for a ten layer $\pm 45^\circ$ laminate. In addition, the convergence is a function of the ratio h/b . In Figure 4.9, Method I is seen to converge as before with mesh refinement. In addition, it is also becoming relatively stiffer as the thickness of the plate increases. We will see later that this is a typical trend for a simplified higher order theory. For thin plates, Method I is shown to converge to the exact solution. In Figure 4.10 Method II again exhibits some peculiar behavior. This time Method II is moving towards the exact solution, but it shows

little signs of convergence. An important point to notice here is that the performance of the element is beginning to look acceptable for the thinner plates, but it quickly diverges for the higher ratios of h/b . Finally, Figure 4.11 and Figure 4.12 present yet another case. This time for the sixteen layer hybrid laminate. Note the same trends are present as in Figure 4.9 and Figure 4.10.

From these observations we can come to several conclusions. First, we can conclude that Method I exhibits acceptable convergence characteristics. The formulation of the element allows the gaps between elements to be easily closed. However, because of these gaps, the solution converges opposite to what is normally found in typical finite element analysis. Normally the finite element method produces a solution guaranteed to be too stiff, but it gets softer with mesh refinement. The presence of gaps between the Least Squares elements invalidates this guarantee. Also, material anisotropy has little effect on the accuracy of the solution, but the model does appear to become too stiff as the thickness to width ratio of the laminate increases. Next, Method II only exhibits convergence for thin to moderately thick plates with several layers. As the thickness to side ratio of the plate increases, gaps between elements soften the model significantly. This phenomenon is also compounded as the number of layers decreases. Despite this apparently poor capability of Method II, further results obtained using it will be presented in the sections to follow. Its performance in estimating natural frequencies will be seen to be fairly accurate for many cases. It is felt that Method II may find use if a better understanding of its convergence can be realized. There seems to be some correlation between the mesh size and the type of problem being solved as to maximizing the accuracy. It is felt that an acceptable element could be realized if some form of hp convergence is implemented. In other words, if the order of the polynomials used to describe the displacement field is manipulated in conjunction with the mesh size, an efficient accurate element may be developed. For

information concerning the *hp*-version of the finite element method see Holzer et al (1990) [35].

4.3 Comparisons to Known Solutions

The literature covering the past twenty years contains a lot of data on the analysis of thick laminated composite plates. A sufficient amount of 3-*D* elasticity data exists to use for comparisons due to the multitude of analysis techniques which have been developed over this period of time. This 3-*D* elasticity data is generally considered to be the exact solution to the laminate problem and is available for specific laminates and boundary conditions. It is with these solutions that authors evaluate the performance of their methods. Unfortunately, the majority of the data are static deformation solutions for various loading cases. This is not to say that there is not a fair amount of vibration and stability data available. The only data which is difficult to come by are detailed stress results based upon the mode shapes obtained from a dynamic analysis. In fact, the only stress distribution data found is in the form of small plots for just a few cases published by Noor (1989) [87, 88], (1990) [89] and (1973) [93]. Therefore, in the comparisons to follow, the majority of the data presented will be in the form of natural frequencies and critical buckling load. Also, as mentioned above in Section 4.1, the specific cases chosen for comparison were picked to represent a range of different types of laminates. It by no means represents all that is available. Also, unless otherwise specified, all finite element analysis were conducted with a quarter plate model with a 3×3 element mesh.

We will start by first discussing how we are going to compare the results of the different techniques to exact as well as to other methods. Figure 4.13 and Figure 4.14 are presented to give a feel for why direct comparison of the non-dimensionalized eigenvalues is not helpful. In these figures the actual values for the natural frequency and buckling

coefficients are so close to the exact solutions that differences are barely discernible. To overcome this problem, two different methods are typically used. One, which was already used above in Section 4.2.2, is to plot $\omega^2/\omega_{Exact}^2$ rather than the actual coefficients. The other is to plot the percent error relative to the exact solution. Both methods give very similar plots, but because the percent relative error provides a well understood measure, it will be used in the following comparisons.

The percent relative error corresponding to Figure 4.13 is presented in Figure 4.15. This data is for the four layer symmetric cross ply laminate with a layup of the form [0/90/90/0]. The differences between the different methods can easily be seen in this figure as compared to the previous. In fact, the errors are exaggerated. Included in the figure is data from a simplified higher order theory, SHOT. This method, developed by Phan and Reddy (1985) [105], uses a displacement field of the form given in eqn (3.2), and implements it into a finite element program through the use of Hermite cubic interpolation functions. The data included in Figure 4.15, including the exact solution, comes from this reference. From the figure it can be seen that Method II behaves quite poorly, while Method I, the Predictor Corrector and SHOT methods all behave similarly with about a $\pm 1\%$ error. In comparing the accuracy of the programs to predict the critical buckling load in Figure 4.16, we see something quite different. This time both Method II and the SHOT have a 3% to 4% error, while Method I is still within a 1% error.

The next case considered is the ten layered $\pm 45^\circ$ laminate. This time we see the comparison as a function of h/a . The data for this comparison was published by Noor and Burton (1990) [89]. Included this time are the results for the SHOT as well as those for a discrete layer theory and a simplified discrete layer theory. As could be expected, the discrete layer theory provides the most accurate results. The simplified discrete layer theory performs rather poorly, with only one data point on the graph. This is because

the simplified discrete layer theory, discussed by Noor [89], is assumed to be a piecewise linear displacement field with no shear correction for the individual layers. Next, the figure shows that the Predictor Corrector technique, along with Method II, remain within 1% of the true solution. Method I and the SHOT approach a 3% error as the plate thickness to width ratio becomes large. In all fairness, the improved accuracy of Method I over the SHOT is not as great in reality as shown in the figure. This is due to the fact that the mesh size used has not allowed Method I to totally converge. (See Figure 4.9.) The same can also be said about the surprising accuracy of Method II. (See Figure 4.10.)

The last comparison is conducted on the sixteen layer hybrid laminate. The results are presented in Figure 4.18. This figure is very similar to the previous figure for the ten layered $\pm 45^\circ$ laminate. This time however, all three of the methods, the Predictor Corrector, Method I and Method II, all perform better than the SHOT and the simplified discrete layer approach. These results give credence to the statement made in Section 1.5.1. With the correct shear correction factor a Mindlin type deformation field can provide as good, if not better, results when compared to a higher order approach. The bottom line is that both Method I and the Predictor Corrector approach can provide accuracies well within a 1% to 2% error.

At this point we should consider known possible reasons why Methods I and II may vary from the published exact solutions. As eluded to earlier, the boundary conditions applied in the Least Squares analysis may be a source of some variances. Recalling from Section 3.2.2, the unknowns in the problem (the degrees of freedom) were chosen to be referenced to the bottom layer. Thus, when setting the boundary conditions, say for instance setting $u_o = 0$, we are fixing this variable equal to zero for the bottom layer and not for the center of the plate, as would normally be desired. Also setting $\varphi_\alpha = 0$ on the boundary sets it equal to zero in every layer (see eqns (3.9)-(3.10)). In addition,

and probably most important, is the fact that in the process of condensing the discrete layer displacement field down to the simplified form, the variables u_o^n , v_o^n , φ_x^n and φ_y^n have lost their direct physical meaning. For instance, u_o^1 is not the membrane stretching at the center of the first layer. It is the membrane stretching of the first layer evaluated at $z = 0$ (the center of the plate). Each of the four variables, u_o^n , v_o^n , φ_x^n and φ_y^n , within a layer, represents a section of a set of curves defined throughout the whole thickness of the plate. The important point is to realize that these variables have different physical meanings as a result of the simplification process. In order to prescribe a particular displacement boundary condition, say for u , one must use the displacement fields and solve the expression for u to get one parameter, say u_o , in terms of another, φ_x . This must be done to get the correct relationship amongst the variables to achieve the desired boundary condition.

Another point to consider is the behavior of the displacement field given in eqns (3.13) when analyzing antisymmetric (even numbered layers) laminates. Looking at eqns (3.11)-(3.12) it can be seen that for these cases, u_o and v_o will have the same value for both layers on either side of the laminate centerline. This effect is not felt to be significant, especially for laminates with six layers or more. However, care should be exercised when analyzing antisymmetric laminates with just a few layers. Most importantly, stress analysis near the center of the plate should be avoided. This is because at the center of the plate the membrane stresses may be the predominant ones.

4.4 Stress Calculations

The capability of an analysis method to accurately predict the internal stress distribution through the thickness of the laminate is almost as important as its ability to predict the primary variables, whatever they may be. The intent of this section is to present some

limited data as to the ability of Method I to provide accurate through-the-thickness stress data for the case of free vibration. Method II is not considered in this analysis because it was found that the eight term quadratic displacement field which was required to achieve accuracy with this method was not sufficient to provide accurate stress distributions. It was found that Method II required at least twelve terms in the polynomial expansion before reasonable stress distributions could be realized. However, as previously pointed out, with this many terms the model becomes too stiff and inaccurate results are obtained. For this reason, stress analysis with Method II will not be discussed beyond this point. In addition, the in-plane stress analysis with the Predictor Corrector technique is essentially that of any first order technique. Therefore, aside from presenting some transverse stress results, this method will not be considered in any detail.

In performing through-the-thickness stress analysis for the free vibration problem, the magnitude of stresses can only be determined within a constant. Thus, displacements and stresses are generally presented after being normalized to unity by dividing each variable by its own maximum. This method destroys the relative magnitudes between the different variables themselves, but in keeping with what little data is available in the literature this technique will be applied except where noted. The through-the-thickness stress data will be presented for three of the cases presented in Section 4.3. The data will be presented in a series of seven plots, namely u , v , σ_{11} , σ_{22} , τ_{12} , τ_{13} and τ_{23} , all as a function of the z position through the thickness. In all of the following graphs, the horizontal grid lines correspond to the layer interfaces.

Figure 4.19 through Figure 4.22 present data for the ten layer crossply laminate. It is interesting to note that in Figure 4.19 the displacement field is seen to be very close to linear for both u and v . This fact provides justification for using a first order shear theory to model such laminates. In fact, the shape of the two curves shows why the

higher order and simplified higher order theories work so well. Thus, the stress fields plotted in the subsequent figures vary little from what would be found using these theories. The transverse shear plots in Figure 4.22 were calculated by integrating the equations of equilibrium as previously discussed. The transverse stress calculations from Method I and the Predictor Corrector technique are compared in Figure 4.22. There are some differences between the two methods which are felt to be functions of the curve fitting and differentiation methods used in the calculations. This particular case for the ten layered crossply laminate happens to be the only one where vibrational stress data could be accurately determined from graphs. Data was hand picked from enlargements of the graphs taken from an article by Noor (1973) [93]. This comparison of Method I to a 3-D elasticity solution is presented in Figure 4.24 for σ_{11} and in Figure 4.25 for τ_{13} . Note that the transverse stress is normalized with respect to the in-plane stress for this case. In subsequent work by Noor [88, 89], this is not done, and data is normalized to unity. In addition, the x - y coordinates of the location in the plate where the data is taken is not given in this particular work. In this research it was found that this ratio was dependent upon where in the plate the data was taken. For this reason, two horizontal axis are provided with Figure 4.25, one corresponding to Method I, and the other for the exact solution. The scales have been adjusted to allow for collocation of the maximum values of τ_{13} . From these two figures, Method I is seen to provide normalized stress values which fall very close, if not identically, on the exact solutions for most locations throughout the thickness of the plate. It is felt that the method used to calculate the stresses through the thickness of the plate can be improved upon through some fine tuning efforts. However, because of the lack of stress data to compare to, the effort is not possible at this time. The force-displacement finite element technique should be applied for which there is a wider range of data available.

The next series of graphs given in Figure 4.26 through Figure 4.30 are very similar to the previous set presented except this time they are for a symmetric nine layer cross-ply laminate. The same observations and statements made above apply to this series. The following set, however, is different. Figure 4.31 through Figure 4.35 are for the sixteen layer hybrid laminate and begin to show a displacement field that is somewhat piecewise continuous. This type of displacement field can still be modeled with a great deal of accuracy with a first order or a higher order displacement field. Stresses would vary somewhat but not significantly. The real difference is found in the τ_{12} plot in Figure 4.33. Note that the shear stress is no longer a smooth function as in the previous plots. This is because of the $\pm 45^\circ$ layers in this laminate. This phenomenon emphasizes the fact that if a laminate is to carry in-plane shear, then it is wise to put in several layers of other than 0° and 90° layers. In doing so, one will reduce large interlaminar shear stresses.

4.5 Conclusions From Method Evaluation

The performance of the Predictor Corrector technique and the Least Squares methods is very good. The Predictor Corrector approach has the capability to extend the performance of the simple Mindlin isoparametric element to exceed that of higher order and simplified higher order theories. The ability to do so rests upon the ability to calculate accurate shear correction coefficients. In this study a method was developed to calculate accurate coefficients for the purpose of demonstrating the technique but was limited to rectangular elements. The method also required a finer mesh for accurate results than may be required using some other techniques. All in all, the Predictor Corrector technique has the potential for being an accurate, computationally cheap method to analyze fiber reinforced composite laminates.

The Least Squares methods also have the ability to perform very well in analyzing

composite laminates. Method I exhibits better convergence characteristics than Method II, making it the immediate choice to use. However, Method II has the potential of possibly being improved through some form of hp -convergence finite element technique. If this is the case, its low number of degrees of freedom give it the potential to be computationally attractive. Method I of the Least Squares technique can give very accurate results, very efficiently, for composite laminates. Its performance is slightly better than the higher order or simplified higher order approaches.

Of particular significance is the ability of the Least Squares method to approximate a C^1 continuous element. The Least Squares element has many advantages over current methods used to solve the C^1 continuity problem, and it can be extended to other applicable areas where this problem exists. The Least Squares element is not in any way limited to the composite laminate problem.

CHAPTER V

NATURAL FREQUENCY AND STABILITY STUDIES FOR LAMINATED COMPOSITE PLATES

5.1 Study Approach

The effect of optimizing the behavior of a laminated fiber reinforced composite plate is an issue which has not been addressed in detail over the past twenty years. The majority of the work in this area, relative to vibration and stability, has been to show simply what effect ply angle has on natural frequency or buckling load for different a/b ratios. It is well accepted that for a square simply supported plate, the natural frequency is maximized for $\theta = \pm 45^\circ$. If the aspect ratio of the plate changes, so does the value of the angle which maximizes the frequency. This behavior is accepted and makes logical sense. Studies of this type have been published by Whitney and Leissa (1969) [143], Bert (1977) [12], Khdir (1988) [50] and Grenestedt (1989) [29] to name a few. It should be stated that some of these studies considered only thin plate theory. This phenomenon will be seen in some of the data to follow. In addition, a typical study found in the literature will consider the frequency not only as a function of θ and a/b , but it will also vary the plate thickness ratio, a/h , and ratio of anisotropy, E_1/E_2 . Also, Liew et al (1989) [64] have presented similar studies for triangular plates. Some studies have limited the number of variables which were considered. For instance, Jones (1973) [40] studied only the effect of a/b and the number of layers on vibration and buckling of cross ply laminates. Buckling

coefficient studies are not as common as vibration studies but are available. Reddy and Phan (1985) [117] and Whitney and Leissa (1969 [143] present graphs of critical buckling load as functions of θ and a/b , while Noor (1974) [94] presents buckling coefficients as functions of E_1/E_2 , h/b , as well as for various values of a/b . Studies including pre-stress effects on plate natural frequency are the least common. Dawe and Craig (1986) [25] looked at pre-stress effects on natural frequency while varying thickness and aspect ratios. Chelladurai et al (1984) [20] have looked at fiber orientation and pre-stress for different aspect ratios, but did so only for single layer lamina. Studies of these types are by no means limited to the ones mentioned above. Many more exist, and the ones listed are intended to provide some basic references to the work that has been done.

One can see from the above discussion that to study the optimization of the fundamental frequency and/or buckling load is not a simple prospect. There are a wide range of variables involved. One could consider ply angle, stacking sequence, material properties, thickness ratios, aspect ratios, boundary conditions and different combinations of pre-stress. A full mathematical optimization study would be insurmountable. At best we can only try to understand how these variables each effects the behavior of the plate. The design engineer, with a basic understanding of how they all influence laminate behavior, can then begin to optimize his design. The intent of this chapter is to present some parametric studies to establish some new understanding into how some of these parameters effect the vibration and stability of laminated composite plates. The study will not attempt to reproduce findings already available in current literature, but it will try to provide some new insight into laminate behavior.

For the following study we will hold the material properties, thickness ratio and number of layers as constants. In other words, we will study a laminate consisting of a fixed number of layers with the material properties and plate thickness ratio also being held as constant.

Table 5.1: Ply Angle Analysis Data/Figure* Correlation Grid.

CASE	BNDRY COND	FREE VIB	PRE- STRESSED VIB†	UNIAXIAL BUCKLING $N_y = 0$	BIAXIAL BUCKLING $N_x = N_y$
A $a/b = 0.7$	6	5.1	5.2	5.1	5.1
	13	5.3	5.4	5.3	5.3
B $a/b = 1.0$	6	5.5	5.6	5.5	5.5
	13	5.7	5.8	5.7	5.7
C $a/b = 1.43$	6	5.9	5.10	5.9	5.9
	13	5.11	5.12	5.11	5.11
D $a/b = 1.7$	6	5.13	5.14	5.13	5.13
	13	5.15	5.16	5.15	5.15

*Numbers indicate Figure number data is displayed in.

†See Table 5.2 for the definitions of the four pre-stressed vibration cases.

The aspect ratio will vary along with the ply angle and boundary conditions. Specifically, the study will look at a six layered laminate with the properties of Material II. The thickness ratio, b/h , was chosen to be 10. The layup is established as $[+\theta/-\theta/+\theta\dots]$, where θ will be varied. The aspect ratios considered will be $a/b = 0.7, 1.0, 1.4286$ and 1.7 . Boundary conditions considered were simply supported and clamped. (All four sides the same.) Data was calculated for the free vibration natural frequencies, critical uniaxial and biaxial buckling loads and natural frequencies for four pre-stress cases. The pre-stress cases were defined relative to the lowest uniaxial buckling load for each case. Two pre-stress loads, one 50% and one 85% of the lowest uniaxial buckling load, were used for both the uniaxial and biaxial pre-stress conditions giving the four pre-stress cases (see Table 5.2). A tabular form of the data collected is presented in Table 5.1. The table also provides the number of the figure on which the data appears.

Table 5.2: Ply Angle Analysis Pre-stress Conditions.

NOMENCLATURE	N_x	N_y
PS1A	$0.50 N_{min}$	0
PS1B	$0.85 N_{min}$	0
PS2A	$0.50 N_{min}$	$0.50 N_{min}$
PS2B	$0.85 N_{min}$	$0.85 N_{min}$

Note: N_{min} indicates the lowest uniaxial buckling load.

5.2 Initial Data Trends

All of the results for cases A, B, C and D are presented in the next series of sixteen figures. Four figures are provided for each aspect ratio. From Figure 5.1 and Figure 5.2 we see that the natural frequency for free vibration and all of the pre-stress cases, as well as the uniaxial and biaxial buckling loads, are all maximized at a value of θ equal to about 32° . This is for Case A and the simply supported boundary condition. For the clamped boundary condition, Figure 5.3 and Figure 5.4 show that, even though the natural frequency is maximized at this same point, the two buckling cases have shifted. The uniaxial buckling load is maximized at about 28° , while the biaxial buckling load is maximized around 39° . The data for the square laminate, case B, is presented in Figure 5.5 through Figure 5.8. Note similar trends here, except that the natural frequencies and biaxial buckling load will be maximized at 45° . One other interesting observation will be made at this time and will continue to be observed in future graphs. We see that in Figure 5.6 the natural frequency curves are bell shaped curves for the 50% buckling loads but are parabolic for the 85% cases. This phenomenon even causes two of the curves to cross over one another for small and large values of θ . This will not be discussed here but merely noted. Moving on to Figure 5.9 and Figure 5.10, we now see that the point at which the uniaxial buckling load is maximized is still around 30° , while the biaxial buckling load and free vibration natural frequency are maximized between 50° and 60° . The pre-stressed vibration cases are all

maximized around 60° . For the clamped boundary conditions Figure 5.11 shows similar results with the exception that the natural frequency does not fall off at the higher ply angles but continues to rise. This increase is negligible, however. Figure 5.12 shows that the pre-stress cases are all maximized around 67° . Again, notice in this figure the sharp drop off in the natural frequency for the two high pre-stress cases. Case D, presented in Figure 5.13 through Figure 5.16, shows the same trends as found for Case C.

5.3 Effects of Plate Aspect Ratio

We can plot all of the data presented in Figure 5.1 through Figure 5.16 in such a way as to more clearly show the effect of plate aspect ratio. For instance, Figure 5.17 shows the free vibration frequencies for the simply supported cases. From this figure we can clearly see how, as the aspect ratio of the plate increases, the optimum θ moves towards the right. This is the trend discussed earlier. This trend is also visible in Figure 5.18 for the clamped cases. Figure 5.19 shows an interesting result. The optimum θ for the uniaxial buckling load does not change with aspect ratio for the simply supported cases. In addition, after the maximum buckling load is achieved, the buckling load is the same for all aspect ratios. For the clamped plates, Figure 5.20 shows that the optimum theta does vary slightly, as do the buckling loads past the optimum θ . For the biaxial buckling loads, Figure 5.21 shows that the optimum value of θ follows trends similar to the natural frequency, as shown in Figure 5.17. It is interesting to note that after the optimum theta is achieved, the buckling loads converge to the same values regardless of the aspect ratio.

5.4 Effects of Pre-Stress on Fundamental Frequency

The effects of pre-stress on the fundamental frequency of simply supported and clamped plates can be seen in the previous figures. Looking back, Figure 5.8 represents a typical

example of such a plot. It is no surprise that the natural frequency of the plate decreases with increased pre-stress load. It is of interest, however, that the shape of the curve changes as the pre-stress load is increased. As mentioned previously, for the larger pre-stress loads the curve no longer maintains a bell shaped curve but more parabolic, and it drops off rapidly at the ends. This trend becomes important when considering the case given in Figure 5.16. If a design engineer wants to choose the optimum θ to maximize the free vibration natural frequency for this particular aspect ratio plate, he would be led to pick $\theta = 90^\circ$. If the plate becomes significantly loaded either uniaxially or biaxially, then serious degradation in the vibration characteristics would occur. Clearly a better choice of θ would be 65° for this case. The important point is the following: In optimizing natural frequency, one should consider the loading conditions which will be present on the laminate in operation, as well as the boundary conditions.

5.5 Optimization of Fundamental Frequency and Buckling Loads

From the above study one can see that optimizing the vibrational and stability characteristics of a laminated composite can become a complicated task. In fact, optimization of one parameter may lead to poor performance in another. For instance, consider the simply supported condition for Case D, presented in Figure 5.13. If the ply lay-up angle is chosen to be 60° , then both natural frequency and biaxial buckling loads are very near their maximum. However, the uniaxial buckling capability of the plate has been reduced by approximately 43%. If we choose a ply lay-up angle of 30° , then the uniaxial buckling capability is maximized, while the fundamental frequency and biaxial buckling load have been degraded by 21% and 38% respectively.

From the above analysis we conclude that the 60° lay-up angle is best from a vibration and biaxial buckling point, while a 30° angle maximizes the uniaxial buckling capability.

One may wonder if better overall performance could be achieved if both 60° and 30° plies were used in the laminate. If we consider a laminate of the form $[-60/ + 30/ - 30]_{AS}$, we find the non-dimensional natural frequency becomes 12.6, while the uniaxial and biaxial coefficients become 27.1 and 12.1 respectively. These numbers translate to a 10% reduction in natural frequency, a 19% reduction in biaxial buckling and a 19% reduction in uniaxial buckling capability. Another option would be to consider a laminate of the form $[-30/ + 60/ - 60]_{AS}$. For this lay-up we find the natural frequency and the uniaxial and biaxial coefficients are 11.8, 27.7 and 10.7 respectively, corresponding to 15.6%, 17.3% and 11.8% reductions from their individual maximums. For a final case, consider a twelve layer laminate of the same thickness. The lay-up is chosen to be $[-60/ - 30/ + 60/ + 30/ - 60/ - 30]_{AS}$. This time we find a non-dimensional natural frequency of 12.9 and buckling coefficients equal to 29.3 for the biaxial case and 11.6 for the uniaxial. These numbers correspond to 7.7%, 12.4% and 21.4% reductions in capabilities. This last case, however, has introduced a new variable, the number of layers, which we have purposefully avoided.

The specific numbers and percentages in the above crude analysis are not meant to provide hard and fast numbers, but they are intended to provide insight into how the natural frequency and critical buckling loads can be affected by ply angle and stacking sequence. The design engineer has countless combinations of these and other parameters to consider. In designing a pressure vessel, a biaxial state stress may be such that $N_x = 2N_y$. For such a case the optimum design would be different yet. One important point which must be made here is that the behaviors observed in Figure 5.1 through Figure 5.22 are for a laminate with a specific number of layers, thickness ratio and set of material properties. If any of these are changed, the trends established above could either be eliminated or accentuated. In addition new trends could be observed.

5.6 General Observations and Conclusions

After investigating the behavior of laminated composite plates for many different cases, some not presented in this research, several conclusions have been reached concerning optimizing design. First of all, the optimization of the performance of a laminated composite plate is not a simple process. Some basic rules always apply. To maximize the natural frequency or buckling load of specific laminate for a given aspect ratio and set of boundary conditions, some ply angle will be optimum. The more plies which are at this angle, the better. If there are a fixed number, and the laminate contains other angles also, the frequency is increased if the optimum angle plies are moved towards the top and bottom of the laminate. Next, the optimum angle for the lamina is dependant upon many factors including boundary conditions, aspect ratio and number of layers. To optimize a specific laminate, the specific conditions under which it will be subjected must be considered. Also of great importance, the optimum ply angles and stacking sequence for maximizing the natural frequency will not be the same required to maximize the buckling loads. Finally, pre-stress can have a significant effect on the frequency of a laminated plate, and the effect must be investigated for the specific case.

CHAPTER VI

CONCLUSIONS AND RECOMMENDATIONS

The work conducted for this research has shed new light upon the effectiveness of different analysis methods used on fiber reinforced composite plates. The trend towards increased accuracy is driving the analysis methods to more computationally intensive approaches. This need not be the case, especially in the area of thick composite laminates. The Predictor Corrector technique, implemented together with the finite element method and the Least Squares elements, are just two ways in which accurate results can be realized for little more effort than for a simple Mindlin plate element. Results obtained using these methods can be every bit as accurate as techniques with increased complexity and many more degrees of freedom.

Of major importance, the Least Squares elements are not limited to analyzing laminated composite plates. The Least Squares elements developed in this work have been shown to be a numerically effective method to approximate a C^1 continuous element. This is an important contribution to the finite element field and can be applied in any situation where C^1 continuity is required. In reality, the Least Squares technique could be extended to even higher orders of continuity with the proper choice of functions describing the primary variables.

The work performed here in developing the Least Squares methods needs to be extended in further research. The element from Method I should be immediately implemented into a static force-displacement finite element program. In doing so, one would

also develop moment curvature relations and plate constitutive equations. Such relationships would be necessary to implement force and moment boundary conditions, and to interpret force results. With the increased data available in the literature, better through-the-thickness stress comparisons can be made allowing fine tuning to be done to the stress calculations. Doing this would also provide more validation data for the technique. Modification of Method II, through the use of an *hp*-convergence technique, should also be investigated. Finally, a more thorough convergence study should be conducted to fully understand the Least Squares method.

Also included in this work was data showing the relationships of ply lay-up angle, boundary conditions and plate aspect ratio on natural frequency and buckling loads. The effect of pre-stress on the natural frequency was also included. Several interesting behaviors were documented but are restricted to a specific thickness ratio, number of layers and type of material. More work of this type needs to be conducted especially in areas not common in the literature. More studies into the effects of boundary conditions, pre-stress and simultaneous optimization of natural frequency and buckling loads must be conducted. In addition, all of these studies should begin to look at the stress distributions through the thickness of the laminates so that propensities towards delamination can be considered.

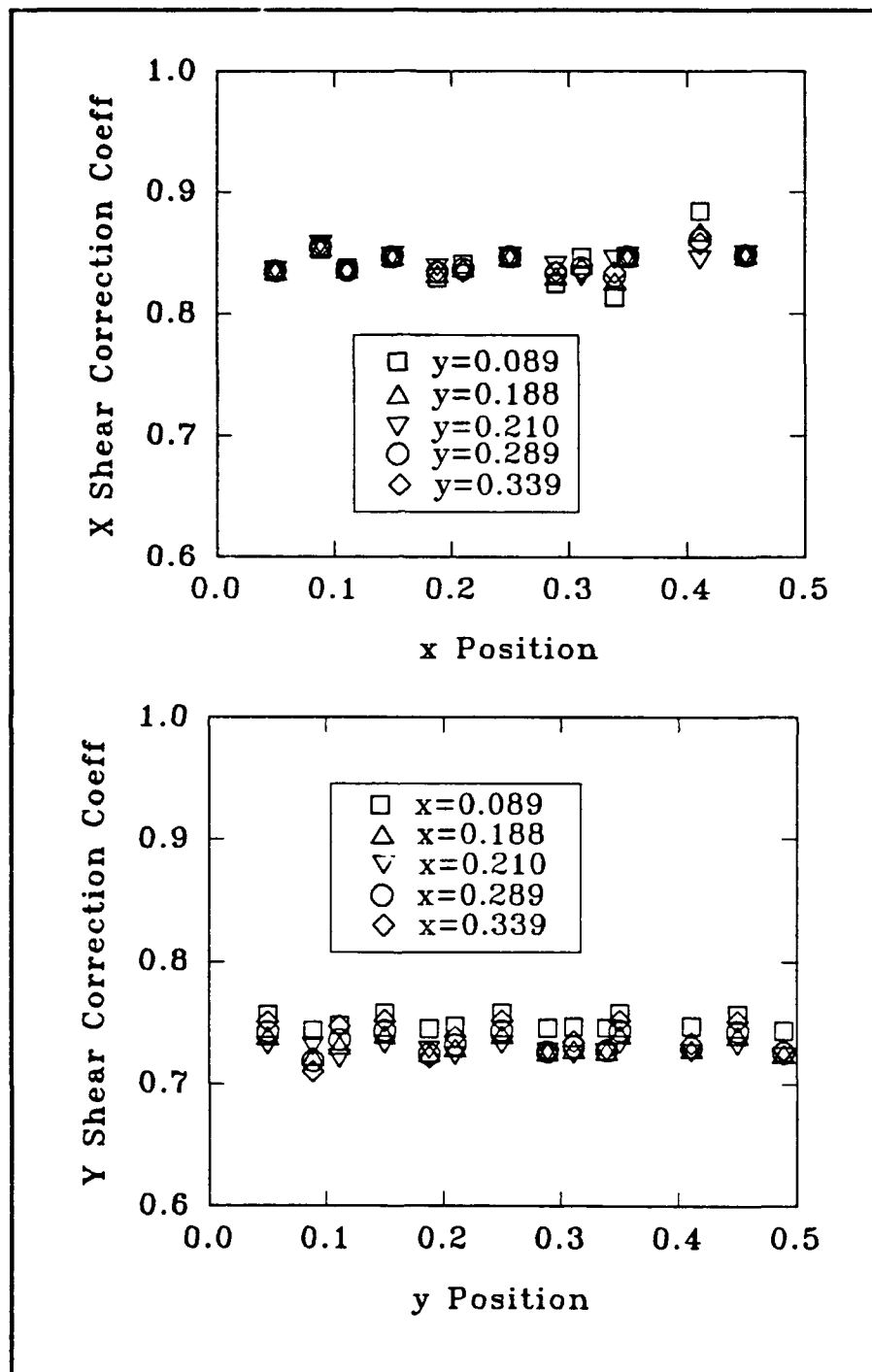


Figure 4.1: Shear Correction Coefficient Variation Across Plate. Material I $a/b = 1$, 9 layer, $[90/0/90/0/\dots]$, $h/b = 0.2$, BC-1, 5×5 quarter plate model.

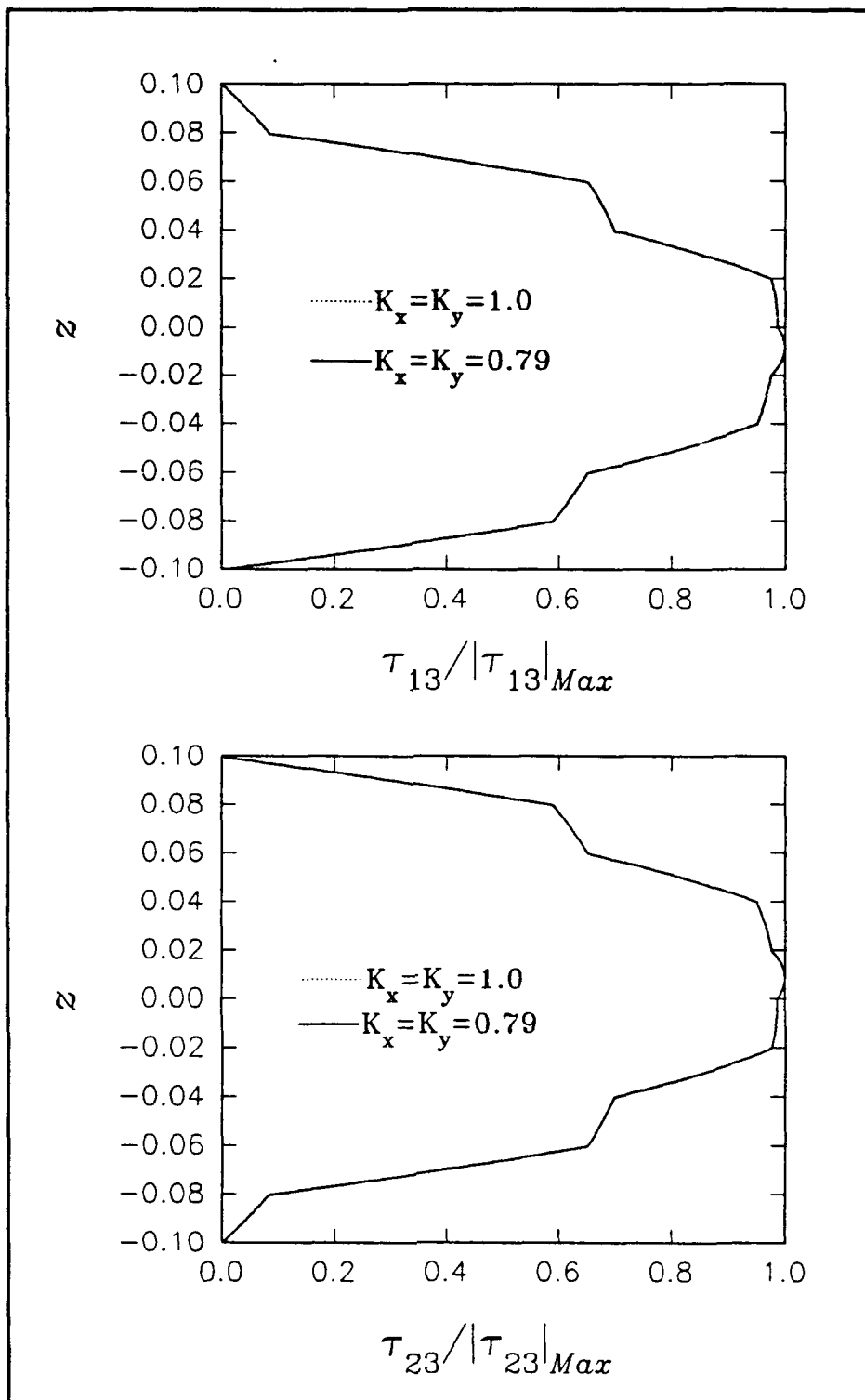


Figure 4.2: Comparison of Transverse Shear Stress with Different Shear Correction Factors. Material I $a/b = 1$, 10 layer, $[90/0/90/0/\dots]$, $h/b = 0.2$, BC-1, 3×3 quarter plate model.

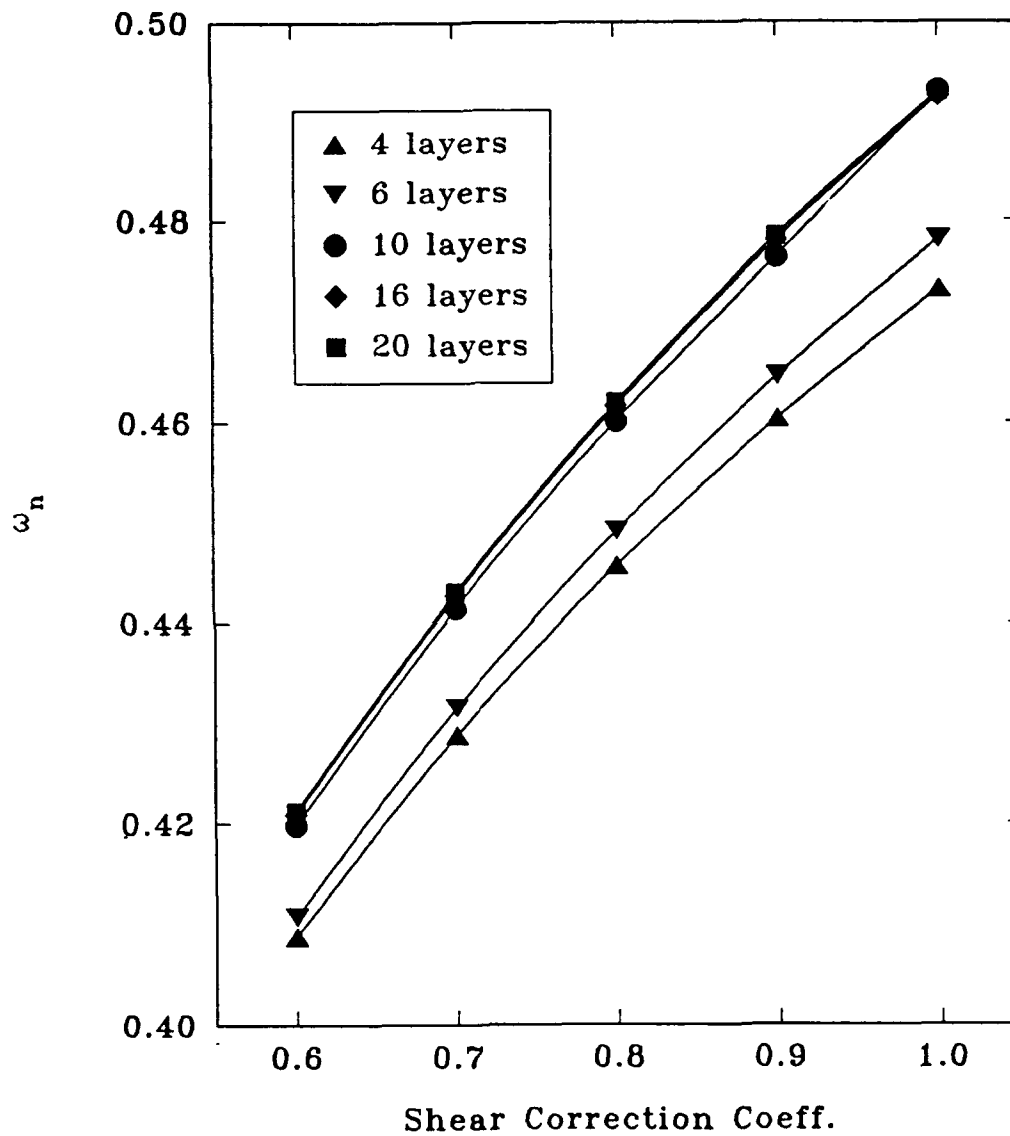


Figure 4.3: Sensitivity of Natural Frequency to Shear Correction Coefficient. Cross ply laminate, Material II $a/b = 1$, $h/b = 0.2$, BC-1, 3×3 quarter plate model.

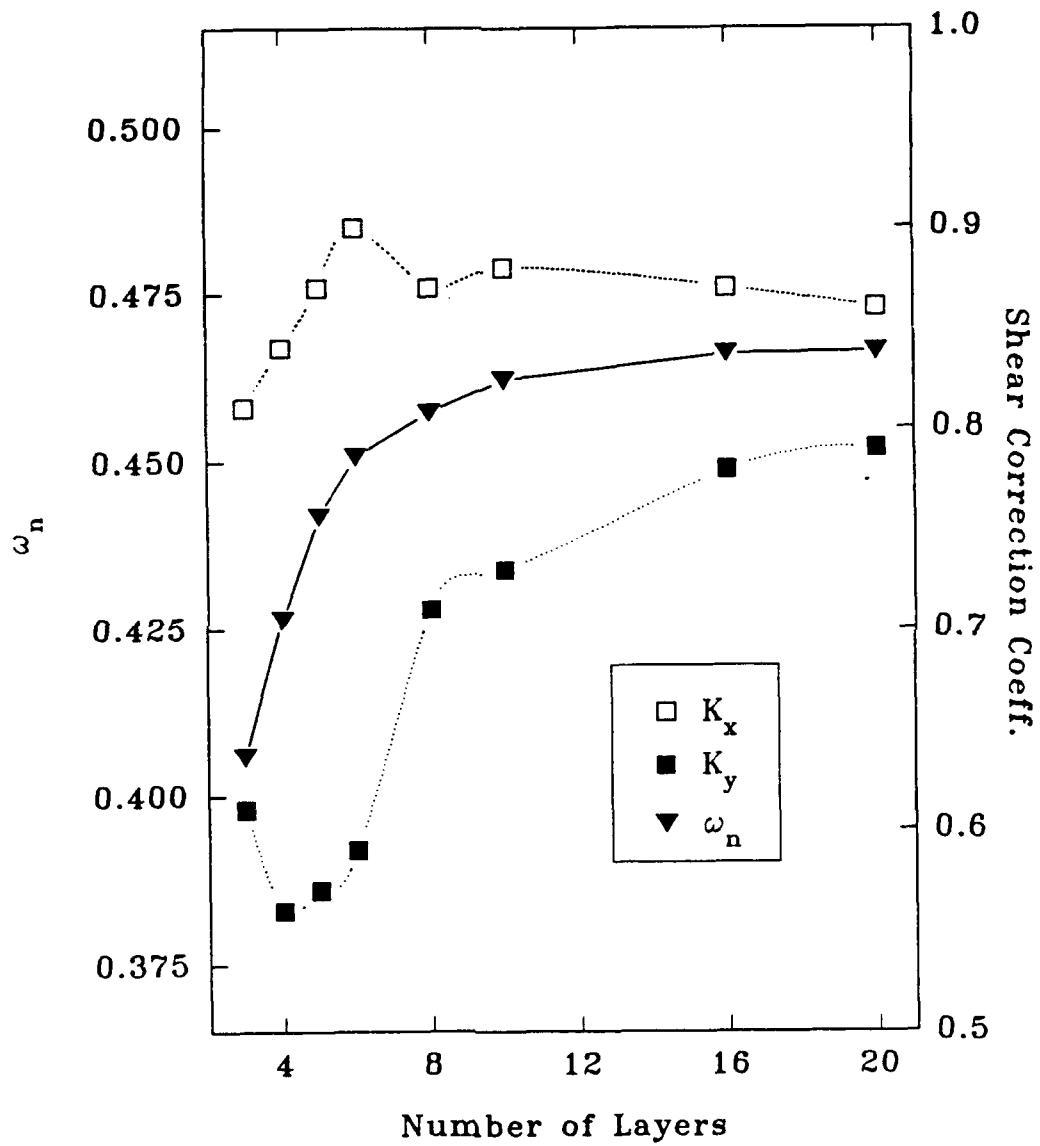


Figure 4.4: Variation of Shear Correction Coefficients with Number of Layers. Cross ply laminate, Material II $a/b = 1$, $h/b = 0.2$, BC-1, 4×4 quarter plate model.

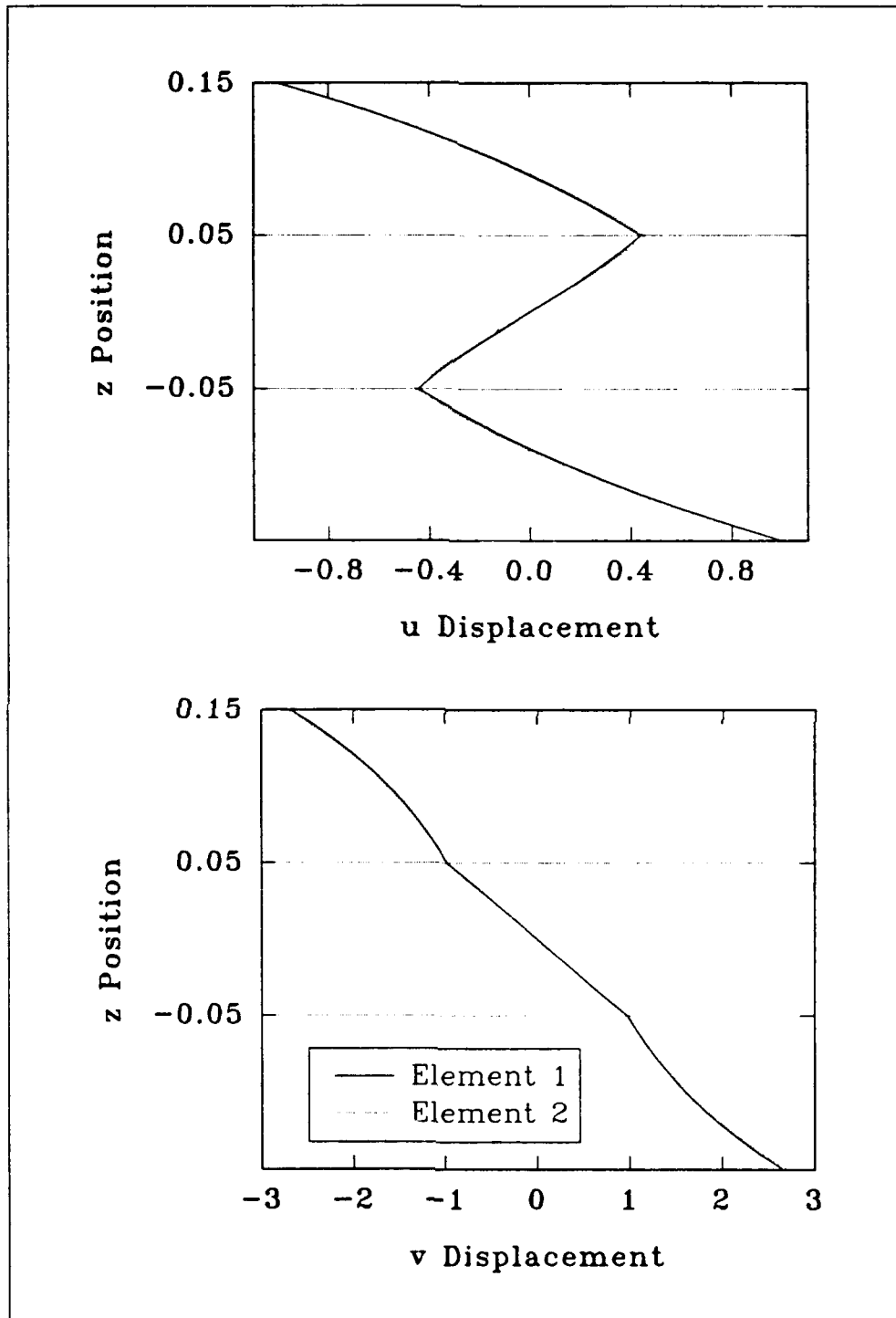


Figure 4.5: Method I Interelement Compatibility. [0/90/0] simply supported $a/b = 1$, Material III, $b/h=4$, Location: $x = 0.16667$, $y = 0.133333$, 3×3 quarter plate model.

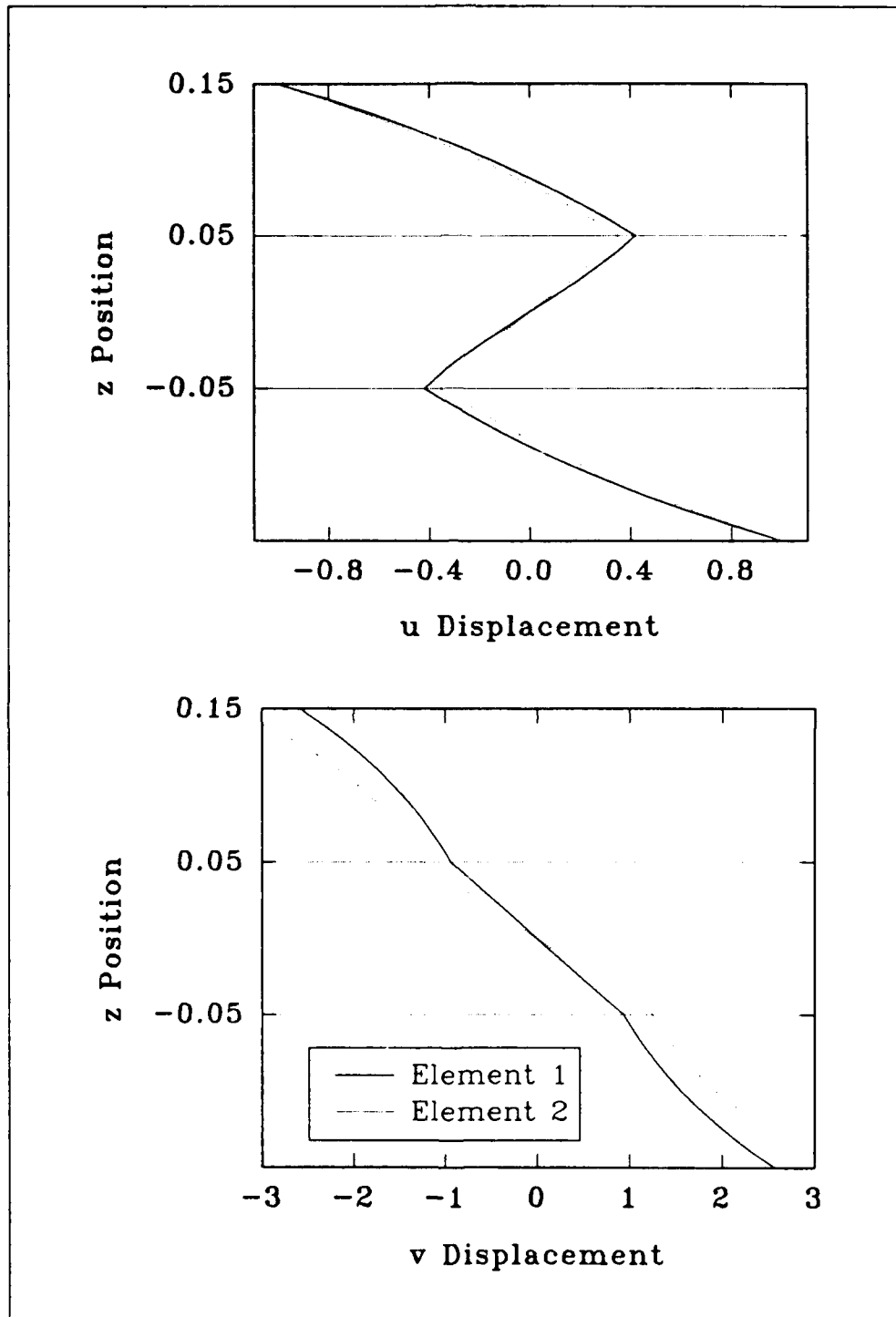


Figure 4.6: Method II Interelement Compatibility. $[0/90/0]$ simply supported $a/b = 1$, Material III, $b/h=4$, Location: $x = 0.16667$, $y = 0.133333$, 3×3 quarter plate model.

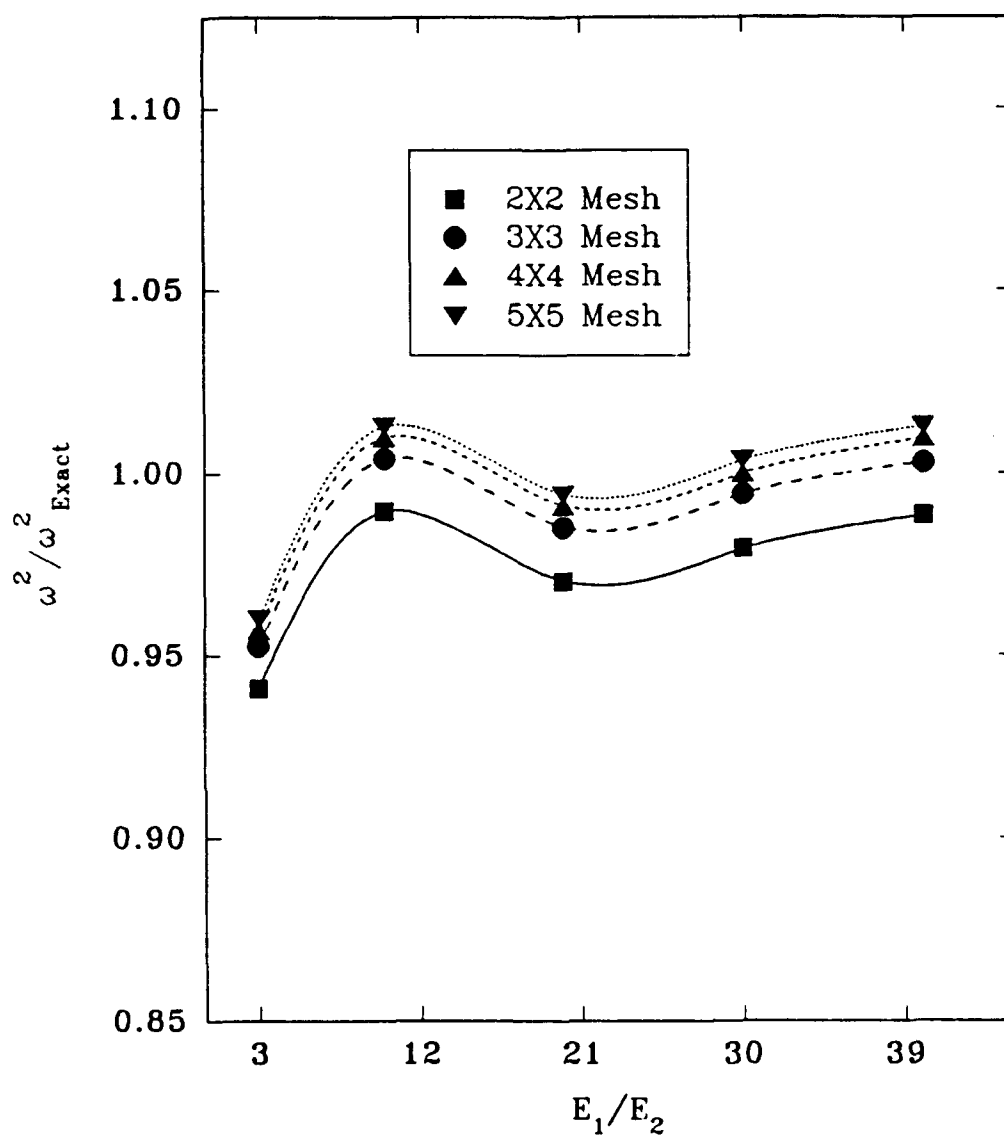


Figure 4.7: Method I Convergence. [0/90/90/0] simply supported (BC-1), $a/b = 1$, Material VII, $b/h=5$, quarter plate model.

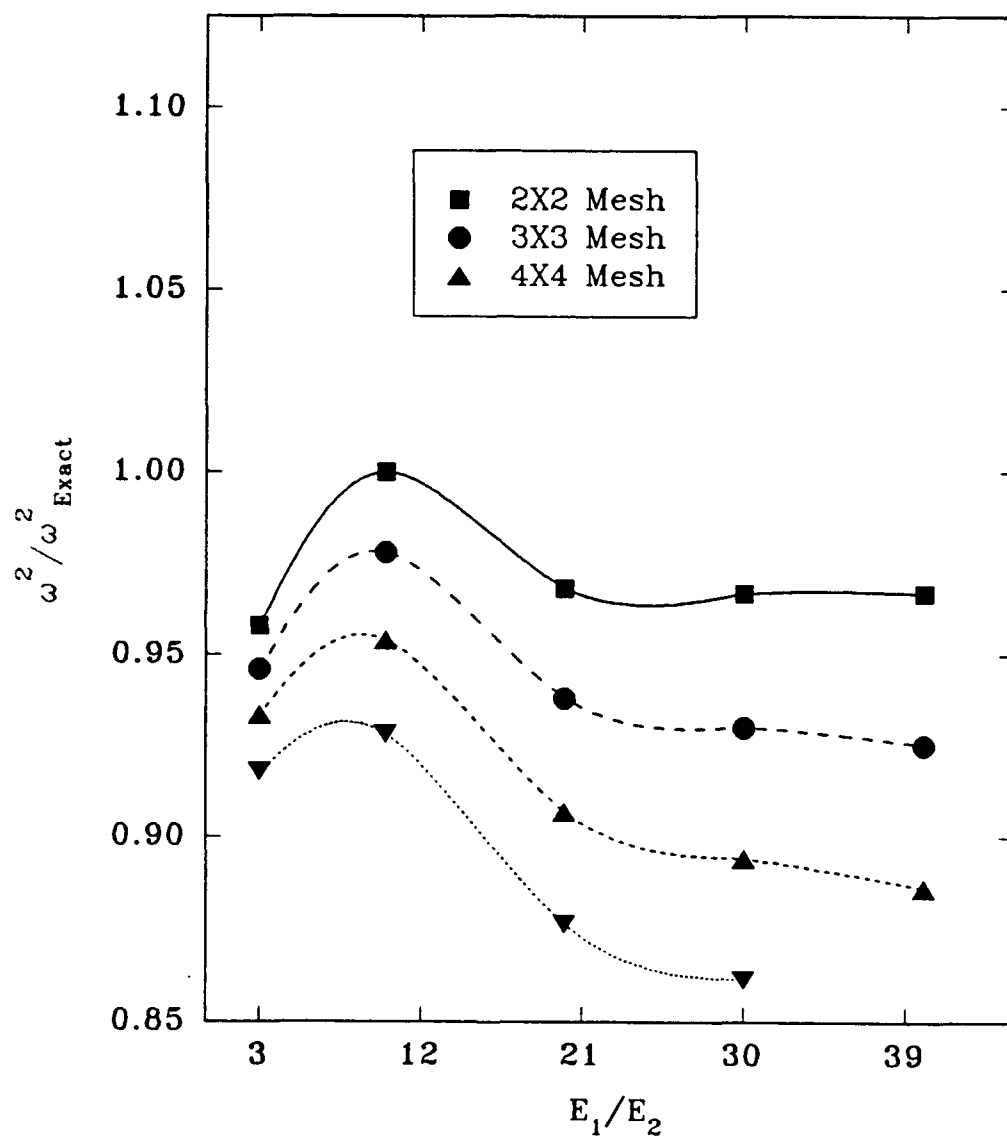


Figure 4.8: Method II Convergence. $[0/90/90/0]$ simply supported (BC-1), $a/b = 1$, Material VII, $b/h=5$, quarter plate model.

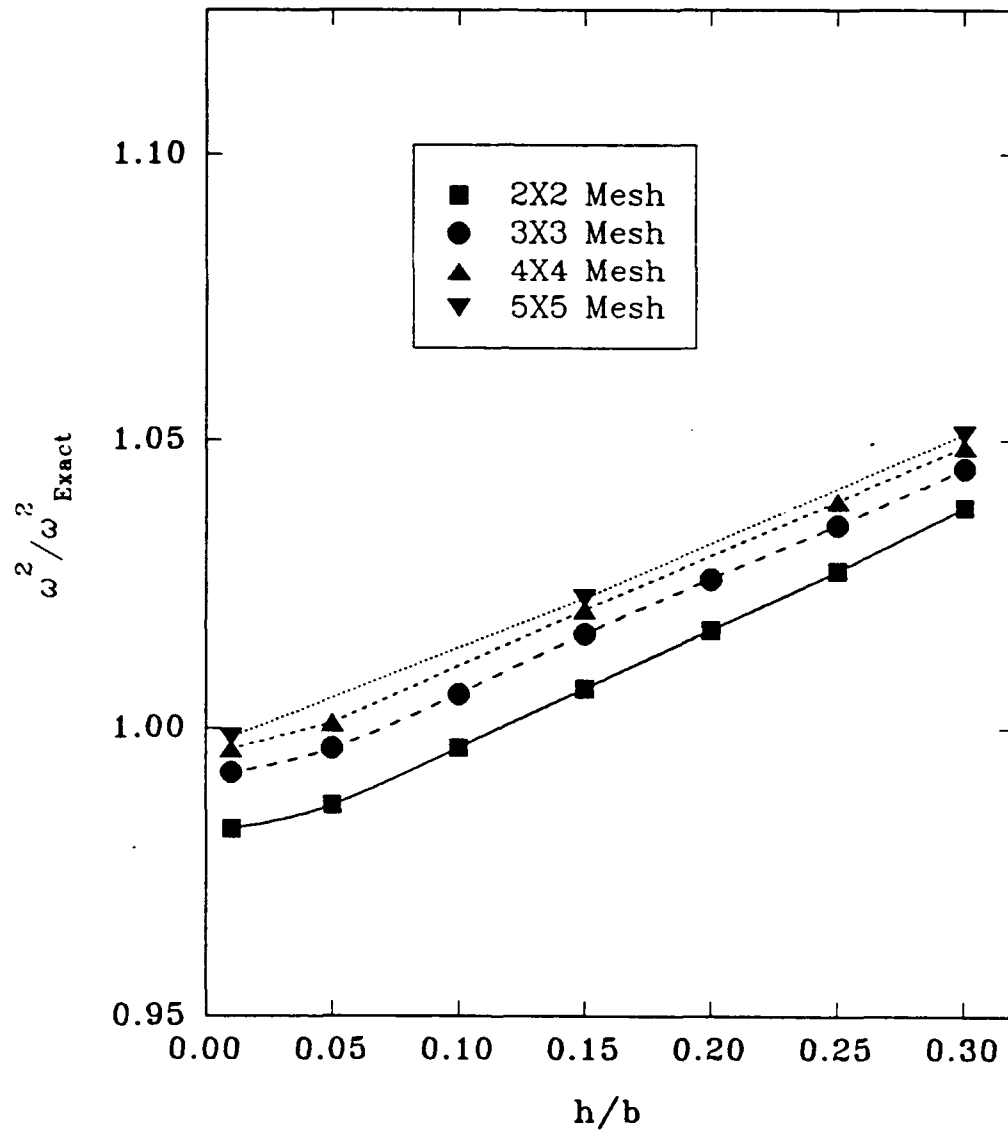


Figure 4.9: Method I Convergence. Ten layer $[-45/ + 45/ - 45/ \dots]$ simply supported (BC-1), $a/b = 1$, Material I, quarter plate model.

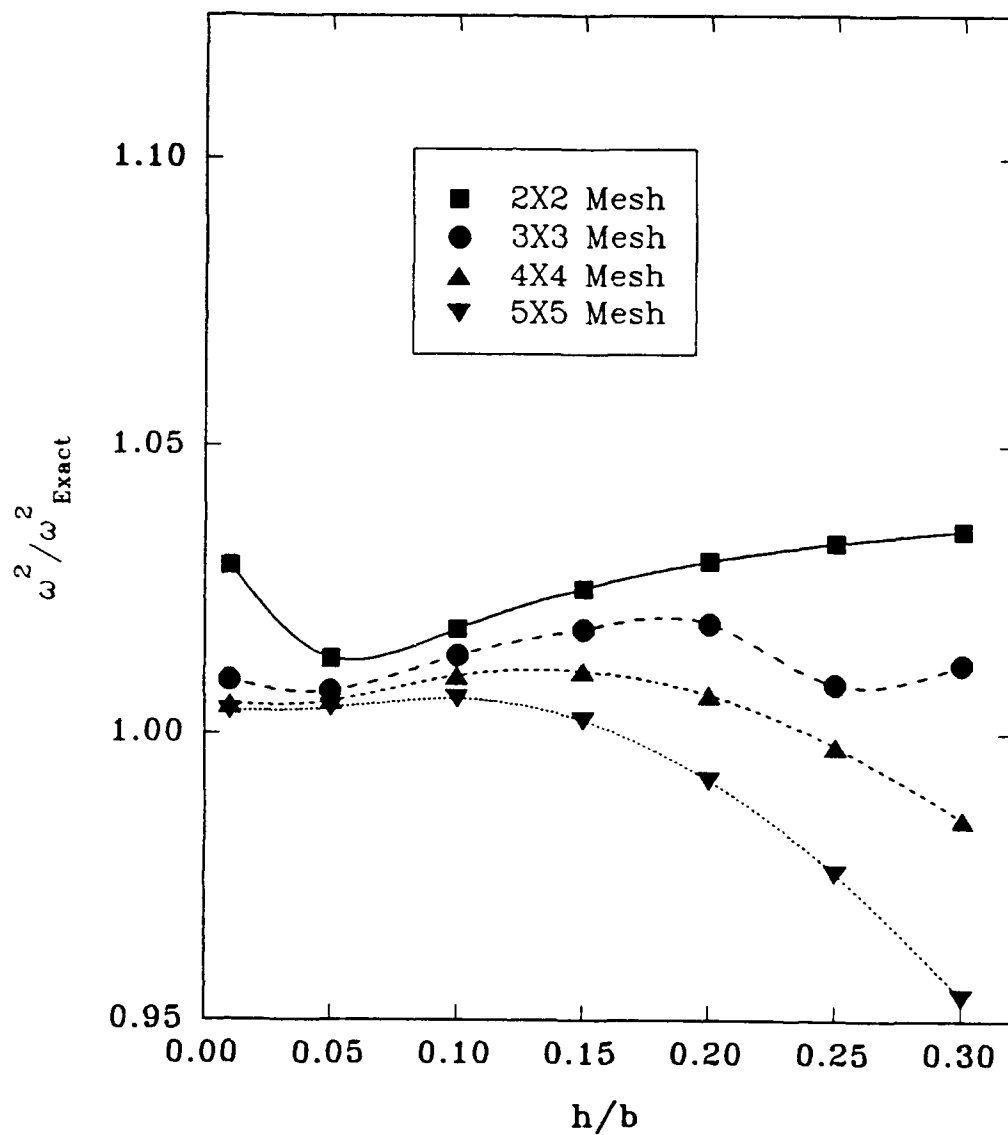


Figure 4.10: Method II Convergence. Ten layer $[-45/+45/-45/\dots]$ simply supported (BC-1), $a/b = 1$, Material I, quarter plate model.

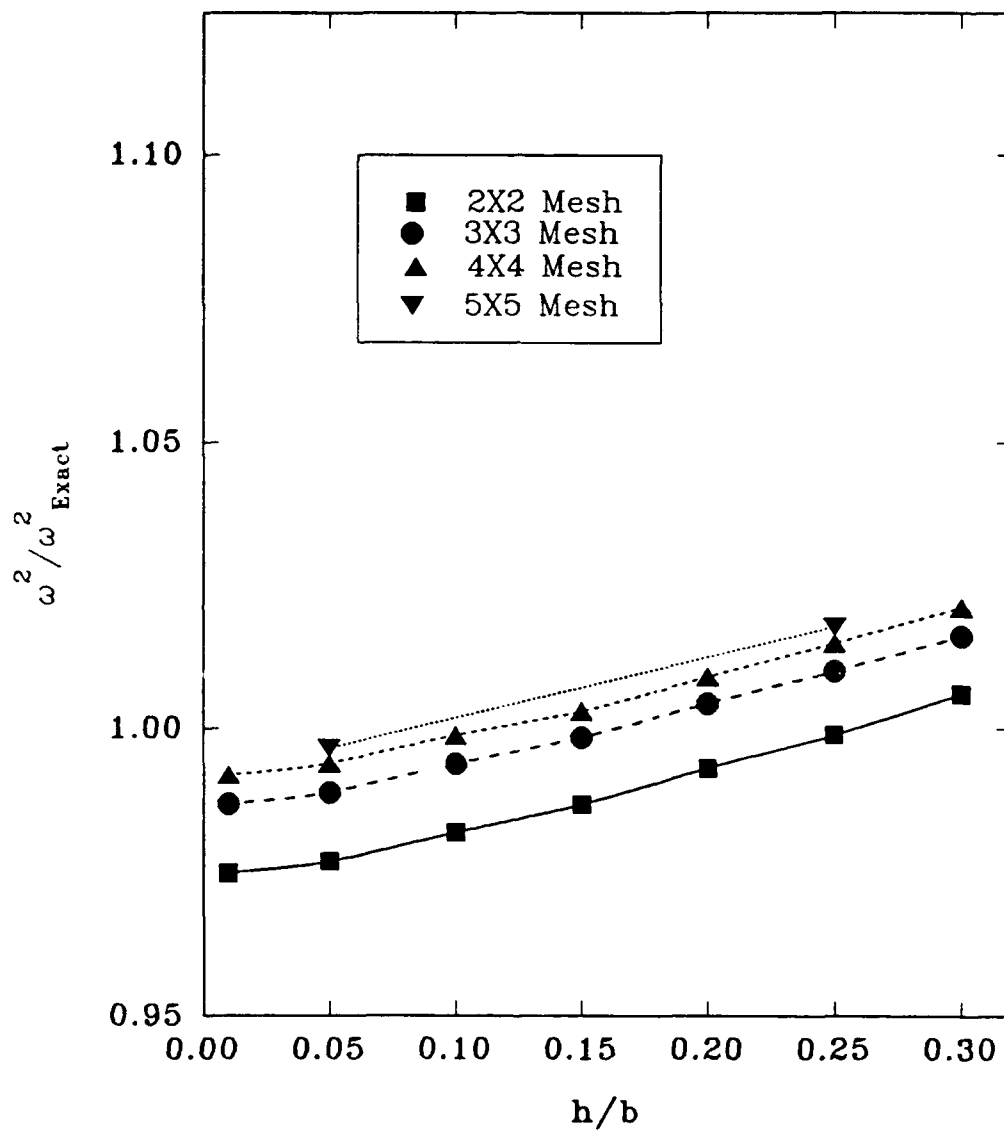


Figure 4.11: Method I Convergence. 16 Layer Hybrid- Materials IV & V, simply supported (BC-1), $a/b = 1$, quarter plate model.

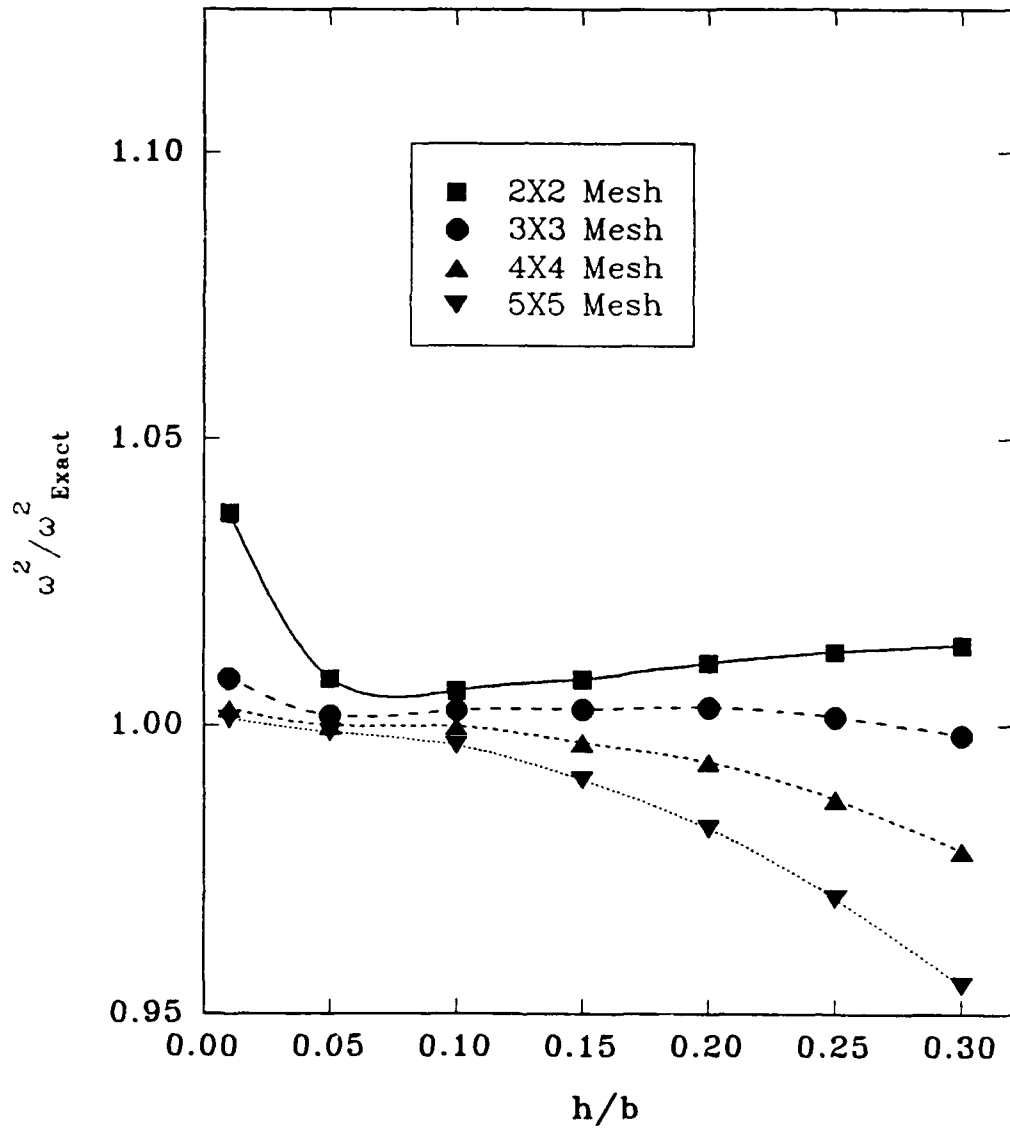


Figure 4.12: Method II Convergence. 16 Layer Hybrid- Materials IV & V, simply supported (BC-1), $a/b = 1$, quarter plate model.

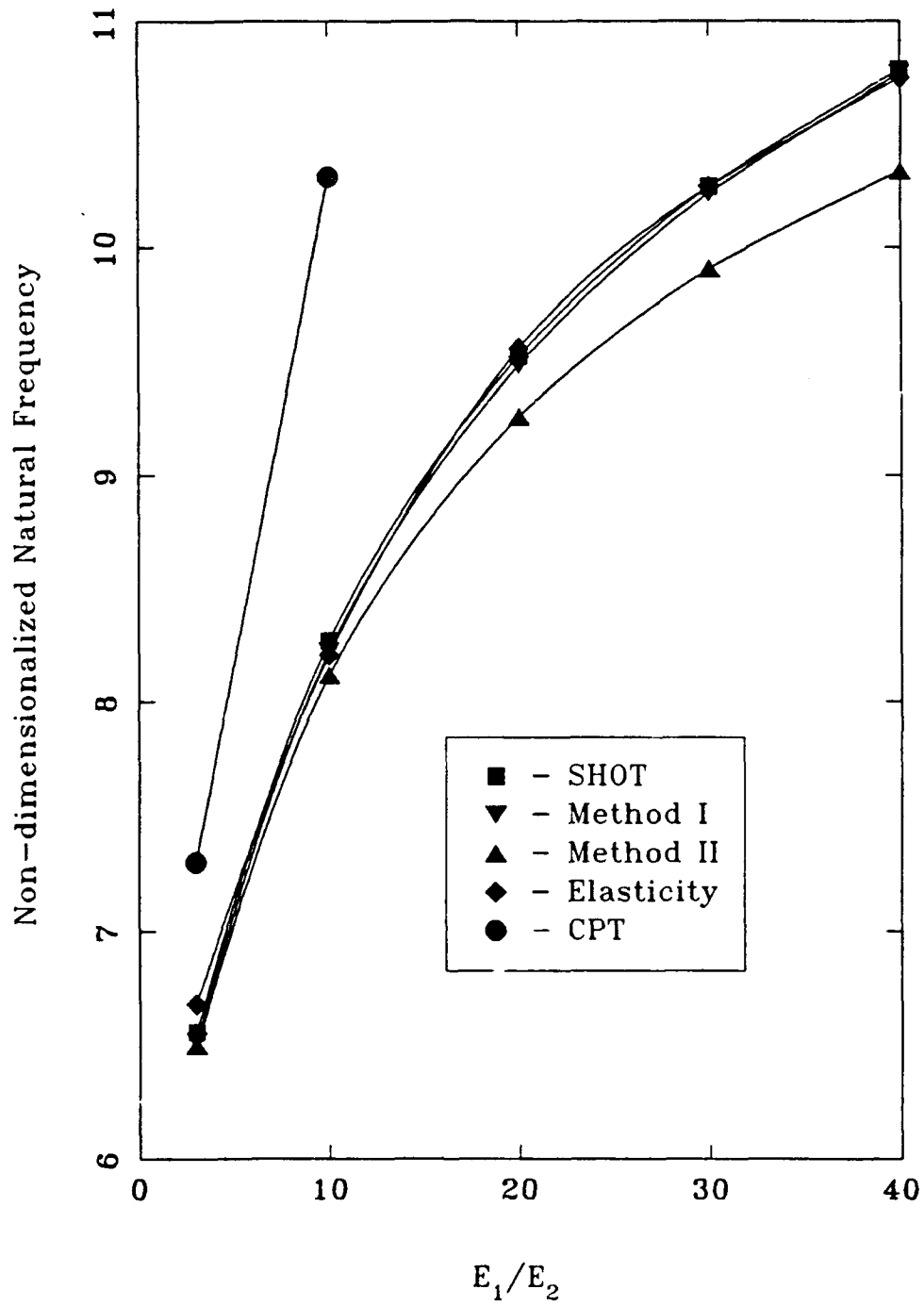


Figure 4.13: Method Comparison of Non-dimensional Natural Frequency -vs- Anisotropy Ratio. [0/90/90/0], Material VII, $b/h = 5$, $\omega_n = (\omega b^2/h) (\rho/E_2)^{1/2}$, $a/b = 1$, Simply supported (BC-1)

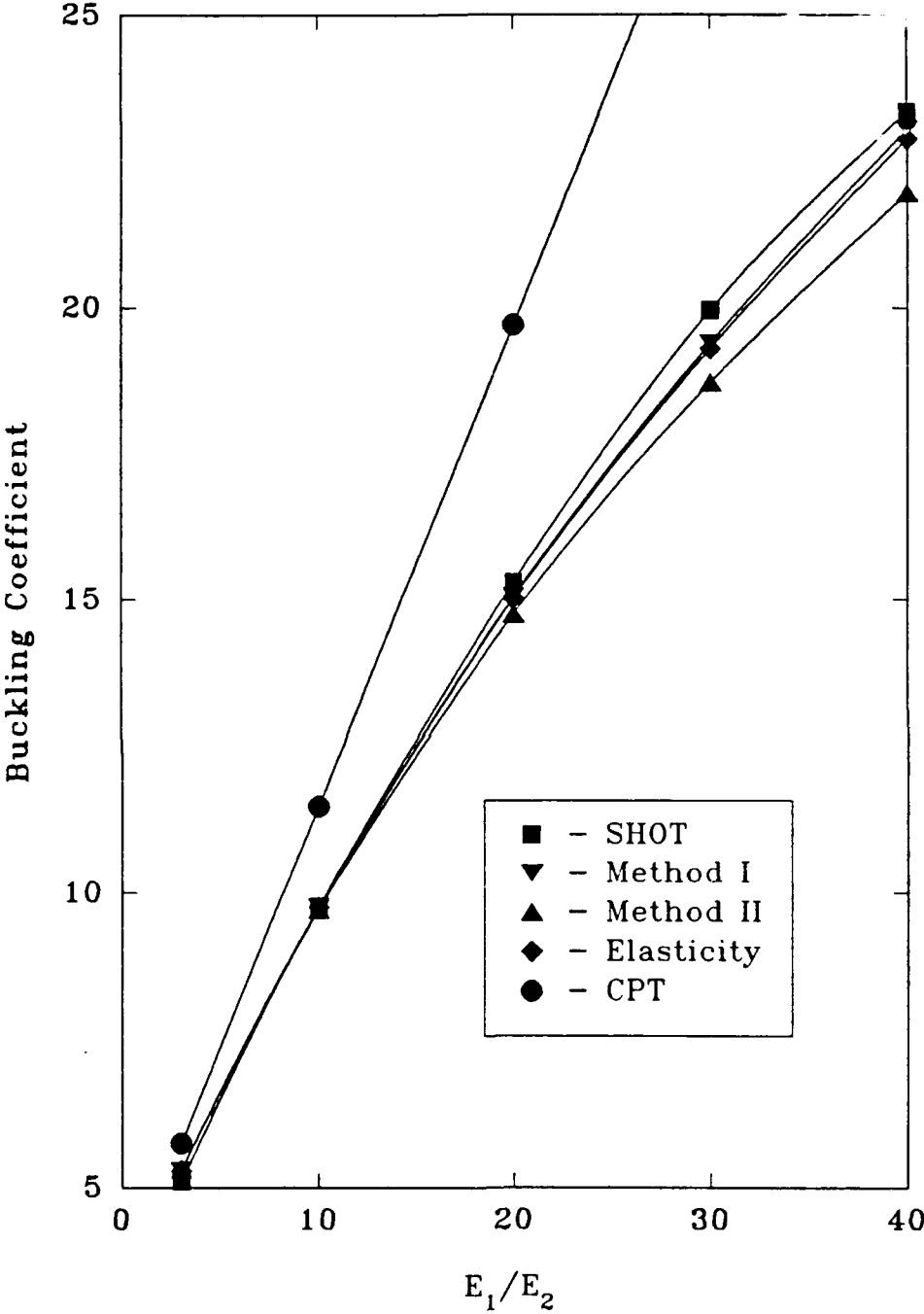


Figure 4.14: Method Comparison of Non-dimensional Buckling Coefficient -vs- Anisotropy Ratio. [0/90/90/0], Material VII, $b/h = 5$, $\lambda_b = n_1 b^2/h^3 E_2$, $a/b = 1$, Simply supported (BC-1)

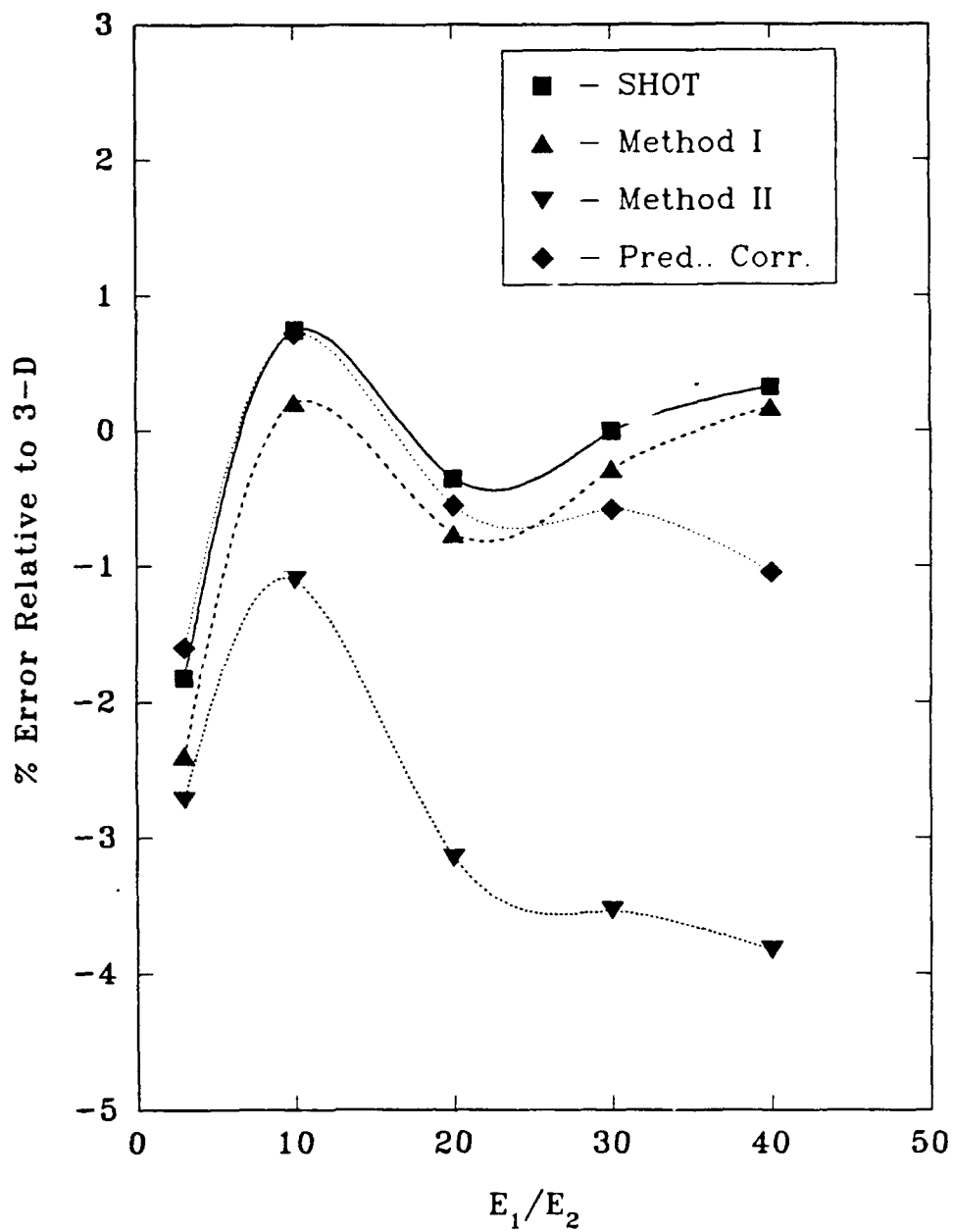


Figure 4.15: Method Comparison of Percent Error in Natural Frequency -vs- Anisotropy Ratio. [0/90/90/0], Material VII, $b/h = 5$, $a/b = 1$, Simply supported (BC-1)

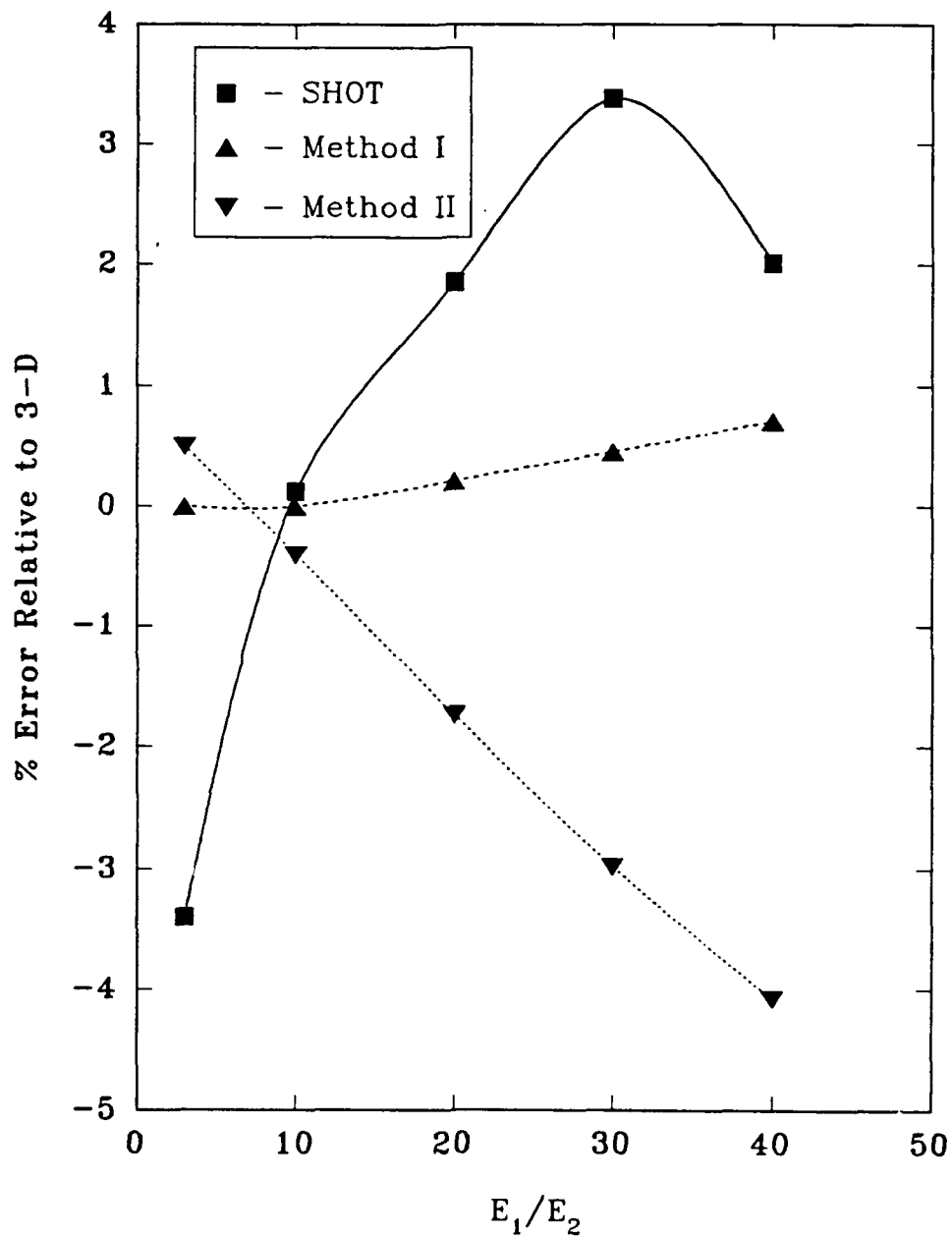


Figure 4.16: Method Comparison of Percent Error in Buckling Coefficient -vs- Anisotropy Ratio. [0/90/90/0], Material VII, $b/h = 5$, $a/b = 1$, Simply supported (BC-1)

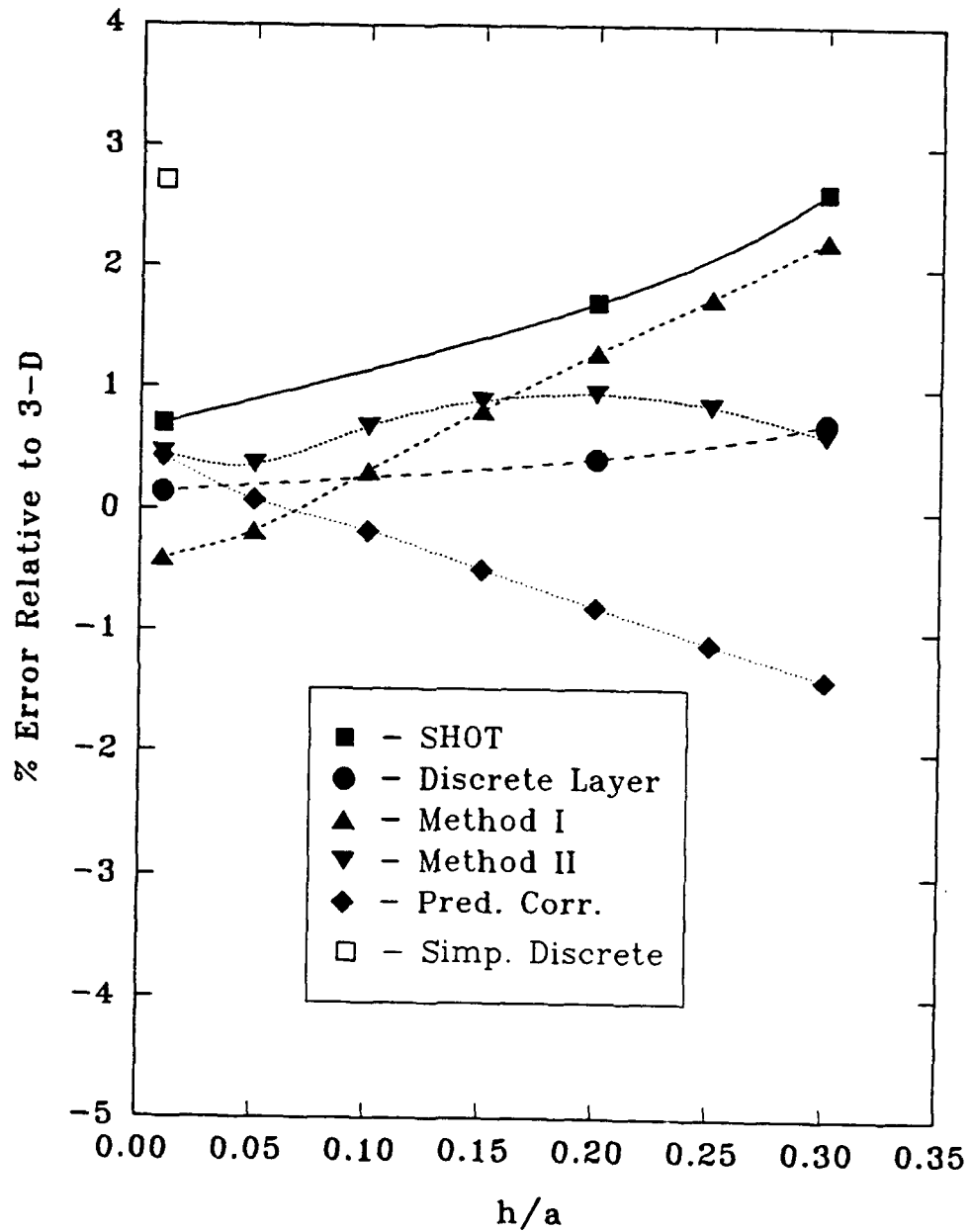


Figure 4.17: Method Comparison of Percent Error in Natural Frequency -vs- Thickness Ratio. 10 layer, $[-45/+45/-45/...]$, Material I, $a/b = 1$, Simply supported (BC-1)

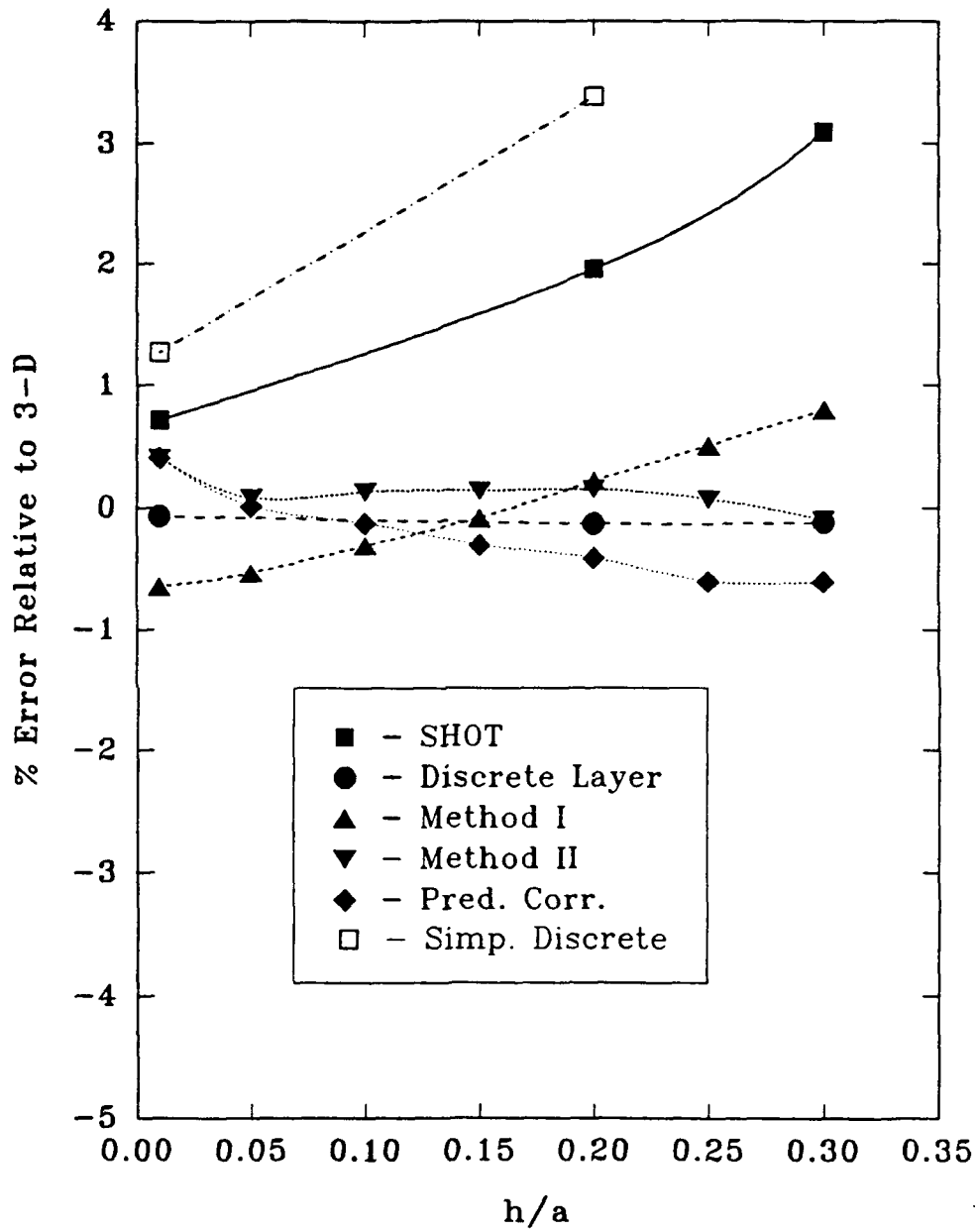


Figure 4.18: Method Comparison of Percent Error in Natural Frequency -vs- Thickness Ratio. 16 layer Hybrid- Materials IV & V, $a/b = 1$, Simply supported (BC-1)

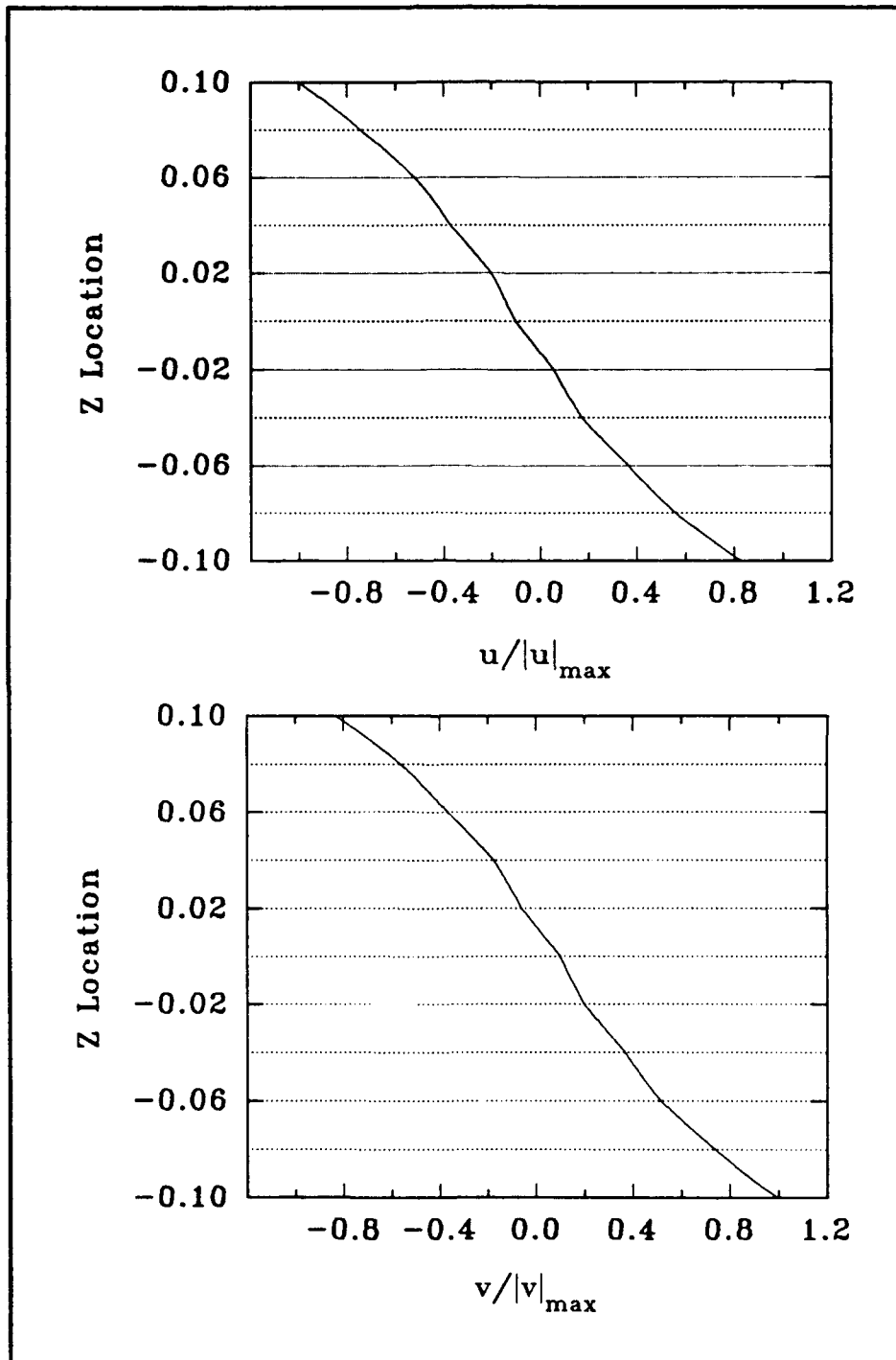


Figure 4.19: In-plane Displacements -vs- z Location. 10 layer, Material I, [90/0/90/...], $a/b = 1$, $h/b = 0.2$, Simply supported (BC-1), 3×3 quarter plate model, $x = 0.29167$, $y = 0.29167$.

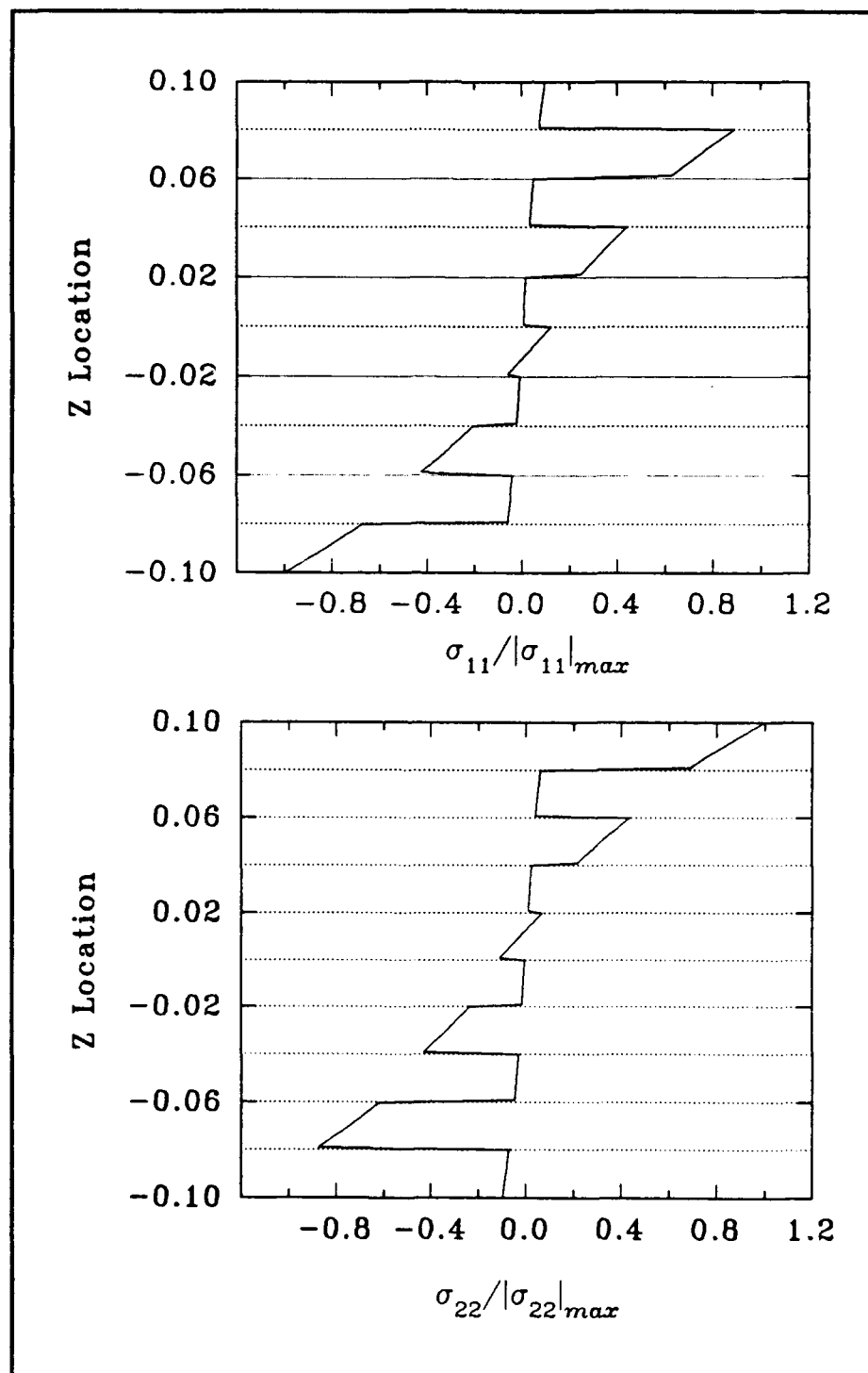


Figure 4.20: In-plane Stresses -vs- z Location. 10 layer, Material I, [90/0/90/...], $a/b = 1$, $h/b = 0.2$, Simply supported (BC-1), 3×3 quarter plate model, $x = 0.29167$, $y = 0.29167$.

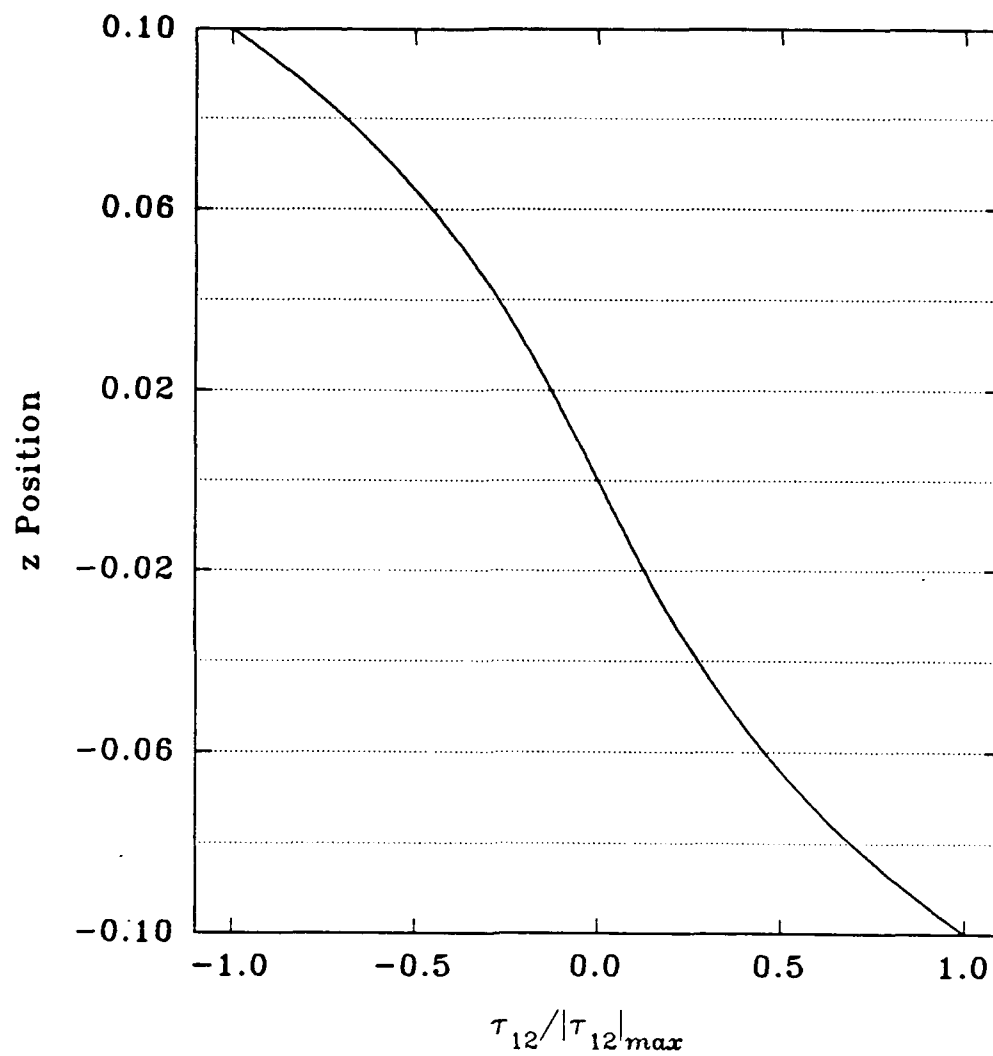


Figure 4.21: In-plane Shear stress -vs- z Location. 10 layer, Material I, [90/0/90/...], $a/b = 1$, $h/b = 0.2$, Simply supported (BC-1), 3×3 quarter plate model, $x = 0.29167$, $y = 0.29167$.

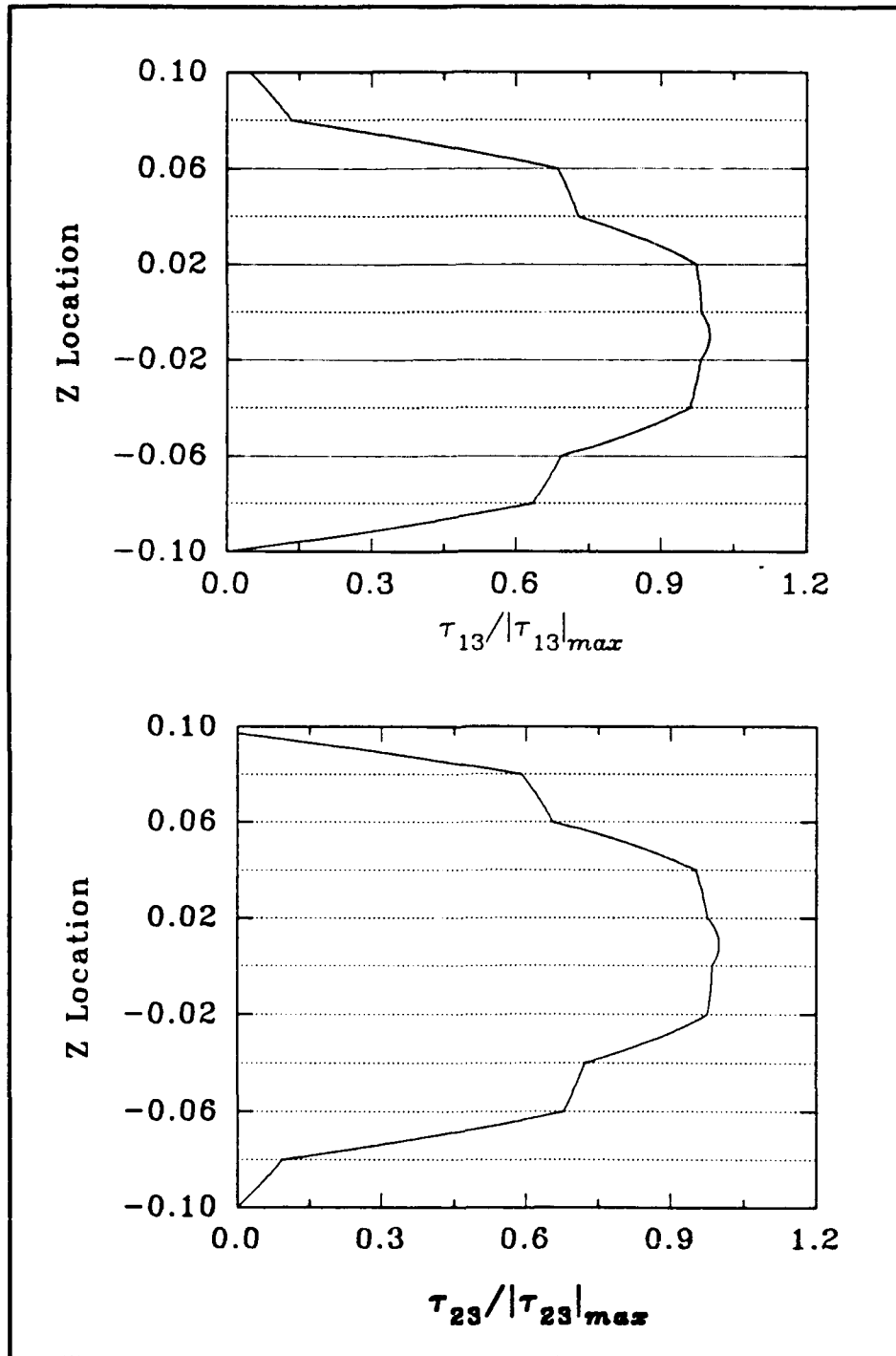


Figure 4.22: Transverse Shear Stresses -vs- z Location. 10 layer, Material I, [90/0/90/...], $a/b = 1$, $h/b = 0.2$, Simply supported (BC-1), 3 \times 3 quarter plate model, $x = 0.29167$, $y = 0.29167$.

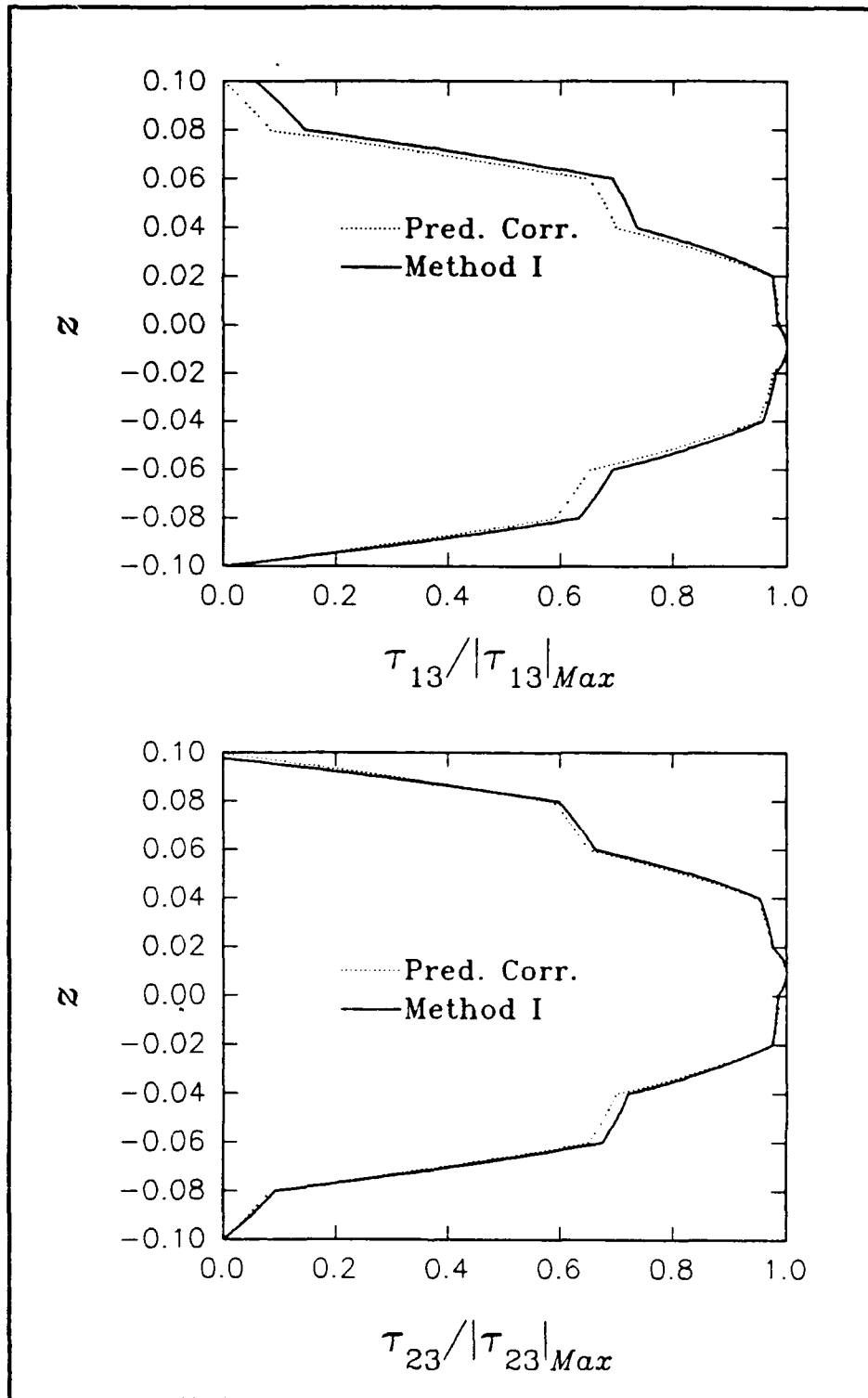


Figure 4.23: Method Comparison of Transverse Shear Stresses. 10 layer, Material I, [90/0/90/...], $a/b = 1$, $h/b = 0.2$, Simply supported (BC-1), 3×3 quarter plate model, $x = 0.29167$, $y = 0.29167$.

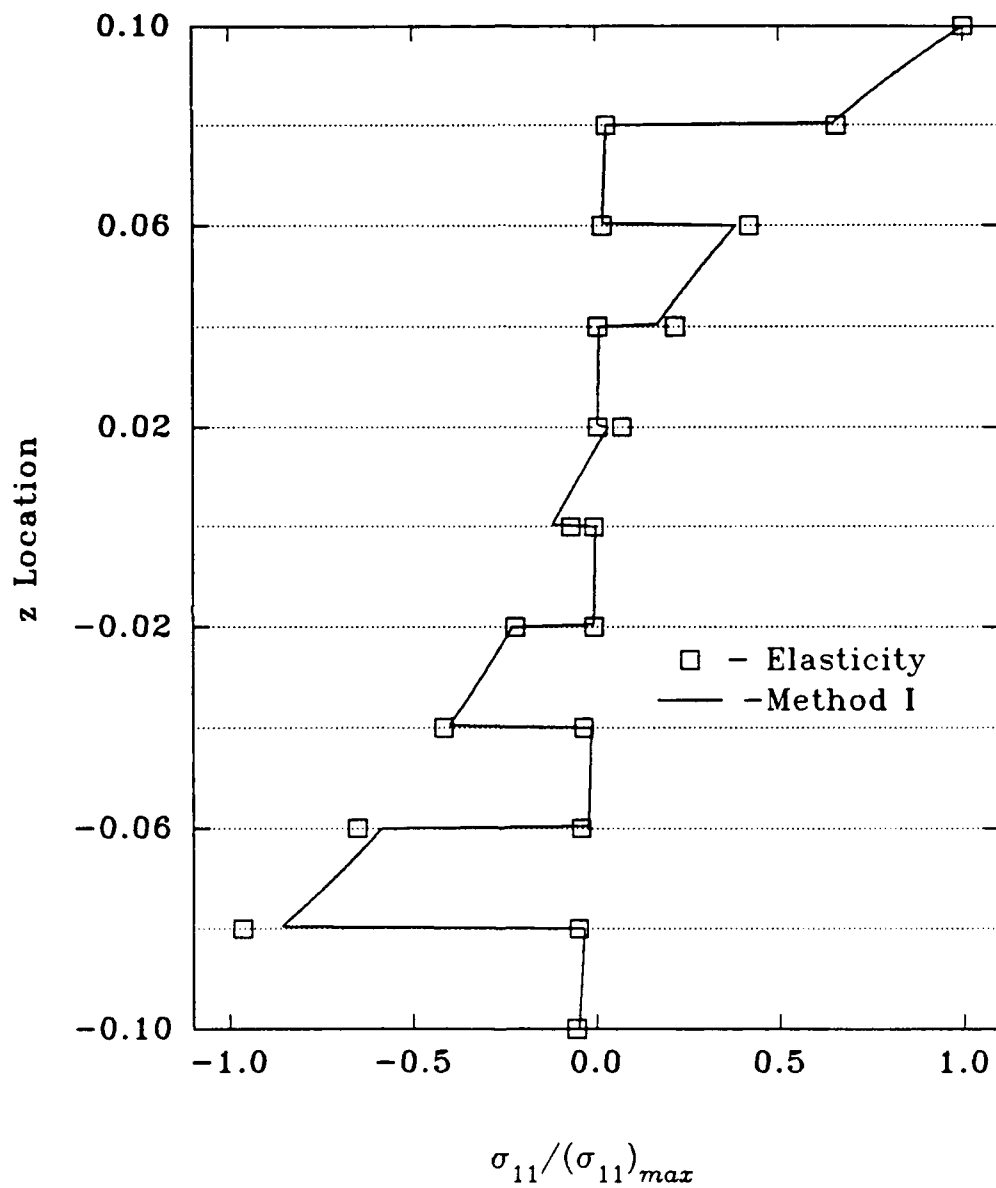


Figure 4.24: In-plane Stress Comparison: Method I -vs- Elasticity. 10 layer, Material VI, [90/0/90/...], $a/b = 1$, $h/b = 0.2$, Simply supported (BC-1), 4×4 quarter plate model, $x = 0.29167$, $y = 0.29167$.

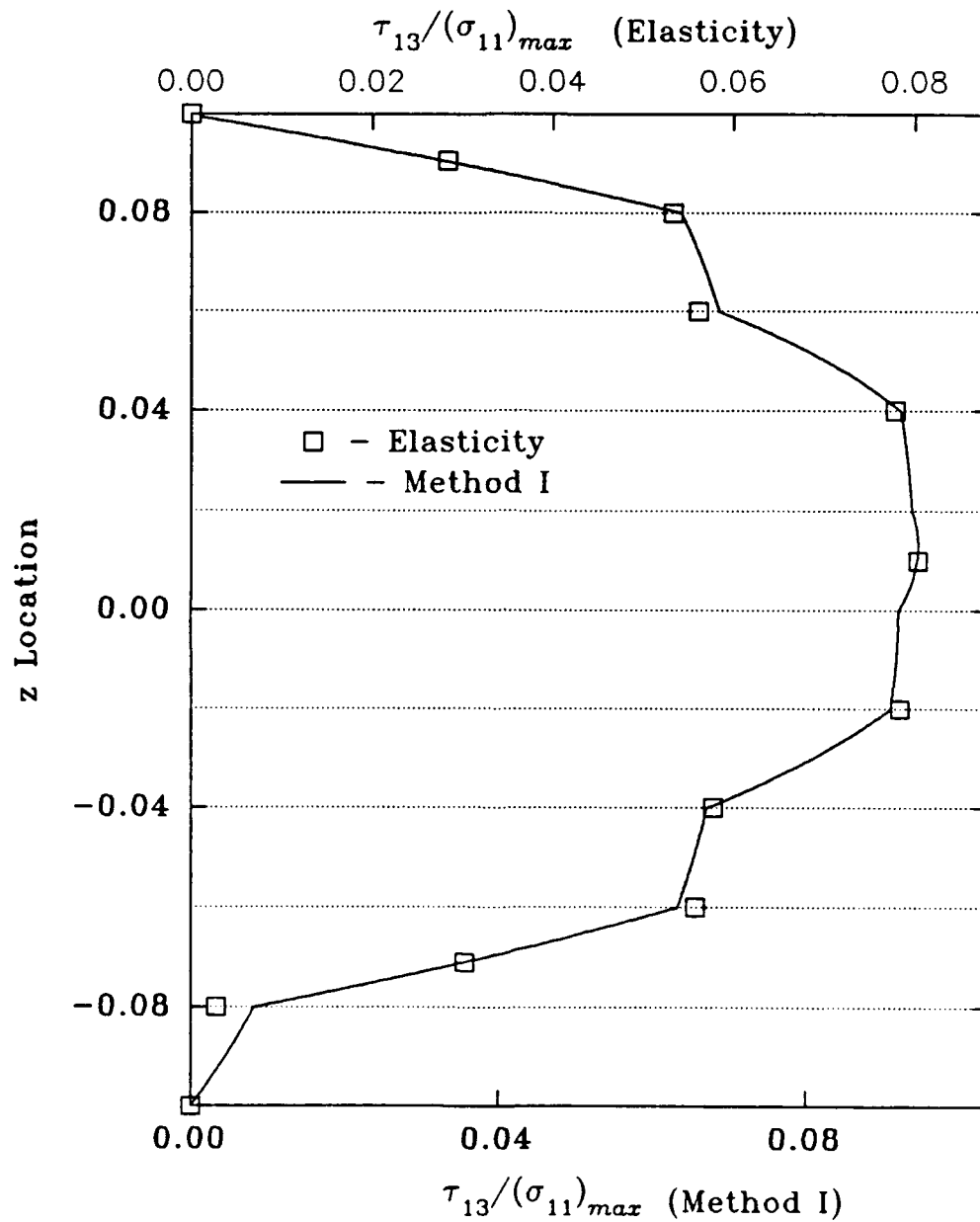


Figure 4.25: Transverse Shear Stress Comparison: Method I -vs- Elasticity. 10 layer, Material VI, [90/0/90/...], $a/b = 1$, $h/b = 0.2$, Simply supported (BC-1), 4×4 quarter plate model, $x = 0.29167$, $y = 0.29167$.

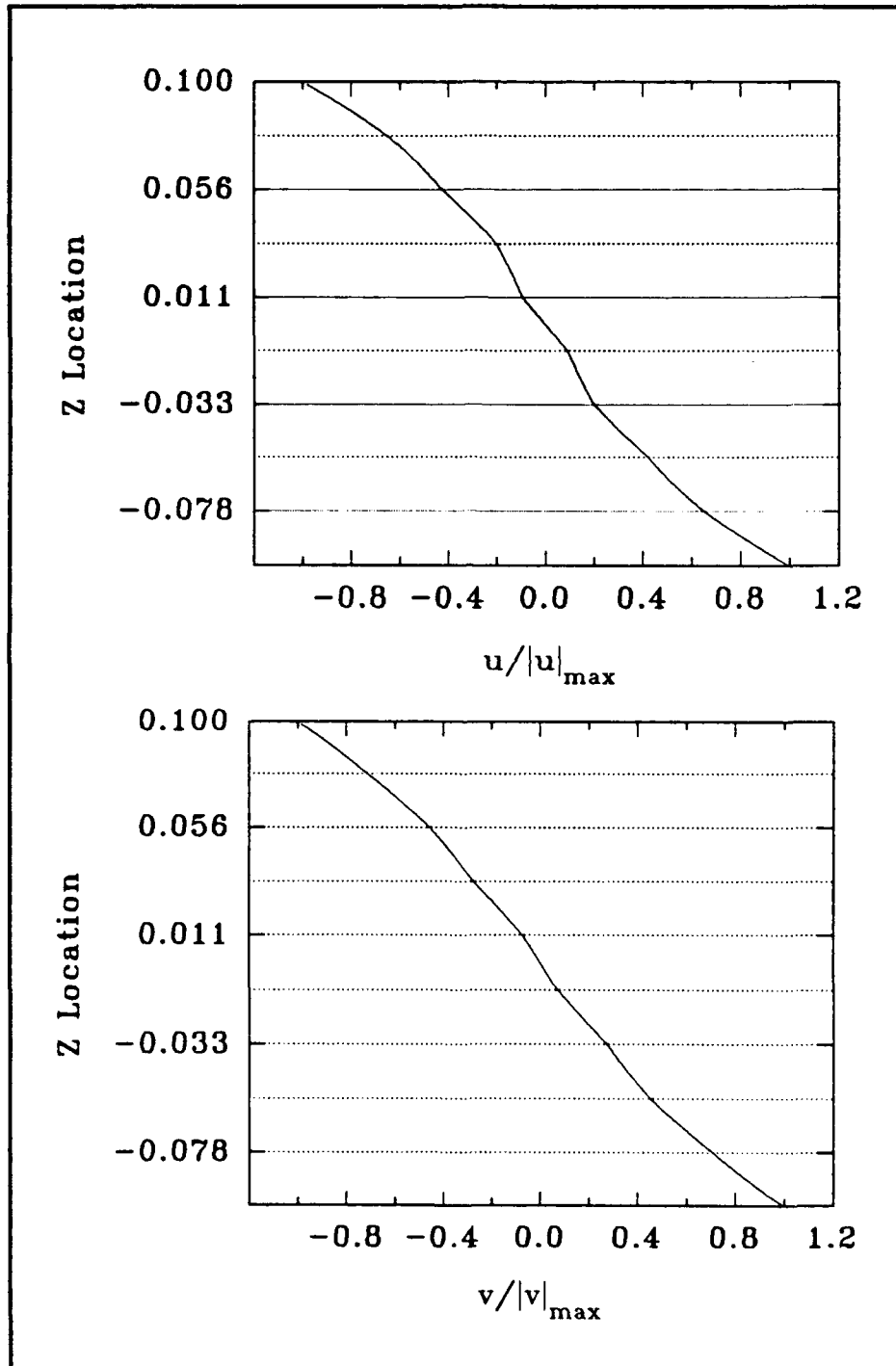


Figure 4.26: In-plane Displacements -vs- z Location. 9 layer, Material I, [90/0/90/...], $a/b = 1$, $h/b = 0.2$, Simply supported (BC-1), 3×3 quarter plate model, $x = 0.29167$, $y = 0.29167$.

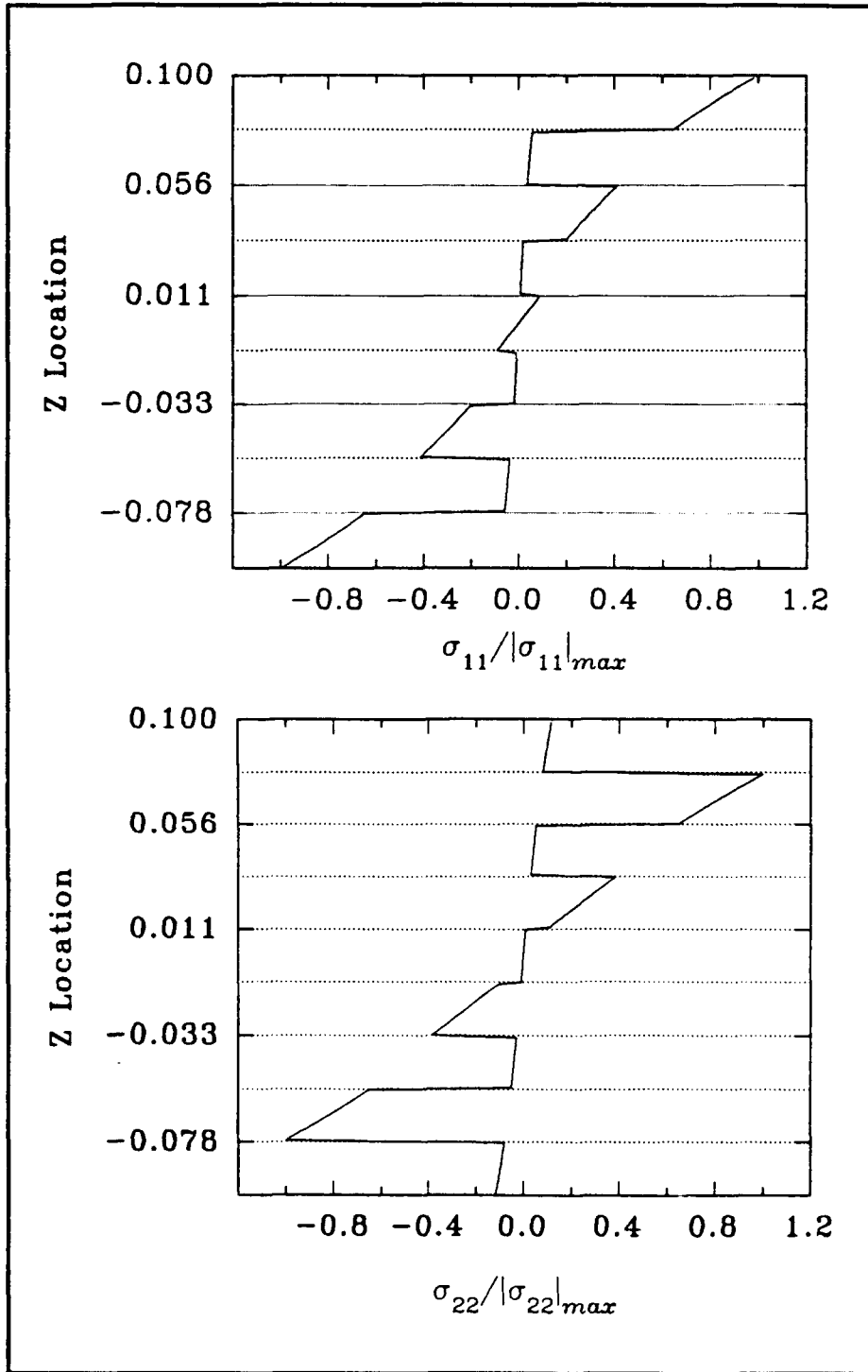


Figure 4.27: In-plane Stresses -vs- z Location. 9 layer, Material I, [90/0/90/...], $a/b = 1$, $h/b = 0.2$, Simply supported (BC-1), 3×3 quarter plate model, $x = 0.29167$, $y = 0.29167$.

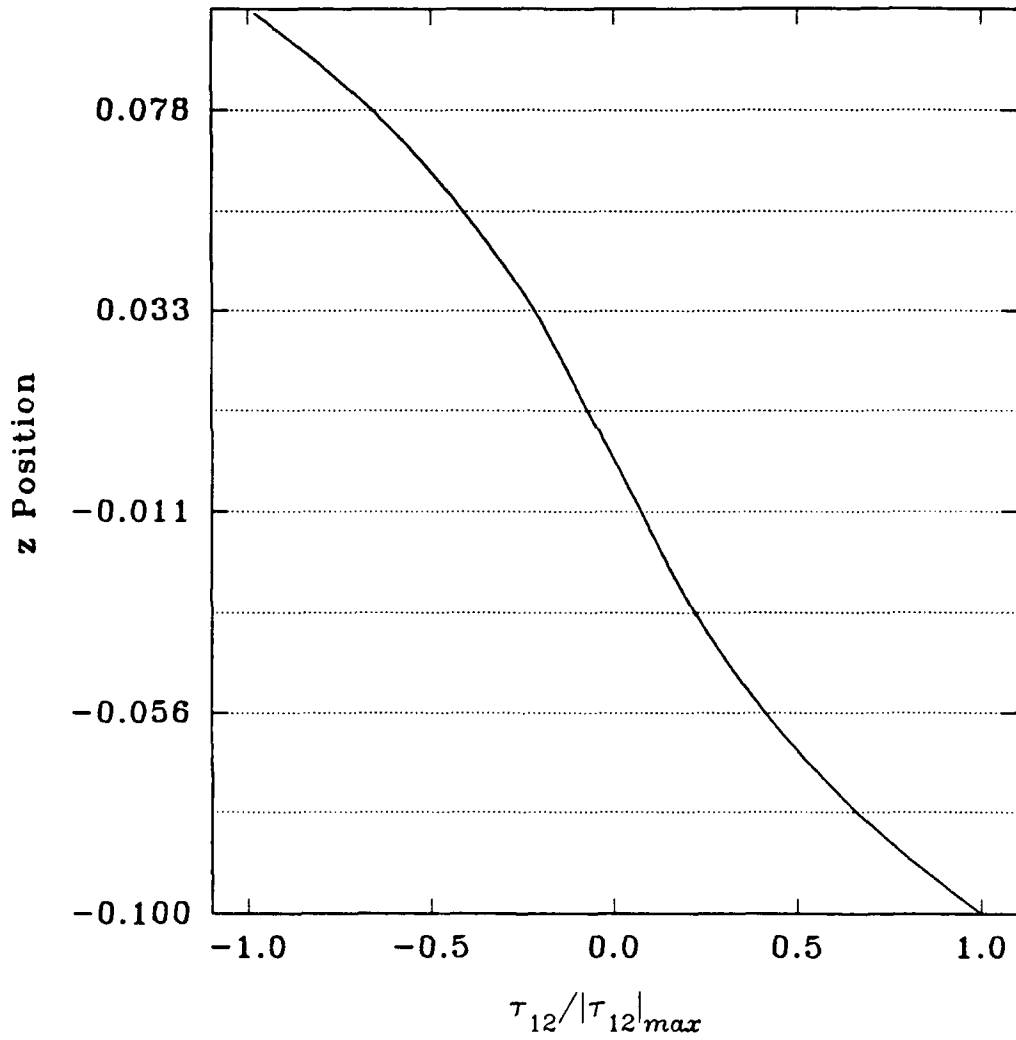


Figure 4.28: In-plane Shear stress -vs- z Location. 9 layer, Material I, [90/0/90/...], $a/b = 1$, $h/b = 0.2$, Simply supported (BC-1), 3×3 quarter plate model, $x = 0.29167$, $y = 0.29167$.

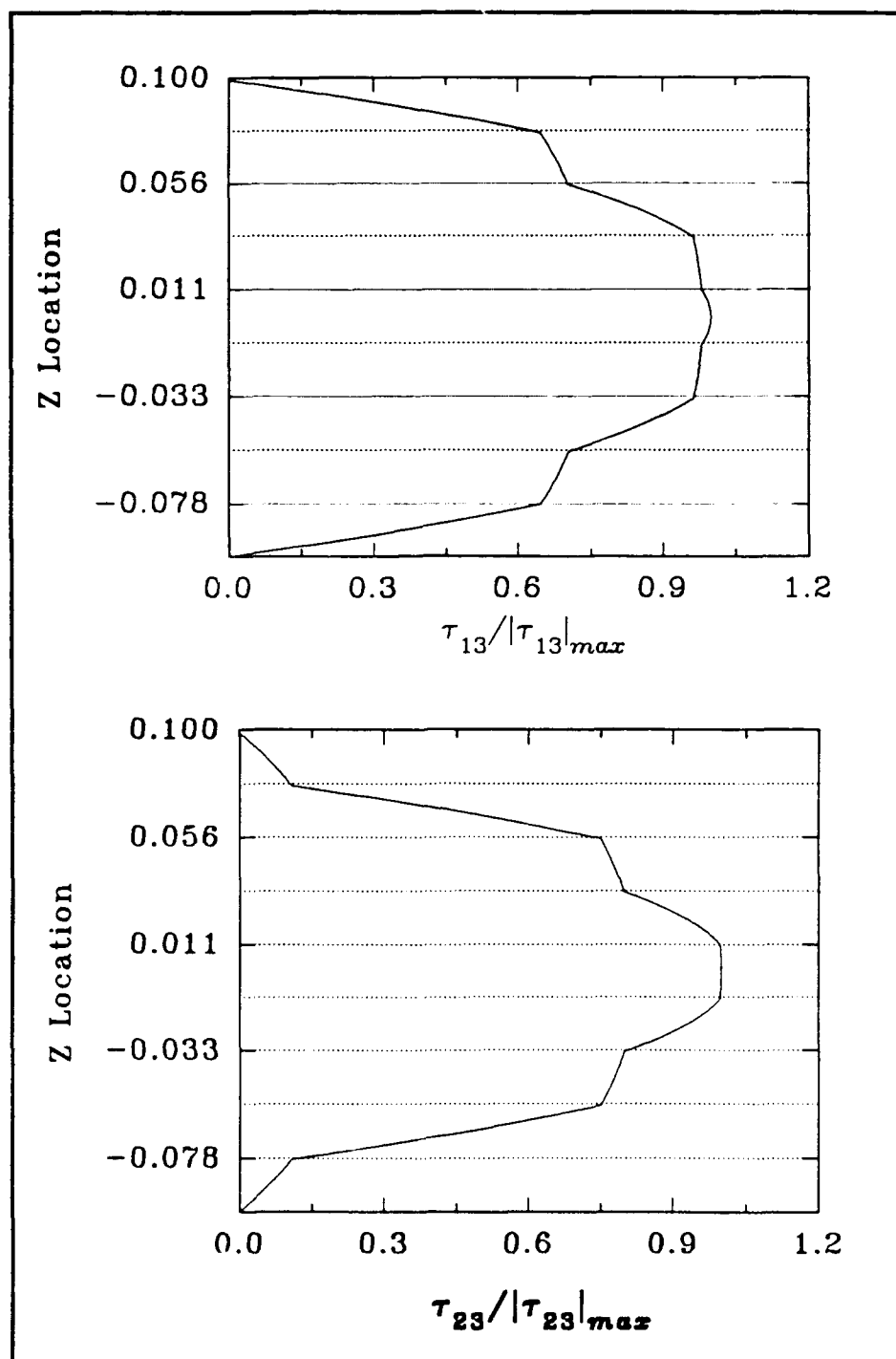


Figure 4.29: Transverse Shear Stresses -vs- z Location. 9 layer, Material I, [90/0/90/...], $a/b = 1$, $h/b = 0.2$, Simply supported (BC-1), 3×3 quarter plate model, $x = 0.29167$, $y = 0.29167$.

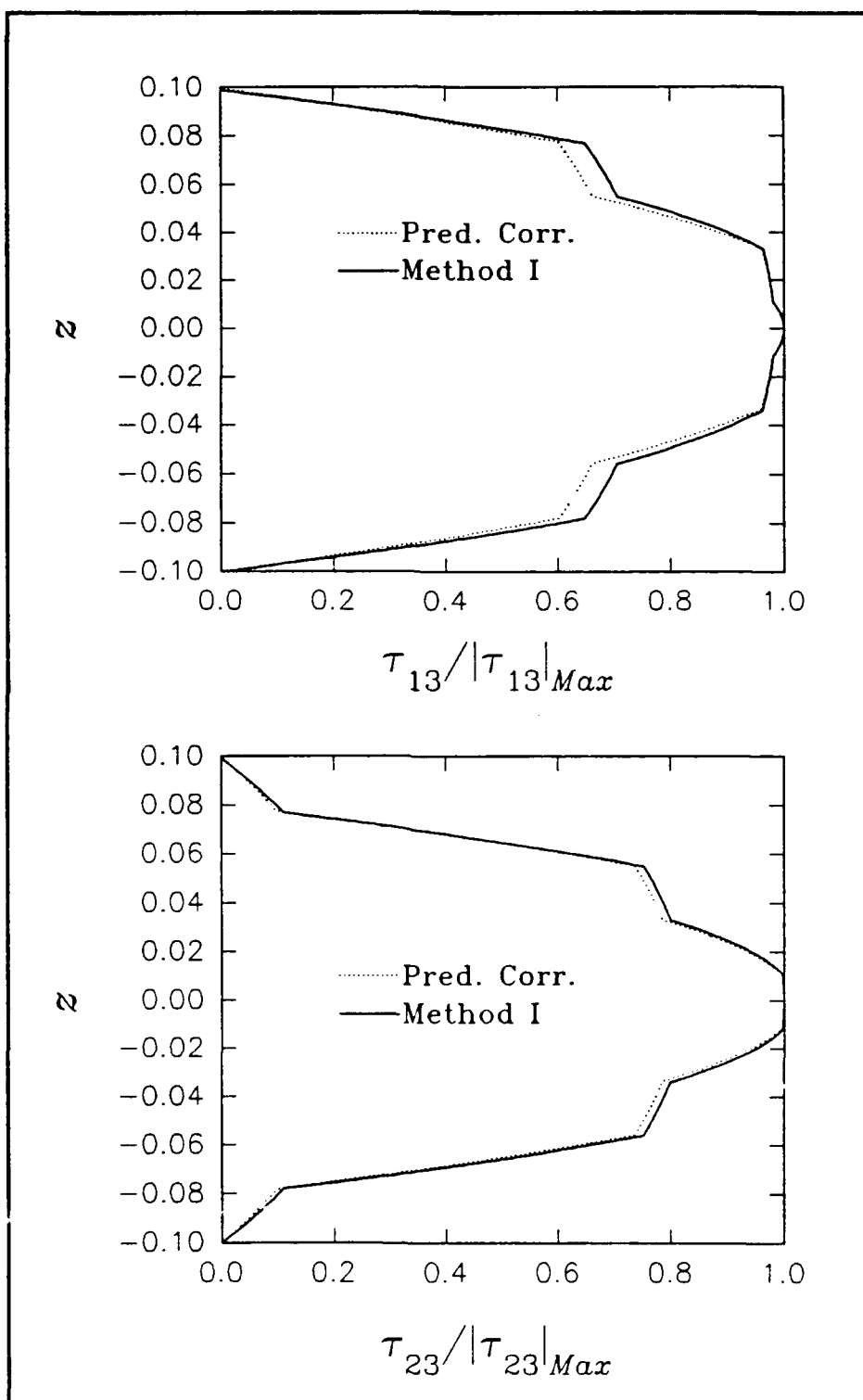


Figure 4.30: Method Comparison of Transverse Shear Stresses. 9 layer, Material I, [90/0/90/...], $a/b = 1$, $h/b = 0.2$, Simply supported (BC-1), 3×3 quarter plate model, $x = 0.29167$, $y = 0.29167$.

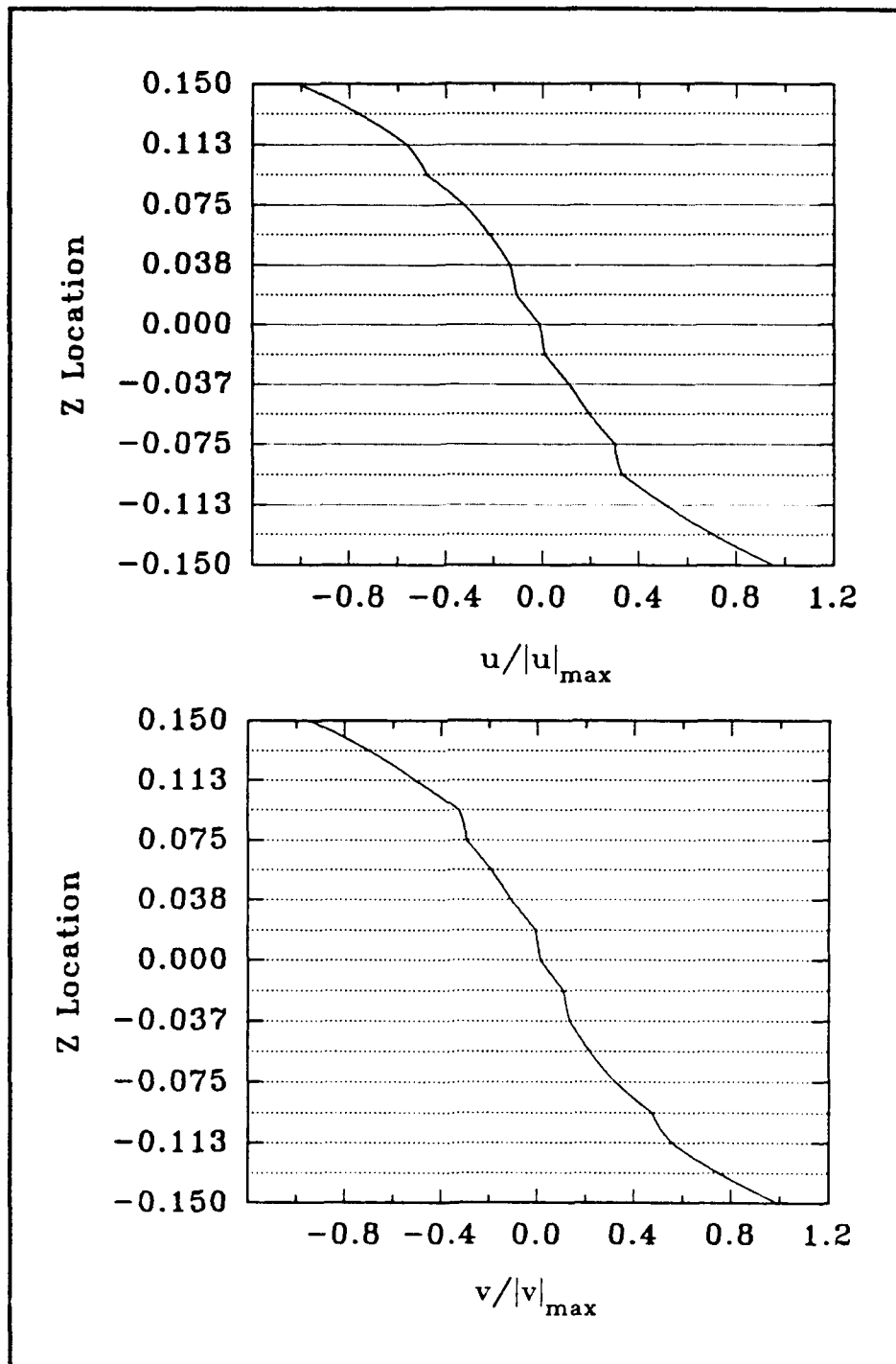


Figure 4.31: In-plane Displacements -vs- z Location. 16 Layer Hybrid, Materials IV & V, $a/b = 1$, $h/b = 0.3$, Simply supported (BC-1), 3×3 quarter plate model, $x = 0.29167$, $y = 0.29167$.

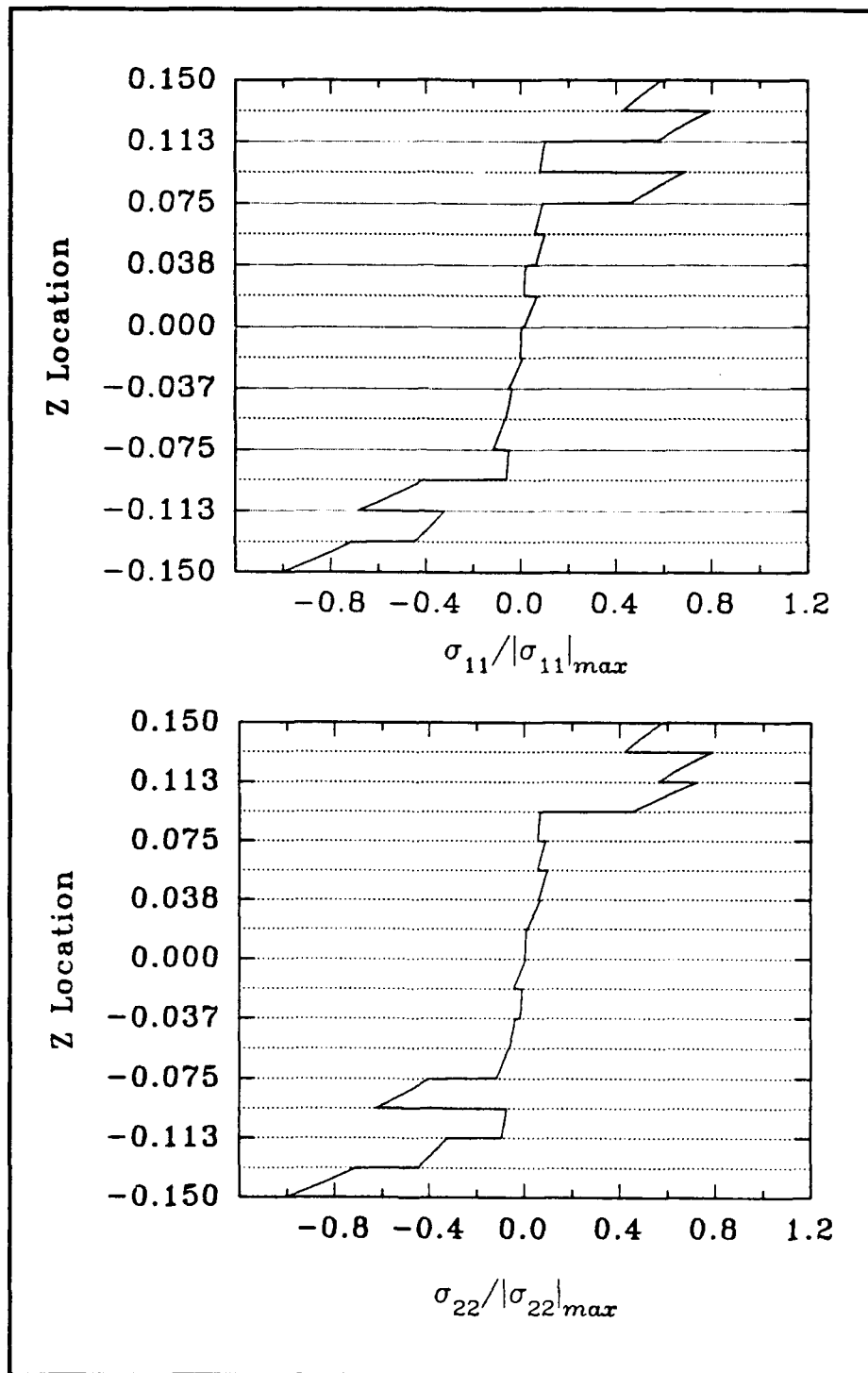


Figure 4.32: In-plane Stresses -vs- z Location. 16 Layer Hybrid, Materials IV & V, $a/b = 1$, $h/b = 0.3$, Simply supported (BC-1), 3×3 quarter plate model, $x = 0.29167$, $y = 0.29167$.

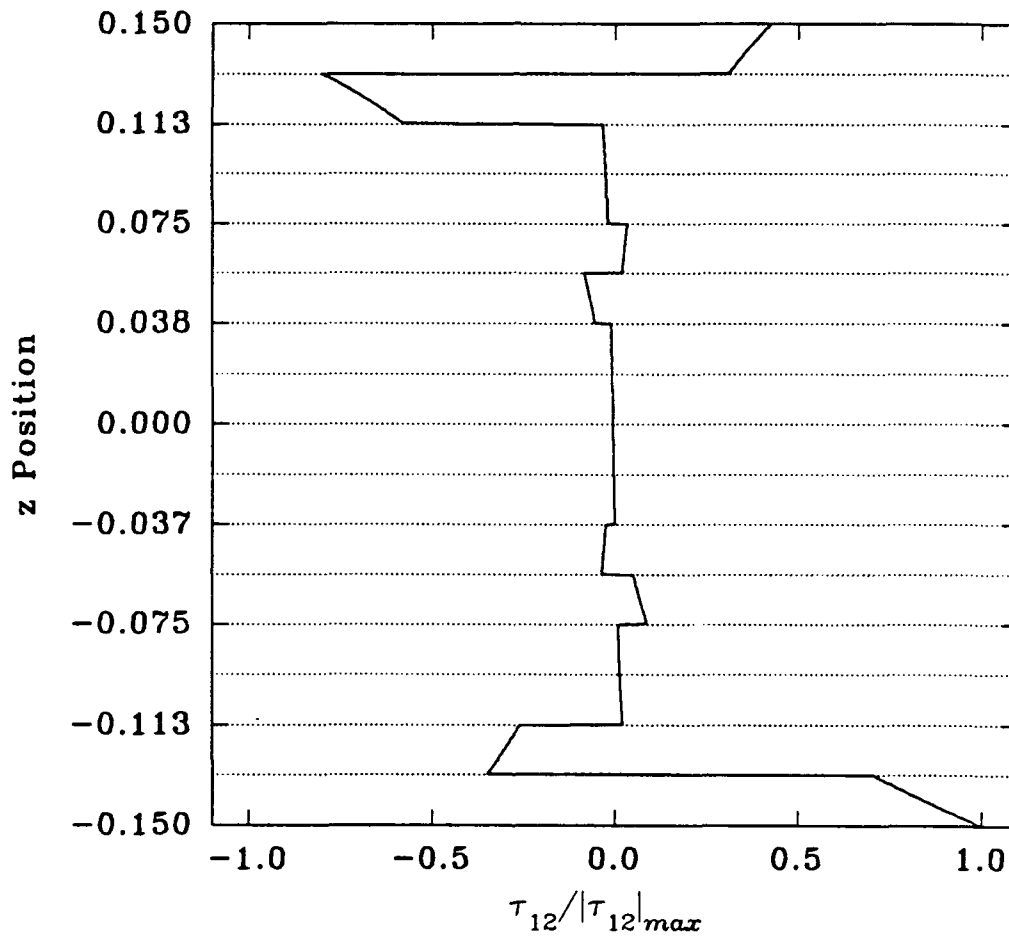


Figure 4.33: In-plane Shear stress -vs- z Location. 16 Layer Hybrid, Materials IV & V, $a/b = 1$, $h/b = 0.3$, Simply supported (BC-1), 3×3 quarter plate model, $x = 0.29167$, $y = 0.29167$.

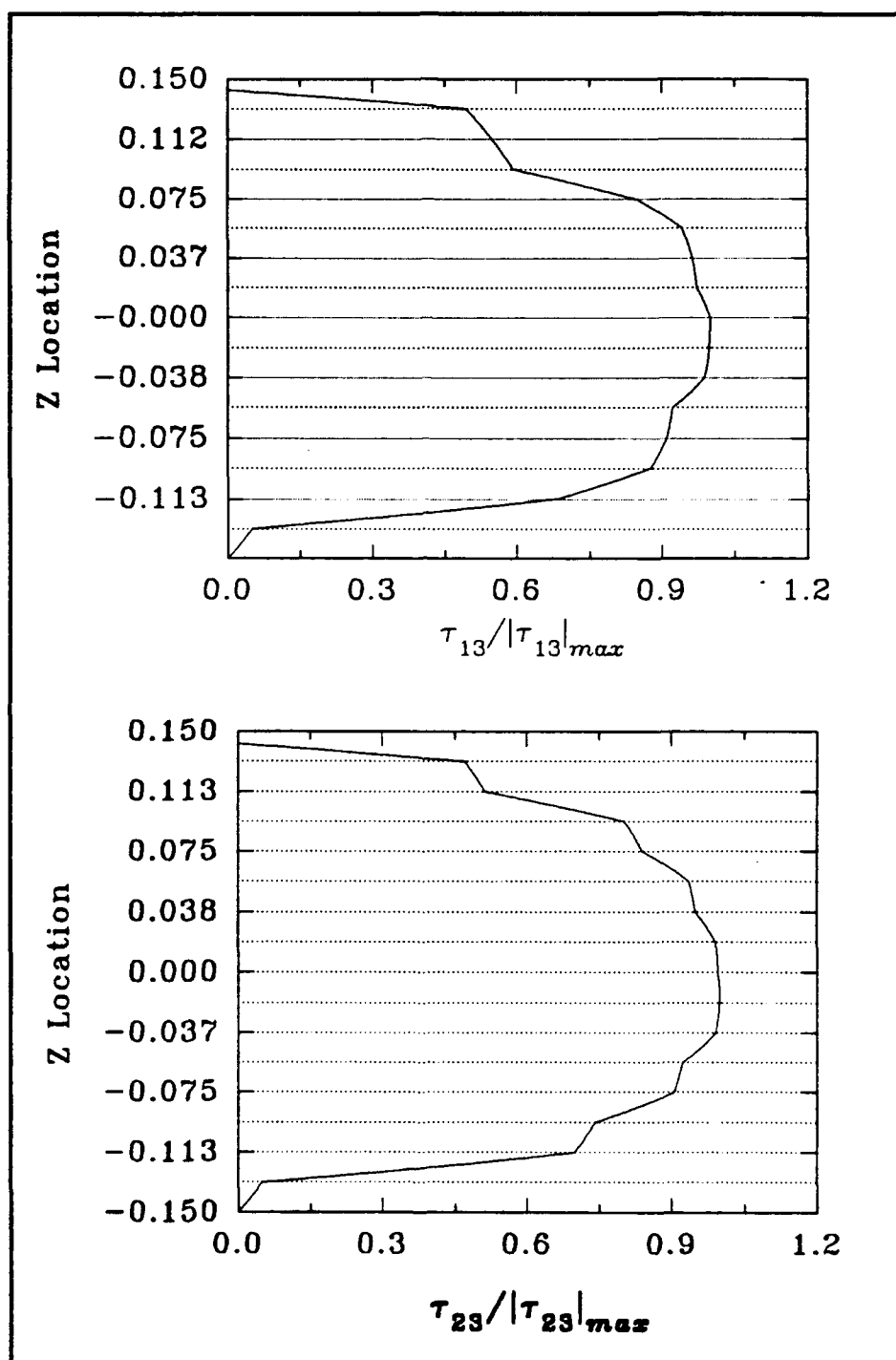


Figure 4.34: Transverse Shear Stresses -vs- z Location. 16 Layer Hybrid, Materials IV & V, $a/b = 1$, $h/b = 0.3$, Simply supported (BC-1), 3×3 quarter plate model, $x = 0.29167$, $y = 0.29167$.

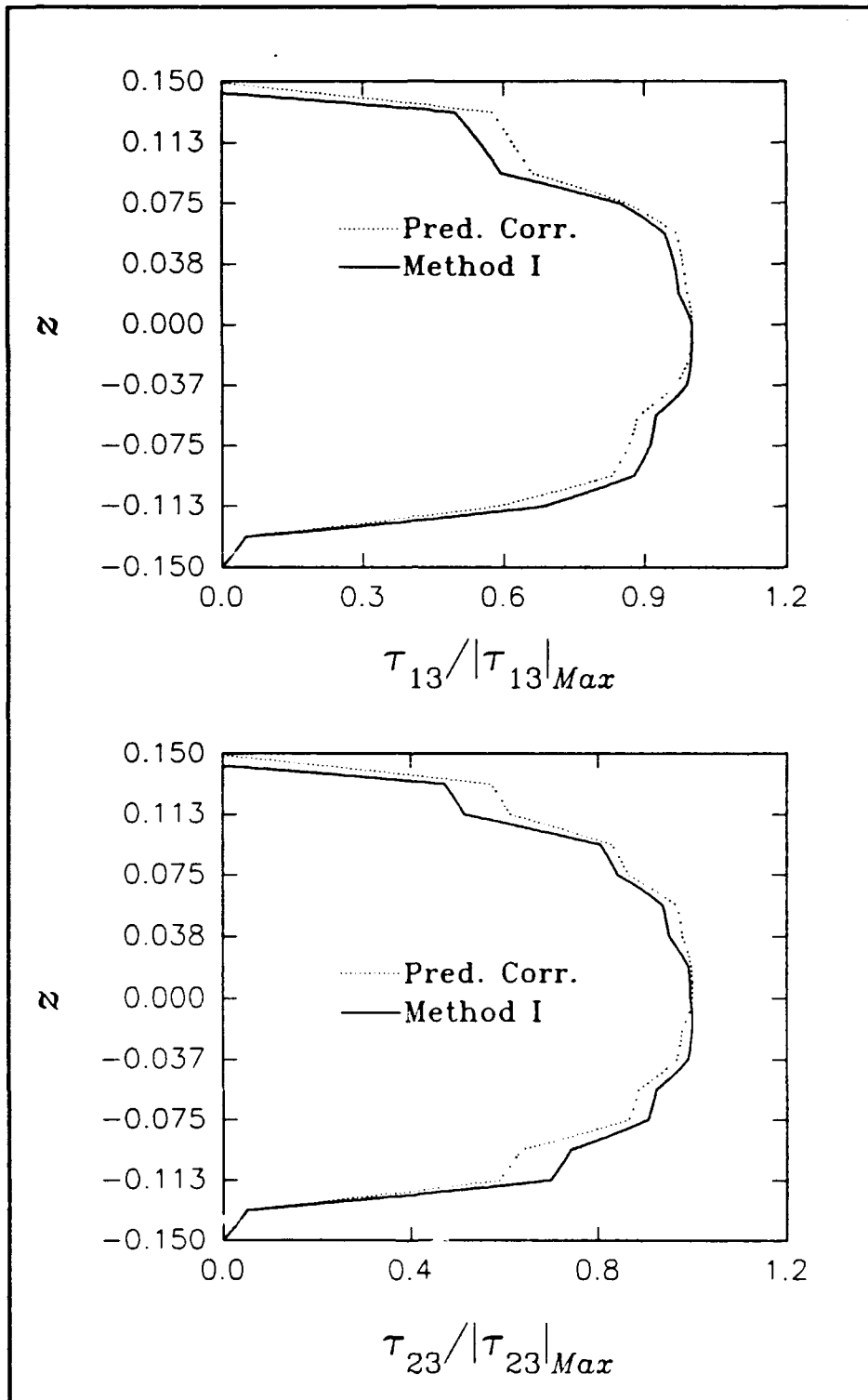


Figure 4.35: Method Comparison of Transverse Shear Stresses. 16 Layer Hybrid, Materials IV & V, $a/b = 1$, $h/b = 0.3$. Simply supported (BC-1), 3×3 quarter plate model, $x = 0.29167$, $y = 0.29167$.

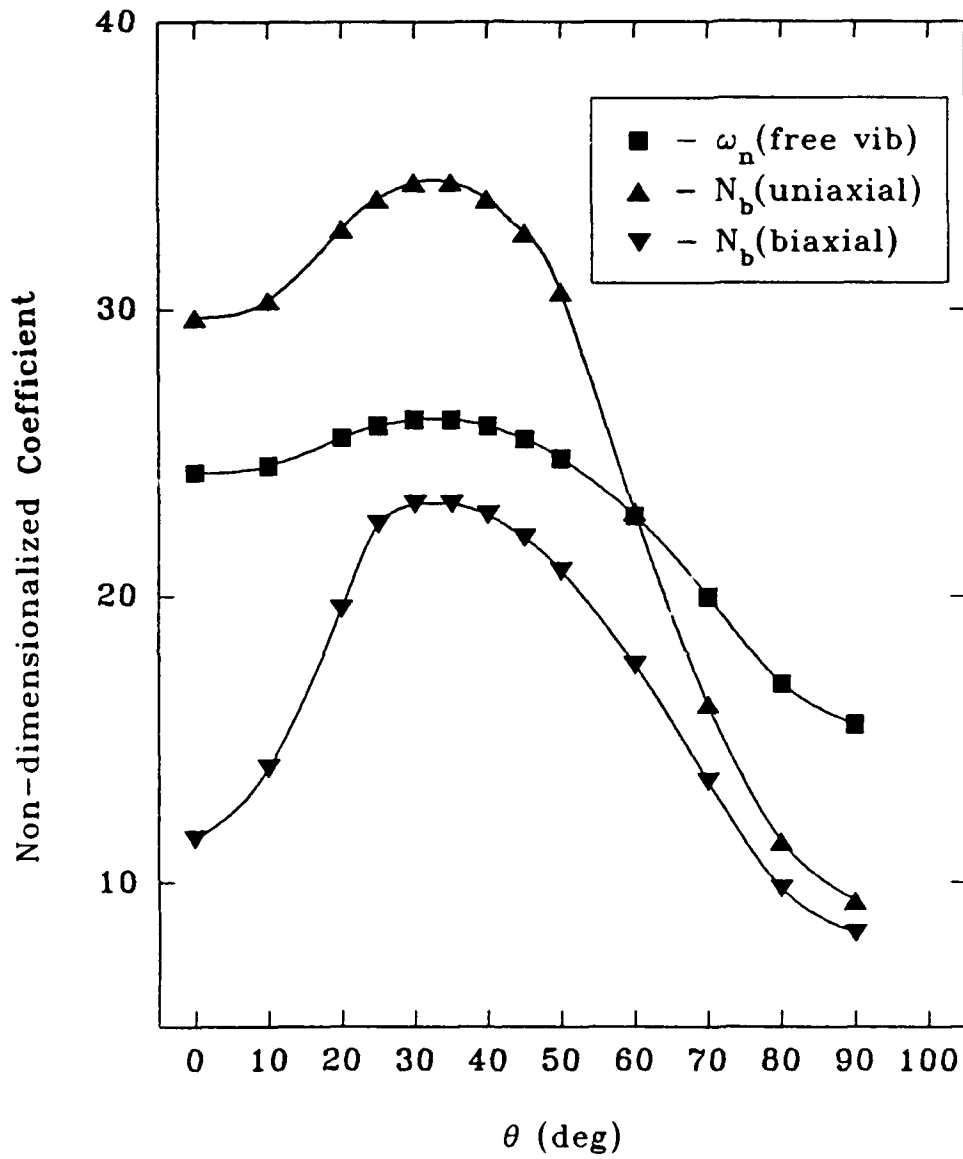


Figure 5.1: Eigenvalue Coefficients -vs- Ply Angle. Case A, 6 Layer $[+\theta/-\theta/\dots]$, Material II, $a/b = 0.7$, $h/b = 0.1$, Simply supported (BC-6), 3×4 full plate model.

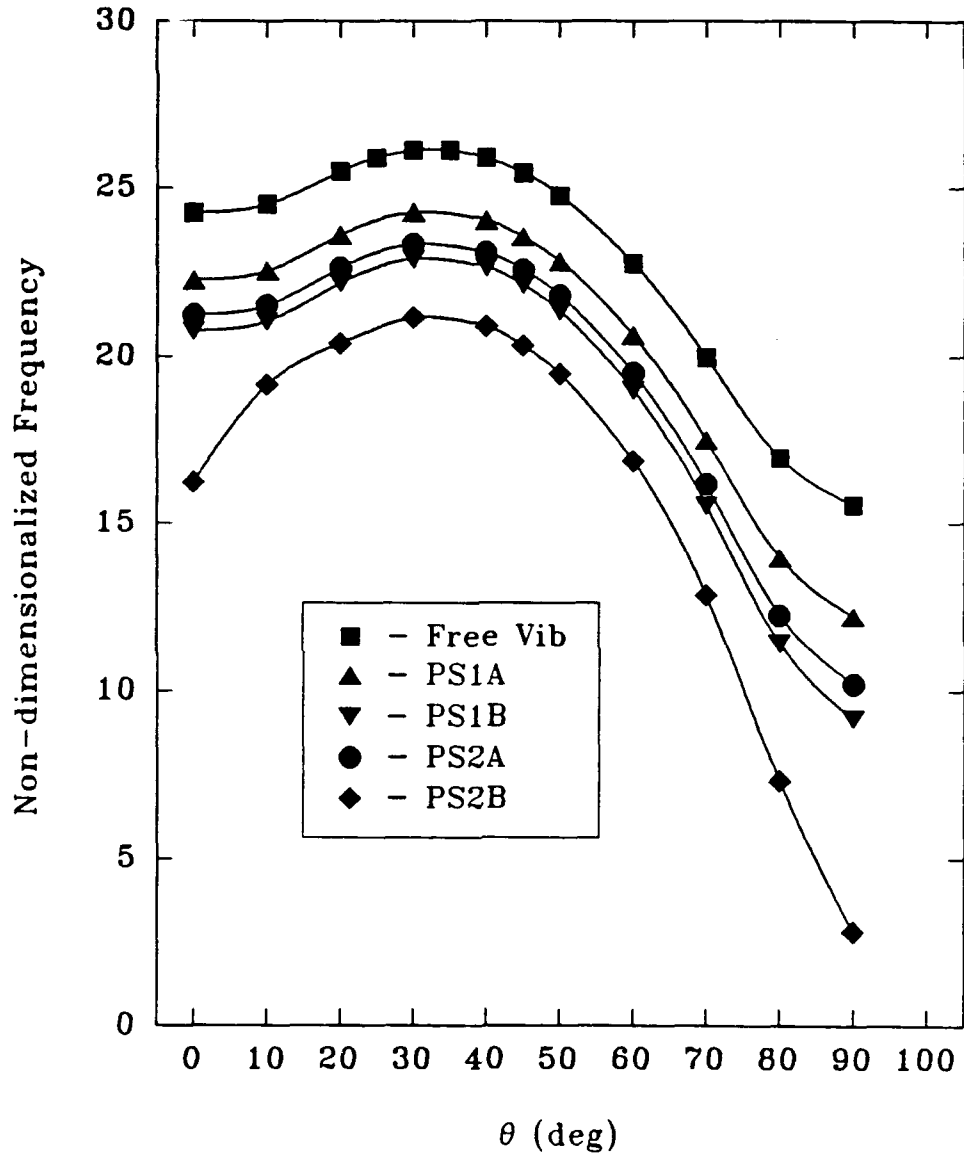


Figure 5.2: Pre-Stressed Natural Frequency -vs- Ply Angle. Case A, 6 Layer $[+\theta/-\theta/\dots]$, Material II, $a/b = 0.7$, $h/b = 0.1$, Simply supported (BC-6), 3×4 full plate model.

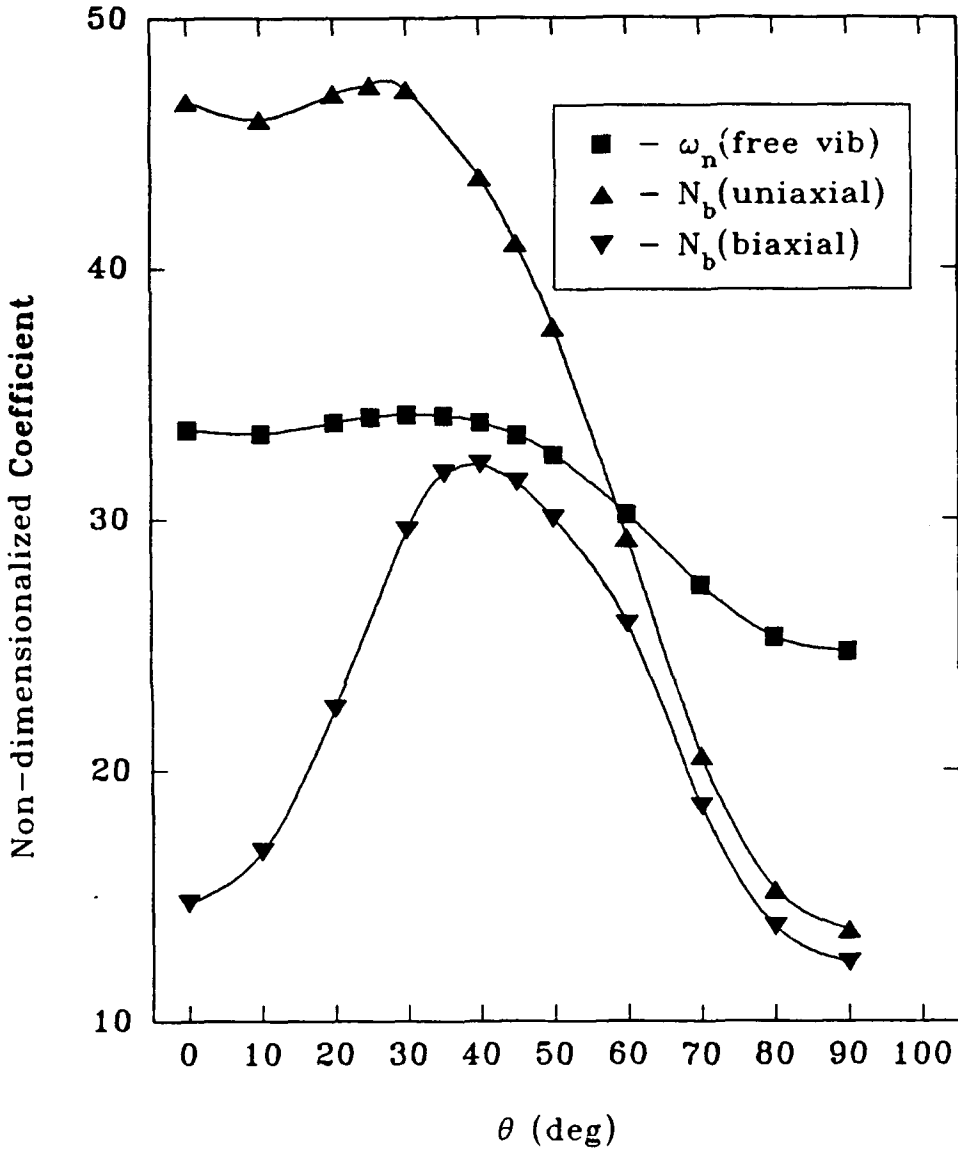


Figure 5.3: Eigenvalue Coefficients -vs- Ply Angle. Case A, 6 Layer [+ θ / $-\theta$ /...], Material II, $a/b = 0.7$, $h/b = 0.1$, Clamped, (BC-13), 3×4 full plate model.

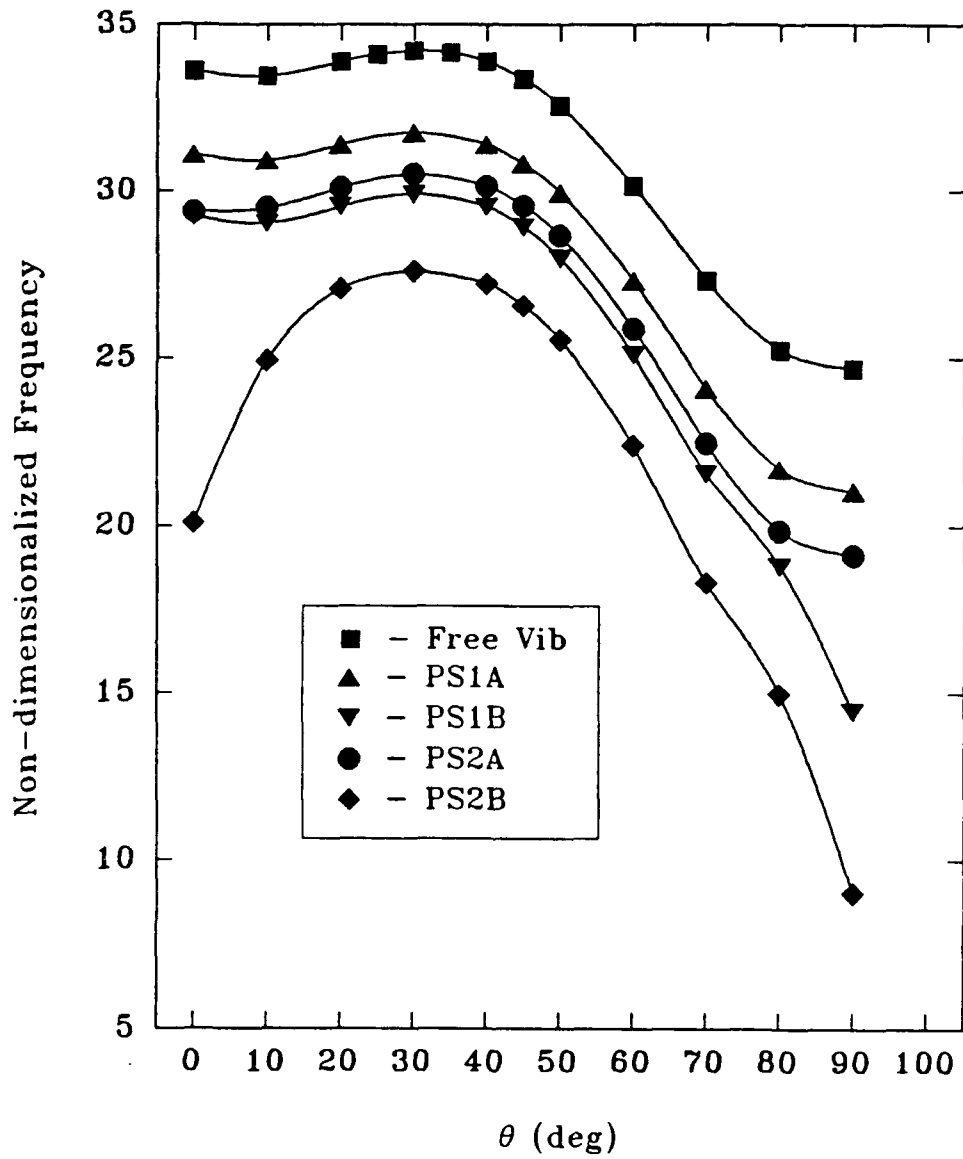


Figure 5.4: Pre-Stressed Natural Frequency -vs- Ply Angle. Case A, 6 Layer [+ θ / $-\theta$ /...], Material II, $a/b = 0.7$, $h/b = 0.1$, Clamped (BC-13), 3×4 full plate model.

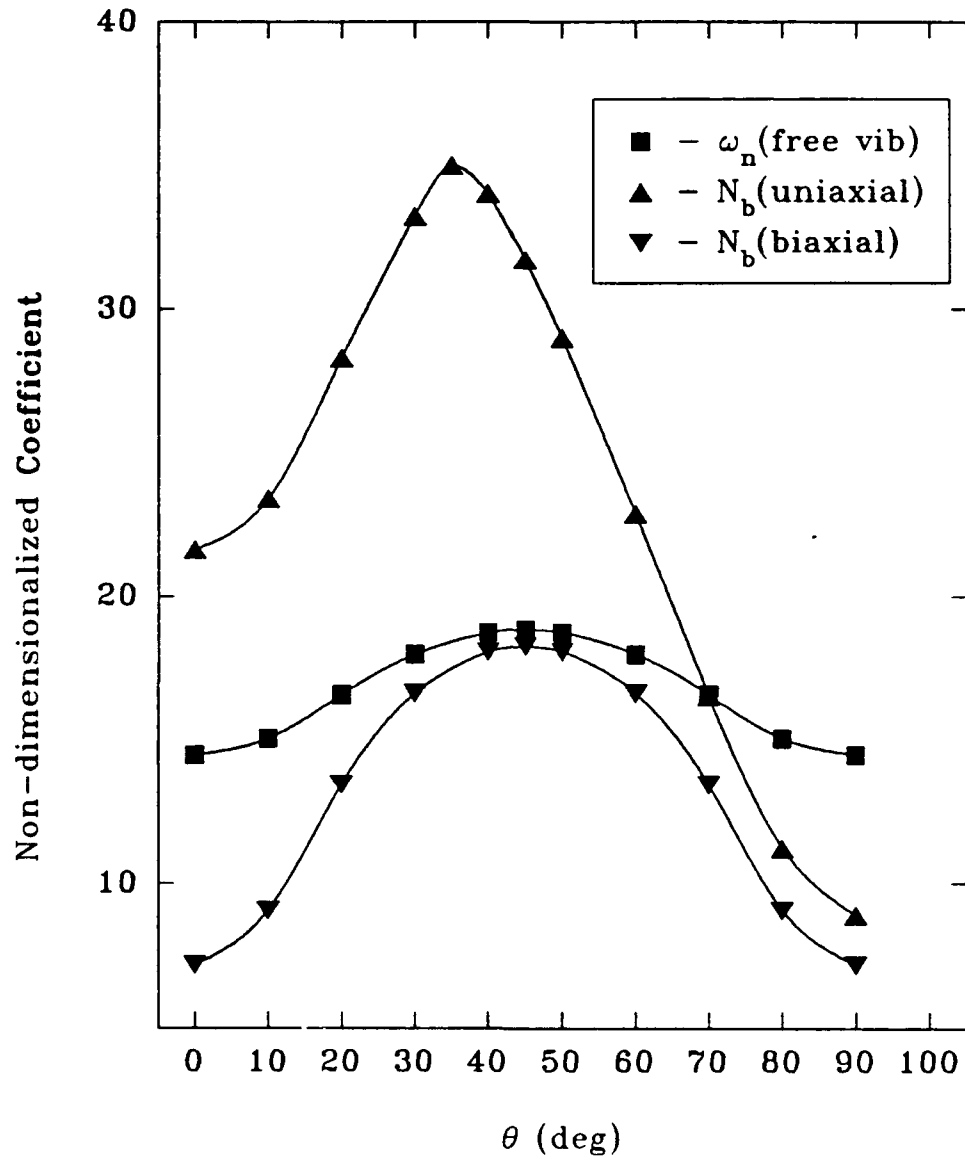


Figure 5.5: Eigenvalue Coefficients -vs- Ply Angle. Case B, 6 Layer [+ θ /- θ /...], Material II, $a/b = 1.0$, $h/b = 0.1$, Simply supported (BC-6), 4×4 full plate model.

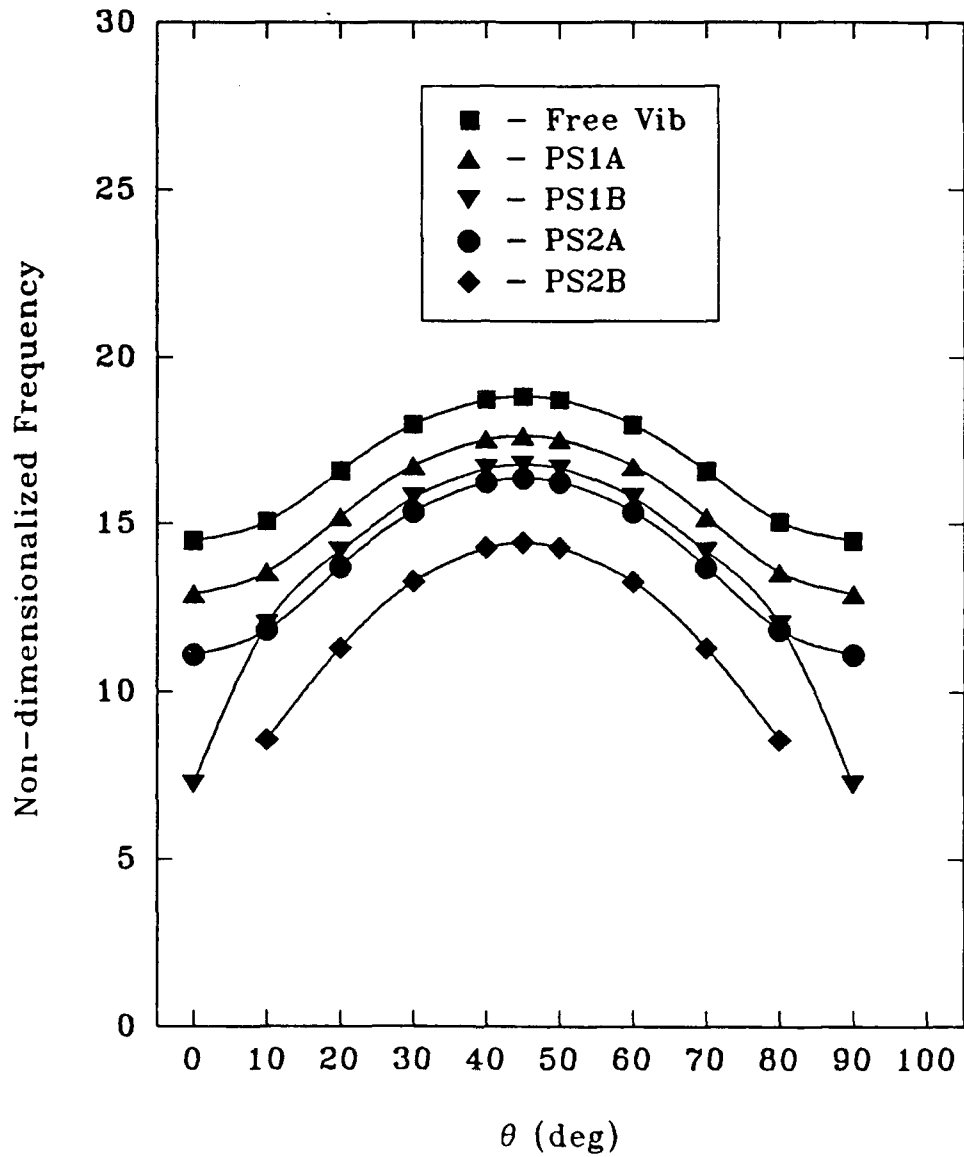


Figure 5.6: Pre-Stressed Natural Frequency -vs- Ply Angle. Case B, 6 Layer $[+\theta/-\theta/\dots]$, Material II, $a/b = 1.0$, $h/b = 0.1$, Simply supported (BC-6), 4×4 full plate model.

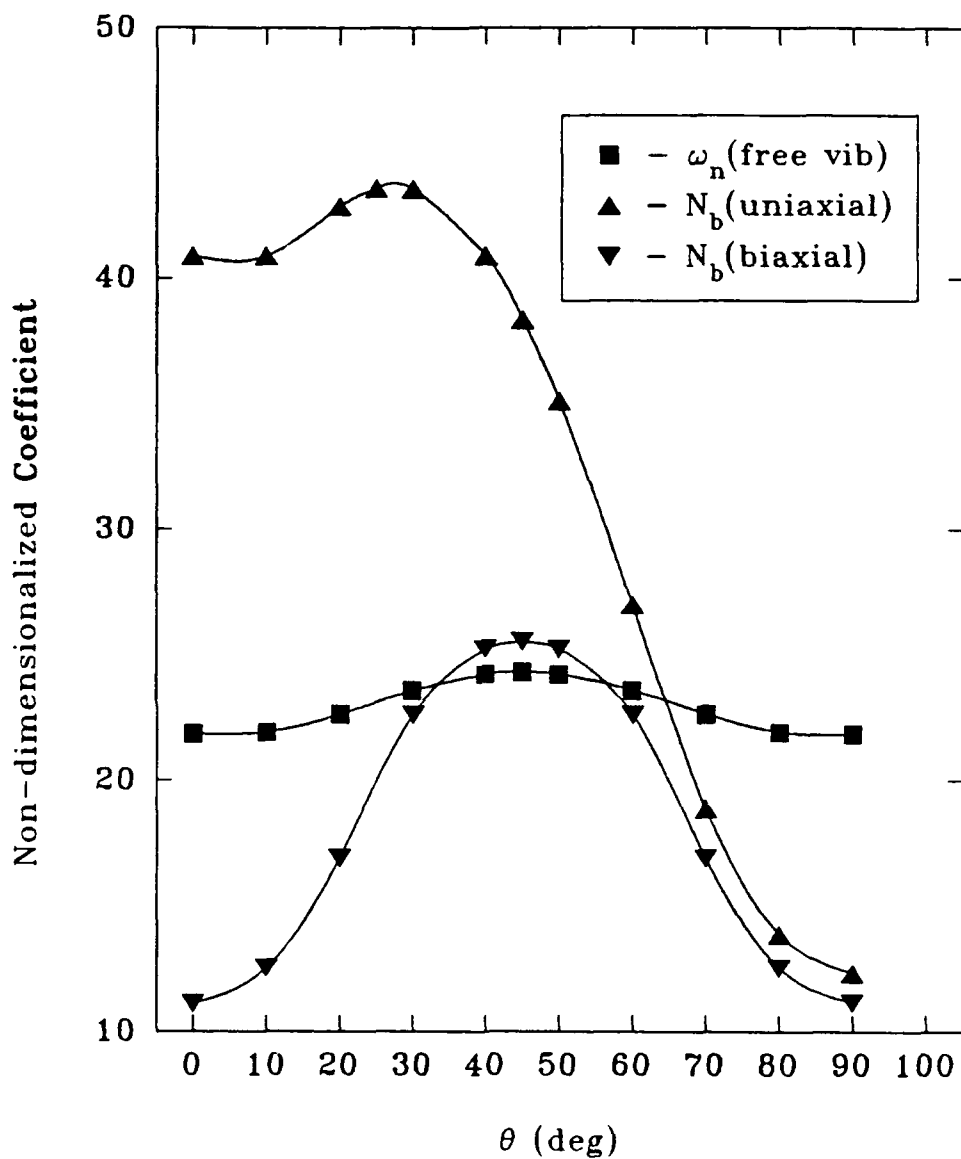


Figure 5.7: Eigenvalue Coefficients -vs- Ply Angle. Case B, 6 Layer $[+\theta/-\theta/\dots]$, Material II, $a/b = 1.0$, $h/b = 0.1$, Clamped, (BC-13), 4×4 full plate model.

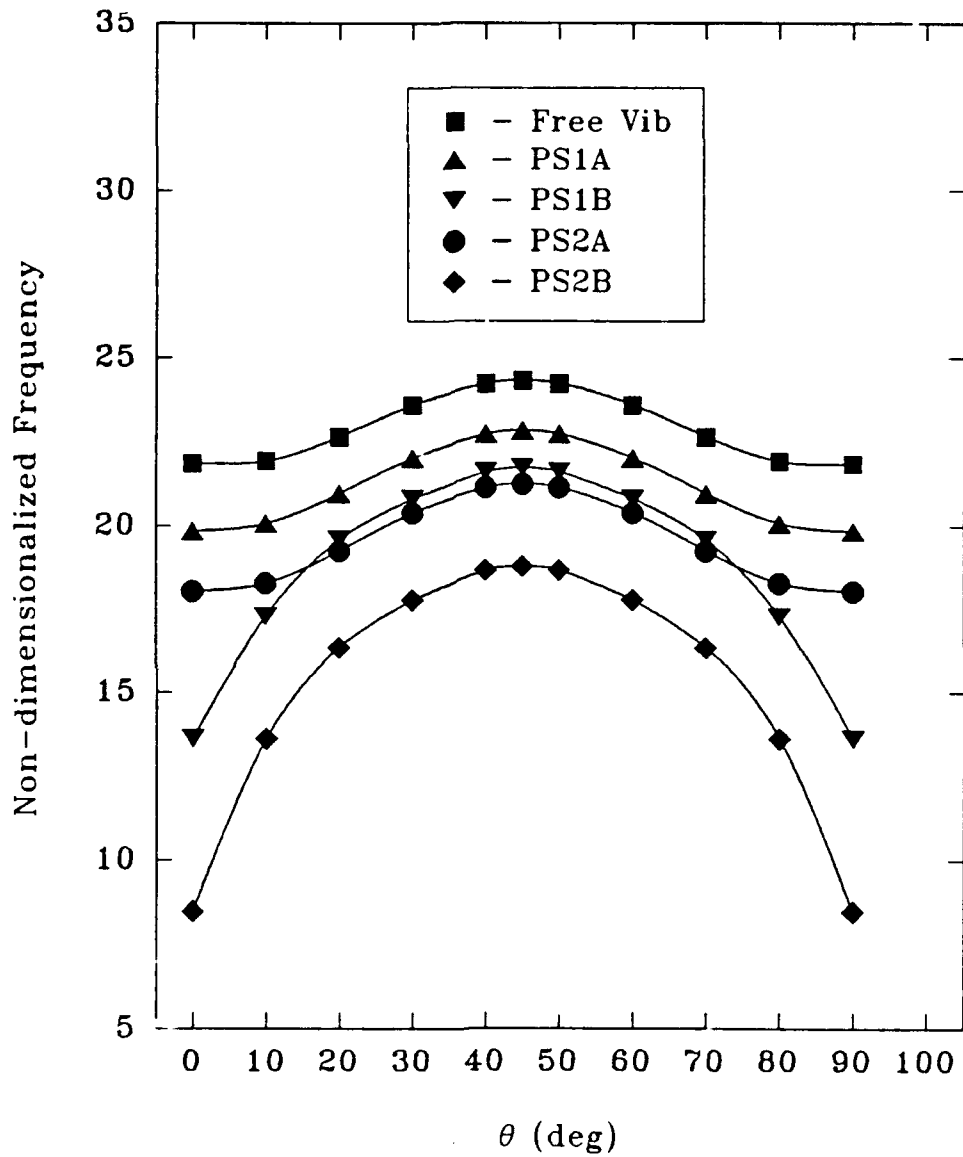


Figure 5.8: Pre-Stressed Natural Frequency -vs- Ply Angle. Case B, 6 Layer [+ θ / $-\theta$ /...], Material II, $a/b = 1.0$, $h/b = 0.1$, Clamped (BC-13), 4×4 full plate model

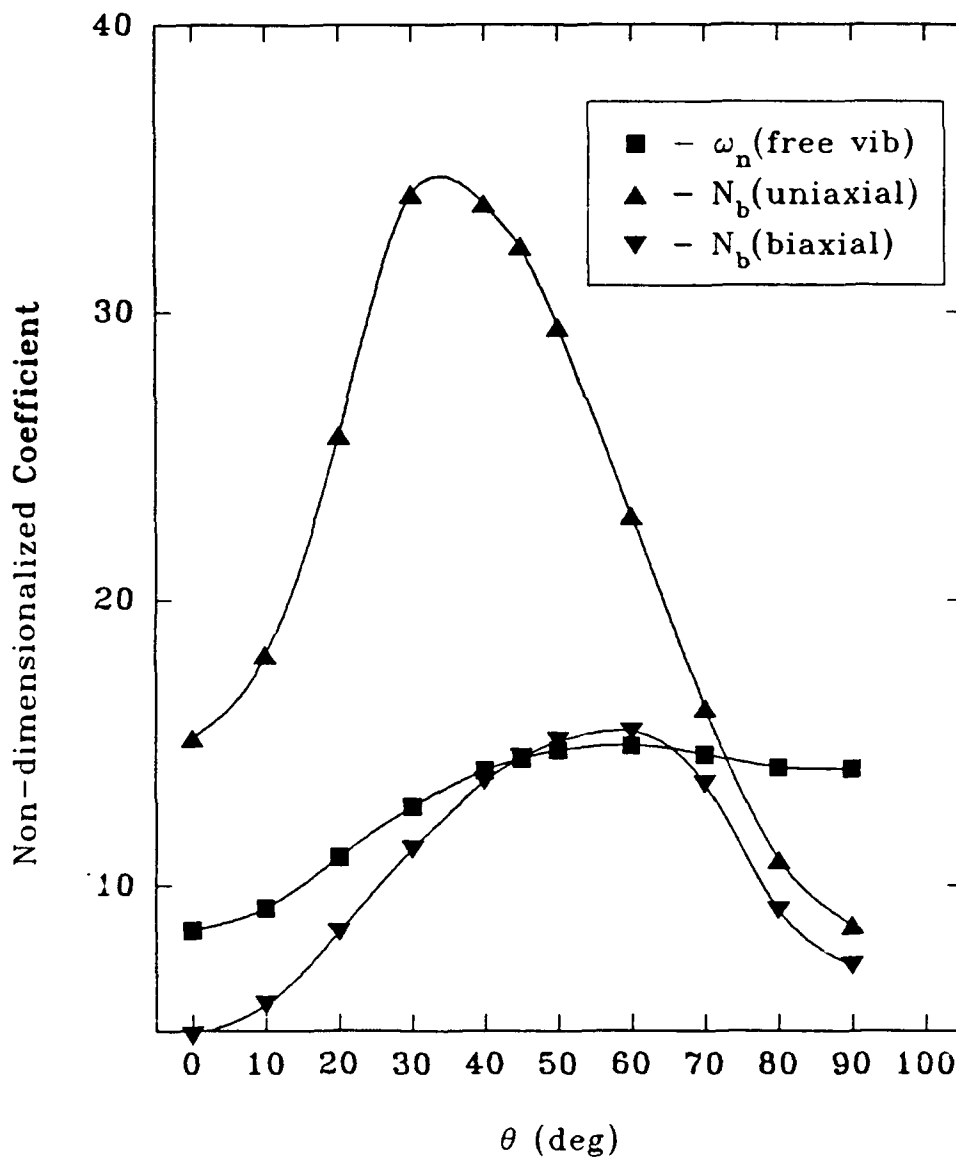


Figure 5.9: Eigenvalue Coefficients -vs- Ply Angle. Case C, 6 Layer [+ θ / $-\theta$ /...], Material II, $a/b = 1.4286$, $h/b = 0.1$, Simply supported (BC-6), 4×3 full plate model.

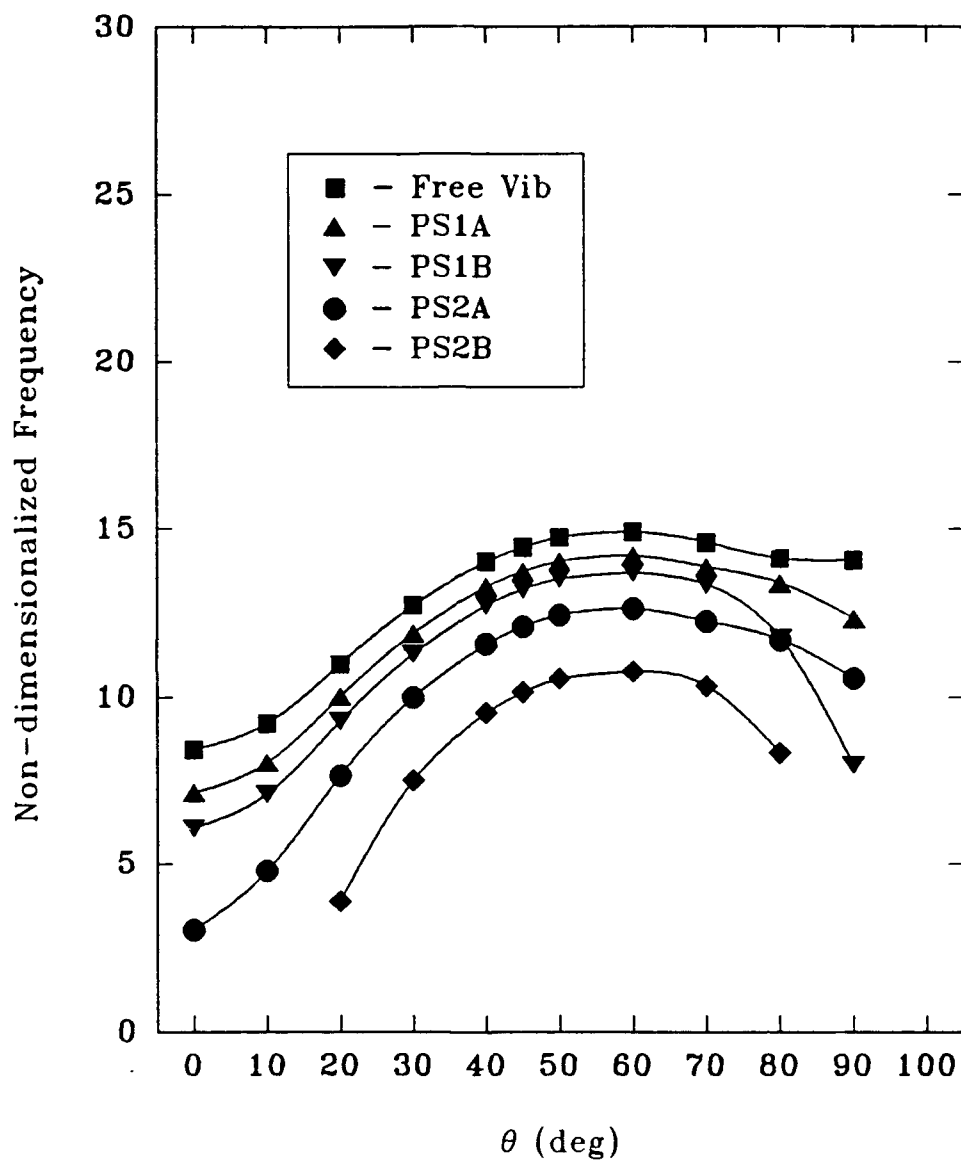


Figure 5.10: Pre-Stressed Natural Frequency -vs- Ply Angle. Case C, 6 Layer $[+\theta/-\theta/\dots]$, Material II, $a/b = 1.4286$, $h/b = 0.1$, Simply supported (BC-6), 4×3 full plate model.

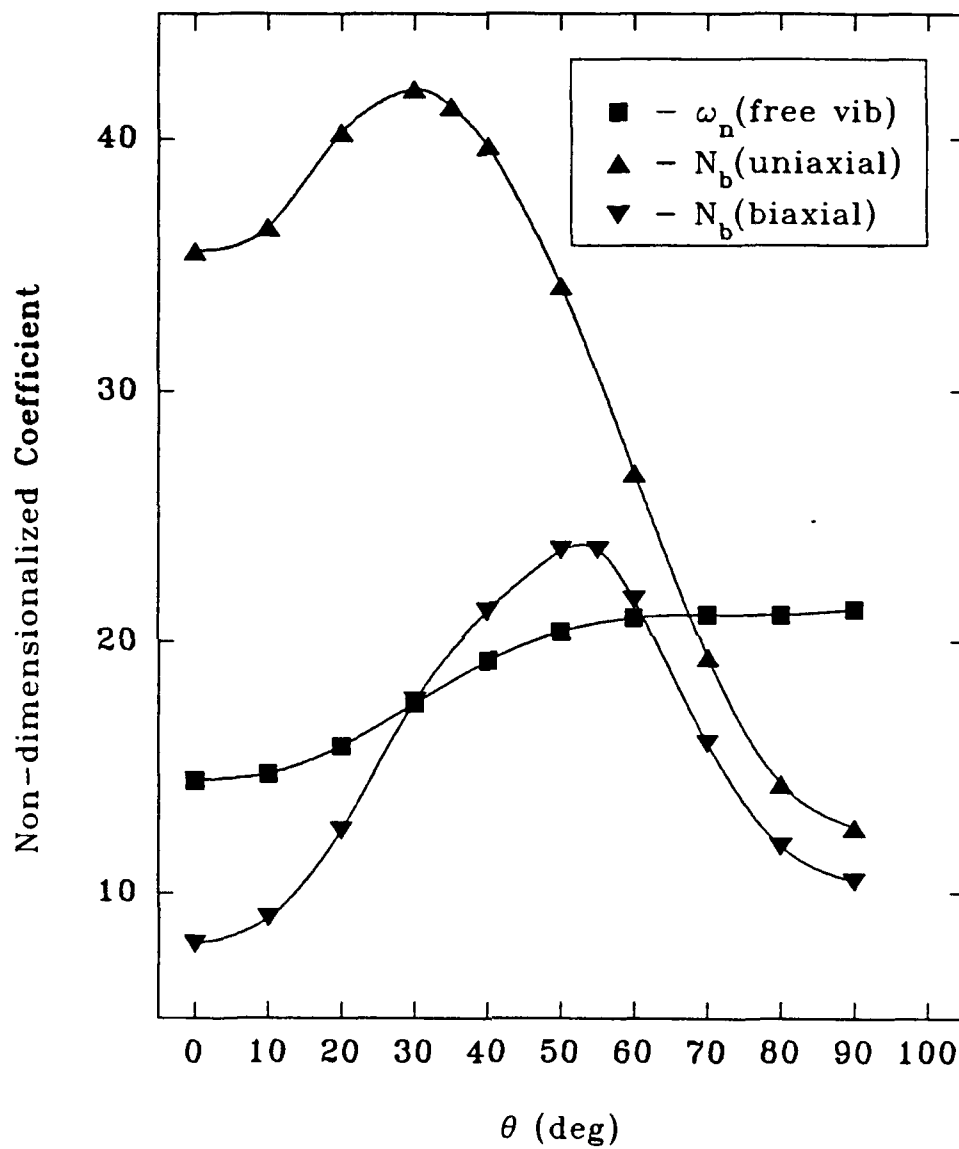


Figure 5.11: Eigenvalue Coefficients -vs- Ply Angle. Case C, 6 Layer [+ θ / - θ /...], Material II, $a/b = 1.4286$, $h/b = 0.1$, Clamped, (BC-13), 4×3 full plate model.

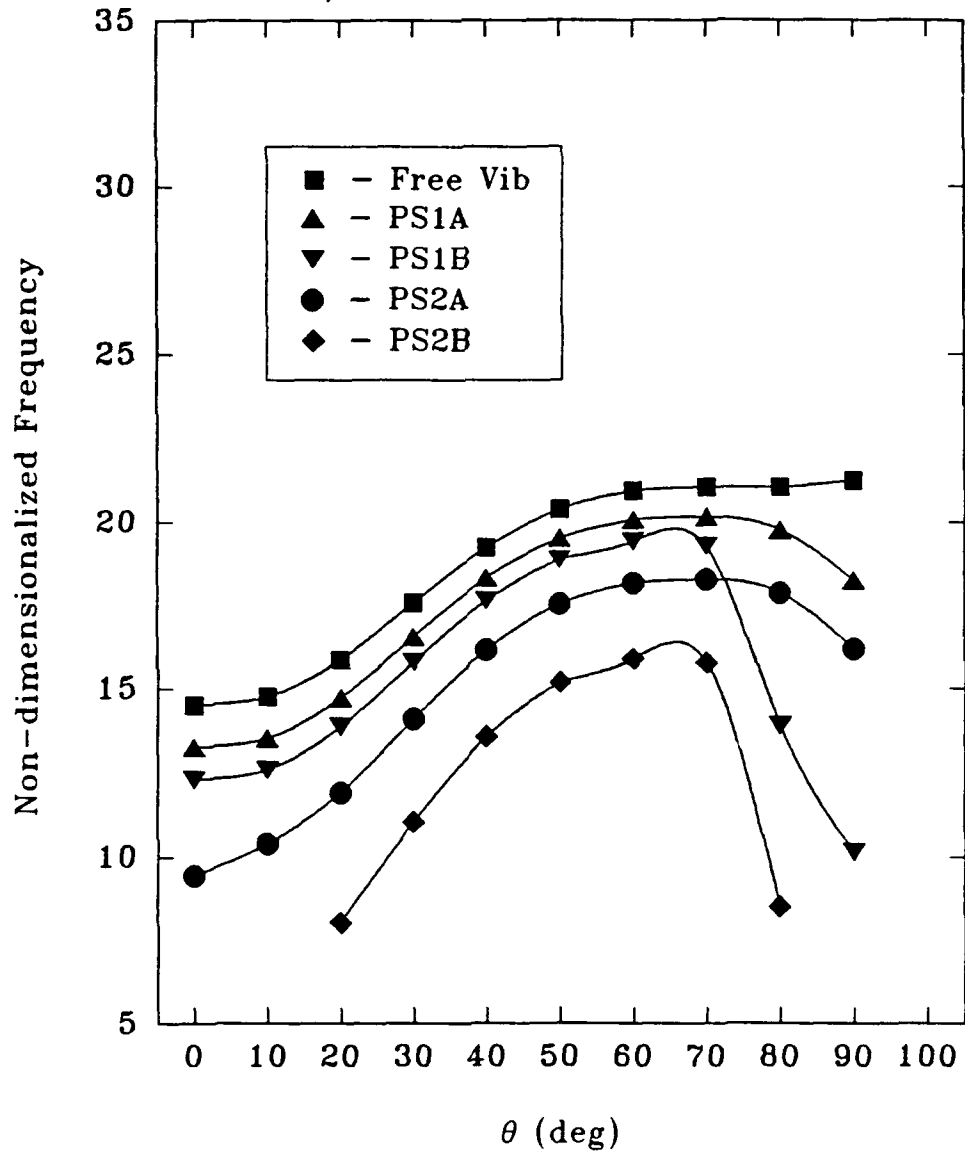


Figure 5.12: Pre-Stressed Natural Frequency -vs- Ply Angle. Case C, 6 Layer $[+\theta/-\theta/\dots]$, Material II, $a/b = 1.4286$, $h/b = 0.1$, Clamped (BC-13), 4×3 full plate model

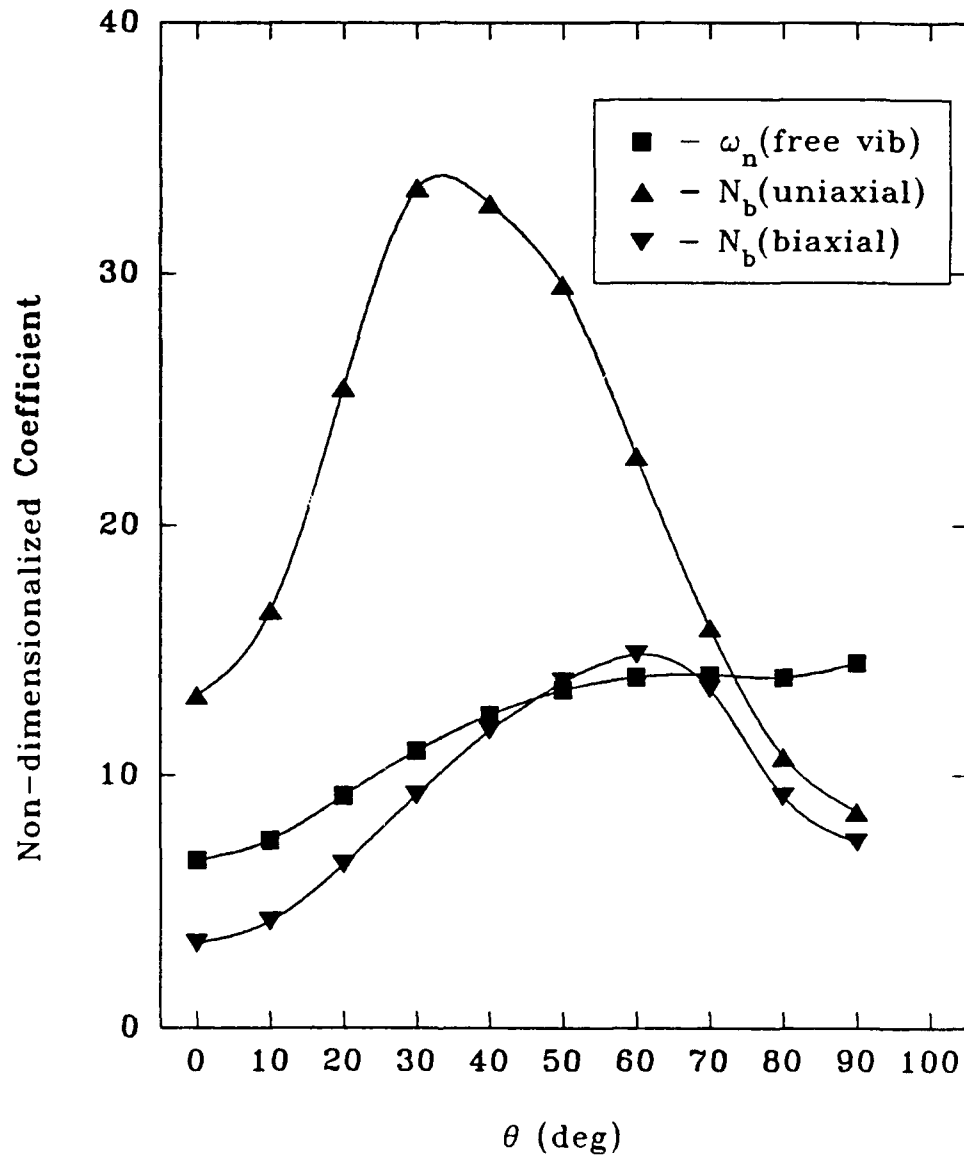


Figure 5.13: Eigenvalue Coefficients -vs- Ply Angle. Case D, 6 Layer [+ θ / - θ /...], Material II, $a/b = 1.7$, $h/b = 0.1$, Simply supported (BC-6), 5×3 full plate model.

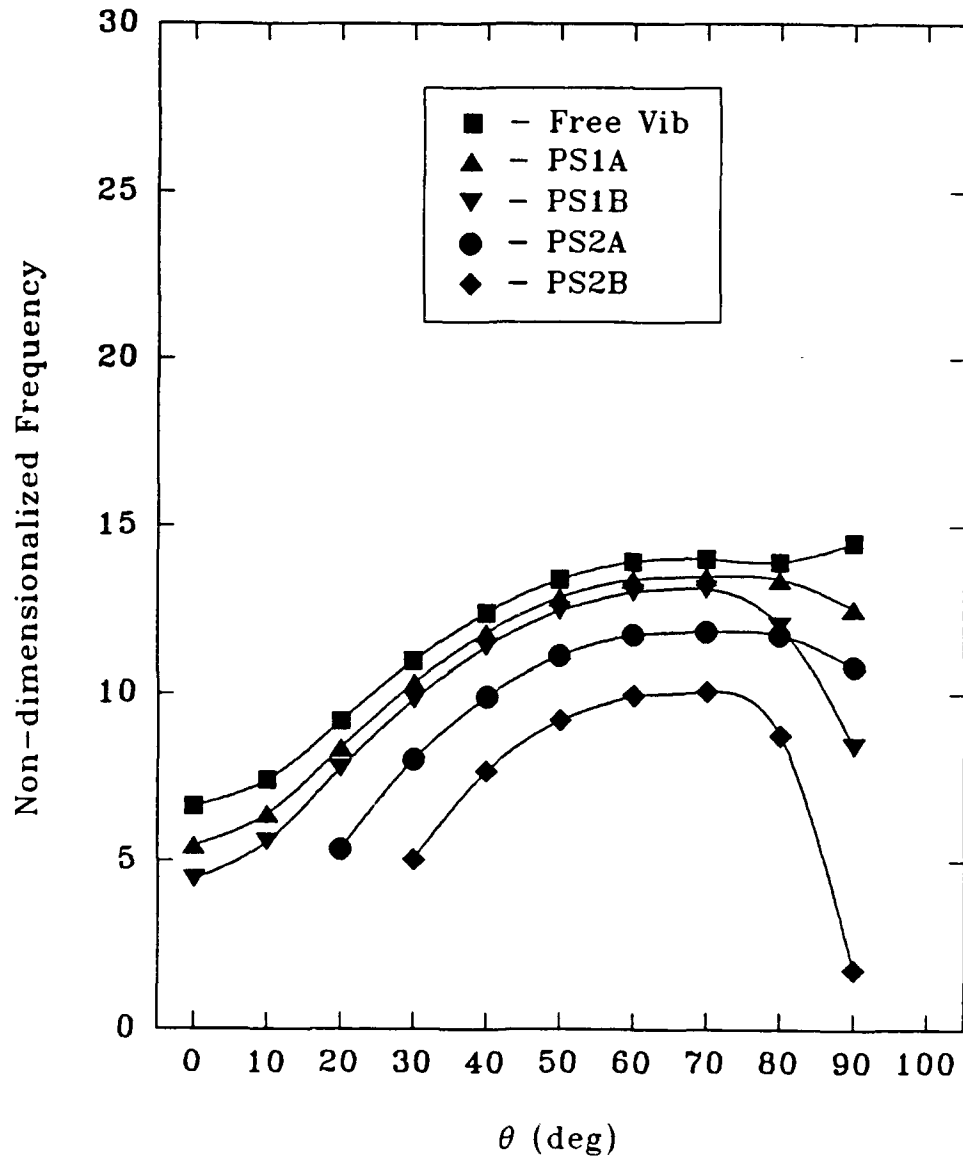


Figure 5.14: Pre-Stressed Natural Frequency -vs- Ply Angle. Case D, 6 Layer $[+\theta/-\theta/\dots]$, Material II, $a/b = 1.7$, $h/b = 0.1$, Simply supported (BC-6), 5×3 full plate model.

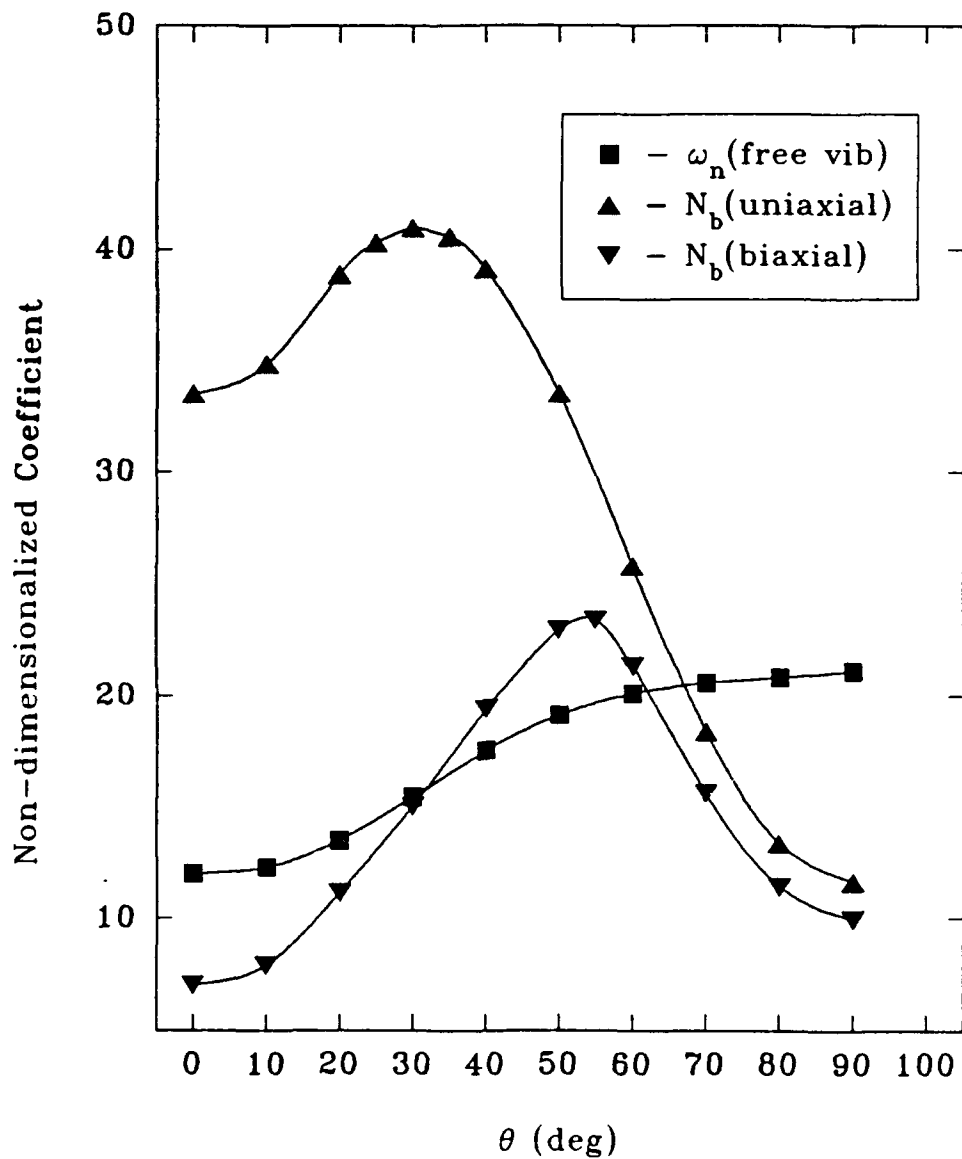


Figure 5.15: Eigenvalue Coefficients -vs- Ply Angle. Case D, 6 Layer [+ θ / - θ /...], Material II, $a/b = 1.7$, $h/l = 0.1$, Clamped, (BC-13), 5×3 full plate model.

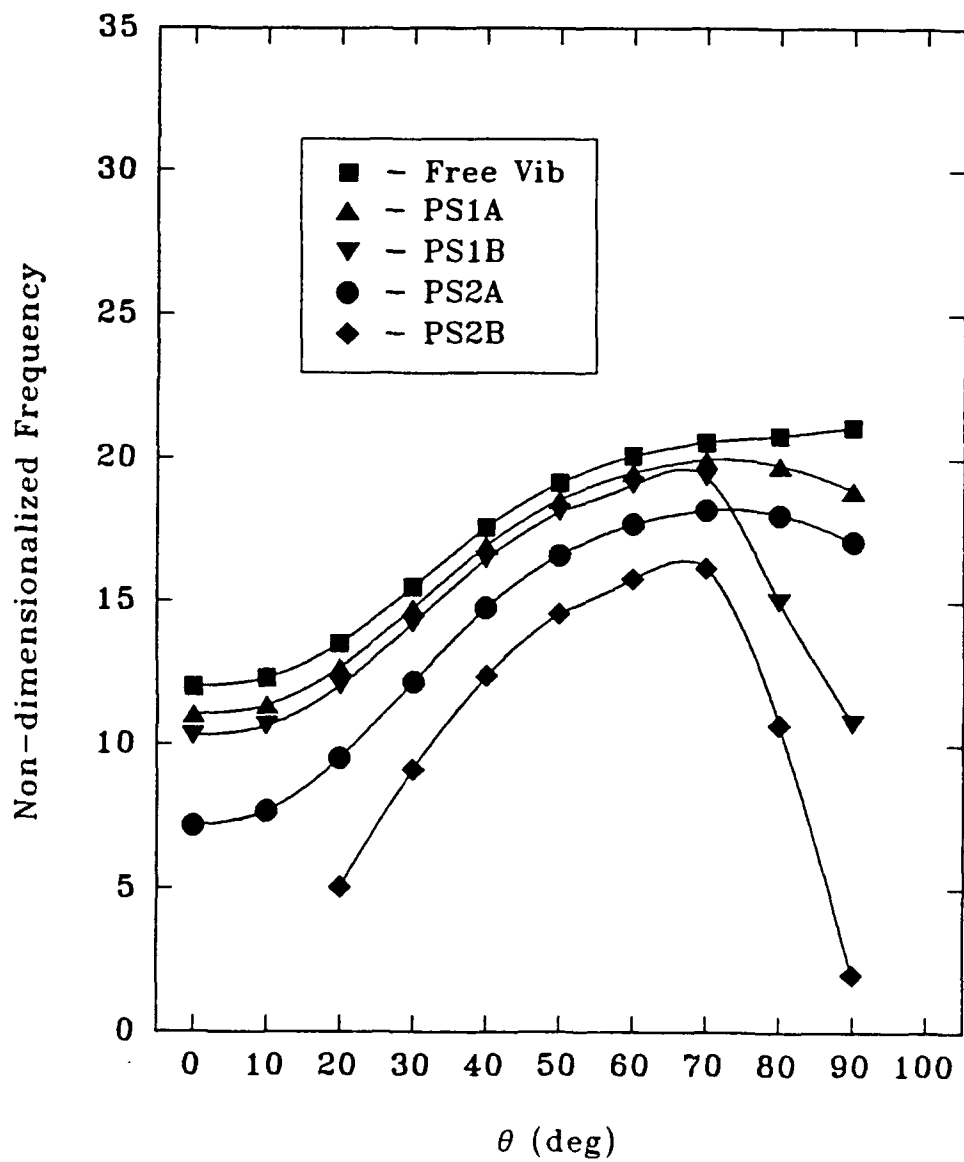


Figure 5.16: Pre-Stressed Natural Frequency -vs- Ply Angle. Case D, 6 Layer $[+\theta/-\theta/\dots]$, Material II, $a/b = 1.7$, $h/b = 0.1$, Clamped (BC-13), 5×3 full plate model.

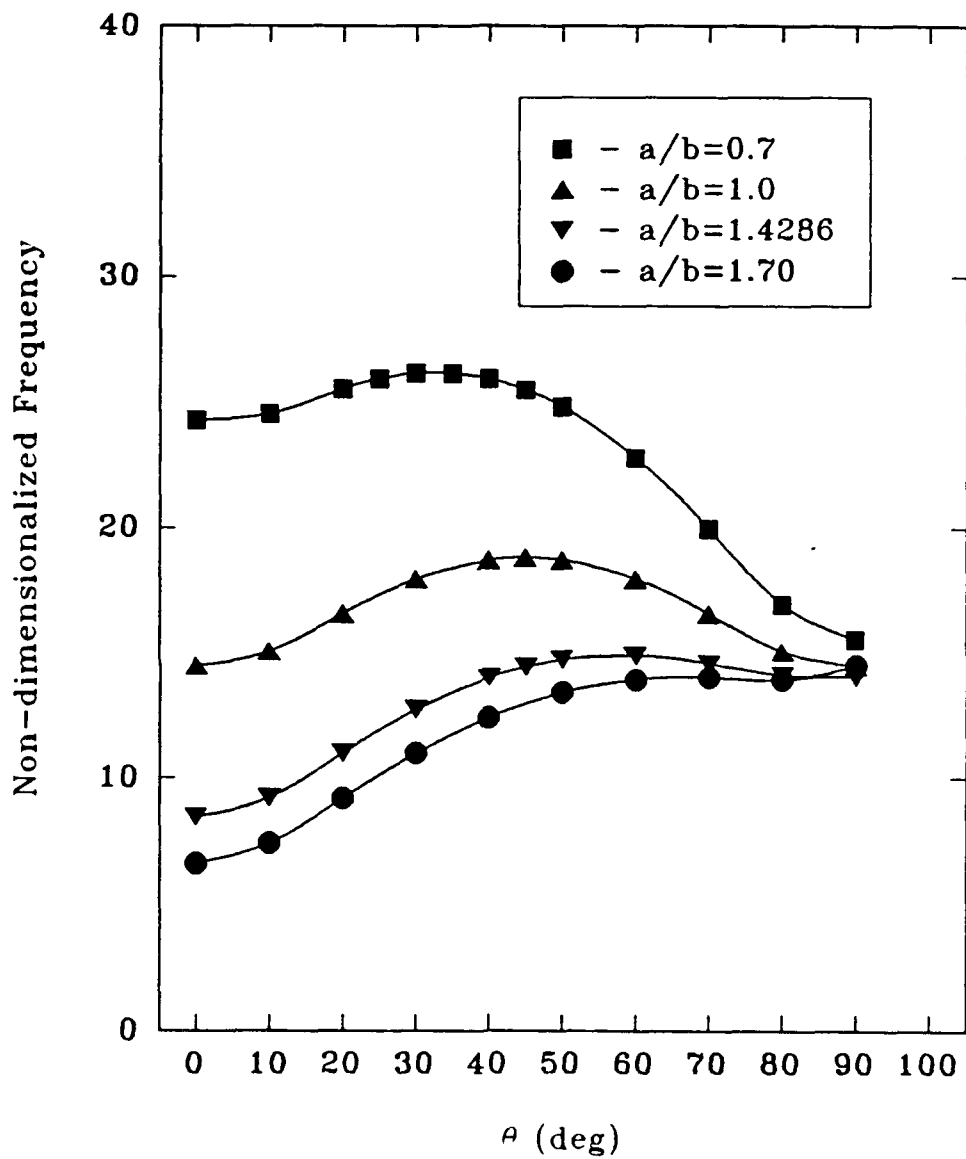


Figure 5.17: Natural Frequency -vs- Ply Angle for All Aspect Ratios. 6 Layer $[+\theta/-\theta/\dots]$, Material II, $h/b = 0.1$, Simply Supported (BC-6), Various mesh full plate models.

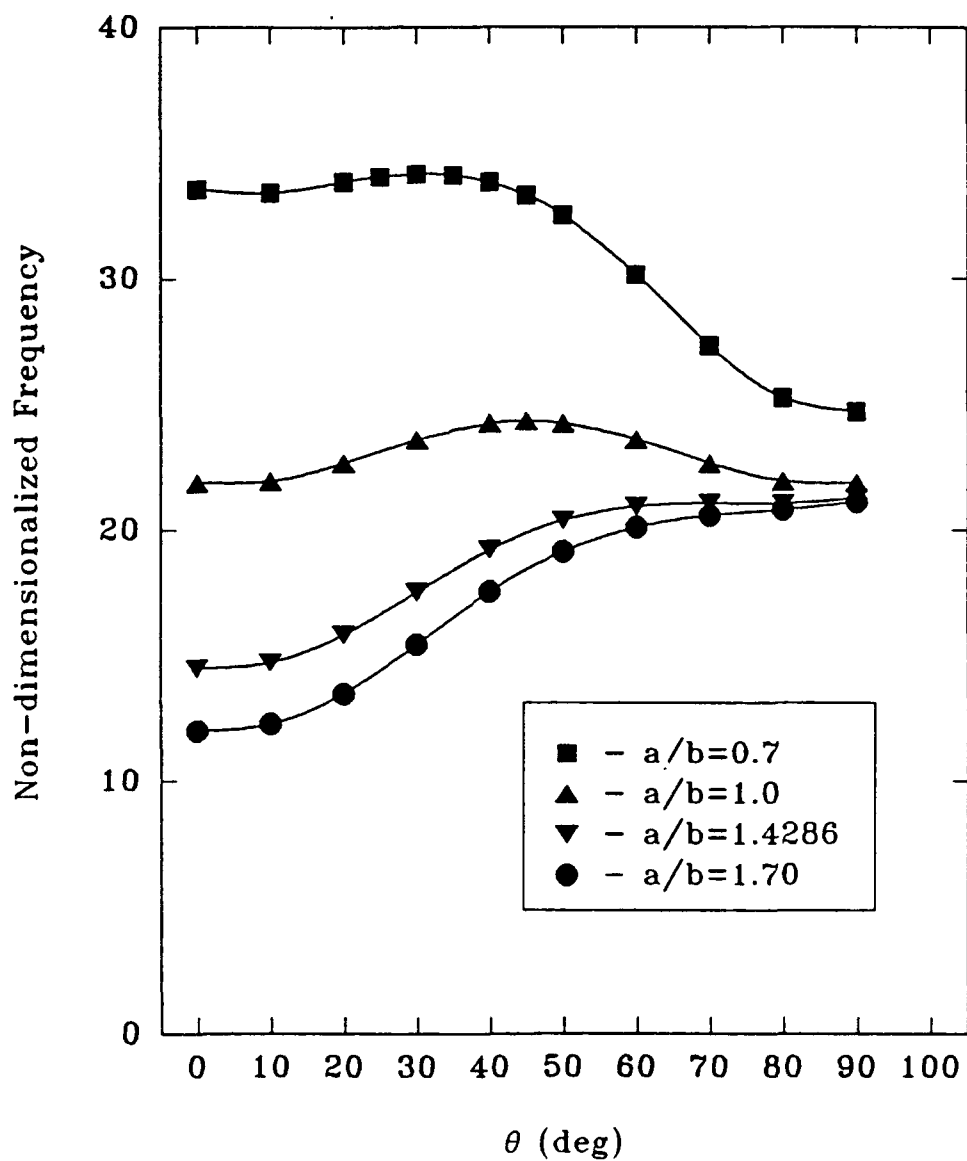


Figure 5.18: Natural Frequency -vs- Ply Angle for All Aspect Ratios. 6 Layer [+ θ /- θ /...], Material II, $h/b = 0.1$, Clamped (BC-13), Various mesh full plate models.

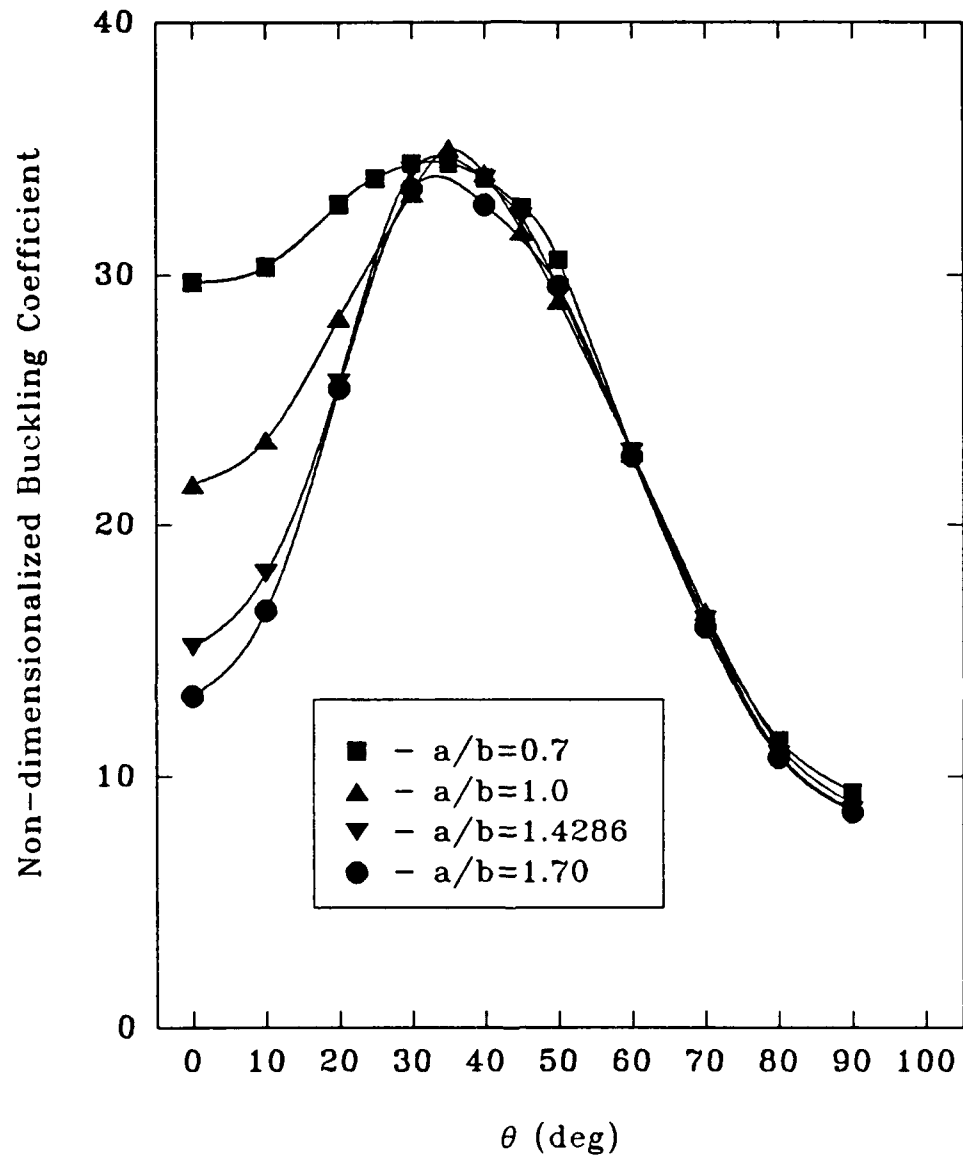


Figure 5.19: Uniaxial Buckling Coefficient -vs- Ply Angle for All Aspect Ratios. 6 Layer [+ θ / - θ / ...], Material II, $h/b = 0.1$, Simply Supported (BC-6), Various mesh full plate models.

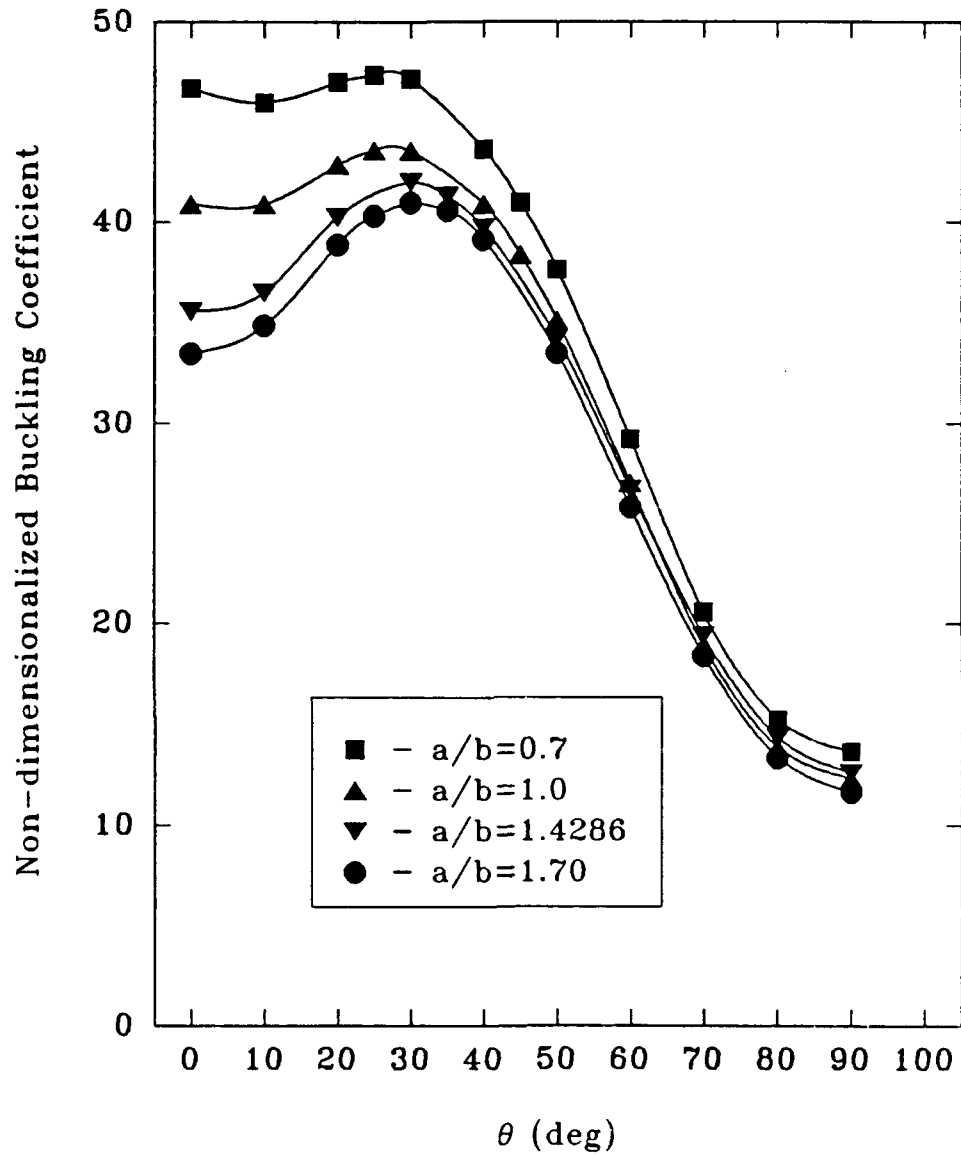


Figure 5.20: Uniaxial Buckling Coefficient -vs- Ply Angle for All Aspect Ratios. 6 Layer $[+\theta/ -\theta/ \dots]$, Material II, $h/b = 0.1$, Clamped (BC-13), Various mesh full plate models.

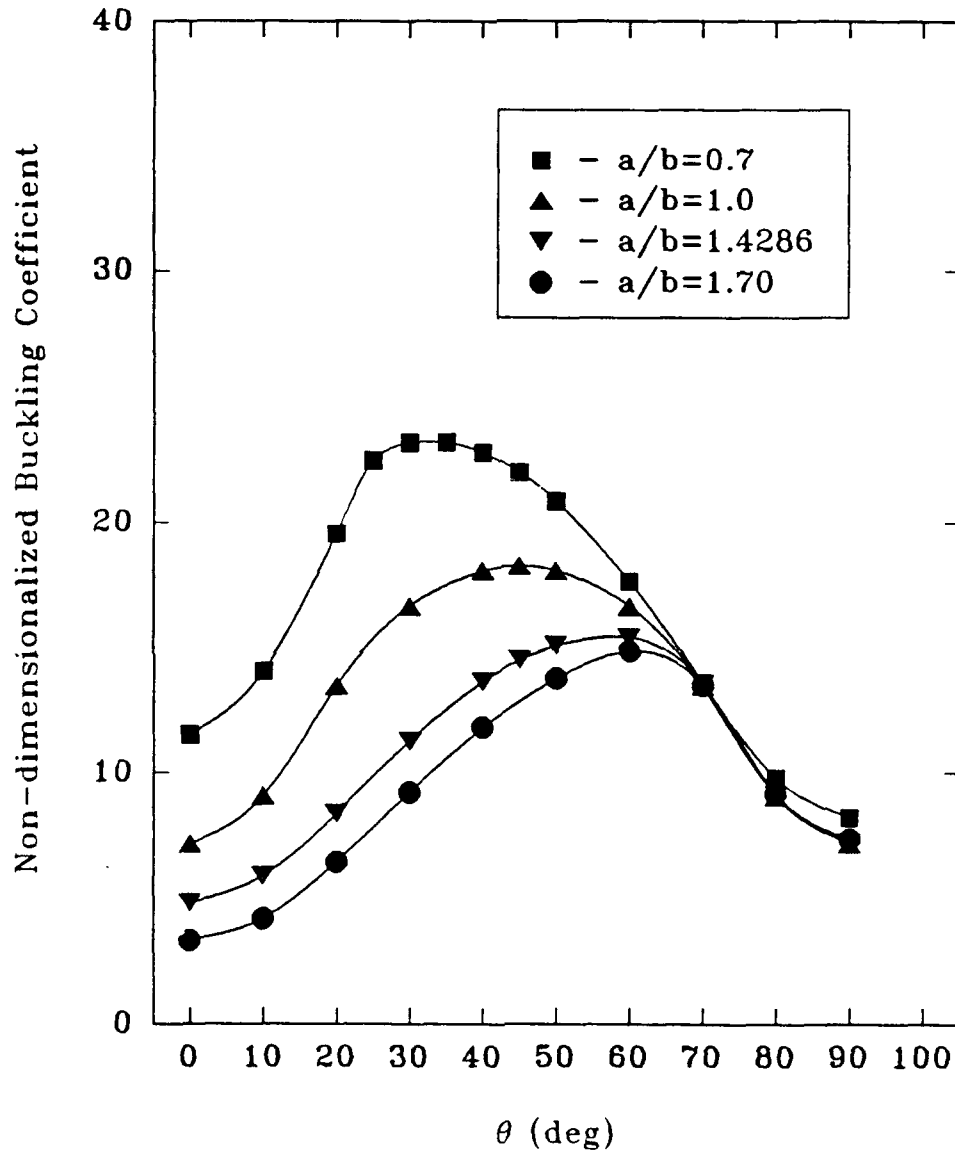


Figure 5.21: Biaxial Buckling Coefficient -vs- Ply Angle for All Aspect Ratios. 6 Layer [+ θ / - θ / ...], Material II, $h/b = 0.1$, Simply Supported (BC-6), Various mesh full plate models.

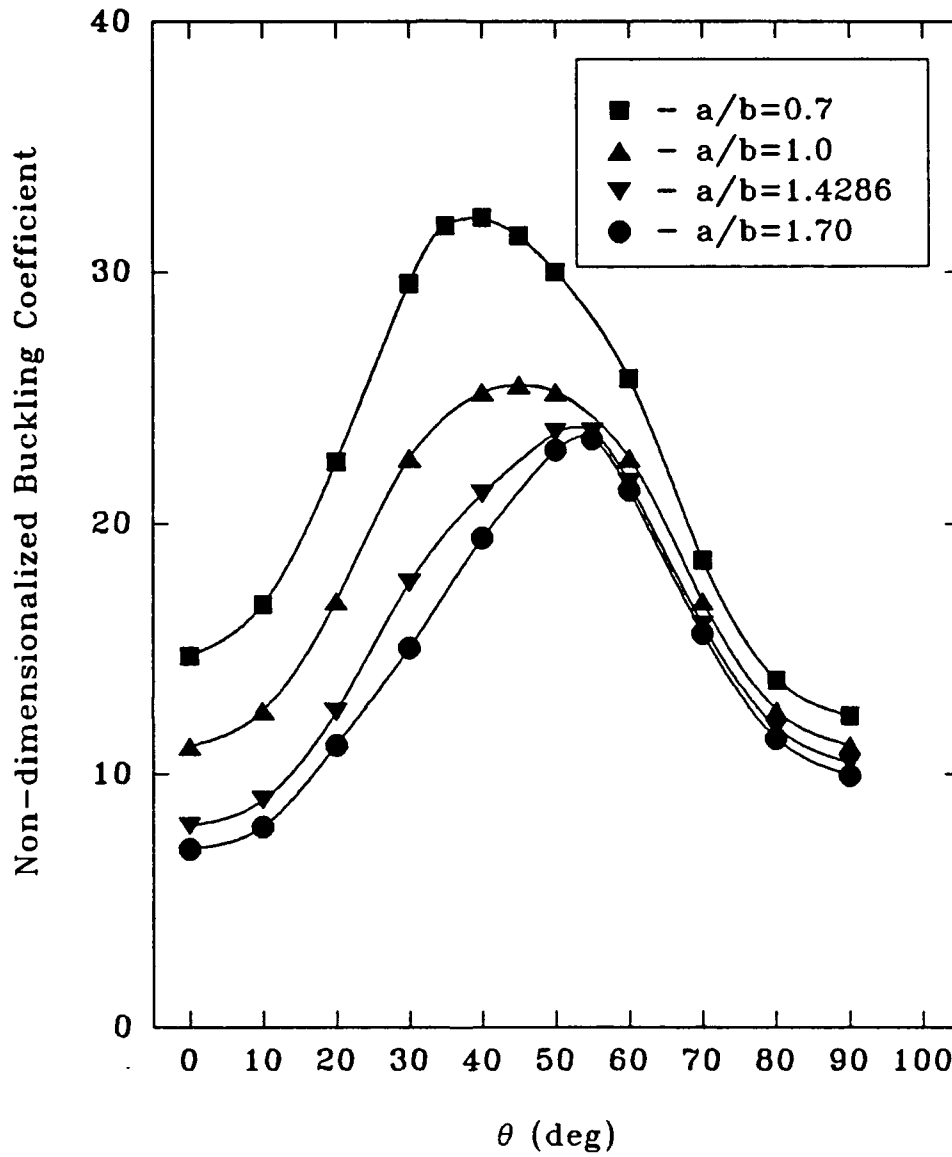


Figure 5.22: Biaxial Buckling Coefficient -vs- Ply Angle for All Aspect Ratios. 6 Layer [+ θ / - θ /...], Material II, $h/b = 0.1$, Clamped (BC-13), Various mesh full plate models.

Appendix A

Supplement to Equations

A.1 Supplement to equations Chapter III

In the derivation of the stiffness matrix, eqn (3.64) was written as

$$\begin{Bmatrix} \epsilon_x \\ \epsilon_y \\ \gamma_{xy} \end{Bmatrix}^k = \{\epsilon\}^k = [S] \{\delta\} \quad (\text{A.1})$$

In this equation, the matrix $[S]$, is of the form:

$$[S] = \begin{bmatrix} A_1 & A_2 & A_3 & A_4 & A_5 \end{bmatrix} \quad (\text{A.2})$$

where

$$\begin{aligned} [A_1] &= \begin{bmatrix} 1 & 0 & 0 \\ 0 & 1 & 0 \\ 0 & 0 & 1 \end{bmatrix} & [A_2] &= \begin{bmatrix} \Gamma_k & 0 & 0 & 0 \\ 0 & \tilde{\Gamma}_k & 0 & 0 \\ 0 & 0 & \Gamma_k & \tilde{\Gamma}_k \end{bmatrix} \\ [A_3] &= \begin{bmatrix} z\alpha_k & 0 & 0 & 0 \\ 0 & z\beta_k & 0 & 0 \\ 0 & 0 & z\alpha_k & z\beta_k \end{bmatrix} & [A_4] &= \begin{bmatrix} \theta\alpha_k & 0 & 0 & 0 \\ 0 & \theta\beta_k & 0 & 0 \\ 0 & 0 & \theta\alpha_k & t\beta_k \end{bmatrix} \\ [A_5] &= \begin{bmatrix} -z & 0 & 0 \\ 0 & -z & 0 \\ 0 & 0 & -z \end{bmatrix} \end{aligned} \quad (\text{A.3})$$

The column matrix $\{\delta\}$ is of the form

In eqn (3.73):

$$[L_1^t] = \begin{bmatrix} 1 & 0 & 0 & 0 \\ 0 & 1 & 0 & 0 \\ 1 & 0 & 0 & 0 \\ 0 & 1 & 0 & 0 \\ 0 & 0 & 1 & 0 \\ 0 & 0 & 0 & 1 \\ 0 & 0 & 0 & 1 \\ 0 & 0 & 1 & 0 \\ 0 & 0 & 0 & 1 \end{bmatrix} \quad (\text{A.5})$$

In eqn (3.76):

$$[L_2] = \begin{bmatrix} [J]^{-1} & 0 & 0 & 0 & 0 \\ 0 & [J]^{-1} & 0 & 0 & 0 \\ 0 & 0 & [J]^{-1} & 0 & 0 \\ 0 & 0 & 0 & [J]^{-1} & 0 \\ 0 & 0 & 0 & 0 & [J_B]^{-1} \end{bmatrix} \quad (\text{A.6})$$

where $[J]^{-1}$ is the 2 by 2 inverse of the Jacobian matrix, and $[J_B]^{-1}$ is the 3 by 3 inverse of the second order Jacobian matrix (See Appendix B).

In eqn (3.77):

$$[L_2^t] = \begin{bmatrix} 1 & 0 & 0 \\ 0 & 1 & 0 \\ 0 & 0 & [J]^{-1} \end{bmatrix} \quad (\text{A.7})$$

where $[J]^{-1}$ is as above

In eqn (3.82):

$$[\mathcal{A}_{\eta\xi}] = \begin{bmatrix} [\mathbf{A}_{\eta/\xi}] & 0 & 0 & 0 & 0 \\ 0 & [\mathbf{A}_{\eta/\xi}] & 0 & 0 & 0 \\ 0 & 0 & [\mathbf{A}_{\eta/\xi}] & 0 & 0 \\ 0 & 0 & 0 & [\mathbf{A}_{\eta/\xi}] & 0 \\ 0 & 0 & 0 & 0 & [\mathbf{A}_{\eta/\xi}] \\ 0 & 0 & 0 & 0 & [\mathbf{A}_{\eta\eta}] \\ 0 & 0 & 0 & 0 & [\mathbf{A}_{\eta\xi}] \\ 0 & 0 & 0 & 0 & [\mathbf{A}_{\xi\xi}] \end{bmatrix} \quad (\text{A.8})$$

where

$$[\mathbf{A}_{\eta/\xi}] = \begin{bmatrix} \mathbf{A}_{,\eta} \\ \mathbf{A}_{,\xi} \end{bmatrix} \quad (\text{A.9})$$

$$[\mathbf{A}_{\eta\eta}] = [\mathbf{A}_{,\eta\eta}] \quad (\text{A.10})$$

$$[\mathbf{A}_{\eta\xi}] = [\mathbf{A}_{,\eta\xi}] \quad (\text{A.11})$$

$$[\mathbf{A}_{\xi\xi}] = [\mathbf{A}_{,\xi\xi}] \quad (\text{A.12})$$

In the above, the matrix $[\mathbf{A}]$ is as defined in eqn (3.16), and the subscripts here denote partial differentiation term by term.

In eqn (3.83):

$$[\mathcal{A}_{\eta\xi}] = \begin{bmatrix} 0 & 0 & [\mathbf{A}] & 0 & 0 \\ 0 & 0 & 0 & [\mathbf{A}] & 0 \\ 0 & 0 & 0 & 0 & [\mathbf{A}_{\eta/\xi}] \end{bmatrix} \quad (\text{A.13})$$

where $[\mathbf{A}]$ is as defined above.

In eqn (3.84):

$$[L_3] = \begin{bmatrix} I & 0 & 0 \\ 0 & I & 0 \\ 0 & 0 & B \end{bmatrix} \quad (\text{A.14})$$

where

$$[I] = \begin{bmatrix} 1 & 0 & 0 & 0 \\ 0 & 1 & 0 & 0 \\ 0 & 0 & 1 & 0 \\ 0 & 0 & 0 & 1 \end{bmatrix} \quad (\text{A.15})$$

and

$$[B] = \begin{bmatrix} \theta_a^1 & \theta_b^1 & 1 & 0 & 0 \\ \theta_a^2 & \theta_b^2 & 0 & 1 & 0 \\ \theta_a^3 & \theta_b^3 & 0 & 0 & 1 \end{bmatrix} \quad (\text{A.16})$$

Here:

$$\begin{aligned} \theta_a^1 &= -x_{,\eta\eta} \Gamma_{11} - y_{,\eta\eta} \Gamma_{21} & \theta_b^1 &= -x_{,\eta\eta} \Gamma_{12} - y_{,\eta\eta} \Gamma_{22} \\ \theta_a^2 &= -x_{,\eta\xi} \Gamma_{11} - y_{,\eta\xi} \Gamma_{21} & \theta_b^2 &= -x_{,\eta\xi} \Gamma_{12} - y_{,\eta\xi} \Gamma_{22} \\ \theta_a^3 &= -x_{,\xi\xi} \Gamma_{11} - y_{,\xi\xi} \Gamma_{21} & \theta_b^3 &= -x_{,\xi\xi} \Gamma_{12} - y_{,\xi\xi} \Gamma_{22} \end{aligned} \quad (\text{A.17})$$

In eqn (3.90)

$$[S_m] = [B_1 \ B_2 \ B_3 \ B_4 \ B_5] \quad (\text{A.18})$$

where

$$\begin{aligned}
 [B_1] &= \begin{bmatrix} 1 & 0 & 0 \\ 0 & 1 & 0 \\ 0 & 0 & 1 \end{bmatrix} & [B_2] &= \begin{bmatrix} \Gamma_k & 0 \\ 0 & \tilde{\Gamma}_k \\ 0 & 0 \end{bmatrix} \\
 [B_3] &= \begin{bmatrix} z\alpha_k & 0 \\ 0 & z\beta_k \\ 0 & 0 \end{bmatrix} & [B_4] &= \begin{bmatrix} \theta\alpha_k & 0 \\ 0 & \theta\beta_k \\ 0 & 0 \end{bmatrix} \\
 [B_5] &= \begin{bmatrix} -z & 0 \\ 0 & -z \\ 0 & 0 \end{bmatrix}
 \end{aligned} \quad (\text{A.19})$$

In eqn (3.107):

$$[I_B] = \begin{bmatrix} 1 & 0 & 0 & 0 & 0 & 0 & 0 & 0 & 0 & 0 & 0 & 0 & 0 \\ 0 & 0 & 1 & 0 & 0 & 0 & 0 & 0 & 0 & 0 & 0 & 0 & 0 \\ 0 & 0 & 0 & 0 & 0 & 0 & 0 & 0 & 0 & 0 & 0 & 1 & 0 \\ 0 & 0 & 0 & 0 & 1 & 0 & 0 & 0 & 0 & 0 & 0 & 0 & 0 \\ 0 & 0 & 0 & 0 & 0 & 0 & 1 & 0 & 0 & 0 & 0 & 0 & 0 \\ 0 & 0 & 0 & 0 & 1 & 0 & 0 & 0 & 0 & 0 & 0 & 0 & 0 \\ 0 & 0 & 0 & 0 & 0 & 0 & 1 & 0 & 0 & 0 & 0 & 0 & 0 \\ 0 & 0 & 0 & 0 & 1 & 0 & 0 & 0 & 0 & 0 & 0 & 0 & 0 \\ 0 & 0 & 0 & 0 & 0 & 0 & 1 & 0 & 0 & 0 & 0 & 0 & 0 \\ 0 & 0 & 0 & 0 & 0 & 0 & 0 & 0 & 1 & 0 & 0 & 0 & 0 \\ 0 & 0 & 0 & 0 & 0 & 0 & 0 & 0 & 0 & 1 & 0 & 0 & 0 \\ 0 & 1 & 0 & 0 & 0 & 0 & 0 & 0 & 0 & 0 & 0 & 0 & 0 \\ 0 & 0 & 0 & 1 & 0 & 0 & 0 & 0 & 0 & 0 & 0 & 0 & 0 \\ 0 & 0 & 0 & 0 & 0 & 0 & 0 & 0 & 0 & 0 & 0 & 0 & 1 \\ 0 & 0 & 0 & 0 & 0 & 1 & 0 & 0 & 0 & 0 & 0 & 0 & 0 \\ 0 & 0 & 0 & 0 & 0 & 0 & 0 & 1 & 0 & 0 & 0 & 0 & 0 \\ 0 & 0 & 0 & 0 & 0 & 1 & 0 & 0 & 0 & 0 & 0 & 0 & 0 \\ 0 & 0 & 0 & 0 & 0 & 0 & 0 & 1 & 0 & 0 & 0 & 0 & 0 \\ 0 & 0 & 0 & 0 & 0 & 0 & 0 & 0 & 1 & 0 & 0 & 0 & 0 \\ 0 & 0 & 0 & 0 & 0 & 0 & 0 & 0 & 0 & 1 & 0 & 0 & 0 \\ 0 & 0 & 0 & 0 & 0 & 0 & 0 & 0 & 0 & 0 & 1 & 0 & 0 \end{bmatrix} \quad (\text{A.20})$$

and

$$\{\delta_{xy}^m\}^T = \left[u_{o,x} \quad u_{o,y} \quad v_{o,x} \quad v_{o,y} \quad \varphi_{x,x} \quad \varphi_{x,y} \quad \varphi_{y,x} \quad \varphi_{y,y} \quad [w_{xy}] \right] \quad (\text{A.21})$$

where

$$[w_{xy}] = [w_{o,xx} \quad w_{o,xy} \quad w_{o,yy} \quad w_{o,x} \quad w_{o,y}] \quad (\text{A.22})$$

Appendix B

Calculation of Higher Order Derivatives

B.1 First Order Derivatives

In relating derivatives in the local coordinate system to those in the global, we use the standard expressions found in any standard finite element text [146] [9] [23] [136]. The equations are nothing more than the application of the chain rule. In finding the derivative of a function, call it N , we have:

$$\frac{\partial N}{\partial \eta} = \frac{\partial N}{\partial x} \frac{\partial x}{\partial \eta} + \frac{\partial N}{\partial y} \frac{\partial y}{\partial \eta} \quad (\text{B.1})$$

$$(\text{B.2})$$

$$\frac{\partial N}{\partial \xi} = \frac{\partial N}{\partial x} \frac{\partial x}{\partial \xi} + \frac{\partial N}{\partial y} \frac{\partial y}{\partial \xi} \quad (\text{B.3})$$

or, in matrix form we have:

$$\begin{aligned} \begin{Bmatrix} \frac{\partial N}{\partial \eta} \\ \frac{\partial N}{\partial \xi} \end{Bmatrix} &= \begin{bmatrix} \frac{\partial x}{\partial \eta} & \frac{\partial y}{\partial \eta} \\ \frac{\partial x}{\partial \xi} & \frac{\partial y}{\partial \xi} \end{bmatrix} \begin{Bmatrix} \frac{\partial N}{\partial x} \\ \frac{\partial N}{\partial y} \end{Bmatrix} \\ &= [J] \begin{Bmatrix} \frac{\partial N}{\partial x} \\ \frac{\partial N}{\partial y} \end{Bmatrix} \end{aligned} \quad (\text{B.4})$$

From this expression we can easily get:

$$\begin{Bmatrix} \frac{\partial N}{\partial x} \\ \frac{\partial N}{\partial y} \end{Bmatrix} = [J]^{-1} \begin{Bmatrix} \frac{\partial N}{\partial \eta} \\ \frac{\partial N}{\partial \xi} \end{Bmatrix} \quad (\text{B.5})$$

B.2 Higher Order Derivatives

To obtain higher order derivatives, we can apply the chain rule successively to the above equations. The results are:

$$\begin{aligned} \frac{\partial^2 N}{\partial \eta^2} &= \frac{\partial N}{\partial x} \frac{\partial^2 x}{\partial \eta^2} + \frac{\partial x}{\partial \eta} \left(\frac{\partial^2 N}{\partial x^2} \frac{\partial x}{\partial \eta} + \frac{\partial^2 N}{\partial x \partial y} \frac{\partial y}{\partial \eta} \right) + \frac{\partial N}{\partial y} \frac{\partial^2 y}{\partial \eta^2} + \frac{\partial y}{\partial \eta} \left(\frac{\partial^2 N}{\partial y^2} \frac{\partial y}{\partial \eta} + \frac{\partial^2 N}{\partial x \partial y} \frac{\partial x}{\partial \eta} \right) \\ &= \frac{\partial N}{\partial x} \frac{\partial^2 x}{\partial \eta^2} + \frac{\partial^2 N}{\partial x^2} \left(\frac{\partial x}{\partial \eta} \right)^2 + 2 \frac{\partial^2 N}{\partial x \partial y} \frac{\partial x}{\partial \eta} \frac{\partial y}{\partial \eta} + \frac{\partial N}{\partial y} \frac{\partial^2 y}{\partial \eta^2} + \frac{\partial^2 N}{\partial y^2} \left(\frac{\partial y}{\partial \eta} \right)^2 \end{aligned} \quad (\text{B.6})$$

and similarly

$$\frac{\partial^2 N}{\partial \xi^2} = \frac{\partial N}{\partial x} \frac{\partial^2 x}{\partial \xi^2} + \frac{\partial^2 N}{\partial x^2} \left(\frac{\partial x}{\partial \xi} \right)^2 + 2 \frac{\partial^2 N}{\partial x \partial y} \frac{\partial x}{\partial \xi} \frac{\partial y}{\partial \xi} + \frac{\partial N}{\partial y} \frac{\partial^2 y}{\partial \xi^2} + \frac{\partial^2 N}{\partial y^2} \left(\frac{\partial y}{\partial \xi} \right)^2 \quad (\text{B.7})$$

The mixed partial turns out to be:

$$\frac{\partial^2 N}{\partial \eta \partial \xi} = \frac{\partial N}{\partial x} \frac{\partial^2 x}{\partial \eta \partial \xi} + \frac{\partial^2 N}{\partial x^2} \frac{\partial x}{\partial \eta} \frac{\partial x}{\partial \xi} + \frac{\partial^2 N}{\partial x \partial y} \left(\frac{\partial x}{\partial \eta} \frac{\partial y}{\partial \xi} + \frac{\partial x}{\partial \xi} \frac{\partial y}{\partial \eta} \right) + \frac{\partial N}{\partial y} \frac{\partial^2 y}{\partial \eta \partial \xi} + \frac{\partial^2 N}{\partial y^2} \frac{\partial y}{\partial \eta} \frac{\partial y}{\partial \xi} \quad (\text{B.8})$$

The next step is to put eqns (B.6)-(B.8) into matrix notation. In doing so directly the result is:

$$\left\{ \begin{array}{l} \frac{\partial^2 N}{\partial \eta^2} \\ \frac{\partial^2 N}{\partial \xi^2} \\ \frac{\partial^2 N}{\partial \eta \partial \xi} \end{array} \right\} = \left[\begin{array}{cccc} \frac{\partial^2 x}{\partial \eta^2} & \left(\frac{\partial x}{\partial \eta}\right)^2 & 2\frac{\partial x}{\partial \eta} \frac{\partial y}{\partial \eta} & \frac{\partial^2 y}{\partial \eta^2} \left(\frac{\partial y}{\partial \eta}\right)^2 \\ \frac{\partial^2 x}{\partial \eta \partial \xi} & \frac{\partial x}{\partial \eta} \frac{\partial x}{\partial \xi} & \left(\frac{\partial x}{\partial \eta} \frac{\partial y}{\partial \xi} + \frac{\partial x}{\partial \xi} \frac{\partial y}{\partial \eta}\right) & \frac{\partial^2 y}{\partial \eta \partial \xi} \frac{\partial y}{\partial \eta} \frac{\partial y}{\partial \xi} \\ \frac{\partial^2 x}{\partial \xi^2} & \left(\frac{\partial x}{\partial \xi}\right)^2 & 2\frac{\partial x}{\partial \xi} \frac{\partial y}{\partial \xi} & \frac{\partial^2 y}{\partial \xi^2} \left(\frac{\partial y}{\partial \xi}\right)^2 \end{array} \right] \left\{ \begin{array}{l} \frac{\partial N}{\partial x} \\ \frac{\partial^2 N}{\partial x^2} \\ \frac{\partial^2 N}{\partial x \partial y} \\ \frac{\partial N}{\partial y} \\ \frac{\partial^2 N}{\partial y^2} \end{array} \right\} \quad (\text{B.9})$$

This equation is not of much use yet, as the rectangular matrix on the right hand side cannot be inverted. In the column vector on the right hand side, we know the first partial terms from eqn (B.5) above, so we can bring those to the left hand side of the equation.

This results in

$$\left\{ \begin{array}{l} \frac{\partial^2 N}{\partial \eta^2} - \frac{\partial N}{\partial x} \frac{\partial^2 x}{\partial \eta^2} - \frac{\partial N}{\partial y} \frac{\partial^2 y}{\partial \eta^2} \\ \frac{\partial^2 N}{\partial \eta \partial \xi} - \frac{\partial^2 x}{\partial \eta \partial \xi} \frac{\partial N}{\partial x} - \frac{\partial^2 y}{\partial \eta \partial \xi} \frac{\partial N}{\partial y} \\ \frac{\partial^2 N}{\partial \xi^2} - \frac{\partial N}{\partial x} \frac{\partial^2 x}{\partial \xi^2} - \frac{\partial N}{\partial y} \frac{\partial^2 y}{\partial \xi^2} \end{array} \right\} = \left[\begin{array}{ccc} \left(\frac{\partial x}{\partial \eta}\right)^2 & 2\frac{\partial x}{\partial \eta} \frac{\partial y}{\partial \eta} & \left(\frac{\partial y}{\partial \eta}\right)^2 \\ \frac{\partial x}{\partial \eta} \frac{\partial x}{\partial \xi} & \frac{\partial x}{\partial \eta} \frac{\partial y}{\partial \xi} + \frac{\partial x}{\partial \xi} \frac{\partial y}{\partial \eta} & \frac{\partial y}{\partial \eta} \frac{\partial y}{\partial \xi} \\ \left(\frac{\partial x}{\partial \xi}\right)^2 & 2\frac{\partial x}{\partial \xi} \frac{\partial y}{\partial \xi} & \left(\frac{\partial y}{\partial \xi}\right)^2 \end{array} \right] \left\{ \begin{array}{l} \frac{\partial^2 N}{\partial x^2} \\ \frac{\partial^2 N}{\partial x \partial y} \\ \frac{\partial^2 N}{\partial y^2} \end{array} \right\} \\ = [J^B] \left\{ \begin{array}{l} \frac{\partial^2 N}{\partial x^2} \\ \frac{\partial^2 N}{\partial x \partial y} \\ \frac{\partial^2 N}{\partial y^2} \end{array} \right\} \quad (\text{B.10})$$

Solving for the desired second derivatives, and substituting in the terms from eqn (B.5) as required we can write

$$\begin{Bmatrix} \frac{\partial^2 N}{\partial x^2} \\ \frac{\partial^2 N}{\partial x \partial y} \\ \frac{\partial^2 N}{\partial y^2} \end{Bmatrix} = [J^B]^{-1} \begin{Bmatrix} \frac{\partial^2 N}{\partial \eta^2} - \frac{\partial^2 x}{\partial \eta^2} \left(\Gamma_{11} \frac{\partial N}{\partial \eta} + \Gamma_{12} \frac{\partial N}{\partial \xi} \right) - \frac{\partial^2 y}{\partial \eta^2} \left(\Gamma_{21} \frac{\partial N}{\partial \eta} + \Gamma_{22} \frac{\partial N}{\partial \xi} \right) \\ \frac{\partial^2 N}{\partial \eta \partial \xi} - \frac{\partial^2 x}{\partial \eta \partial \xi} \left(\Gamma_{11} \frac{\partial N}{\partial \eta} + \Gamma_{12} \frac{\partial N}{\partial \xi} \right) - \frac{\partial^2 y}{\partial \eta \partial \xi} \left(\Gamma_{21} \frac{\partial N}{\partial \eta} + \Gamma_{22} \frac{\partial N}{\partial \xi} \right) \\ \frac{\partial^2 N}{\partial \xi^2} - \frac{\partial^2 x}{\partial \xi^2} \left(\Gamma_{11} \frac{\partial N}{\partial \eta} + \Gamma_{12} \frac{\partial N}{\partial \xi} \right) - \frac{\partial^2 y}{\partial \xi^2} \left(\Gamma_{21} \frac{\partial N}{\partial \eta} + \Gamma_{22} \frac{\partial N}{\partial \xi} \right) \end{Bmatrix} \quad (\text{B.11})$$

Appendix C

BOUNDARY CONDITIONS

Note: In the following tables all boundary conditions are various versions of the simply supported case, with the exception of BC-13 and BC-14 which are for the clamped-clamped and clamped-simply supported cases respectively.

C.1 Boundary Conditions- Predictor Corrector Method

The boundary conditions used for the Predictor Corrector Method are given in Table C.1.

C.2 Boundary Conditions- Method I

The boundary conditions used for Method I are given in Table C.2.

C.3 Boundary Conditions- Method II

The boundary conditions used for Method II are given in Table C.3.

Table C.1: Boundary Conditions: Predictor Corrector Method.

Variable Order: $(u_o \ v_o \ w_o \ \phi_x \ \phi_y)^*$

MODEL TYPE	BC NO.	$x = 0$	$x = a/2$ $x = a$	$y = 0$	$y = b/2$ $y = b$
Qrtr Plate	1	(01101)	(10010)	(10110)	(01001)
	2	(10101)	(01010)	(01110)	(10001)
	3	(10101)	(10010)	(01110)	(01001)
	4	(01100)	(10010)	(10100)	(01001)
Full Plate	5	(01101)	(01101)	(10110)	(10110)
	6	(10101)	(10101)	(01110)	(01110)
	13	(11111)	(11111)	(11111)	(11111)
	14	(10101)	(10101)	(11111)	(11111)

*(1 indicates FIXED - 0 indicates FREE)

Table C.2: Boundary Conditions: Method I.

Variable Order:
 $(u_o \ v_o \ \varphi_x \ \varphi_y \ w \ w_x \ w_y)^*$

MODEL TYPE	BC NO.	$x = 0$	$x = a/2$ $x = a$	$y = 0$	$y = b/2$ $y = b$
Qrtr Plate	1	(0101101)	(1010010)	(1010110)	(0101001)
	2	(1001101)	(0110010)	(0110110)	(1001001)
	3	(1001101)	(1010010)	(0110110)	(0101001)
	4	(1001101)	(1110010)	(0110110)	(1101001)
Full Plate	5	(0101101)	(0101101)	(1010110)	(1010110)
	6	(1001101)	(1001101)	(0110110)	(0110110)
	13	(1111111)	(1111111)	(1111111)	(1111111)
	14	(1001101)	(1001101)	(1111111)	(1111111)

*(1 indicates FIXED - 0 indicates FREE)

Table C.3: Boundary Conditions: Method II.

Variable Order: $(u_o \ v_o \ \varphi_x \ \varphi_y \ w)^*$

MODEL TYPE	BC NO.	$x = 0$	$x = a/2$ $x = a$	$y = 0$	$y = b/2$ $y = b$
Qrtr Plate	1	(01011)	(10100)	(10101)	(01010)
	2	(10011)	(01100)	(01101)	(10010)
	3	(10011)	(10100)	(01101)	(01010)
	4	(10011)	(11100)	(01101)	(11010)
Full Plate	5	(01011)	(01011)	(10101)	(10101)
	6	(10011)	(10011)	(01101)	(01101)
	13	(11111)	(11111)	(11111)	(11111)
	14	(10011)	(10011)	(11111)	(11111)

*(1 indicates FIXED - 0 indicates FREE)

Bibliography

- [1] N. Alam and N. T. Asnani. Vibration and damping analysis of fibre reinforced composite material plates. *Journal of Composite Materials*, 20:2-18, January 1986.
- [2] Naiyar Alam and N. T. Asnani. Vibration and damping analysis of a multilayered cylindrical shell, Part I: Theoretical analysis. *American Institute of Aeronautics and Astronautics Journal*, 22(6):803-810, June 1984.
- [3] Naiyar Alam and N. T. Asnani. Vibration and damping analysis of a multilayered cylindrical shell, Part II: Numerical results. *American Institute of Aeronautics and Astronautics Journal*, 22(7):975-981, July 1984.
- [4] Edoardo Anderheggen. A conforming triangular finite element plate bending solution. *International Journal of Numerical Methods in Engineering*, 2:258-264, 1970.
- [5] B. Baharlou and A. W. Leissa. Vibration and buckling of generally laminated composite plates with arbitrary edge conditions. *Int. J. Mech. Sci.*, 29(8):545-555, 1987.
- [6] E. J. Barbero and J. N. Reddy. An accurate determination of stresses in thick laminates using a generalized plate theory. *International Journal of Numerical Methods in Engineering*, 29:1-14, 1990.
- [7] John Barlow. Optimal stress locations in finite element models. *International Journal of Numerical Methods in Engineering*, 10:243-251, 1976.
- [8] A.B. Basset. On the extension and flexure of cylindrical and spherical thin elastic shells. *Philos. Trans. Royal Soc. (London) Ser. A*, 181:433-480, 1890.
- [9] Klaus-Jürgen Bathe. *Finite Element Procedures in Engineering Analysis*. Prentice-Hall, Inc., 1982.
- [10] Jean-Louis Batoz, Klaus-Jürgen Bathe, and Lee-Wing Ho. A study of three-node triangular plate bending elements. *International Journal of Numerical Methods in Engineering*, 15:1771-1812, 1980.
- [11] Kolbein Bell. A refined triangular plate bending finite element. *International Journal of Numerical Methods in Engineering*, 1:101-122, 1969.
- [12] C. W. Bert. Optimal design of a composite-material plate to maximize its fundamental frequency. *Journal of Sound and Vibration*, 50(2):229-237, 1977.
- [13] C. W. Bert. Recent research in composite and sandwich plate dynamics. *Shock and Vibration Digest*, 11:13-23, October 1979.

- [14] C. W. Bert. Comparison of new plate theories applied to laminated composites. *Mechanics of Composite Materials*, pages 9–17, 1983.
- [15] C. W. Bert and T. L. C. Chen. Effect of shear deformation of vibration of antisymmetric angle-ply laminated rectangular plates. *International Journal of Solids and Structures*, 14:465–473, 1978.
- [16] A. Bhimaraddi and L. K. Stevens. A higher order theory for free vibration of orthotropic, homogeneous, and laminated rectangular plates. *Journal of Applied Mechanics*, 51:195–198, March 1984.
- [17] J. A. Bowlus, A. N. Palazotto, and J. M. Whitney. Vibration of symmetrically laminated rectangular plates considering deformation and rotary inertia. *American Institute of Aeronautics and Astronautics Journal*, 25(11):1500–1511, November 1987.
- [18] G. Cederbaum, I. Elishakoff, and L. Librescu. Random vibrations of laminated plates modeled within the first order shear deformation theory. *Composite Structures*, 12:97–111, 1989.
- [19] K. Chandrashekara, A. H. Yahyavi, and P. R. Rao. Bending of cross-ply laminated clamped plates using lagrange multipliers. *Composite Structures*, 15:169–179, 1990.
- [20] T. Chelladurai, B. P. Shastry, and G. V. Rao. Effect of fibre orientation on the initially stressed vibration behaviour of orthotropic rectangular plates. *Fibre Science and Technology*, 21:247–253, 1984.
- [21] K. N. Cho, A. G. Striz, and C. W. Bert. Bending analysis of thick bimodular laminates by higher-order individual-layer theory. *Composite Structures*, 15:1–24, 1990.
- [22] R. M. Christensen. *Mechanics of Composite Materials*. John Wiley and Sons, 1979.
- [23] Robert D. Cook. *Concepts and Applications of Finite Element Analysis*. John Wiley and Sons, 2nd edition, 1981.
- [24] T. J. Craig and D. J. Dawe. Vibration of shear-deformable laminated plate structures by the finite strip method. *Computers and Structures*, 27(1):61–72, 1987.
- [25] D. J. Dawe and T. J. Craig. The vibration and stability of symmetrically-laminated composite rectangular plates subjected to in-plane stresses. *Composite Structures*, pages 281–307, 1986.
- [26] J. P. Fuehne and J. J. Engblom. A shear-deformable, doubly-curved finite element for the analysis of laminated composite structures. *Composite Structures*, 12:81–95, 1989.
- [27] Chin-Ping Fung and Ji-Liang Doong. Bending of a bimodulus laminated plate based on a higher-order shear deformation theory. *Composite Structures*, 10:121–144, 1988.
- [28] Faramarz Gordaninejad. Effect of shear deformation on bending of bimodular composite-material plates. *Composite Structures*, 12:161–170, 1989.
- [29] Joachim L. Grenestedt. Layup optimization and sensitivity analysis of the fundamental eigenfrequency of composite plates. *Composite Structures*, 12:193–209, 1989.

- [30] H. Hencky. Über die berücksichtigung der schubverzerrungen in ebenen platten. *Ing.-Arch*, 16, 1947.
- [31] L. R. Herrmann, K. R. Welch, and C. K. Lim. Composite FEM analysis for layered systems. *Journal of Engineering Mechanics*, 110(9):1284–1302, September 1984.
- [32] F.B. Hildebrand, E. Reissner, and G.B. Thomas. Notes on the foundations of the theory of small displacements of orthotropic shells. In *NACA Technical Note No. 1833*, Mar 1949.
- [33] E. Hinton and J. S. Campbell. Local and global smoothing of discontinuous finite element functions using a least squares method. *International Journal of Numerical Methods in Engineering*, 8:461–480, 1974.
- [34] E. Hinton, F. C. Scott, and R. E. Ricketts. Local least squares stress smoothing for parabolic isoparametric elements. *International Journal of Numerical Methods in Engineering*, 9:235–256, 1975.
- [35] Stefan Holzer, Ernst Rank, and Heinrich Werner. An implementation of the *hp*-version of the finite element method for Reissner-Mindlin plate problems. *International Journal of Numerical Methods in Engineering*, 30:459–471, 1990.
- [36] T. J. R. Hughes. *The Finite Element Method*. Prentice Hall, 1987.
- [37] Bruce M. Irons. A conforming quartic triangular element for plate bending. *International Journal of Numerical Methods in Engineering*, 1:29–45, 1969.
- [38] Bruce M. Irons and O. C. Zienkiewicz. Analysis of thick and thin shell structures by curved finite elements. *International Journal of Numerical Methods in Engineering*, 2:419–451, 1970.
- [39] Hung-Sying Jing and Ming-Liang Liao. Partial hybrid stress element for the analysis of thick laminated composite plates. *International Journal of Numerical Methods in Engineering*, 28:2813–2827, 1989.
- [40] Robert. M. Jones. Buckling and vibration of unsymmetrically laminated cross-ply rectangular plates. *American Institute of Aeronautics and Astronautics Journal*, 11(12):1626–1632, December 1973.
- [41] Robert M. Jones. *Mechanics of Composite Materials*. McGraw-Hill Book Company, 1975.
- [42] C. W. Pryor Jr. and R. M. Barker. A finite-element analysis including transverse shear effects for applications to laminated plates. *American Institute of Aeronautics and Astronautics Journal*, 9(5):912–917, May 1971.
- [43] Henrique Hiroshi Kanematsu and Yoichi Hirano. Bending and vibration of CFRP-faced rectangular sandwich plates. *Composite Structures*, 10:145–163, 1988.
- [44] T. Kant and B.N.Pandya. A simple finite element formulation of a higher-order theory for unsymmetrically laminated composite plates. *Composite Structures*, 9:215–246, 1988.

- [45] T. Kant and Mallikarjuna. Vibrations of unsymmetrically laminated plates analyzed by using a higher order theory with a c^0 finite element formulation. *Journal of Sound and Vibration*, 134(1):1-16, 1989.
- [46] T. Kant, R.V. Ravichandran, B. N. Pandya, and Mallikarjuna. Finite element transient dynamic analysis of isotropic and fibre reinforced composite plates using a higher-order theory. *Composite Structures*, 9:319-342, 1988.
- [47] C. Kassapoglou and P. A. Lagace. Closed form solutions for the interlaminar stress field in angle-ply and cross-ply laminates. *Journal of Composite Materials*, 21:292-308, April 1987.
- [48] C. Kassapoglou and P.A. Lagace. An efficient method for the calculation of interlaminar stresses in composite materials. *Journal of Applied Mechanics*, 53:744-750, December 1986.
- [49] T. P. Khatua and Y. K. Cheung. Bending and vibration of multilayer sandwich beams and plates. *International Journal of Numerical Methods in Engineering*, 6:11-24, 1973.
- [50] A. A. Khdeir. Free vibration of antisymmetric angle-ply laminated plates including various boundary conditions. *Journal of Sound and Vibration*, 122(2):377-388, 1988.
- [51] A. A. Khdeir. Comparison between shear deformable and Kirchhoff theories for bending, buckling and vibration of antisymmetric angle-ply laminated plates. *Composite Structures*, 13:159,172, 1989.
- [52] A. A. Khdeir. An exact approach to the elastic state of stress of shear deformable antisymmetric angle-ply laminated plates. *Composite Structures*, 11:245-258, 1989.
- [53] A. A. Khdeir. Free vibration and buckling of unsymmetric cross-ply laminated plates using a refined theory. *Journal of Sound and Vibration*, 128(3):377-395, 1989.
- [54] A. A. Khdeir and J. N. Reddy. Exact solutions for the transient response of symmetric cross-ply laminates using a higher-order plate theory. *Composite Science and Technology*, 34:205-224, 1989.
- [55] G. Kirchhoff. Uber das gleichgewicht und die bewegung einer elastischen scheinbe. *Journal fuer die reine und angewandte mathematik*, 40:51-88, 1850.
- [56] S. V. Kulkarni and N. J. Pagano. Dynamic characteristics of composite laminates. *Journal of Sound and Vibration*, 23(1):127-143, 1972.
- [57] R. Ramesh Kumar and Y. V. K. Sadasiva Rao. Free vibrations of multilayered thick composite shells. *Computers and Structures*, 28(6):717-722, 1988.
- [58] P. Lardeur and J. L. Batoz. Composite plate analysis using a new discrete shear triangular finite element. *International Journal of Numerical Methods in Engineering*, 27:343-359, 1989.
- [59] K. H. Lee N. R. Senthilnathan, S. P. Lim, and S. T. Chow. An improved zig-zag model for the bending of laminated composite plates. *Composite Structures*, 15:137-148, 1990.

- [60] S. W. Lee and S. C. Wong. Mixed formulation finite elements for Mindlin theory plate bending. *International Journal of Numerical Methods in Engineering*, 18:1297-1311, 1982.
- [61] A. W. Leissa and Yoshihiro Narita. Vibration studies for simply supported symmetrically laminated rectangular plates. *Composite Structures*, 12:113-132, 1989.
- [62] S. G. Lekhnitsky. *Anisotropic Plates*. Gordon and Breach, 1968. Translated from the second Russian edition by Tsai, S. W. and Cheron, T.
- [63] L. Librescu and J. N. Reddy. A few remarks concerning several refined theories of anisotropic composite laminated plates. *International Journal of Engineering Science*, 27(5):515-527, 1989.
- [64] K. M. Liew, K. Y. Lam, and S. T. Chow. Study on flexural vibration of triangular composite plates influenced by fibre orientation. *Composite Structures*, 13:123-132, 1989.
- [65] S. P. Lim, K. H. Lee, S. T. Chow, and N. R. Senthilnathan. Linear and nonlinear bending of shear-deformable plates. *Computers and Structures*, 30(4):945-952, 1988.
- [66] Wen-Jinn Liou and C. T. Sun. A three-dimensional hybrid stress isoparametric element for the analysis of laminated composite plates. *Computers and Structures*, 25(2):241-249, 1987.
- [67] K. H. Lo, R.M. Christensen, and E.M. Wu. A high-order theory of plate deformation, Part 1: Homogeneous plates. *Journal of Applied Mechanics*, 44:663-668, Dec 1977.
- [68] K. H. Lo, R.M. Christensen, and E.M. Wu. A high-order theory of plate deformation, Part 2: Laminated plates. *Journal of Applied Mechanics*, 44:669-676, Dec 1977.
- [69] P. P. Lynn and S. K. Arya. Finite elements formulated by the weighted discrete least squares method. *International Journal of Numerical Methods in Engineering*, 8:71-90, 1974.
- [70] P. P. Lynn and Santosh K. Arya. Use of the least squares criterion in the finite element formulation. *International Journal of Numerical Methods in Engineering*, 6:75-88, 1973.
- [71] Mallikarjuna and T. Kant. Free vibration of symmetrically laminated plates using a higher-order theory with finite element technique. *International Journal of Numerical Methods in Engineering*, 28:1875-1889, 1989.
- [72] S. T. Mau, P. Tong, and T. H. H. Pian. Finite element solutions for laminated thick plates. *Journal of Composite Materials*, 6:304-311, 1972.
- [73] A. S. Mawenya and J. D. Davies. Finite element bending analysis of multilayer plates. *International Journal of Numerical Methods in Engineering*, 8:215-225, 1974.
- [74] D. E. McFarland, B. L. Smith, and W. D. Bernhart. *Analysis of Plates*. Spartan Books, 1972.
- [75] S. J. Medwadowski. A refined theory of elastic orthotropic plates. *Journal of Applied Mechanics*, 25:437-443, Dec 1958.

- [76] R.D. Mindlin. Influence of rotatory inertia and shear on flexural motions of isotropic, elastic plates. *Journal of Applied Mechanics*, 73:31-38, Mar 1951.
- [77] K. Moser and A. Schmid. Composite structures-modelling, finite element analysis and evaluation. *Composite Structures*, 11:33-56, 1989.
- [78] J. T. Mottram. High-order analysis of generally symmetrical laminated plates under transverse loading. *Composite Structures*, 12:211-237, 1989.
- [79] H. Murakami. Laminated composite plate theory with improved in-plane responses. *Journal of Applied Mechanics*, 53:661-666, September 1986.
- [80] A. V. Krishna Murty. Higher order theory for vibrations of thick plates. *American Institute of Aeronautics and Astronautics Journal*, 15(12):1823-1824, December 1977.
- [81] A. V. Krishna Murty. Flexure of composite plates. *Composite Structures*, 7:161-177, 1987.
- [82] A. V. Krishna Murty. Theoretical modelling of laminated composite plates. *Sadhana*, 11(3 and 4):357-365, December 1987.
- [83] A. V. Krishna Murty and S. Vellaichamy. On higher order shear deformation theory of laminated composite panels. *Composite Structures*, 8:247-270, 1987.
- [84] R. B. Nelson and D. R. Lorch. A refined theory for laminated orthotropic plates. *Journal of Applied Mechanics*, 41(1):177-183, March 1974.
- [85] Toshihisa Nishioka and Satya N. Atluri. Fracture-stress analysis of through-cracks in angle-ply laminates: An efficient assumed-stress finite element approach- Part I. In *A Collection of Technical Papers on Structures, AIAA/ASME/ASCE/AHS 20th Structures, Structural Dynamics and Materials Conference*, pages 315-325, Apr 1979.
- [86] A. J. Noor and M. D. Mathers. Anisotropy and shear deformation in laminated composite plates. *American Institute of Aeronautics and Astronautics Journal*, 14(2):282-285, February 1976.
- [87] A. K. Noor and W. Scott Burton. Assessment of shear deformation theories for multilayered composite plates. *Applied Mechanics Review*, 42(1):1-12, January 1989.
- [88] A. K. Noor and W. Scott Burton. Stress and free vibration analyses of multilayered composite plates. *Composite Structures*, 11:183-204, 1989.
- [89] A. K. Noor and W. Scott Burton. Assessment of computational models for multilayered anisotropic plates. *Composite Structures*, 14:233-265, 1990.
- [90] A. K. Noor and M. D. Mathers. Finite element analysis of anisotropic plates. *International Journal of Numerical Methods in Engineering*, 11:289-307, 1977.
- [91] A. K. Noor and J. M. Peters. A posteriori estimates for shear correction factors in multi-layered composite cylinders. *Journal of Engineering Mechanics*, 115(6):1225-1244, June 1989.

- [92] Ahmed Noor and Jeanne Peters. Buckling and postbuckling analyses of laminated anisotropic structures. *International Journal of Numerical Methods in Engineering*, 27:383-401, 1989.
- [93] Ahmed K. Noor. Free vibrations of multilayered composite plates. *American Institute of Aeronautics and Astronautics Journal*, 11(7):1038-1039, July 1973.
- [94] Ahmed K. Noor. Stability of multilayered composite plates. *Fibre Science and Technology*, 8:81-89, 1975.
- [95] E. Onate and B. Suarez. A comparison of the linear, quadratic and cubic Mindlin strip elements for the analysis of thick and thin plates. *Computers and Structures*, 17(3):427-439, 1983.
- [96] N. J. Pagano. Exact solutions for composite laminates in cylindrical bending. *Journal of Composite Materials*, 3:398-411, July 1969.
- [97] N. J. Pagano. Exact solutions for rectangular bidirectional composites and sandwich plates. *Journal of Composite Materials*, 4:20-34, January 1970.
- [98] N. J. Pagano. Influence of shear coupling in cylindrical bending of anisotropic laminates. *Journal of Composite Materials*, 4:330-343, July 1970.
- [99] N. J. Pagano. On the calculation of interlaminar normal stress in composite laminate. *Journal of Composite Materials*, 8:65-74, January 1974.
- [100] N. J. Pagano. Stress fields in composite laminates. *International Journal of Solids and Structures*, 14:385-400, 1978.
- [101] N. J. Pagano and S. D. Wang A. Further study of composite laminates under cylindrical bending. *Journal of Composite Materials*, 5:521-527, October 1971.
- [102] N. J. Pagano and S. J. Hatfield. Elastic behavior of multilayered bidirectional composites. *American Institute of Aeronautics and Astronautics Journal*, 10(7):931-933, July 1972.
- [103] Suresh C. C. Panda and R. Natarajan. Finite element analysis of laminated composite plates. *International Journal of Numerical Methods in Engineering*, 14:69-79, 1979.
- [104] B. N. Pandya and T. Kant. Finite element analysis of laminated composite plates using a higher-order displacement model. *Composite Science and Technology*, 32:137-155, 1988.
- [105] N. D. Phan and J. N. Reddy. Analysis of laminated composite plates using a higher-order shear deformation theory. *International Journal of Numerical Methods in Engineering*, 21:2201-2219, 1985.
- [106] N. S. Putchu and J. N. Reddy. Stability and natural vibration analysis of laminated plates by using a mixed element based on a refined plate theory. *Journal of Sound and Vibration*, 104(2):285-300, 1986.
- [107] K. M. Rao and H.-R. Meyer-Piening. Analysis of thick laminated anisotropic composite plates by the finite element method. *Composite Structures*, 15:185-213, 1990.

- [108] Y. V. K. Sadasiva Rao. Vibrations of layered shells with transverse shear and rotatory inertia effects. *Journal of Sound and Vibration*, 86(1):147-150, 1983.
- [109] Abdur Razzaque. Program for triangular bending elements with derivative smoothing. *International Journal of Numerical Methods in Engineering*, 6:333-343, 1973.
- [110] J. N. Reddy. A penalty plate-bending element for the analysis of laminated anisotropic composite plates. *International Journal of Numerical Methods in Engineering*, 15:1187-1206, 1980.
- [111] J. N. Reddy. Finite-element modeling of layered, anisotropic composite plates and shells: A review of recent research. *Shock and Vibration Digest*, 13:3-12, 1981.
- [112] J. N. Reddy. A refined nonlinear theory of plates with transverse shear deformation. *International Journal of Solids and Structures*, 20(9/10):881-896, 1984.
- [113] J. N. Reddy. A simple higher-order theory for laminated composite plates. *Journal of Applied Mechanics*, 51:745-752, December 1984.
- [114] J. N. Reddy. A review of the literature on finite-element modeling of laminated composite plates. *Shock and Vibration Digest*, 17:3-8, 1985.
- [115] J. N. Reddy. On refined computational models of composite laminates. *International Journal of Numerical Methods in Engineering*, 27:361-382, 1989.
- [116] J. N. Reddy, E. J. Barbero, and J. L. Teply. A plate bending element based on a generalized laminate plate theory. *International Journal of Numerical Methods in Engineering*, 28:2275-2292, 1989.
- [117] J. N. Reddy and N. D. Phan. Stability and vibration of isotropic, orthotropic and laminated plates according to a higher-order shear deformation theory. *Journal of Sound and Vibration*, 98(2):157-170, 1985.
- [118] E. Reissner. The effect of transverse shear deformation on the bending of elastic plates. *Journal of Applied Mechanics*, 12(2):69-77, June 1945.
- [119] E. Reissner. On bending of elastic plates. *Quarterly of Applied Mathematics*, 5:55-68, 1947.
- [120] E. Reissner. On a certain mixed variational theorem and proposed application. *International Journal of Numerical Methods in Engineering*, 20:1366-1368, 1984.
- [121] E. Reissner and Y. Stavsky. Bending and stretching of certain types of heterogeneous anisotropic elastic plates. *Journal of Applied Mechanics*, 28:402-408, September 1961.
- [122] M. Sathyamoorthy. Effects of transverse shear and rotatory inertia on large amplitude vibration of composite plates and shells. *Sadhana*, 11(3 and 4):367-377, December 1987.
- [123] M. Di Sciuva. An improved shear-deformation theory for moderately thick multilayered anisotropic shells and plates. *Journal of Applied Mechanics*, 54:589-596, September 1987.

- [124] N. R. Senthilnathan, S. P. Lim, K. H. Lee, and S. T. Chow. Vibration of laminated orthotropic plates using a simplified higher-order deformation theory. *Composite Structures*, 10:211-229, 1988.
- [125] K. Shirakawa. Effects of shear deformation and rotatory inertia on vibration and buckling of cylindrical shells. *Journal of Sound and Vibration*, 91(3):425-437, 1983.
- [126] V. Soamidass and N. Ganesan. Effect of fibre orientation of the vibration characteristics of the orthotropic annular plates. *Journal of Sound and Vibration*, 121(3):567-570, 1988.
- [127] B. R. Somashekar, G. Prathap, and C. Ramesh Babu. A field-consistent, four-noded, laminated, anisotropic plate/shell element. *Computers and Structures*, 25(3):345-353, 1987.
- [128] R. L. Spilker. Hybrid-stress eight-node elements for thin and thick multilayer laminated plates. *International Journal of Numerical Methods in Engineering*, 18:801-828, 1982.
- [129] R. L. Spilker, S. C. Chou, and O. Orringer. Alternate hybrid-stress elements for analysis of multilayer composite plates. *Journal of Composite Materials*, 11:53-70, January 1977.
- [130] S. Srinivas. A refined analysis of composite laminates. *Journal of Sound and Vibration*, 30(4):495-507, 1973.
- [131] S. Srinivas and A. K. Rao. Bending, vibration and buckling of simply supported thick orthotropic rectangular plates and laminates. *International Journal of Solids and Structures*, 6:1463-1481, 1970.
- [132] S. Srinivas, C. V. Joga Rao, and A. K. Rao. An exact analysis for vibration of simply-supported homogeneous and laminated thick rectangular plates. *Journal of Sound and Vibration*, 12(2):187-199, 1970.
- [133] Y. Stavsky. *On the Theory of Heterogeneous Anisotropic Plates*. PhD thesis, Massachusetts Institute of Technology, Cambridge, Mass., September 1959.
- [134] C. T. Sun, J. D. Achenbach, and G. Herrmann. Continuum theory for a laminated medium. *Journal of Applied Mechanics*, 35(3):467-475, September 1968.
- [135] A. Toledano and H. Murakami. A composite plate theory for arbitrary laminate configurations. *Journal of Applied Mechanics*, 54:181-189, March 1987.
- [136] Pin Tong and John N. Rossettos. *Finite-Element Method- Basic Technique and Implementation*. The MIT Press, 1977.
- [137] Stephen W. Tsai and H. Thomas Hahn. *Introduction to Composite Materials*. Technomic Publishing Co., Inc, 1980.
- [138] G. Z. Voyiadjis and M. H. Baluch. Refined theory for thick composite plates. *Journal of Engineering Mechanics*, 114(4):671-687, April 1988.
- [139] G. Z. Voyiadjis, M. H. Baluch, and W. K. Chi. Effect of shear and normal strain on plate bending. *Journal of Engineering Mechanics*, 111(9):1130-1143, September 1985.

- [140] G. Z. Voyiadjis and Robert W. Pecquet Jr. Bending and stretching elements for analysis of thick composite plates. *Journal of Engineering Mechanics*, 114(11):1973-1995, November 1988.
- [141] J. M. Whitney. The effect of transverse shear deformation on the bending of laminated plates. *Journal of Composite Materials*, 3:534-547, July 1969.
- [142] J. M. Whitney. Shear correction factors for orthotropic laminates under static load. *Journal of Applied Mechanics*, pages 302-305, March 1973.
- [143] J. M. Whitney and A. W. Leissa. Analysis of heterogeneous anisotropic plates. *Journal of Applied Mechanics*, 36:261-266, June 1969.
- [144] J. M. Whitney and N. J. Pagano. Shear deformation in heterogeneous anisotropic plates. *Journal of Applied Mechanics*, 37:1031-1036, December 1970.
- [145] P. C. Yang, C. H. Norris, and Y. Stavsky. Elastic wave propagation in heterogeneous plates. *International Journal of Solids and Structures*, 2:665-684, 1966.
- [146] O. C. Zienkiewicz. *The Finite Element Method*. McGraw-Hill Book Company, 1977.
- [147] O. C. Zienkiewicz and D. Lefebvre. A robust triangular plate bending element of the Reissner-Mindlin type. *International Journal of Numerical Methods in Engineering*, 26:1169-1184, 1988.